The Role of the Leaving Group in the Photo-Favorskii Rearrangement of *p*-Hydroxyphenacyl

By

Copyright 2008
Elizabeth D. Cope
M.S., Illinois State University, 2003

Submitted to the Department of Chemistry and
the Faculty of the Graduate School of the University of Kansas
in partial fulfillment of the requirements for the degree of
Doctor of Philosophy

Richard S. Givens, Committee Chair

Jeffrey Aubé, Committee Member

David R. Benson, Committee Member

Heather Desaire, Committee Member

Paul R. Hanson, Committee Member

Date

The Dissertation Committee for Elizabeth Cope certifies
that this is the approved version of the following dissertation:

The Role of the Leaving Group in the Photo-Favorskii
Rearrangement of *p*-Hydroxyphenacyl

Committee:

_____
Chairperson

_____

_____

_____

_____

Date Approved: _____

ABSTRACT

The Role of the Leaving Group in the Photo-Favorskii Rearrangement of *p*-Hydroxyphenacyl

By

Elizabeth D. Cope

Department of Chemistry, May 2008

University of Kansas

The p-hydroxyphenacyl group has several features that make it an attractive photoremovable protecting group. Literature examples support this statement and the benzoate, formate, and sulfonate derivatives are not exceptions. The synthesis of these targets is straight forward involving few synthetic steps that produce the desired product in good to excellent yield. The purification of these targets is simplified by the fact that these derivatives are all solids. Their solubility and stability in polar

organic solvents and in water at low concentrations, the formate solubility in water is the exception, make them ideal for use in organic synthesis and in biological applications.

The bulk of the photochemical reactions on these derivatives were performed using a low intensity commercially available Southern New England Photoreactor fitted with RPR 3000 Å lamps in order to excite the chromophore in the region where reasonable absorptivity is displayed, at or above 300 nm. Departure of the substrate or leaving group from the p-hydroxyphenacyl chromophore occurs by the heterolytic rupture of the covalent bond connecting the two and is a primary photochemical process. The reaction results in the formation of two major photoproducts, the released substrate and a product resulting from the rearrangement of chromophore. Their lack of photochemical or chemical reactivity with other reagents, solvent, or other products established the stability of these two products. Finally, the photochemical release is fast ($>10^8$ s^{-1}) and efficient ($\Phi_{dis} = 0.20 – 1.00$).

p-Hydroxyphenacyl (pHP) caged compounds release substrates through a novel photo-Favorskii rearrangement. In an effort to systematically explore the effects of the leaving group on the efficacy of photorelease, a series of pHP substituted phenol, benzoate, formate, phosphate, and sulfonate esters have been examined. The quantum yields (Φ), Stern-Volmer quenching rates (k_q), and release rates (k_r) were determined. When this data was combined with the data from laser flash photolysis data, a correlation between the release rate and the pK_a of the leaving group was observed. The β_{LG} for this correlation was calculated to be roughly -0.24

showing that photorelease of the substrate is less sensitive to the structure and pK_a of the leaving group than is the reference deprotonation reaction of water. The modest value of β_{LG} suggests a small amount of bond cleavage to leaving group in the transition state.

The mechanism of photorelease in aqueous or mixed aqueous solvents follows an ionic pathway with the substrate and a proton release occurring from the triplet ester forming a triplet biradical. This biradical then decays forming a spirodienedione intermediate which can either react with water as part of a Favorskii-like rearrangement yielding *p*-hydroxyphenylacetic acid, or it can undergo decarbonylation to form *p*-quinone methide. Subsequent reaction of *p*-quinone methide with water results in the formation of *p*-hydroxybenzyl alcohol. This mechanism is supported by the results of the quenching of the reaction of the benzoates by a triplet quencher (piperylene), the formation of only photoproducts when pHP formate, mesylate, and tosylate were photolyzed in the presence of a triplet sensitizer (acetone), the absorption bands for the triplet biradical and *p*-quinone methide that were observed using laser flash photolysis, and the appearance and decay of singlet and triplet species in the time resolved spectra of pHP benzoate and tosylate. A Brønsted correlation relating the rate constant for photorelease to the pK_a of the substrate leaving group for several pHP derivatives, including the benzoate, formate, and sulfonate esters, which indicated there is a moderate degree of bond cleavage in the transition state for the adiabatic triplet fragmentation step. These

results have added further insight into the mechanism for the photo-Favorskii rearrangements of *p*-hydroxyphenacyl derivatives.

ACKNOWLEDGEMENTS

There are a number of people that I would like to thank for their help and support. These people have been important during my academic career at the University of Kansas. They each deserve a grateful thank you for everything they have done.

I have appreciated the advice, encouragement, and support of my friends and colleagues within the Department. They have made the difficult bearable and the rest of it great. I look forward to the things we are going to do in the future.

Several people have contributed valuable information and data to this work. I would like to thank Benjamin Neuenswander and Todd Williams for teaching me about HLPC. Their leadership taught me the basics in instrument care and usage and how to troubleshoot when things did not go as planned. The X-ray diffraction data confirmed the structures of the derivates I synthesized. For these, I thank Victor Day. Special thanks to Dr. Jakob Wirz and to Dr. Dominik Heger for their analysis of my derivatives using laser flash photolysis. The results were spectacular.

I would like to thank my parents for instilling the morals, values, and good work ethic that have gotten me where I am today. Without the constant support of my family, I would not be who I am today.

My deepest gratitude goes to Dr. Givens for his guidance and support over the years. His guidance and encouragement have pushed me to accomplish more. My best wishes for him in the years to come.

Without funding none of this would have been possible. I would like to thank NIH Grants GM72910 and P50 BM 069663 (CMLD) for their financial support.

E.D.C.

TABLE OF CONTENTS

	page
ABSTRACT	iii
ACKNOWLEDGEMENTS	vii
LIST OF EQUATIONS	ix
LIST OF FIGURES	xii
LIST OF SCHEMES	xvi
LIST OF TABLES	xviii
ABBREVIATIONS	xxiii
INTRODUCTION	1
STATEMENT OF PROBLEM	47
RESULTS AND DISCUSSION	49
CONCLUSION	115
EXPERIMENTAL	117
REFERENCES	154
APPENDIX A: Spectral Data	159
APPENDIX B X-Ray Diffraction Data	Supplementary Files

LIST OF EQUATIONS

Equation 1. 2

Equation 2. 5

Equation 3. 5

Equation 4. 6

Equation 5. 11

Equation 6. 13

Equation 7. 14

Equation 8. 17

Equation 9. 17

Equation 10. 19

Equation 11. 20

Equation 12. 21

Equation 13. 26

Equation 14. 28

Equation 15. 28

Equation 16. 30

Equation 17. 33

Equation 18. 34

Equation 19. 37

Equation 20. 39

Equation 21. 39

Equation 22. 40

Equation 23. 50

Equation 24. 52

Equation 25. 58

Equation 26. 59

Equation 27. 60

Equation 28. 66

Equation 29. 75

Equation 30. 76

Equation 31. 77

Equation 32. 89

Equation 33. 109

Equation 34. 109

Equation 35. 110

Equation 36. 110

Equation 37. 110

LIST OF FIGURES

Figure 1.	Linear Free Energy Relationship between log(k_1) and the pK_a values of the acids released during photolysis of DMACM **25a-f** and 7-MCM **26a-f** esters in CH_3CN/HEPES	18
Figure 2.	Quantum efficiency for release of GABA as a function of the ^3pK_a of Substituted pHP GABA derivatives	45
Figure 3.	X-Ray Crystal Structure – pHP Formate **70a**	53
Figure 4.	X-Ray Crystal Structure – pHP Benzoate **70c**	55
Figure 5.	X-Ray Crystal Structure – pHP *p*-Methoxybenzoate **70d**	55
Figure 6.	X-Ray Crystal Structure – pHP Mesylate **72a**	62
Figure 7.	X-Ray Crystal Structure – pHP Tosylate **72b**	62
Figure 8.	Stern-Volmer Quenching with Piperylene of pHP Benzoate **70c**	84
Figure 9.	Stern-Volmer Quenching with Piperylene of pHP $pOCH_3$ Benzoate **70d**	84
Figure 10.	Stern-Volmer Quenching with Piperylene of pHP pCF_3 Benzoate **70e**	85
Figure 11.	Time Resolved Spectra for pHP Benzoate **70c**	100
Figure 12.	Time Resolved Spectra for pHP Tosylate **72b**	100
Figure 13.	Numbering of Atoms in X-Ray Crystal Structures of pHP Carboxylates and Sulfonates	104
Figure 14.	Optimized Structure of Ground State pHP Acetate **60**	107

Figure 15. Optimized Structure of Triplet pHP Acetate **60** 107

Figure 16. Brønsted Linear Free Energy Relationship 111

Figure 17. IR of pHP Formate **70a** (KBr) 159

Figure 18. Laser Flash Photolysis Transient Spectra for pHP Formate **70a** in Aqueous Acetonitrile 160

Figure 19. Laser Flash Photolysis Transient Spectra for pHP Formate **70a** in Water 160

Figure 20. UV-VIS of pHP Formate **70a** (3:1 water/acetonitrile) 161

Figure 21. ^{1}H NMR of pHP Formate **70a** (DMSO-d_6) 162

Figure 22. ^{13}C NMR of pHP Formate **70a** (DMSO-d_6) 163

Figure 23. X-Ray Crystal Structure of pHP Formate **70a** 164

Figure 24. Orientation of pHP Formate **70a** Molecules in the Crystal Lattice 164

Figure 25. IR of pHP Benzoate **70c** (KBr) 175

Figure 26. Laser Flash Photolysis Transient Spectra for pHP Benzoate **70c** in Aqueous Acetonitrile 176

Figure 27. UV-VIS of pHP Benzoate **70c** (7:3 acetonitrile/water) 176

Figure 28. ^{1}H NMR of pHP Benzoate **70c** (DMSO-d_6) 177

Figure 29. ^{13}C NMR of pHP Benzoate **70c** (DMSO-d_6) 178

Figure 30. X-Ray Crystal Structure of pHP Benzoate **70c** 179

Figure 31. Orientation of pHP Benzoate **70c** in the Crystal Lattice 179

Figure 32. IR of pHP $pOCH_3$ Benzoate **70d** (KBr) 190

Figure 33. Laser Flash Photolysis Transient Spectra for pHP $pOCH_3$ Benzoate **70d** in Aqueous Acetonitrile 191

Figure 34. UV-VIS of pHP $pOCH_3$ Benzoate **70d** (7:3 acetonitrile/water) 191

Figure 35. ^{1}H NMR of pHP $pOCH_3$ Benzoate **70d** (DMSO-d_6) 192

Figure 36. ^{13}C NMR of pHP $pOCH_3$ Benzoate **70d** (DMSO-d_6) 193

Figure 37. X-Ray Crystal Structure of pHP *p*-Methoxybenzoate **70d** 194

Figure 38. Orientation of $pOCH_3$ Benzoate **70d** in the Crystal Lattice 194

Figure 39. IR of pHP pCF_3 Benzoate **70e** (KBr) 205

Figure 40. Laser Flash Photolysis Transient Spectra for pHP pCF_3 Benzoate **70e** in Aqueous Acetonitrile 206

Figure 41. UV-VIS of pHP pCF_3 Benzoate **70e** (7:3 acetonitrile/water) 206

Figure 42. ^{1}H NMR of pHP pCF_3 Benzoate **70e** (DMSO-d_6) 207

Figure 43. ^{13}C NMR of pHP pCF_3 Benzoate **70e** (DMSO-d_6) 208

Figure 44. IR of pHP Mesylate **72a** (KBr) 209

Figure 45. Laser Flash Photolysis Transient Spectra for pHP Mesylate **72a** in Aqueous Acetonitrile 210

Figure 46. Laser Flash Photolysis Transient Spectra for pHP Mesylate **72a** in Water 210

Figure 47. UV-VIS of pHP Mesylate **72a** (3:1 acetonitrile/water) 211

Figure 48. ^{1}H NMR of pHP Mesylate **72a** (DMSO-d_6) 212

Figure 49. ^{13}C NMR of pHP Mesylate **72a** (DMSO-d_6) 213

Figure 50. X-Ray Crystal Structure of pHP Mesylate **72a** 214

Figure 51. Orientation of pHP Mesylate **72a** in the Crystal Lattice 214

Figure 52. IR of pHP Tosylate **72b** (KBr) 225

Figure 53. Laser Flash Photolysis Transient Spectra for pHP Tosylate **72b** in Aqueous Acetonitrile 226

Figure 54. UV-VIS of pHP Tosylate **72b** (1:1 acetonitrile/water) 226

Figure 55. ^{1}H NMR of pHP Tosylate **72b** (DMSO-d_6) 227

Figure 56. ^{3}C NMR of pHP Tosylate **72b** (DMSO-d_6) 228

Figure 57. X-Ray Crystal Structure – pHP Tosylate **72b** 229

Figure 58. Orientation of pHP Tosylate **72b** in the Crystal Lattice 229

LIST OF SCHEMES

Scheme 1.	*o*-Nitrobenzyl Photorelease Mechanism	7
Scheme 2.	Revised *o*-Nitrobenzyl Photorelease Mechanism	9
Scheme 3.	Pincock Benzyl Acetate Photorelease Mechanism	13
Scheme 4.	Coumarin Photorelease Mechanism	16
Scheme 5.	Benzoin Photorelease Mechanism	23
Scheme 6.	Revised Benzoin Photorelease Mechanism	24
Scheme 7.	Photorelease Mechanism for *p*-Methoxyphenacyl Esters	27
Scheme 8.	Dhavale Mechanism	31
Scheme 9.	Synthesis of pHP ATP **55**	37
Scheme 10.	Synthesis of pHP Glutamate **57a** and pHP GABA **57b**	38
Scheme 11.	Givens *p*-Hydroxyphenacyl Photorelease Mechanism	43
Scheme 12.	Corrie and Wan *p*-Hydroxyphenacyl Photorelease Mechanism	43
Scheme 13.	Proposed Synthesis of pHP Carboxylates	50
Scheme 14.	Chimilio pHP Sulfonate Synthesis	56

Scheme 15. Phillips Synthetic Sequence 57

Scheme 16. Emmons and Ferris Synthesis of Benzyl Mesylate (**77a**) and Benzyl Tosylate (**77b**) 60

Scheme 17. Synthesis of pHP Mesylate **72a** and pHP Tosylate **72b** 61

Scheme 18. Synthesis of pHP Caged Biological Molecules 66

Scheme 19. Radical Pathway of Photorelease 68

Scheme 20. Ionic Pathway of Photorelease 69

Scheme 21. Formation of *p*-Hydroxybenzyl Alcohol (**87**) 78

Scheme 22. Proposed Mechansim of Photoreleaes from the Conjugate Base of pHP Esters 98

Scheme 23. Revised pHP Photorelease Mechanism 113

LIST OF TABLES

Table 1.	Efficiencies and Excitation Wavelengths for cAMP and cGMP Coumaryl Esters	15
Table 2.	Photophysical and Photochemical Data for (7-Methoxycoumarin-4-yl)methyl Esters in 30:70 (vol/vol) CH_3CN/H_2O-HEPES (pH 7.2)	17
Table 3.	Photophysical and Photochemical Data for (Coumarin-4-yl)methyl Esters in CH_3CN/H_2O-HEPES Buffer Mixtures at Various Concentrations (pH7.2)	18
Table 4.	Efficiencies for Benzoin Phosphate Esters	20
Table 5.	Quantum Efficiencies for Photolysis of Benzoin Cyclic Adenosine 3',5'-Monophosphate **30**	22
Table 6.	Yields for the Release of Acids from 4-Methocyphenacyl Esters	26
Table 7.	Quantum Efficiencies and Solvent Isotope Effects (k_H/k_D) for Photolysis of 4-Methoxyphenacyl Diethyl Phosphate **38a**	29
Table 8.	Photolysis of α-Chloroacetophenones **42a-d**: Yields Obtained for Photoproducts under Various Conditions	30
Table 9.	Product Formation from Photolysis of Substituted Phenacyl Chlorides	32
Table 10.	Product Distribution from Photolysis of **47a-i** in Aqueous Acetone or Aqueous Methanol	33
Table 11.	Disappearance and Product Efficiencies for Aryl-Substituted Phenacyl Phosphates **51a-f** in TRIS Buffer (pH 7.2) at 300 nm	35
Table 12.	Phosphorescence Emission for a Series of *p*-Hydroxy-acetophenone Esters at 77 K	41

Table 13.	Substituent Effects on Photorelease of GABA from pHP Esters	45
Table 14.	Leaving Group pK_a	49
Table 15.	Yields of Bromination Reactions	51
Table 16.	Product Yields of pHP Carboxylates	53
Table 17.	UV-VIS Absorption Maxima (λ_{max}) and Extinction Coefficients (log ε) of pHP Derivatives	74
Table 18.	Disappearance and Product Appearance Quantum Efficiencies for pHP Benzoate Ester Photolyses	79
Table 19.	Quantum Efficiencies for pHP Formate and Sulfonate Esters	81
Table 20.	Stern-Volmer Results for Piperylene Quenching of pHP Benzoates	85
Table 21.	LFP Results for pHP Derivatives	88
Table 22.	UV-VIS Absorption Maxima (λ_{max}) and Extinction Coefficients (log ε) of pHP Derivatives in Buffered Solutions	93
Table 23.	Quantum Efficiencies of pHP Mesylate at Different pHs	95
Table 24.	Comparison of Stern-Volmer Quenching and Laser Flash Photolysis	101
Table 25.	Dihedral Angles for pHP Derivatives	105
Table 26.	Calculated Structural Parameters of the Ground and Triplet State of pHP Acetate **60**	106
Table 27.	Summary of Brønsted LFER Data	112
Table 28.	Crystal Data and Structure Refinement for pHP Formate **70a**	167

Table 29.	Atomic Coordinates (x 10^4) and Equivalent Isotropic Displacement Parameters ($Å^2$ x 10^3) for pHP Formate **70a**	168
Table 30.	Bond Lengths [Å] for pHP Formate **70a**	169
Table 31.	Bond Angles [°]pHP Formate **70a**	170
Table 32.	Anisotropic Displacement Parameters ($Å^2$ x 10^3) for pHP Formate **70a**	171
Table 33.	Hydrogen Coordinates (x 10^4) and Isotropic Displacement Parameters ($Å^2$ x 10^3) for pHP Formate **70a**	172
Table 34.	Torsion Angles [°] for pHP Formate **70a**	173
Table 35.	Hydrogen Bonds for pHP Formate **70a** [Å and °]	174
Table 36.	Crystal Data and Structure Refinement for pHP Benzoate **70c**	182
Table 37.	Atomic Coordinates (x 10^4) and Equivalent Isotropic Displacement Parameters ($Å^2$ x 10^3) for pHP Benzoate **70c**	183
Table 38.	Bond Lengths [Å] for pHP Benzoate **70c**	184
Table 39.	Bond Angles [°] pHP Benzoate **70c**	185
Table 40.	Anisotropic Displacement Parameters ($Å^2$ x 10^3) for pHP Benzoate **70c**	186
Table 41.	Hydrogen Coordinates (x 10^4) and Isotropic Displacement Parameters ($Å^2$ x 10^3) for pHP Benzoate **70c**	187
Table 42.	Torsion Angles [°] for pHP Benzoate **70c**	188
Table 43.	Hydrogen Bonds for pHP Benzoate **70c** [Å and °]	189

Table 44.	Crystal Data and Structure Refinement for pHP $pOCH_3$ Benzoate **70d**	197
Table 45.	Atomic Coordinates (x 10^4) and Equivalent Isotropic Displacement Parameters ($Å^2$ x 10^3) for pHP $pOCH_3$ Benzoate **70d**	198
Table 46.	Bond Lengths [Å] for pHP $pOCH_3$ Benzoate **70d**	199
Table 47.	Bond Angles [°] pHP $pOCH_3$ Benzoate **70d**	200
Table 48.	Anisotropic Displacement Parameters ($Å^2$ x 10^3) for pHP $pOCH_3$Benzoate **70d**	201
Table 49.	Hydrogen Coordinates (x 10^4) and Isotropic Displacement Parameters ($Å^2$ x 10^3) for pHP $pOCH_3$ Benzoate **70d**	202
Table 50.	Torsion Angles [°] for pHP $pOCH_3$Benzoate **70d**	203
Table 51.	Hydrogen Bonds for pHP $pOCH_3$ Benzoate **70d** [Å and °]	204
Table 52.	Crystal Data and Structure Refinement for pHP Mesylate **72a**	217
Table 53.	Atomic Coordinates (x 10^4) and Equivalent Isotropic Displacement Parameters ($Å^2$ x 10^3) for pHP Mesylate **72a**	218
Table 54.	Bond Lengths [Å] for pHP Mesylate **72a**	219
Table 55.	Bond Angles [°] for pHP Mesylate **72a**	220
Table 56.	Anisotropic Displacement Parameters ($Å^2$ x 10^3) for pHP Mesylate **72a**	221
Table 57.	Hydrogen Coordinates (x 10^4) and Isotropic Displacement Parameters ($Å^2$ x 10^3) for pHP Mesylate **72a**	222
Table 58.	Torsion Angles [°] for pHP Mesylate **72a**	223

Table 59.	Hydrogen Bonds for pHP Mesylate **72a** [Å and °]	224
Table 60.	Crystal Data and Structure Refinement for pHP Tosylate **72b**	233
Table 61.	Atomic Coordinates (x 10^4) and Equivalent Isotropic Displacement Parameters (Å^2 x 10^3) for pHP Tosylate **72b**	234
Table 62.	Bond Lengths [Å] for pHP Tosylate **72b**	235
Table 63.	Bond Angles [°] for pHP Tosylate **72b**	236
Table 64.	Anisotropic Displacement Parameters (Å^2 x 10^3) for pHP Tosylate **72b**	237
Table 65.	Hydrogen Coordinates (x 10^4) and Isotropic Displacement Parameters (Å^2 x 10^3) for pHP Tosylate **72b**	238
Table 66.	Torsion Angles [°] for pHP Tosylate **72b**	239
Table 67.	Hydrogen Bonds for pHP Tosylate **72b** [Å and °]	240

ABBREVIATIONS

^{1}H NMR	Proton Nuclear Magnetic Resonance
^{3}pHA	Triplet *p*-Hydroxyacetophenone
^{3}pK_a	Triplet pK_a
Ala-Ala	Alanine-Alanine
ATP	Adenosine 5'-Triphosphate
ADP	Adenosine Diphosphate
cAMP	Cyclic adenosine Monophosphate
cGMP	Cyclic Guanosine Monophosphate
DBU	1,8-Diazabicyclo[5.4.0]undec-7-ene
DDB	Dioxane Dibromide
DFT	Density Function Theory
DMACM	(7-Methoxycoumarin-4-yl)methyl Esters
DMAP	Dimethylaminopyridine
DMF	*N*,*N*-Dimethylformamide

DNA	Deoxyribonucleic Acid
GABA	Gamma-aminobutyric Acid
GC-MS	Gas Chromatography-Mass Spectroscopy
h	hour(s)
HPLC	High Performance Liquid Chromatography
ISC	Intersystem Crossing
k_{diff}	Rate of Diffusion
k_{dis}	Rate of the Disappearance of Starting Material
k_{ISC}	Rate of Intersystem Crossing
k_f	Rate of Fluorescence
k_q	Rate of Quenching
k_{rel}	Rate of Substrate Release
k_{ST}	Rate of Intersystem Crossing
$k_{\tau 3\ decay}$	Rate of Triplet Decay
$k_{\tau 3\ rise}$	Rate of the Rise of the Triplet
K_{SV}	Stern-Volmer Constant

λ_{max}	Absorption Maxima
LC-MS	Liquid Chromatography- Mass Spectroscopy
LC-UV/MS	Liquid Chromatography-Ultraviolet/Mass Spectroscopy
LFER	Linear Free Energy Relationship
LF	Laser Flash
LFP	Laser Flash Photolysis
MCM	(Coumarin-4-yl)methyl Esters
MS	Mass Spectroscopy
NB	2-Nitrobenzyl ester
NPE	1-(2-Nitrophenyl)ethyl Ester
pHBA	*p*-Hydroxybenzyl Alcohol
Φ_{acid}	Quantum Efficiency of Appearance of Released Substrate
Φ_{dis}	Quantum Efficiency of the Disappearance of Starting Material
Φ_{pHBA}	Quantum Efficiency of the Appearance of *p*-Hydroxybenzyl Alcohol
Φ_{pHPAA}	Quantum Efficiency of the Appearance of *p*-Hydroxyphenyl-acetic Acid
Φ_{pHPOH}	Quantum Efficiency of the Appearance of 2,4'-Dihydroxyacetophenone

Φ_{rel}	Quantum Efficiency for the Release of Substrate
pHP	*p*-Hydroxyphenacyl
pHPAA	*p*-Hydroxyphenylacetic Acid
ppm	Parts per Million
ps	Picosecond
RP-HPLC	Reverse Phase High Performance Liquid Chromatography
SES	Singlet Excited State
ST	Intersystem Crossing (Singlet to Triplet)
TBDPS	Tert-Butyldiphenyl silyl
TEA	Triethylamine
TFA	Trifluoroacetic Acid
TLC	Thin Layer Chromatography
UV-VIS	Ultraviolet-Visible

INTRODUCTION

A need to safeguard spectator groups in multiple functional group transformations in the synthesis of organic molecules has led to the development and use of many types of protecting groups. In general, protecting groups are covalently attached organic appendages that render the functional group inert to subsequent reaction conditions until their removal.[1] They have become a necessity in modern organic synthesis and have been applied in biologically active molecules by blocking key functional groups, which suspend their normal mode of action. The molecule's activity can be fully restored upon treatment with the proper reagent(s) to remove the protecting group allowing for the mechanisms and action of the molecule to be studied in biological processes. However, there are limitations that traditional protecting groups encounter when they are used in biological systems in that the reaction conditions needed for the incorporation or removal of these groups may be too harsh. These harsh conditions, which usually involve the use of an acid or a base, may interfere with the normal biological processes or be incompatible with the chemistry of the biologogical processes under investigation. Another limitation is that a typical process for protecting group removal, hydrolysis, is far too slow to serve as a means of investigating the initial rates of reactions involving rapid biochemical processes. An ideal solution to these limitations would involve the use of a protecting group that can be removed under mild, neutral conditions thus avoiding any

alterations to the natural biological environment and where release occurs on a fast enough timescale for kinetic analysis for the most rapid biological processes. Such a group may be a photoremovable protecting group.

The concept of a photoremovable protecting group was first envisioned by Barltrop and coworkers almost fifty years ago.[2] In 1962, they reported the photochemical deprotection of glycine (**1**), a biological substrate (**Equation 1**). This discovery initiated the development of several additional photoremovable protecting

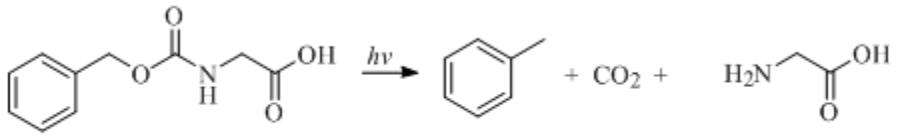

1

Equation 1.

groups. With the continued success of photoremovable protecting groups, especially in the area of biology by Kaplan[3], they became referred to as "cages". To describe the notion of caging, physiologically significant substrates[4-7] were protected by covalently attaching a photoremovable protecting group. It was said that these compounds had been trapped inside a cage and were unable to interact with receptors, catalytic sites, or other substrates. The cage could be opened with the use of light freeing the substrate, which could then act in a normal fashion and is the basic requirement for this type of protecting group.

Light offers several advantages over previously mentioned agents for protecting group removal. These advantages include a measure of control over the caged compound's spatial, temporal, and concentration variables that have an enormous impact on where, when, and how much of the substrate is released. Several researchers in the field, including Sheehan[8] and Lester[9], compiled a list of benchmarks and requirements for evaluating the efficacy of a photoremovable protecting group under given circumstances, or for evaluating the potential of a chromophore. The following is a generalized list adapted for the Sheehan and Lester criteria.

i. The substrate, caged substrate, and the photoproducts should have good aqueous solubility for biological studies. For synthetic applications, this requirement is relaxed.

ii. The photochemical release must be efficient, i.e. $\Phi > 0.10$.

iii. The departure of the substrate from the protecting group by rupture of the covalent bond to the protecting group should be a primary photochemical process, *i.e.* a rapid process occurring directly from an excited state of the caged chromophore

iv. All photoproducts should be stable to the surrounding media.

v. Excitation wavelengths should be ≥ 300 nm and must not be absorbed by the media or photoproducts.

vi. The chromophore should have reasonable absorptivity (a) to efficiently capture the incident light.

vii. The caged compounds as well as the photoproduct(s) from the cage portion should be inert or at least benign with respect to the media, the other reagents, and the other products.

viii. A general, high yielding synthetic procedure, for the attachment of the cage to the substrate, must be available.

ix. In the synthesis of a caged substrate, the separation of caged and uncaged derivatives must be quantitative. This also is necessary for the deprotection products for synthetic applications.

While the above guidelines are highly desirable for an ideal photoremovable protecting group, a cage or potential cage that lacks one or two of these properties may still be useful. However, the absence of several of these qualities may diminish the viability of that group as a useful photoremovable protecting group for specific applications.

In the literature, there are several examples of photoremovable protecting groups which include α-substituted acetophenones[10], benzoins[11], benzyl groups[12], cinnamate esters[7], coumaryl groups[6], and *o*-nitrobenzyl esters and their analogs. Among these, the most popular and widely used is the *o*-nitrobenzyl series. The first report of an *o*-nitrobenzyl group being used as a cage was by Barltrop and coworkers in 1966.[13] Photolysis of *o*-nitrobenzyl benzoate **2** resulted in the formation of 2-nitrosobenzaldehyde (**3**) and the release of benzoic acid (**4**, 17% yield) (**Equation 2**). It was later determined that the poor deprotection yield was the result of the

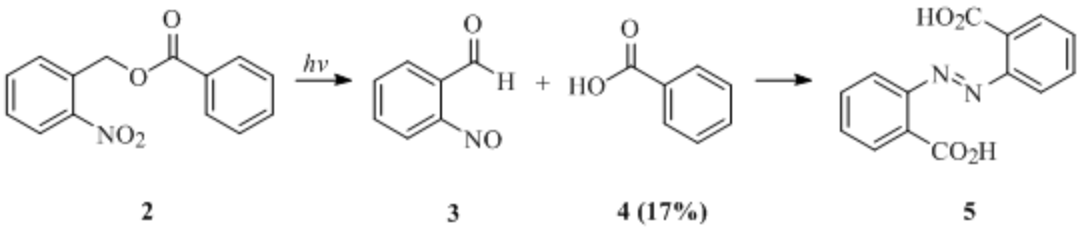

2 **3** **4 (17%)** **5**

Equation 2.

competitive light absorption between the starting material and azobenzene-2,2'-dicarboxylic acid (**5**), which is a secondary photoproduct produced from 2-nitrobenzaldehyde (**3**).[14] Yields were dramatically improved to 75-95% conversion with the use of α-substituted nitrobenzyl esters (**Equation 3**) due to the photoproduct of the chromophore being a less reactive nitroso benzophenone derivative **6**.

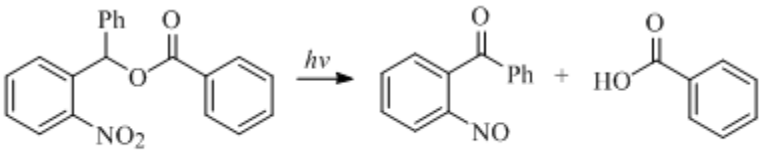

6

Equation 3.

As the status of the *o*-nitrobenzyl chromophore grew, so did the number of biological compounds caged by this chromophore. Investigators applied this chemistry to amino acids, peptides, glycosides, amino sugars, and to nucleotides. The

release of ATP was first published in 1978 by Kaplan and coworkers[3] (**Equation 4**). In their report, ATP was caged as either the corresponding 2-nitrobenzyl (NB) ester

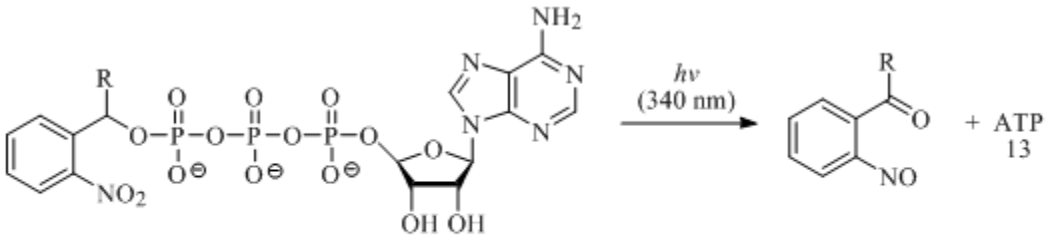

7a R = H,
7b R = Me

Equation 4.

7a or as the 1-(2-nitrophenyl)ethyl (NPE) ester **7b**. Although they are similar in structure, these two cages exhibited very different quantum yields. NPE ester **7b** released 80% of the caged ATP in less than 60 seconds while NB ester **7a** only released 25% of the caged ATP in the same amount of time, indicating a quantum efficiency three times greater than that of NPE. These results suggested that the α-substituted *o*-nitrobenzyl derivatives were better suited to be photoremovable protecting groups than the unsubstituted derivatives.

Kaplan's report also investigated the use of photoremovable protecting groups in a physiological environment. The enzyme responsible for sodium/potassium transportation through cell walls, Na^+,K^+-ATPase, served as a model for exploring the effect of NPE caged ATP **7b** on the Na^+:K^+ transport associated with enzymatic

activity. The enzyme acquires ATP as the energy source through hydrolysis of the terminal γ-phosphate, which can be monitored by the detection of the inorganic phosphate generated from the free ATP consumed by the enzyme. In the absence of light, NPE-ATP **7b** was shown to be resistant to hydrolysis by the enzyme, but upon irradiation the liberated ATP triggered enzyme activity, and inorganic phosphate was released. The successful introduction of *o*-nitrobenzyl caged ATP into physiological media instigated interest in expanding the applications of caged release to a wide variety of biochemical systems. Several mechanistic investigations of photorelease reactions at the molecular level using biologically significant phosphates have since been extensively studied. The list includes the mechanism of release of inorganic phosphate in skeletal muscle[15], the function of cAMP in the relaxation of distal muscle[16], the ATP-induced mechanism of actomyosin in muscle contraction[17], and the activation of antitumor antibiotics to highly reactive pyrrole intermediates responsible for DNA cross linking reactions.[18]

The mechanism of substrate photorelease from the corresponding *o*-nitrobenzyl ester (**Scheme 1**) occurs via an intramolecular redox reaction.[19] Upon

Scheme 1. *o*-Nitrobenzyl Photorelease Mechanism[19]

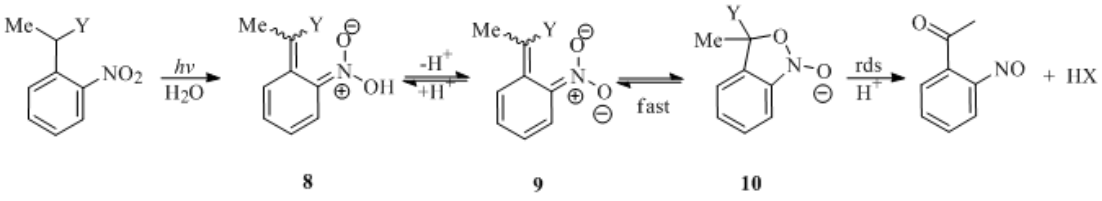

irradiation, the chromophore is excited to its singlet excited state. An intramolecular hydrogen abstraction then occurs to form aci-nitro intermediate **8**, which after deprotonation cyclizes to form isoxazole intermediate **9**. The final step of this mechanism, the rate-determining step for the release of the substrate, is the collapse of intermediate **10**. Several groups have questioned the validity of this mechanism. Ab initio and density functional theory calculations for 2-nitrotoluene and its isomers have predicted a higher energy barrier for the cyclization of **9** to **10** and predict this transformation to be exothermic and essentially irreversible. These findings question the validity of the proposed mechanism (**Scheme 1**) by suggesting that the rate-determining step is cyclization of **9** to **10** instead of substrate release from intermediate **10**. Recent laser flash photolysis (LFP) studies by Wirz and coworkers[19,20] on 1-(methoxymethyl)-2-nitrobenzene (**11**) and 1-(1-methoxyethyl)-2-nitrobenzene led to the observation of three transient intermediates **12**, **13**, and **14** using time resolved infrared spectroscopy. With the observation of these intermediates by Wirz and coworkers, a new mechanism (**Scheme 2**) was proposed. Based upon these findings, it was concluded that photorelease in an aqueous environment proceeds via one of two mechanisms: direct hydrolysis of aci-nitro intermediate **12** (not shown in **Scheme 2**) or isoxazole formation followed by hydrolysis of the intermediate **13**. In buffered solutions, a competing acid catalyzed degradation of aci-nitro intermediate **12** occurs shortening the intermediate lifetime, and the decay of intermediate **14** limits the release of methanol up to pH 8 to 10. The

breakdown of intermediate of type **13** is the limiting step for the release rate of ATP at pH values ≤ 6.

Scheme 2. Revised *o*-Nitrobenzyl Photorelease Mechanism[19,20]

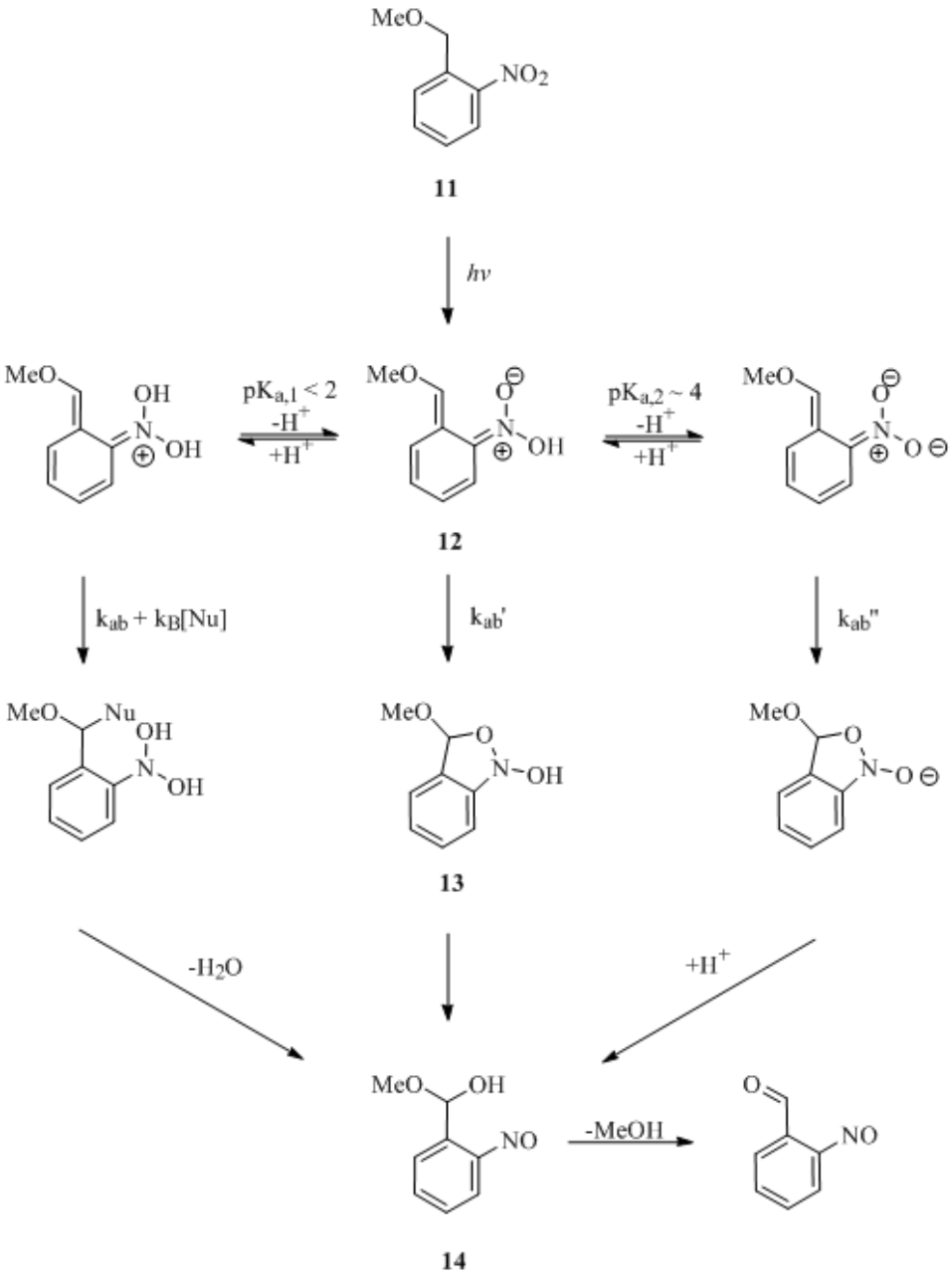

The *o*-nitrobenzyl group has been used in many applications, but this cage suffers from a number of disadvantages. The first disadvantage is that the nitrosoaldehyde or nitrosoketone is a highly absorbing chromophore in the excitation region of the caged substrate. This results in lower quantum efficiencies and in lower conversion for the release process because of the competition for incident radiation between the starting material and the product. Another disadvantage is that these photoproducts are toxic and reactive with nucleophilic components of the surrounding media. This is particularly problematic in biological studies where side reactions with proteins or other substrates can complicate the analyses. It has been shown that substrate release by hydrolysis of the hemiacetal or hemiketal intermediate in the ground state is the rate-determining step in this reaction. The rate of release has been reported by independent researchers[19-21] to be $< 10^3$ s^{-1}. This very slow process severely limits the range of biochemical rates and processes that can be examined with this chromophore. In addition, it has been reported that the aci-nitro intermediate can be trapped by buffer solutions (e.g. acetate and presumably other adventitious nucleophiles) further delaying the release of the substrate.[20] The final disadvantage is that several *o*-nitrobenzyl esters are not stable in biological media, which can oftentimes lead to premature release of the substrate, which may or may not be an issue during the photolysis. These numerous disadvantages would lead to the belief that, based upon the criteria for an ideal photoremovable protecting group, the *o*-nitrobenzyl derivatives are poor cages. However, this cage is the most widely used with the majority of synthetic and biochemical applications employing this

photoremovable protecting group due to its success in a wide variety of applications.[22] Nonetheless, the demand remains for photoremovable protecting groups with faster release rates and a wider range of excitation wavelengths. These demands have driven the design of numerous other photoremovable protecting groups, some of which will be discussed below.

Early studies by Zimmerman[23] on the photosolvolysis of benzyl acetates in 50% aqueous dioxane set the stage for attempts to use 3,5-dimethoxybenzyl acetate (**15**) as a photoremovable protecting group. In general, the photofragmentation reactions of benzyl acetates (**Equation 5**) are primarily singlet processes and occur rapidly ($k > 10^8\ s^{-1}$). It was observed that substituents in the *para* position led to homolytic bond fission and radical derived products while substituents in the *meta* position lead to heterolytic bond fission resulting in an ionic pathway. According to Zimmerman, *meta* and *ortho* activation of the singlet excited state occurs through the approach of the excited and ground state energy surfaces funneling the excited state toward heterolytic cleavage of the benzyl-ester bond. The required course for

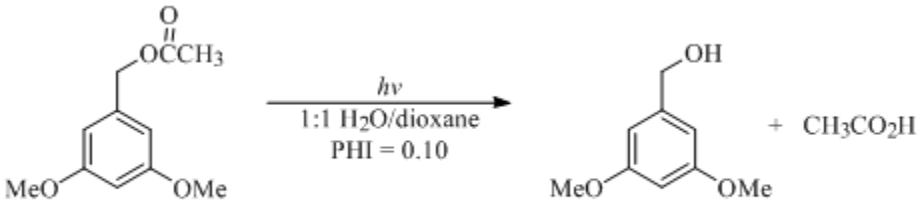

15

Equation 5.

substrate photorelease is the direct heterolytic fission of the substrate-photoremovable protecting group bond. This process avoids the generation of radicals that could result in reactions such as decarboxylation, radical dimerization, or redox processes.

Recent studies by both Zimmerman[24,25] and Pincock[26,27] on the nature of the *meta* effect have raised questions about whether the primary photochemical process is a heterolytic or homolytic bond cleavage. According to Pincock, the mechanistic pathway for most *meta* substituted arylmethyl substrates begins with homolytic cleavage of the benzyl ester bond. This is followed by either electron transfer to give an ion pair or by typical radical ground state reactions (**Scheme 3**).[27] For arylmethyl derivatives with a *meta* electron donating group the electron transfer reaction occurs more rapidly than competing radical processes due to favorable redox properties of the radical pair. Normally, the details of the steps leading to the ion pair would not play a significant role in the outcome of the photorelease process. However, in the case of carboxylate esters, there is a competing pathway between decarbonylation of the initially generated carboxy radical and electron transfer to the ion pair. This process can become significant leading to the destruction of the released substrate. The product determining process for *meta* and especially di-*meta*-substituted arylmethyl chromophores leads to an ion pair, an intermediate arylmethyl carbocation, and the conjugate base of the leaving group, by either mechanism. Thus, the effect of *meta* substitution of the photochemistry of benzyl, naphthyl, and other aromatic chromophores has received attention in an attempt to design the ideal photoremovable protecting group.

Scheme 3. Pincock Benzyl Acetate Photorelease Mechanism[27]

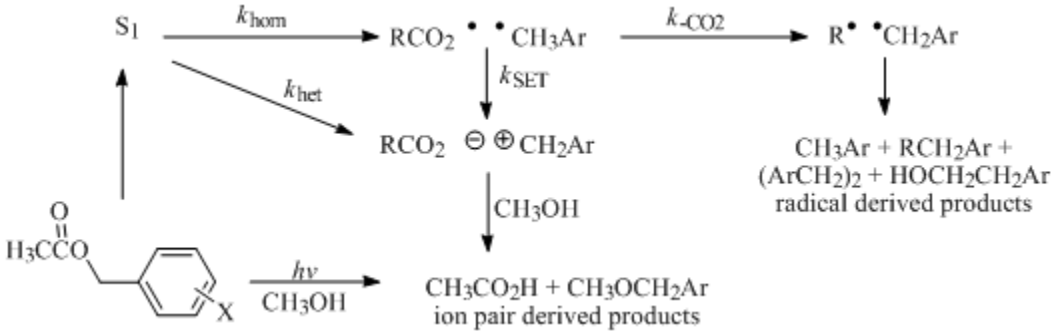

Another arylmethyl analog that has been pursued as a photoremovable protecting group is the coumaryl group. It is an attractive cage because of high yields of fluorescence emission, which is sometimes a useful property for following the course of substrate release processes. One of the earliest studies using coumarin as a photoremovable protecting group was the photorelease of diethyl phosphate from coumarylmethyl diethyl phosphate **16** (**Equation 6**). During the photorelease process,

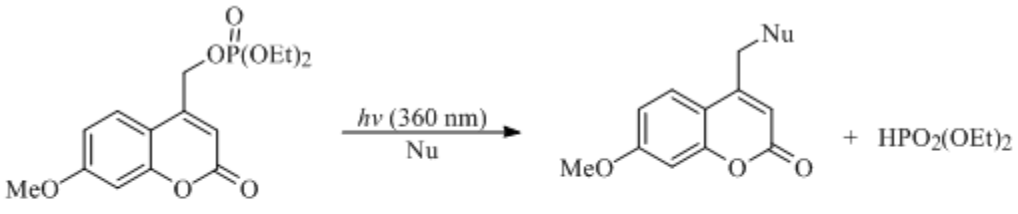

16

Nu = CH_3OH, piperidine, cysteine, tyrosine, alpha-chymotrypsin, HMT

Equation 6.

a coumarylmethyl cation is formed, which reacts with a wide variety of nucleophiles. In addition to phosphates, the coumaryl group has been used to cage several other substrates. These include carboxylates[28], alcohols[29], and cyclic nucleotides[30]. In the literature recent work involving the cyclic nucleotides cAMP and cGMP was reported by Hagen and coworkers[31]. In this case, the chromophore was substituted with carboxyl and amino substituents in order to increase water solubility and to extend the chromophore into the visible region of the spectrum. Photolysis of coumarin caged cAMP or cGMP **17a** in aqueous buffer (**Equation 7**) resulted in the release of the free cyclic phosphate along with hydrolyzed chromophore **18a** in good quantum efficiencies (**Table 1**). The carboxymethoxy groups were more effective in enhancing the water solubility of caged compounds **17b** and **17c** but their quantum efficiencies were not as high as the less water soluble **17a**, which also exhibited the most red shifted absorption maximum in the series. This series shows the versatility of the coumarin group so that it can be applied and used to cage a wide range of substrates.

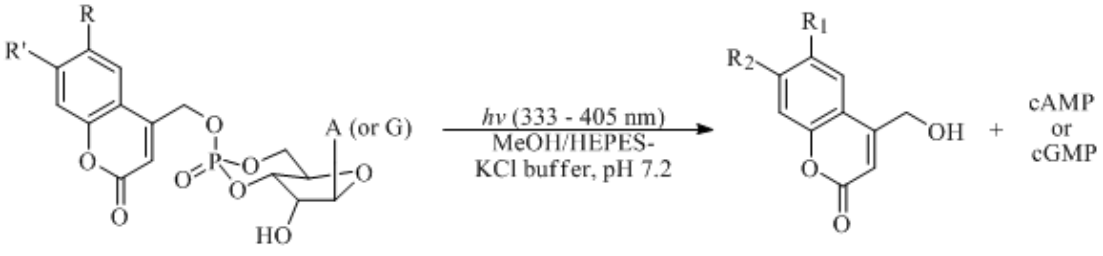

17a R = H, R' = Et_2N
17b R = H, R' = OCH_2CO_2H
17c R = R' = OCH_2CO_2H

18a R = H, R' = Et_2N

Equation 7.

Table 1. Efficiencies and Excitation Wavelengths for cAMP and cGMP Coumaryl Esters[31]

Coumaryl Derivative	Solvent	Φ_{dis_cAMP}	Φ_{dis_cGMP}	λ_{max} (nm)
17a	80:20 HEPES-KCl buffer/MeOH	0.21	0.25	402
17b	HEPES-KCl buffer, pH 7.2	0.12	0.16	326
17c	HEPES-KCl buffer, pH 7.4	0.1	0.14	346

The use of laser flash photolysis (LFP) aided Bendig and coworkers in their kinetic[32] and mechanistic[33] studies of coumarin-4-ylmethyl esters. The proposed mechanism of photorelease (**Scheme 4**) involves excitation of the coumaryl chromophore to its singlet-excited state (SES) **19**. Deactivation of SES **19** occurs by fluorescence (k_{fl} = 1.01 ± 0.08 x 10^8 s^{-1}) and non-radiative decay (k_{nr} = 0.76 ± 0.06 x 10^8 s^{-1}) which compete with heterolytic bond cleavage that form the singlet ion pair **20** with rate constant (k_1 = 2.0 x 10^{10} s^{-1}) as the initial reaction step. Recombination of ion pair **20** leads back to the ground state ester **21** (k_{rec}). Product formation is proposed to happen in two steps[28,34]: escape from the solvent cage affords first the solvent separated ions **22** and **23**; then coumarin-4-ylmethyl cation **22** reacts with water and undergoes a very fast deprotonation to yield product alcohol **24** and H^+. The respective first order and pseudo-first order rate constants are k_{esc} and k_{hyd}. Since no distinction was made between these two reactions they were denoted k_2.

Scheme 4. Coumarin Photorelease Mechanism[33]

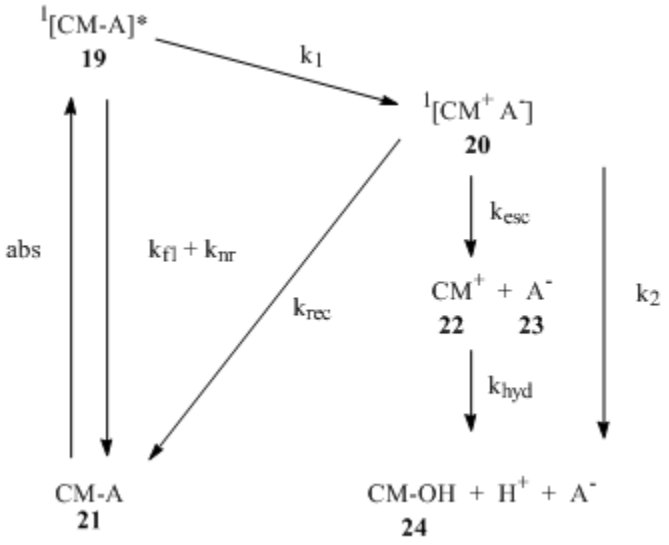

In their most recent publication, Bendig and coworkers[33] reported their results into an investigation as to how the molecular properties of alcohol and acidic moieties influence the rate and efficiency of photorelease (**Equations 8 and 9, Tables 2 and 3**). From these data, a linear free energy relationship (LFER) was derived (**Figure 1**) comparing the log k_2 (rate of substrate release) versus the pK_a of the substrate/leaving group, a Brønsted β_{LG} relationship. The straight line (slope = -0.35) is the result of a linear least squares fit of all of the data and demonstrates that as the pK_a of the leaving group decreases both the rate of the initial reaction and the efficiency of product formation increase.

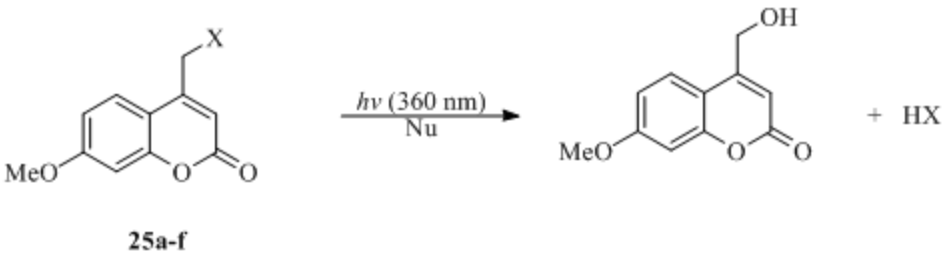

25a-f

Equation 8.

Table 2. Photophysical and Photochemical Data for (7-Methoxycoumarin-4-yl)methyl Esters in 30:70 (vol/vol) CH_3CN/H_2O-HEPES (pH 7.2)[33]

Caged Compound	HX	pK_a LG	Φ_{fl}^C	Φ_{ch}^C	Φ_1	k_1 (10^9 s^{-1})	τ_C (ns)
25a	HSO_3Me	-1.54	0.007	0.081	0.99	52	0.02
25b	$HPO_2(OEt)_2$	0.71	0.052	0.037	0.9	6.6	0.14
25c	$HCO_2C_6H_4$-pCN	3.54	0.08	0.0064	0.85	4.0	0.21
25d	$HCO_2C_6H_5$	3.99	0.43	0.0052	0.20	0.18	1.1
25e	$HCO_2C_6H_4$-pOMe	4.41	0.42	0.0045	0.22	0.20	1.1
25f	$HCO_2(CH_2)_5CH_3$	4.89	0.37	0.0043	0.31	0.32	0.98

Φ_{fl}^C = Fluorescence quantum efficiency; Φ_{ch}^C = Photochemical quantum efficiency; Φ_1 = Quantum efficiency for ion pair formation; k_1 = Rate of intersystem crossing; τ_C = Fluorescence lifetime

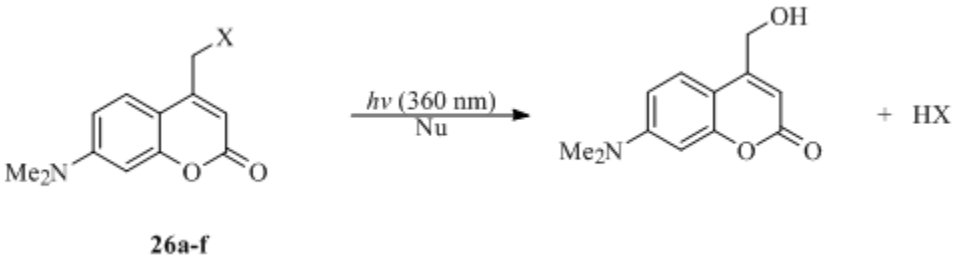

26a-f

Equation 9.

Table 3. Photophysical and Photochemical Data for (Coumarin-4-yl)methyl Esters in CH_3CN/H_2O-HEPES Buffer Mixtures at Various Concentrations[a-c] (pH 7.2)[33]

Caged Compound	HX	pK_a LG	Φ_{fl}^{C}	Φ_{ch}^{C}	Φ_1	k_1 (10^9 s^{-1})	τ_C (ns)
26a	HSO_3Me	-1.54	0.002[b,e]	0.79[b,f]	0.98[f]	56[g]	0.2[g]
26b	$HPO_2(OEt)_2$	0.71	0.006[a,e]	0.36[a,f]	0.95[f]	18[g]	0.05[g]
26c	HSO_3	1.92	0.011[a,c]	0.46[c,f]	0.92[f]	9.5[g]	0.10[g]
26d	GTP	6.5	0.12[a,f]	0.05[c,e]	0.08[k]	0.07[k]	1.06[h]
26e	$HPO_3(OEt)$	6.62	0.10[a,f]	0.03[c,h]	0.23[g]	0.26[k]	0.88[h]
26f	H_2PO_4	7.21	0.14[a,f]	0.03[c,h]		- 0.06[m]	1.23[h]

[a-c]CH_3CN/H_2O (vol/vol): a, 5:95; b, 20:80; c 0:100. [d](ax). [e-h]Average uncertainties: e, ± 15%; f, ± 10%; g, ± 30%; h, ± 20%. [i]Single-pulse experiment. [j]Limit of accuracy. [k]Factor of 2. [l]Factor of 6. [m]Meaningless negative value of k_1 is cause by the fact that $\Phi_{fl}^{C} > \Phi_{fl}^{OH}$. $\Phi_{fl}^{C} - \Phi_{fl}^{OH}$ = in the mutual error limits of Φ_{fl}^{C} and Φ_{fl}^{OH} (5%).

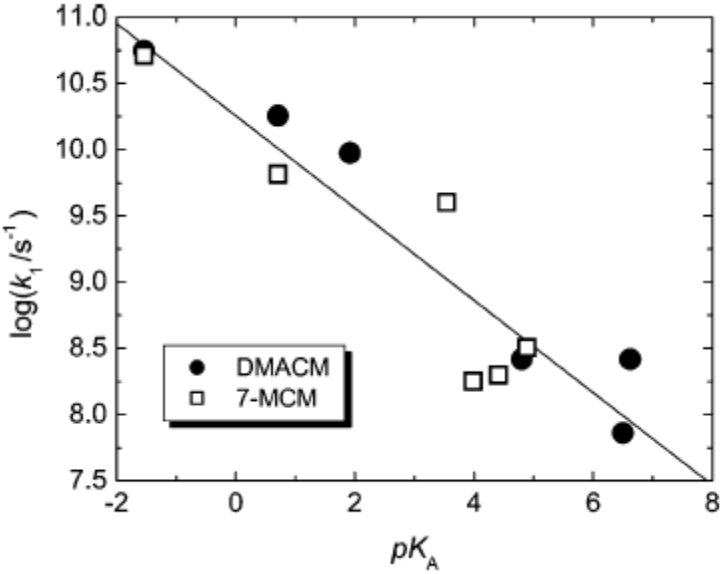

Figure 1. Linear free energy relationship between log(k_1) and the pK_a values of the acids released during photolysis of DMACM **25a-f** and 7-MCM **26a-f** esters in CH_3CN/HEPES. The straight line with slope = -0.35 and intercept = 10.26 results from a linear fit to the respective data. (Reprinted with permission from Reference 33. Copyright 2007 American Chemical Society.)

Sheehan and Wilson were the first to investigate the photochemical rearrangement of benzoin derivatives[11] and then to explore the possibility of using this chromophore as a photoremovable protecting group[35]. When irradiated, the strongly absorbing benzoin group **27a** rearranges to 2-phenylbenzofuran (**28a**) with concurrent release of the substrate (**Equation 10**). It was suggested that benzoin chromophore, especially the 3',5'-dimethoxybenzoin chromophore **27b** could serve as a photoremovable protecting group for carboxylic acids. In 1984, Givens and coworkers[36] demonstrated the quantitative expulsion of phosphates from the ungarnished benzoin cage (**Equation 11**).[37,38] The benzoin diethyl phosphate, isopropyl phosphate, and phosphate derivatives were examined in detail and the results extended the range of applications and the nature of the parent chromophore. In these photochemical reactions, the only major product accompanying the released phosphate was 2-phenylbenzofuran (**28a**). These reactions were quenched with either naphthalene, piperylene, or, for the aqueous studies, sodium 2-naphthalenesulfonate. All three of these compounds are well-known triplet quenchers; this established the short-lived triplet (3 – 14 ns) as the reactive excited state for benzoin.

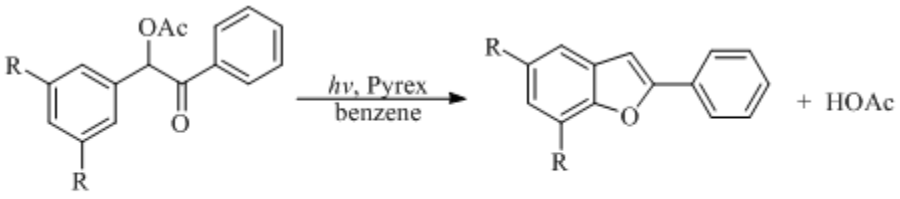

27a R = H
27b R = OCH_3

28a R = H
28b R = OCH_3

Equation 10.

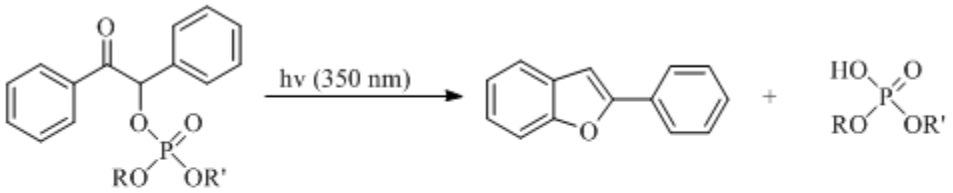

29a R = R' = Et
29b R = ^{i}Pr, R' = $^{+}$Na or $^{+}$H
29c R = R' = $^{+}$Na or $^{+}$H

28a

Equation 11.

Further information was revealed from Stern-Volmer quenching analyses utilizing nanosecond LFP.[39] From these data, the release of phosphate (Φ_{dis} = 0.28 – 0.38) for this reaction (**Table 4**) was determined. The multiplicity assignment was supported by phosphorescence spectra, which also established the triplet energy (73 ± 1 kcal/mol). The triplet-triplet absorption of diethyl benzoin phosphate **29a**, which was quenched by naphthalene, gave good Stern-Volmer values (τ^3 = 24 ± 2 ns) in

Table 4. Quantum Efficiencies for Benzoin Phosphate Esters[37,38]

Phosphate Ester	Solvent	pH	Φ_{dis}	Φ_{furan}	$\Phi_{phosphate}$
29a	C_6H_6	nd	0.28	0.26	nd
29b	H_2O/CH_3CN	2	0.37	0.20	0.12
29b	H_2O/CH_3CN	7	nd	0.07	0.013
29c	H_2O/CH_3CN	2	0.38	0.14	0.15
29c	H_2O/CH_3CN	7	nd	0.08	0.01

All reactions were run in 60% aqueous acetonitrile, except **30a** as indicated.
Phosphate esters were irradiated at 350 nm and monitored with ^{31}P NMR.
nd = not determined.

trifluoroethanol.[39] The efficiencies for the disappearance of caged phosphates as well as the appearance of 2-phenylbenzofuran (**28a**) and the phosphate were determined to be pH dependent with higher efficiencies reported under acidic conditions. The greater efficiency at the lower pH suggests that the protonated phosphate is a more favorable leaving group than its conjugate base.

This study was extended to nucleotide release from the benzoin cage through the synthesis and photolysis of benzoin cAMP **30** (**Equation 12**). The efficient release of cAMP (**31**) as the exclusive product with quantum efficiencies on the same order of magnitude as the model phosphate esters first demonstrated the application of benzoin as a cage for nucleotides (**Table 5**). ^{31}P spectra of the photolyzed sample demonstrated that cAMP was the only phosphate present after release. As **Table 5** indicates, the quantum efficiencies remained relatively constant throughout the pH range examined, following the anticipated pH independence for the release process of the phosphate triester.

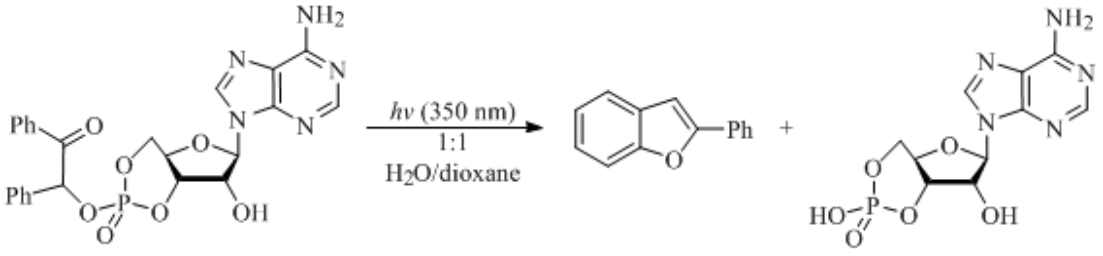

30 **28a** **31**

Equation 12.

Table 5. Quantum Efficiencies for Photolysis of Benzoin Cyclic Adenosine 3',5'-Monophosphate **30**[37]

Aqueous buffer	pH	Φ_{dis}	Φ_{furan}	Φ_{cAMP}
Tris (D_2O)	7.3	0.39	0.19	0.34
Tris (H_2O)	7.3	0.37	0.17	0.34
Phosphate (D_2O)	8.4	nd	0.17	nd
Phosphate (H_2O)	8.4	nd	0.17	nd
Perchloric (D_2O)	1.6	0.40	0.16	0.36

Irradiations were carried out in 1:1 buffer/1,4-dioxane at 350 nm. Quantum efficiencies were measured using ^{31}P NMR except were indicated (nd).

Sheehan, Wilson, and Oxford[35] determined that carboxylate derivatives were released more readily when electron donating groups were present at the *meta* and *meta'* positions of the benzyl ring. The absorption spectra of the benzoin esters along with the observations that cyclization was enhanced by *meta* electron donating groups led observers to believe that the reaction was taking place through an n,π* singlet (**Scheme 5**). The authors suggested that excitation of the phenacyl group would be followed by attachment of the electrophilic carbonyl oxygen on the distal aromatic ring, forming ground state oxetane **32** by way of a biradical intermediate. The electron donating methoxy group would then facilitate the ring opening and concurrent release of the carboxylate. Re-aromatization via loss of a proton would provide benzofuran **28b**. The inability to quench the reactions with high concentrations of piperylene suggests that the reaction originated from the singlet-excited state or from a very short lived, unquenchable triplet.

Scheme 5. Benzoin Photorelease Mechanism[35]

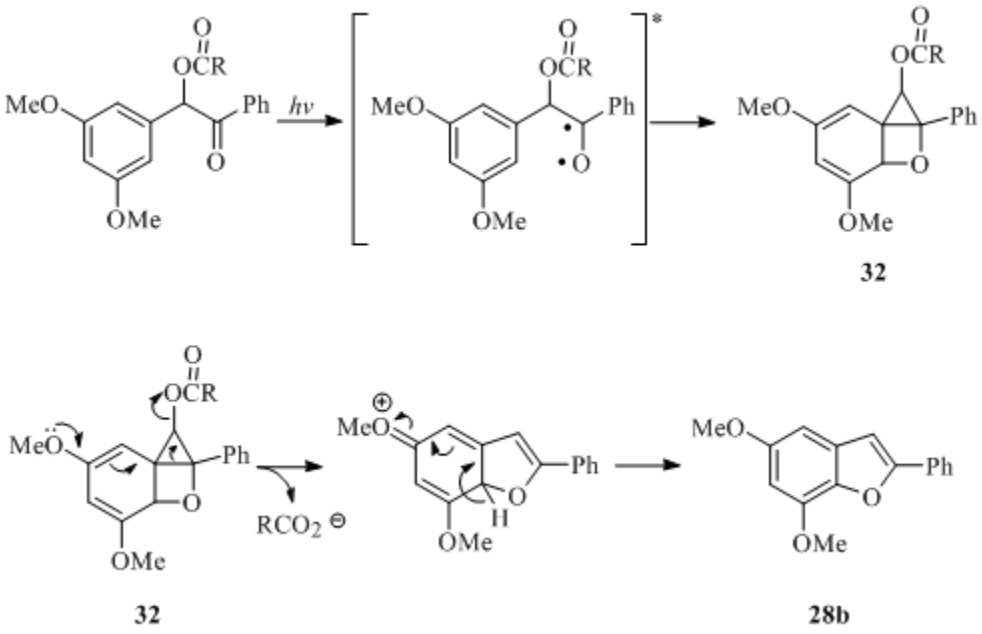

Recent LFP analysis performed by Wirz and coworkers[40] led to the proposal of a new reaction pathway for substrate release from benzoin caged derivatives (**Scheme 6**). Transient spectra from two species were obtained at delays of around 50 ps with respect to the laser pump pulse; one with bands at 330 and 420 nm and a second with a strong maximum at 355 nm. The first species was identified as the triplet state of the chromophore. The decay of the latter ($\tau \approx 2$ ns) was accompanied by the growth of a broad band in the visible region ($\lambda_{max} = 480$ nm). This species has been assigned as cyclic cation **33**. These observations support the earlier assignments of a triplet excited state and cation **33** but require that cation **33** not be the primary photoproduct. The species with $\lambda_{max} = 355$ nm was tentatively identified, and later

confirmed, as biradical **34**. This biradical had been previously proposed by Rock and Chan[41] as the primary photoproduct in their mechanistic investigation. During this investigation, several solvent addition products were observed. It is possible that benzofuran **28b** can be formed through this pathway from addition product **35**.

Scheme 6. Revised Benzoin Photorelease Mechanism[40]

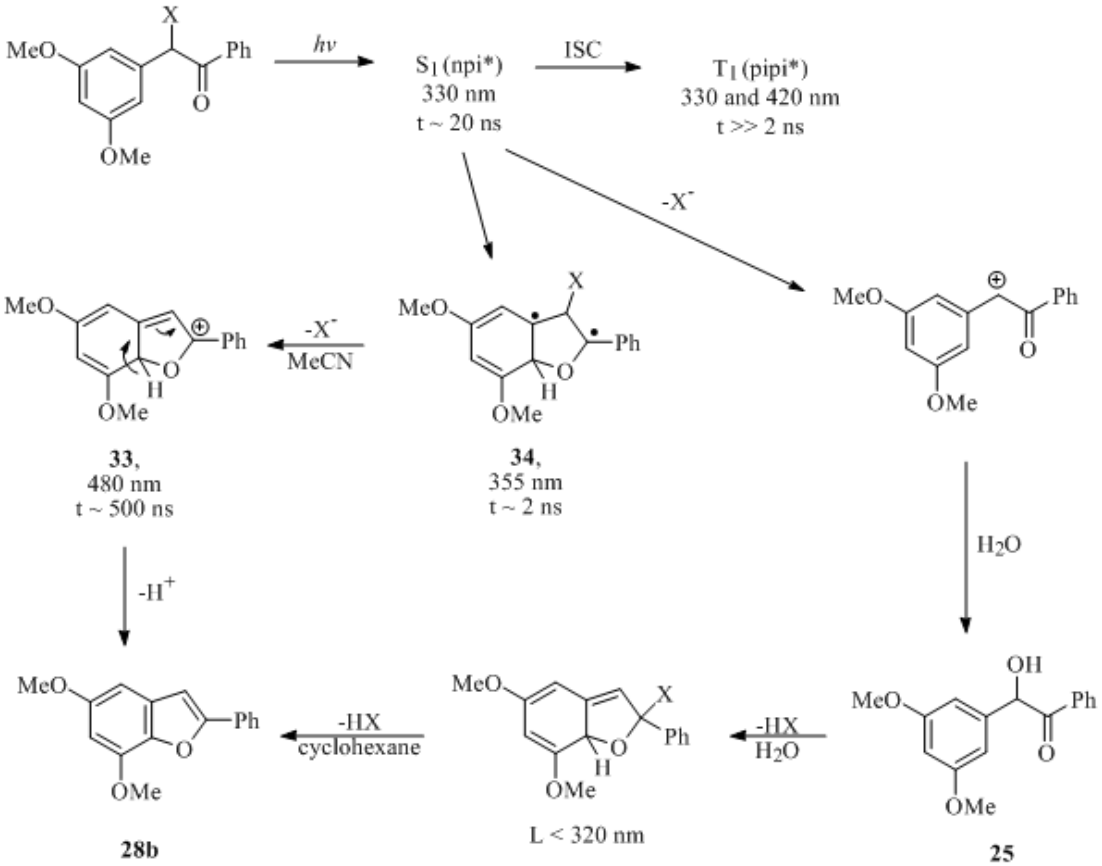

Based on these observations, Corrie and Trentham[42] re-examined the photochemistry of several substituted benzoin phosphates. They found that the 3',5'-

dimethoxybenzoin cage was best suited among those investigated for the release of inorganic phosphate. The formation of 3',5'-dimethoxy-2-phenylbenzofuran (**28b**) occurred at a rate that exceeded 10^5 s^{-1} and with a quantum efficiency of 0.78. While the rate of product formation was lower than that reported by Givens and Matuszewski[36], the efficiency for the substituted benzofuran analog was much higher, reflecting the effect of the different substituents (methoxy or hydrogen) in reaction environment and monitoring protocols for this very fast and efficient photorelease process. The fast release and high quantum efficiencies for benzoin caged substrates have significant advantages over the *o*-nitrobenzyl group but do have limitations of their own. The primary photoproduct of the protecting group, such as benzofuran **28**, is strongly absorbing and can compete with the caged compound for light. This product can also react to form photodimers that are insoluble in aqueous media along with several other products upon subsequent irradiation. In addition, the presence of a stereocenter alpha to the carbonyl causes problems with isolation and purification in the synthesis of benzoin-protected chiral compounds. Again, this photoremovable protecting group does not contain all of the characteristics to make it ideal but has disadvantages that can be worked around when applied in chemistry or biology.

With the success of the benzoin cage as a photoremovable protecting group, a simplified version of this chromophore, *p*-methoxyphenacyl, was employed by Sheehan and Umezawa[8] for the release of benzoic acid (**4**), several amino acids, and peptides (**Equation 13, Table 6**). It was noted that the phenacyl group's low-lying excited state, from the conjugation between the carbonyl group and the phenyl ring,

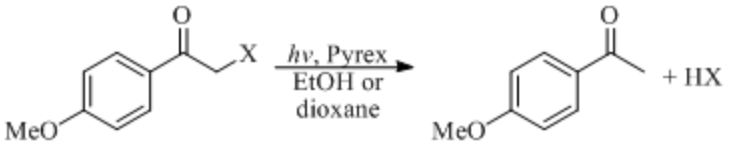

36a-j **37**

Equation 13.

Table 6. Yields for the Release of Acids from 4-Methoxyphenacyl Esters[8]

Caged Compound	HX	Solvent	Yield of ROOH (%)
36a	PhCOOH 4	Dioxane	81
36a	PhCOOH 4	Ethanol	96
36b	Boc-L-Ala	Dioxane	82
36b	Boc-L-Ala	Ethanol	93
36c	Boc-Gly	Ethanol	94
36d	Boc-L-Phe	Dioxane	89
36e	Z-D, L-Ala	Dioxane	84
36f	Phthaloyl-Gly	Dioxane	80
36g	Tri-Gly	Dioxane	58
36h	Z-L-Trp	Ethanol	33
36i	Z-Gly-Gly	Ethanol	77
36j	Z-L-Asp(OBz)-L-Ser	Dioxane	49

All reactions were carried out below rt at 5 x 10^{-3} – 10^{-2} M using a Pyrex filter.
Irradiations were complete in 6 h in ethanol and 11 – 17 h in dioxane.
Yields were determined from product isolation following photolysis.

made the phenacyl group a potential candidate for useful photoremovable protecting group applications for other carbonyl moieties. The proposed mechanism (**Scheme 7**) involved homolytic bond cleavage of the chromophore-substrate carbon-oxygen bond to form two radicals. The phenacyl radical abstracted a hydrogen (probably from ethanol) to form *p*-methoxyacetophenone (**37**) and the free acid. When this reaction

was run in the presence of 1 M benzophenone (E_T = 68 kcal/mol) or naphthalene (E_T = 62 kcal/mol) the reaction was completely quenched indicating a triplet reaction pathway.

Scheme 7. Photorelease from *p*-Methoxyphenacyl Esters[8]

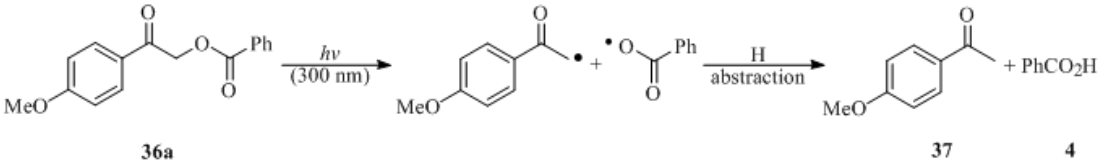

36a **37** **4**

Epstein and Garrossian[43] reported the release of ethyl and phenyl phosphates from the corresponding p-methoxyphenacyl phosphate esters. The reactions were performed in dioxane with high yields (ethyl: 74%, methyl: 86%) reported for the release of the two phosphates. This contrasts with reports by Anderson and Reese[44] for substituted α-chloroacetophenones (*vide infra*). They reported that the carbonyl stretching frequencies at 1678 cm^{-1} and 1690 cm^{-1} had been replaced with two strong bands at 1670 cm^{-1} and 1725 cm^{-1} during photolysis of *p*-methoxyphenacyl diethyl phosphate **38** in a 1% ethanol solution. Separation and isolation of the products revealed two new major photoproducts: rearrangement photoproduct **39** and reduction photoproduct **40** (**Equation 14**). The authors proposed that the rearranged ester resulted from spiro-intermediate **41**, following a Favorskii-like rearrangement reaction. The rationale for the discrepancy advanced by Epstein was an altered mechanism due to a change in the solvent. The solvent, 1,4-dioxane, may not be

sufficiently polar to support the formation of the zwitterionic precursor to the Favorskii-like rearrangement that was proposed by Anderson and Reese (*vide infra*). Reinvestigation of the photolytic cleavage using polar solvents would be necessary to support or disprove that statement.

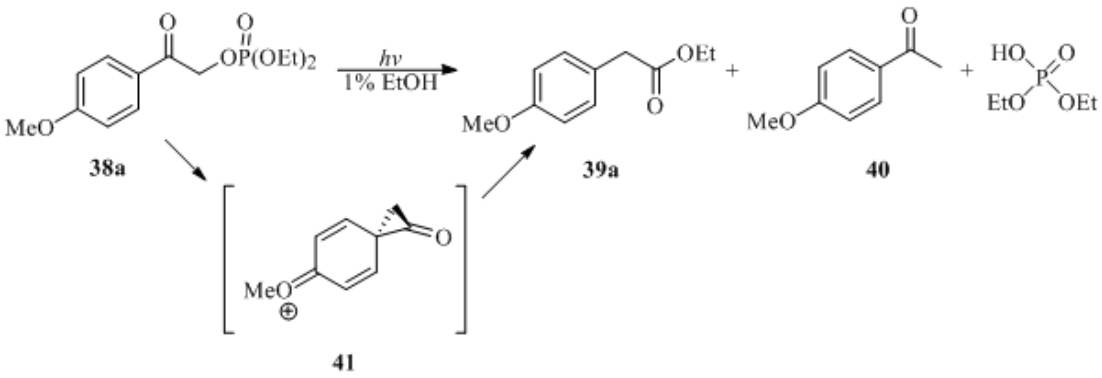

Equation 14.

Givens and coworkers[38] examined the photorelease of phosphate esters using *tert*-butanol and methanol as solvents; the former being a poor hydrogen atom donor and both having increased polarity compared with 1,4-dioxane (**Equation 15**). The

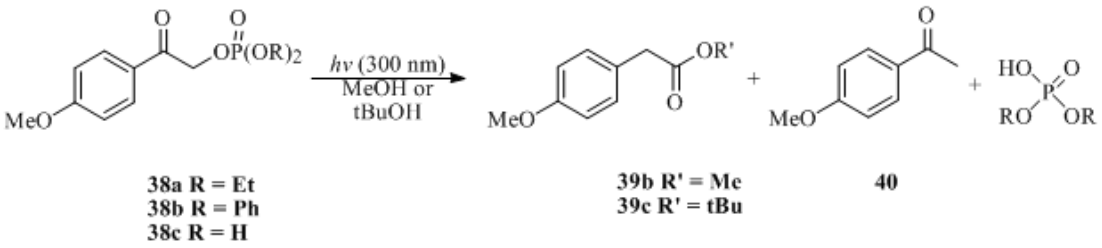

Equation 15.

results correlated well with those of Anderson and Reese in that the major photoproduct was rearranged ester **39b-c** and not photoreduction product **40**. The amount of photoreduction product **40** was decreased to 21% in methanol and to 14% in *tert*-butanol. Further investigation of the solvent dependency for the release of phosphates revealed a solvent isotope effect with deuterated versus protiated methanol as the solvent (**Table 7**). The formation of *p*-methoxyacetophenone was suppressed by a factor of five when the photolysis was carried out in CD_3OD compared with CH_3OD or CH_3OH. This observation suggests that the rate-determining step in the photoreduction process is hydrogen abstraction. This mechanistic pathway, which was first described by Sheehan, was discussed earlier.

Table 7. Quantum Efficiencies and Solvent Isotope Effects (k_H/k_D) for Photolysis of 4-Methoxyphenacyl Diethyl Phosphate **38a**[38]

Solvent	Φ_{dis}	Φ_{rear}	k_H/k_D	Φ_{red}	k_H/k_D
C_6H_6, ^{t}BuOH (3:1)	0.036	0.026	-	0.074	-
CH_3OH	0.42	0.2	-	0.07	-
CD_3OD	-	0.14	1.4	0.013	5.4
CH_3OD	-	0.11	1.8	0.053	1.3

Irradiations were performed in the indicated solvent at 300 nm. k_H/k_D is a relative efficiency for H vs. D abstraction. Error limits are ± 10%.

Solvent comparisons by Dhavale and coworkers[45] did indeed show that the ratio of rearrangement product to reduction product is solvent-dependent (**Equation 16, Table 8**). The authors reported that irradiation of starting material **42** in methanol results in more photoreduction product **43** whereas in aqueous acetonitrile

rearrangement to the phenylacetate esters **44** and **45** becomes the major pathway. For a given solvent, the ratio of rearrangement product to reduction product increases

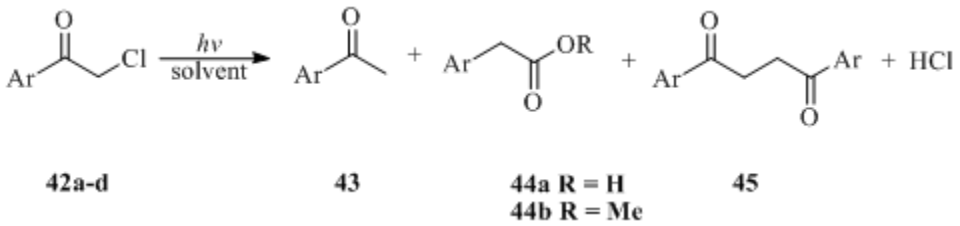

42a-d **43** **44a R = H** **44b R = Me** **45**

Equation 16.

Table 8. Photolysis of α-Chloroacetophenones 42a-d: Yields Obtained for Photoproducts under Various Conditions[45]

		Methanol		Acetone$_{(aq)}$			Acetonitrile$_{(aq)}$		
	Ar	43	44	43	44	45	43	44	45
42a	phenyl	60	0	29	24	37	18	47	14
42b	4-methyl-phenyl	62	6	23	47	24	11	70	14
42c	4-methoxy-phenyl	35	34	14	43	16	8	54	9
42d	4-chloro-phenyl	60	0	31	14	10	18	35	6

Photolysis of 2% degassed solution of **42a-d** in methanol, 95:5 acetone/water, or 95:5 acetonitrile water using 300 nm lamps was carried out in the presence of propylene oxide as an HCl scavenger. Irradiations were 4 h and yields are isolated products.

with the electron donating power of the substituent. Dhavale's proposed mechanism for chloride loss and subsequent rearrangement begins with homolytic cleavage of the CH_2-Cl bond to form an ion pair (**Scheme 8**). Electron transfer from the α-ketoradical to the chlorine atom leads to ion pair **46**. The ion pair is more susceptible to Favorskii-like rearrangement in polar solvents, and therefore the rearranged

phenylacetic acid (**44**) is favored in polar, protic solvents. Hydrogen atom abstraction, leading to **42**, prevails in good hydrogen atom donating solvents.

Scheme 8. Dhavale Mechanism[45]

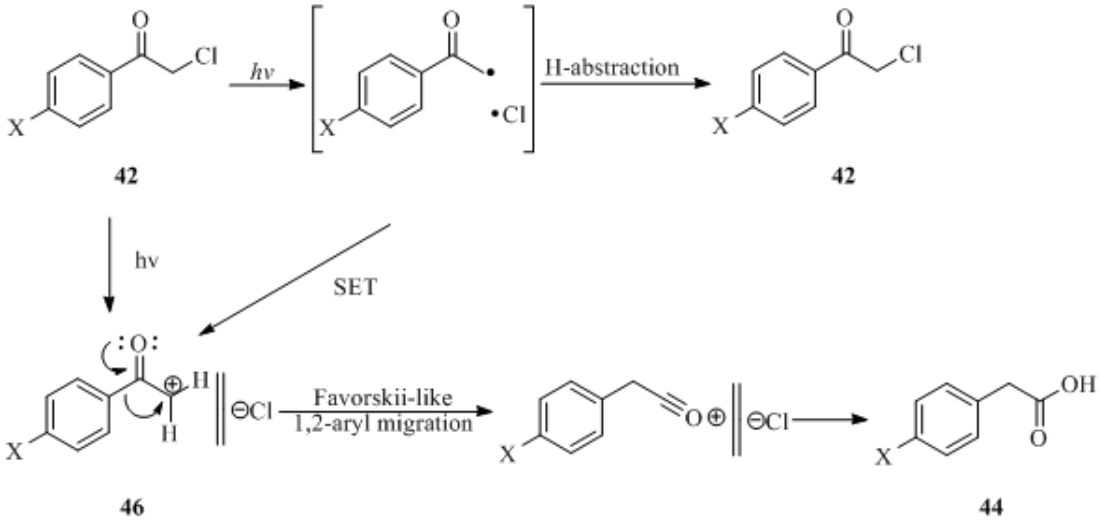

Investigation into the effects of the substituents on the ring by Anderson and Reese[44] led to the observation that electron donating groups in the *ortho* and *para* positions were necessary for rearrangement to occur (**Table 9**). Sonawane and coworkers[46] investigated the photorearrangement of several *para* substituted

Table 9. Product Formation from Photolysis of Substituted Phenacyl Chlorides[44]

Caged Compound	Aryl Substitution, X	**45** (%)	**46** (%)
42e	*p*-OH	32	26
42f	*p*-OMe	32	30
42g	*o*-OH	-	3
42h	*o*-OMe	32	16
42i	*p*-Me	4	58
42j	H	-	53
42k	*p*-CO_2Me	-	48
42l	*p*-Cl	-	55
42m	*o*-Cl	-	45
42n	*m*-OMe	-	15

Photolyses were carried out in 1% alcoholic solutions using a 500W Hanovia mercury lamp. Reactions were carried out for 1 – 2 h. Products were isolated via GLC.

propiophenones as a convenient entry in the synthesis of substituted α-arylpropionic acids (**Equation 17**) and observed that *para* substitution promoted rearrangement in almost every case (**Table 10**). Phenyl and chloro substitution in the *para* position were the only cited examples where rearrangement did not dominate in methanol. These cases also showed significant reduced and hydrolyzed products. While the chlorine atom has lone pairs of electrons to donate into the aromatic ring, like *p*-methoxy, chlorine is formally treated as an electron withdrawing group because of its inductive effect. Instead, chlorine exerts its influence on the aromatic ring by inductive and field effects by polarizing the σ-electrons toward chlorine. By this rationale, para chlorine effectively reduces the amount of rearranged product formed.

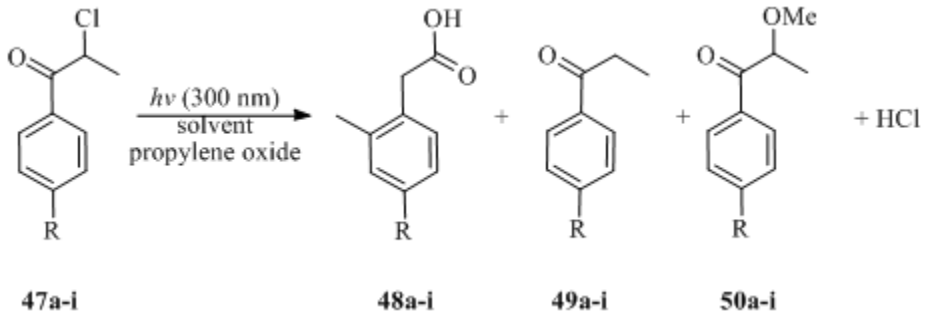

47a-i **48a-i** **49a-i** **50a-i**

Equation 17.

Table 10. Product Distribution from Photolysis of **47a-i** in Aqueous Acetone or Aqueous Methanol[46]

	Substrate	Acetone$_{(aq)}$			Methanol$_{(aq)}$		
47	R	**48**	**49**	**50**	**48**	**49**	**50**
a	H	58	25	-	39	30	-
b	CH_3	84	5	-	76	8	-
c	C_2H_5	82	6	-	74	9	-
d	*n*-C_3H_7	84	5	-	77	9	-
e	*i*-C_4H_9	74	10	-	65	15	-
f	*t*-C_4H_9	78	7	-	69	8	-
g	Cl	45	25	20	30	51	30
h	Ph	40	25	35	18	26	35
i	OCH_3	32	10	50	80	12	70

Irradiations were carried out in 95:5 solvent/water solutions employing a Hanovia 200W medium pressure mercury vapor lamp with a Pyrex filter until the disappearance of starting material. The photoreaction was monitored and yields were determined with GLC and ^{1}H NMR.

Promotion of the rearranged product is realized more efficiently through the use of electron donating substituents with lone pair electrons in the *para* position. Givens and Park[47] investigated the role and efficiency of several phenacyl derivatives **51** possessing other nitrogen and oxygen based electron donating groups as substituents in the *meta* and *para* positions (**Equation 18**). Phosphate derivatives

served as leaving groups since they previously had been established as good nucleofuges. Only the *para* alkoxy and hydroxy derivatives gave the rearranged photoproduct under the photolysis conditions explored (**Table 11**). The three *p*-amino derivatives yielded only the corresponding acetophenones, despite their superior resonance electron donation capabilities. The unsubstituted and *m*-methoxy derivatives gave complex mixtures of dimers and reduction products. Of all substituents examined, Park[47] found that the most versatile derivative was the *p*-hydroxyphenacyl group. Rearrangement of the *p*-hydroxyphenacyl derivative to *p*-hydroxyphenylacetic acid (**52a**) in aqueous media occurred efficiently and virtually free of byproducts. This result coupled with the results of Anderson and Reese[44] sparked interest in developing *p*-hydroxyphenacyl as a photoremovable protecting group.

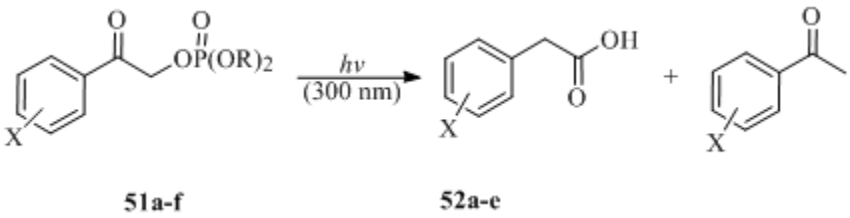

51a-f **52a-e**

Equation 18.

Table 11. Disappearance and Product Efficiencies for Aryl-Substituted Phenacyl Phosphates **51a-f** in TRIS Buffer (pH 7.2) at 300 nm[47]

Aryl Substituent (X)	R	Φ_{dis}	Φ_{rear}	Φ_{red}	Φ_{other}
p-OH	Et	0.77	0.33	0.05	-
p-OMe	Et	0.42	0.20	0.07	-
p-OH	NH_4^+	0.38	0.12	0	-
p-NH_2	NH_4^+	< 0.05	-	< 0.05	-
p-$NHCOCH_3$	NH_4^+	0.38	-	0.11	dimers
p-$NHOCOCH_3$	NH_4^+	0.34	-	-	2 unknown

Solvent was methanol and phosphate or diethyl phosphate were the leaving groups. The diammonium salt of the mono ester; 10% acetonitrile was added to the solvent. dis = disappearance, rear = rearrangement, and red = reduction.

The *p*-hydroxyphenacyl group has several features that make it an attractive photoremovable protecting group. It was rationalized by Givens and coworkers[47,48] that the introduction of the phenolic hydroxy group would enhance the aqueous solubility of this chromophore. The absence of the attendant α aryl moiety that is present in benzoin caged substrates alleviated the stereogenic center problem mentioned earlier. Furthermore, the reported Favorskii-like rearrangement of the chromophore from *p*-hydroxyphenacyl to *p*-hydroxyphenylacetate leads to a significant hypsochromatic shift in the chromophore. This alleviates the problem of incident light competition between the starting material and the photoproduct. Finally, the attachment of the substrate to a primary α-keto methylene group stabilizes the derivative against ground state hydrolysis for almost all of the derivatives. Only direct nucleophilic substitution or ester hydrolysis appears to affect the stability of the caged compounds. The initial discovery that photolysis of diethyl *p*-hydroxyphenacyl (pHP)

phosphate **51a** exclusively followed a rearrangement pathway in aqueous buffer or water was followed by the study of pHP caged ATP **55**.[49] Protection of a substrate with a pHP group was facilitated through a direct displacement of bromide from 2-bromo-4'-hydroxyacetophenone (**53**) (**Scheme 9**). The synthesis of pHP ATP required the coupling of ADP to pHP mono-phosphate **51c**. In addition, prior steps required the protection of the ketone against hydrogenolysis of the benzyl groups in phosphate triester **54**. Irradiation of pHP ATP **55** at 300 nm released ATP **56** and *p*-hydroxyphenylacetic acid (**52a**) with a quantum efficiency of 0.37 ± 0.01 and a rate constant of $6.9 \pm 1.2 \times 10^8\ s^{-1}$ (**Equation 19**). The solvolytic stability was tested and this compound was found to be completely stable in D_2O for 100 hours. HPLC and NMR studies showed that the protected phosphate ester had not degraded or hydrolyzed under such conditions.

Scheme 9. Synthesis of pHP ATP **55**[49]

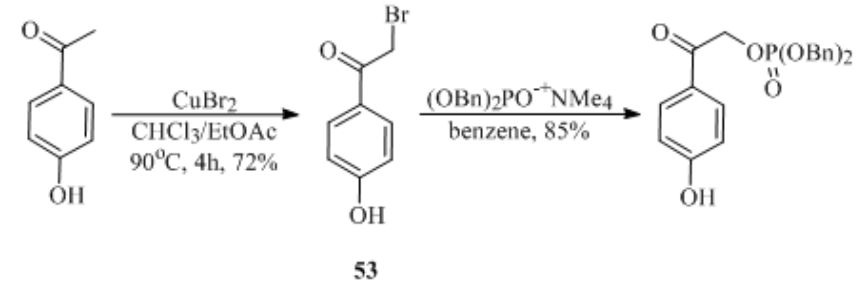

53

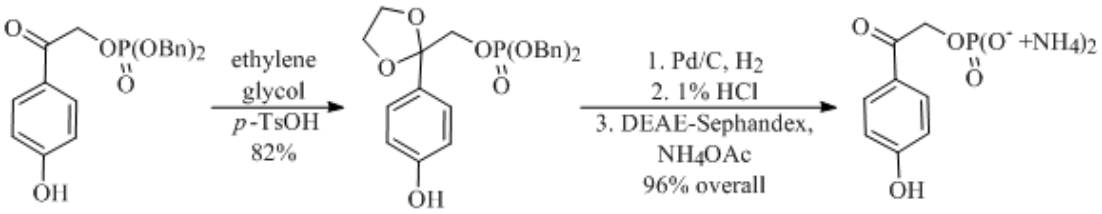

54 **51c**

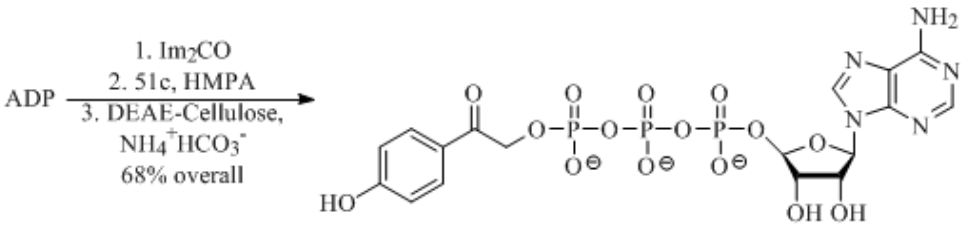

55

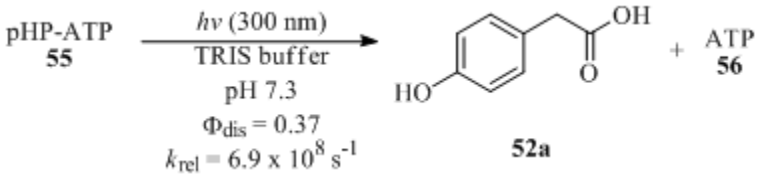

52a

Equation 19.

The highly successful results with the release of phosphates warranted additional examination of other nucleofugal groups that have demonstrated biological importance. L-Glutamate and γ-amino butyric acid (GABA) were chosen by Givens and coworkers[48] because of their well-known importance as neurotransmitters.[50-56] Protection of the C-terminus of amino acids with pHP was accomplished by treating the *N*-Boc protected amino acid with 1,8-diazabicyclo[5.4.0]undec-7-ene (DBU) followed by deprotection at the N-terminus with trifluoroacetic acid (TFA) (**Scheme 10**).[48] The resulting esters were quite stable, resisting hydrolysis in water, D_2O, Ringers solution, and TRIS buffer at room temperature over a 24 hour period.

Scheme 10. Synthesis of pHP Glutamate **57a** and pHP GABA **57b**[48]

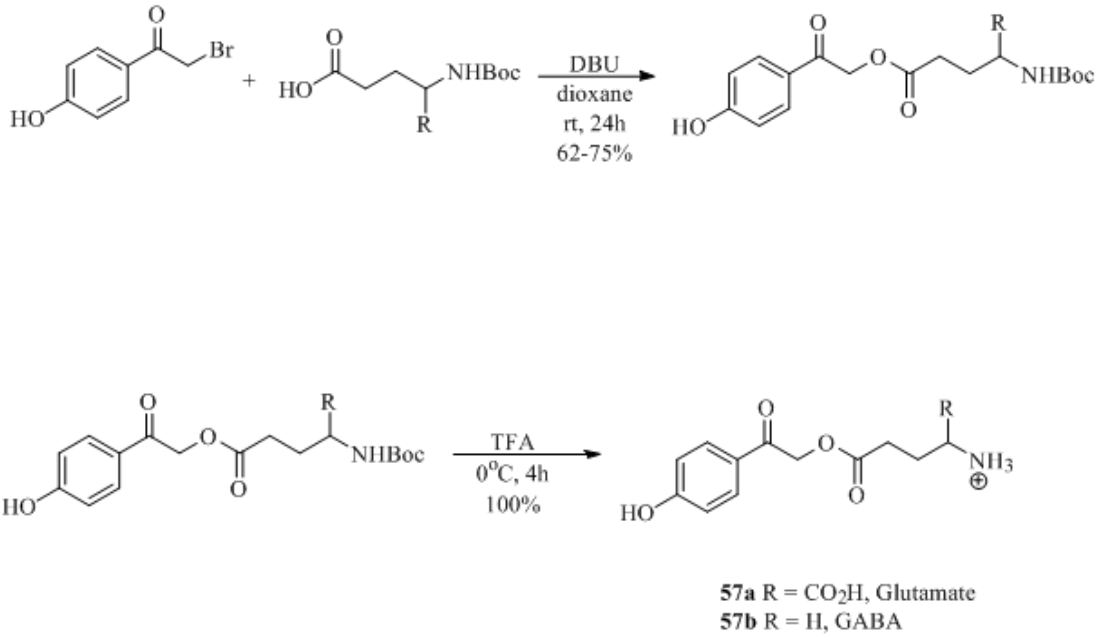

57a R = CO_2H, Glutamate
57b R = H, GABA

Irradiation of buffered solutions of pHP GABA **57a** and pHP glutamate **57b** released the free amino acid, and conversion of the phenacyl group to *p*-hydroxyphenylacetic acid (**52a**) accompanied the photorelease process (**Equation 20**).[48] The rate constants for release were comparable to that determined for pHP ATP. Caged derivatives of neurotransmitters, such as pHP glutamate, have been used

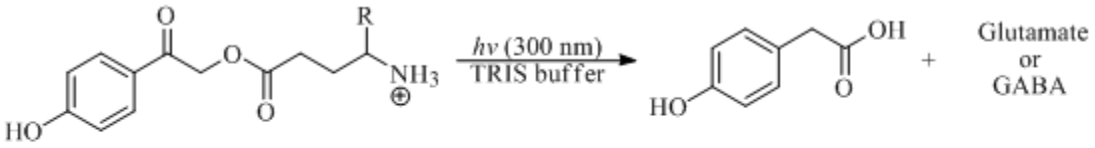

57a R = CO_2H, Glutamate
57b R = H, GABA

52a

Equation 20.

to study chemical synaptic transmission in brain cells in order to understand the processes involved in learning and memory.[57] Photorelease of Ala-Ala from starting material **58** was rapid and the reaction was complete in less than 20 minutes (**Equation 21**). This reaction has served as a model for further studies on the release

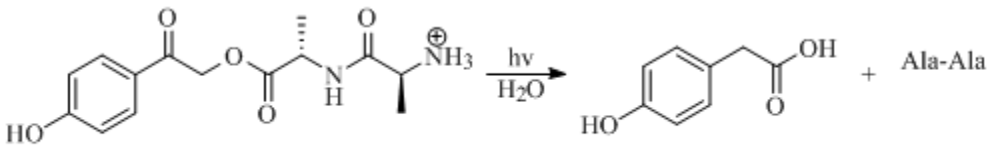

58 **52a**

Equation 21.

of oligopeptides. The most dramatic example of an application to a small oligopeptide was the release of synthetic bradykinin from pHP bradykinin **59** (**Equation 22**).[49] Applications using caged second messengers such as bradykinin have aided our understanding of the biological functions of BK2 receptor[49] and the role of astrocytes, i.e. glial cells, in neurotransmission processes[58].

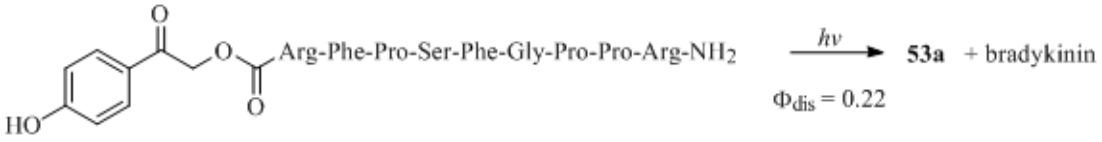

59

Equation 22.

The photochemical attributes of the carboxylate analogs are equivalent to those determined for pHP phosphates in that they both are very clean processes with similar quantum efficiencies (Φ_{dis} = 0.1 – 0.3) and rates of release ($k_{rel} \sim 10^8\ s^{-1}$). Both were shown to be triplet processes via phosphorescence emission studies of pHP esters **51a, 57b, 58, 60,** and **61** and *p*-hydroxyacetophenone (**62**) and 2,4'-dihydroxyacetophenone (**63**) which displayed triplet energies of 68.9 – 70.6 kcal/mol (**Table 12**) and the excited triplets were quenchable by triplet quenchers[49]. The triplet energies of the pHP esters were » 3 kcal/mol above those of the triplet quenchers sodium 2-naphthalenesulfonate or potassium sorbate which were employed in these studies. Stern-Volmer analysis of sodium 2-naphthalenesulfonate quenching of the

release of Ala-Ala from pHP Ala-Ala confirmed a reactive, short-lived triplet excited state (τ^3 = 5.5 ns) and a rate constant for release (k_{rel}) of 1.82 x 10^8 s^{-1}. These results are consistent with earlier reports by Banerjee and coworkers[59,60], Savéant and coworkers[61,62], and Andersen and coworkers[62] confirming that release of the radical and carboxylate anion occurs from the phenacyl triplet.

Table 12. Phosphorescence Emission for a Series of *p*-Hydroxyacetophenone Esters at 77 K[49]

Ketone	Solvent	[M]	λ_{ex} (nm)	$\lambda_{0,0}$ (nm)	E_T (kcal/mol)
pHP Ala-Ala **58**	EPA	0.003	302	408	70.1
pHP GABA **57b**	EG:W	0.05	345	415	68.9
62	EPA	0.03	350	407	70.2
63	EPA	0.02	324	405	70.6
pHP Acetate **60**	EPA	0.01	309	403	71
pHP Phenylacetate **61**	EPA	0.02	305	415	68.9
pHP Diethyl Phosphate **51a**	EPA	0.02	320	405	70.6

Solvent ratios: EPA = 5:2:2 ether/isopentane/methanol; EG:W = 2:1 ethylene glycol/water.

Extensive research in the Givens lab[22,63] led to a proposed mechanism for the photorelease of substrates from the pHP group in aqueous media (**Scheme 11**). According to this mechanism, initial excitation generates the singlet excited state which rapidly undergoes quantitative singlet-triplet (ST) intersystem crossing (k_{ST} = 2.7 x 10^{11} s^{-1}) to generate the triplet state[64]. The triplet excited state phenolic group rapidly undergoes an adiabatic proton transfer to solvent generating triplet phenoxide anion **64**. It was speculated that triplet anion **64** is the precursor to the rate

determining release of the substrate, or alternatively that concerted proton transfer is coupled with the expulsion of the leaving group (not shown). Decay to the putative ground state spirodienedione **65** follows. Finally, hydrolysis of spirodienedione **65** yields *p*-hydroxyphenylacetic acid (**52a**), the only major photoproduct of the pHP chromophore. Phillips and coworkers[65-67] reported results observed during a time-resolved resonance Raman study that supports the triplet nature of the photorelease mechanism proposed above. Previous mechanistic hypotheses involving the direct heterolytic cleavage of the pHP substrate bond from the triplet phenol **66**, or homolytic cleavage followed by rapid electron transfer also suggest intermediate **65**[63,68] but do not incorporate the seminal role of the phenolic hydroxy group, nor the importance of an aqueous environment that appear to be necessary for this triplet photo-Favorskii rearrangement. In a few instances, photohydrolysis of the starting material competes with the Favorskii reaction and results in the appearance of 10% or less of 2,4'-dihydroxyacetophenone (**63**).

Scheme 11. Givens *p*-Hydroxyphenacyl Photorelease Mechanism[63]

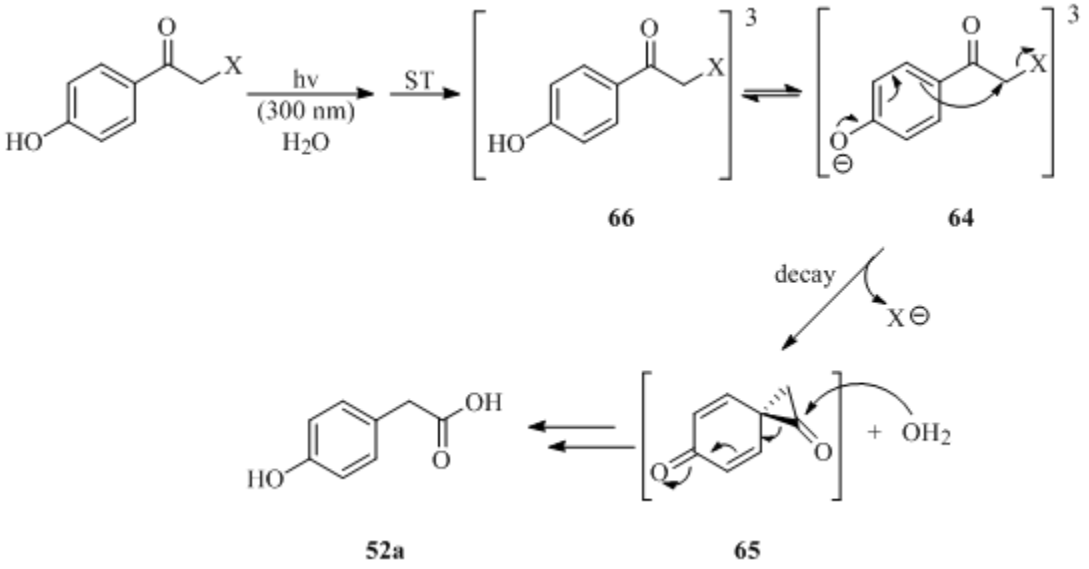

Scheme 12. Corrie and Wan *p*-Hydroxyphenacyl Photorelease Mechanism[69]

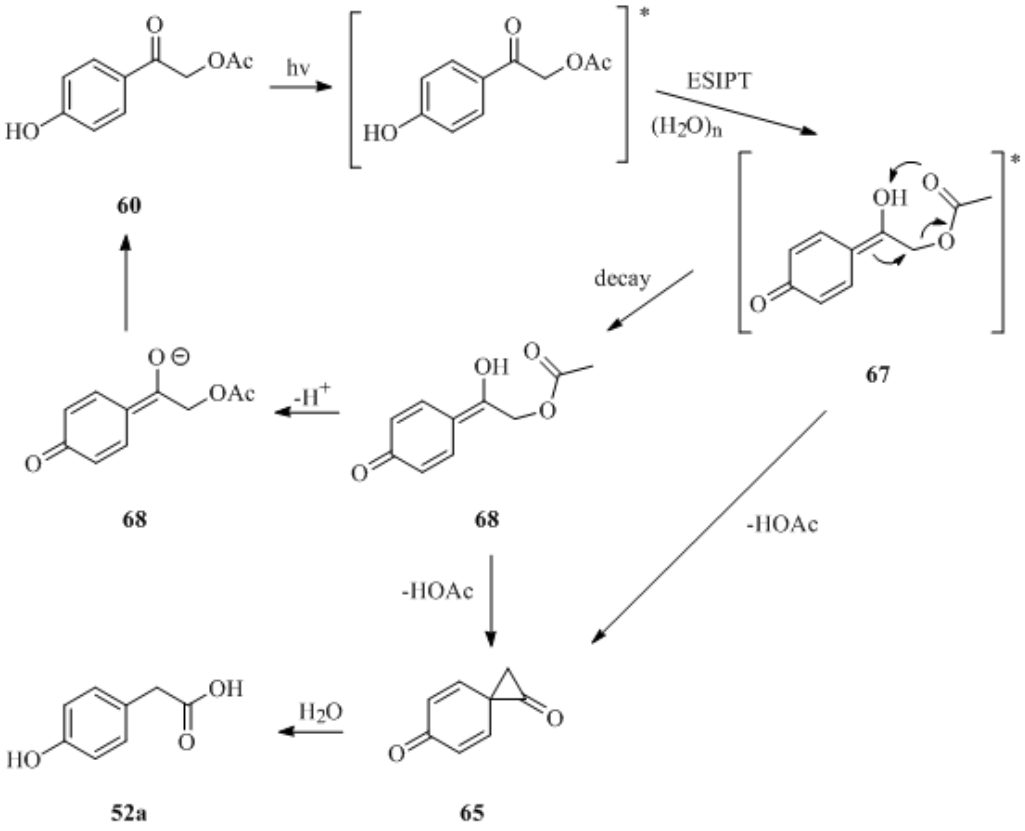

An independent investigation into the mechanism of photosolvic rearrangement by Wan and coworkers[69] using nanosecond LFP was done using pHP acetate **60** as the model. From their results, a pathway differing from that previously proposed was suggested (**Scheme 12**). This mechanism differs from the previous one in that the reaction proceeds through a singlet pathway and that, upon returning to the ground state, intermediate **67** undergoes deprotonation to enolate/phenolate **68** followed by another deprotonation reaction to reform starting material or goes through a ground state Favorskii rearrangement with release of the substrate.

In the mechanism proposed by Givens and coworkers (**Scheme 11**), substrate release occurs from triplet *p*-hydroxyphenacyl group **66**. This is supported by LFP studies of *p*-hydroxyacetophenone (**62**) in aqueous acetonitrile[70]. A 60-fold increase in the acidity of ^{3}pHA **62** when compared to the ground state was reported[71]. An increase in acidity was also observed for several pHP chromophores (**Table 13**) suggesting substrate release from the phenoxide ion is driven by the adiabatic ionization of the phenol on the triplet excited state energy surface. Further evidence of the importance of the role of the phenolic proton transfer was found when a correlation between the efficiency of release (Φ_{rel}) and the $^{3}pK_a$ was observed (**Figure 2**)[64]. It is noteworthy that the electron donating groups cause much less of an increase in acidity than do the electron withdrawing groups. The exact timing of proton transfer and the departure of the substrate are not known but from the evidence above, however, it is known that the separation of the phenoxide ion **64** is important in the release mechanism.

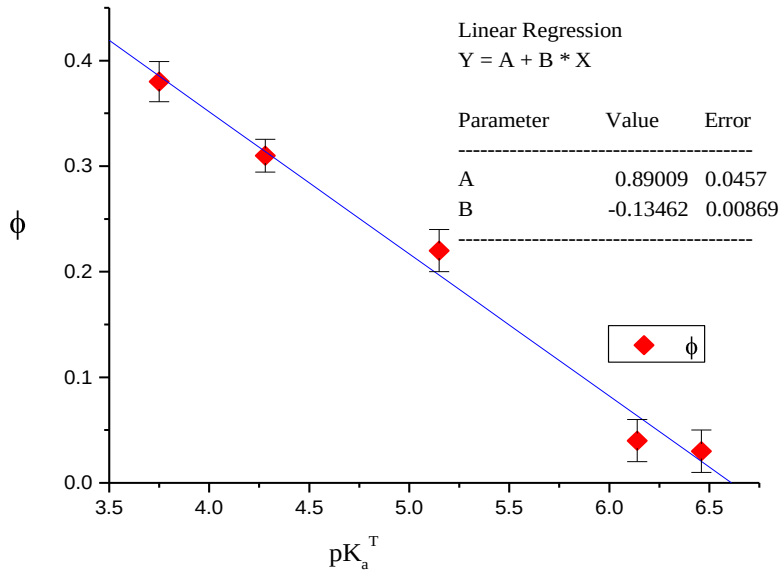

Figure 2. Quantum efficiency for release of GABA as a function of the ^3pK_a of Substituted pHP GABA derivatives. See **Table 13** for the ^3pK_a and appearance quantum efficiencies.[22] (Reprinted with permission from Wiley-VCH.)

Table 13. Substituent Effects on Photorelease of GABA from pHP Esters[22]

pHP Derivative	Φ_{rel}[a]	Φ_{GABA}[a,b]	K_{SV} (M^{-1})[c]	$^3\tau$ (ns)[c]	k_{rel} (10^7 s^{-1})[c,d]	^3pK_a[e]
3-$CONH_2$	0.48	0.38	106	14.3	3.4	3.75
3-CO_2Me	0.31	0.31	5.7	0.77	40	4.28
H	0.22	0.21	38	5.1	4.3	5.15
3-OMe	0.04	0.04	3.2	0.43	9.3	6.14
3,5'-$(OMe)_2$	0.03	0.03	343	46.3	0.065	6.46

[a]Quantum efficiencies for pHP ester disappearance and GABA appearance were measured for 0.01 M aerated (not degassed) aqueous solutions of caged GABA at 300 nm. Error limits are ± 10%. [b]GABA appearance. [c]k_{diff} = 7.4 x 10^9 M^{-1} s^{-1} (H_2O) was used for the rate of diffusion in the quenching experiments (k_q, K^+ sorbate quencher) for calculation of τ^3 and $K_{SV} = (k_q)(\tau^3)$. [d]The rate constants were calculated by the equation $k_{rel} = \Phi_{GABA}/\tau^3$. [e]The ^{3}pKa was determined from ionization and tautomerization equilibria of the corresponding *p*-hydroxyacetophenones by LFP.

Several other newer, photoremovable protecting groups have been designed and are being developed in addition to the ones described above. While these will not be discussed here, information regarding their chemical and biological attributes may be found by consulting other reviews on photoremovable protection groups.[68,71-73] Suffice it to say that the pHP group possesses several advantages that make it superior to many other photoremovable protecting groups; among these advantages are improved water solubility, fast release rates, relatively high quantum efficiencies, relative ease of installation, and quantitative conversions to products, including a blue shifted, rearranged chromophore.

STATEMENT OF THE PROBLEM

Prior to the 1980s, photoremovable protecting groups were employed primarily as a synthetic tool. In the last two decades, there has been an explosion of the use of photoremovable protecting groups as cages in biological studies. In fact, the most exciting development of photoremovable protecting groups hinges upon their applications as cages for biologically important molecules. Thus, an understanding of the mechanism of substrate photorelease is important for future development. The *p*-hydroxyphenacyl group has gained popularity in the last decade. Despite its increase in use, the mechanism remains uncertain. Thus, a major goal of this work is the synthesis and the study of various derivatives that will be used in the investigation of the photorelease mechanism

Another major goal for this investigation is to explore the effects of the leaving group on the efficacy of photorelease. Through the years, many types of leaving groups have been employed in the investigation of photorelease reactions and their mechanisms investigated. Previously mentioned groups involve chromophore-leaving group linkages through a carboxylate[8,40,69,74-76], phosphate[32,38,39,64,67,77], or a sulfonate linkage[11,32,35,78-82]. The influence of the leaving group had not been thoroughly explored until very recently. While this work was in progress, Bendig and coworkers[33] published their findings on the release of a series of conjugate bases from with the coumarin chromophore (**Tables 2 and 3, Figure 1**). Their result, paralleled

our efforts to search for the same type of trend with the *p*-hydroxyphenacyl group. In an effort to systematically explore the effect of the leaving group on substrate photorelease, the quantum efficiencies (Φ), Stern-Volmer quenching rates (k_q), and release rates (k_{rel}) for a series of pHP formate, benzoate, and sulfonate esters have been determined. These results and their mechanistic implications will be presented and discussed.

RESULTS AND DISCUSSION

A. Synthesis

1. pHP Formate and Trifluoroacetate

The synthetic targets needed to explore the role of the leaving group on the efficacy of photorelease are pHP caged benzoic acids, formic acid, and sulfonic acids.

Table 14. Leaving Group pK_a

Leaving Group	pK_a
Methanesulfonic Acid	-1.54
p-Toluenesulfonic Acid	-0.43
Diethyl Phosphate	0.71
p-Trifluoromethylbenzoic Acid	3.69
Formic Acid	3.75
pMethoxybenzoic Acid	4.09
Benzoic Acid	4.21
GABA	4.76
4-Hydroxybenzonitrile	7.17
Phenol	9.8

These leaving groups were chosen for their range of pK_a's (**Table 14**) to test the effect of the pK_a on the rates and quantum efficiencies of photorelease. The synthesis of pHP carboxylate derivatives (**Scheme 13**), *i.e.* the formates and the benzoates, was based upon the previously reported synthesis of pHP GABA and glutamate (**Scheme 10**) where a carboxylic acid was successfully coupled to 2-bromo-4'-hydroxy-acetophenone **53** in the presence of a base.

Scheme 13. Proposed Synthesis of pHP Carboxylate Derivatives

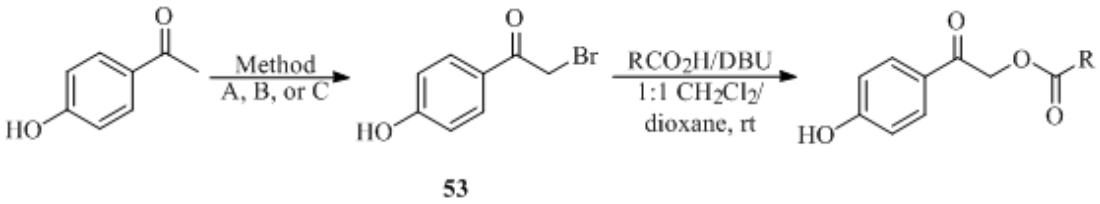

53

The bromination of *p*-hydroxyacetophenone (**62**) is the first synthetic step of the sequence (**Equation 23**) in the synthesis of the pHP carboxylate derivatives. Three different methods were employed to perform this transformation (**Table 15**). The first method, which had been previously used in the group, was based on the method reported by Durden, Juorio, and Davis[83,84] (Method A). In this method copper (II) bromide is reacted with *p*-hydroxyacetophenone **62** resulting in the formation of 2-bromo - 4' - hydroxyacetophenone **53** in good yield (60%) as the major product. However, the reaction also produced the undesired side product 2,2-dibromo-4'-hydroxy-acetophenone **69** in low yields (20%). This side product creates

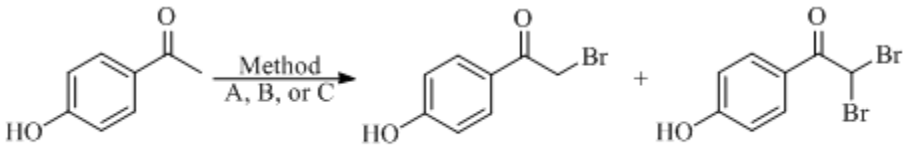

62 **53** **69**

Equation 23.

a couple of problems. The first problem encountered with these products is that they have almost indistinguishable R_f values in thin layer chromatography (TLC). This

makes monitoring the reaction by TLC and stopping the reaction before the side product formation begins to appear nearly impossible. Because the two compounds are very similar, good separation by column chromatography is very difficult and isolated yields of pure mono-bromo product were moderate. This prompted the search for a different synthetic method that would produce **53** in good yield while avoiding the formation of dibromo side product **69**.

Table 15. Yields of Bromination Reactions

Method	Reagent	Solvent	Temperature (°C)	Yield (%)
A[83]	Cu (II) Br_2	EtOAc/$CHCl_3$	reflux	60
B[85]	Br_2	Et_2O	0	50
C[86]	DDB	Et_2O/dioxane	0	93

For reaction details see Experimental Section.

The second method performed was developed by Rather and Reid[85] (Method B) which formed 2-bromo-4'-hydroxyacetophenone (**53**) though the slow addition of bromine to *p*-hydroxyacetophenone (**62**, **Table 15**). Preliminary results were promising with quantitative product yields, but subsequent reactions did not produce the same high yield of the desired product. Reproducible results showed small amounts of dibromo derivative **69** being formed at low conversions of *p*-hydroxyacetophenone (**62**) to 2-bromo-4'-hydroxyacetophenone (**53**). Attempts to push the reaction to completion were made by increasing the amount of bromine used, either at the beginning of the reaction or with a second addition. This consistently resulted in a significant increase in the amount of dibromo side product

70 produced. The reaction mixtures were purified by column chromatography, which eliminated unreacted starting material **63** and side product **69** from the mixture. Even though the resulting product was a mixture, it was used without further purification. Repeated attempts to reproduce the preliminary results were unsuccessful.

The third method employed was adapted from the method reported by Pasaribu and Williams[86] (Method C). Dioxane dibromide (DDB) is the bromine source for the bromination of *p*-hydroxyacetophenone (**62**) and resulted in very good yields (93%). A very small amount of the dibromo derivative **69** formed resulting in a very clean product by ^{1}H NMR, when compared with the Methods A and B. This reaction consistently gave very reproducible results.

The second step in the synthesis (**Equation 24**) involved the formation of pHP esters **70a-e** and **61** via an S_N2 displacement of bromide by carboxylate. The method employed in the synthesis of pHP Glutamate **57a** and GABA **57b** was based upon the method reported by Buu-Hoi and Lavit[87]. Chimilio[88] used this method in the

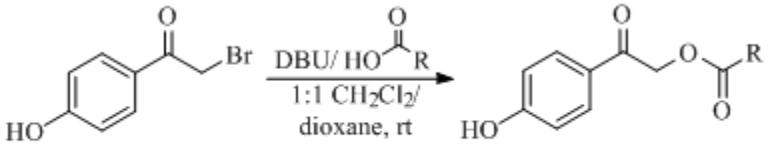

53 **70a-e**

Equation 24.

synthesis of pHP formate using formic acid (**71a**) and 2-bromo-4'-hydroxyacetophenone (**53**). The results (**Table 16**) were again successful in that pHP

Table 16. Product Yields of pHP Carboxylates

Carboxylic Acid	pHP Derivative	R	Time (h)	Yield (%)
71a	**70a**	H	8	82
71b	**70b**	CF_3	5	48
4	**70c**	C_6H_5	24	83
71d	**70d**	$pOCH_3$-C6H4	6	75
71e	**70e**	pCF_3-C_6H_4	120	51
52a	**62**	CH_2- pOH-C_6H_4	48	60

See Experimental for details.

formate **70a** was formed in good yield (82%), was easily purified and characterized. The crystalline product was submitted for x-ray crystallography for structure confirmation. These crystals were suitable for analysis and the structure was confirmed (**Figure 3**). The same method was applied in the synthesis of pHP trifluoroacetate **70b**. pHP trifluoroacetate **70b** was formed in moderate yield (48%) but purification using flash chromatography (3:2 hexanes/ethyl acetate (EtOAc)) was unsuccessful.

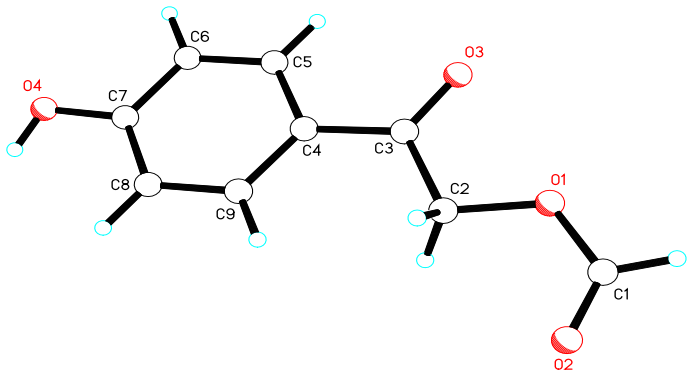

Figure 3. X-Ray Crystal Structure – pHP Formate **70a**. See Appendix A for details.

2. pHP Benzoates

The same method was then employed for the synthesis of the three pHP benzoate derivatives (**Equation 24, Table 16**). DBU and benzoic acid (**4**), *p*-methoxybenzoic acid (**71d**), or *p*-trifluoromethylbenzoic acid (**71e**) were each reacted with 2-bromo-4'-hydroxyacetophenone (**53**) to form pHP benzoate **70c** (benzoate), pHP *p*-methoxybenzoate **70d** ($pOCH_3$ benzoate), and pHP *p*-trifluoromethylbenzoate **70e** (pCF_3 benzoate), respectively. The syntheses were straightforward with the only variation being the amount of time needed for the reaction reach completion. Unsubstituted benzoate **70c** was purified by recrystallization in absolute ethanol while benzoates **70d** and **70e** were purified using column chromatography (1:1 hexanes/EtOAc) and then recrystallized. Crystals of each compound were submitted for x-ray crystallography for structure conformation, and the crystals of benzoates **70c** and **70d** were suitable for analysis (**Figures 4 and 5**). *p*-Hydroxyphenylacetate **61** was also synthesized by reacting 2-bromo-4'-hydroxyacetophenone (**53**) with DBU/*p*-hydroxyphenylacetic acid (**52a**) using this method. Purification with column chromatography (1:1 hexanes/EtOAc) was performed, giving pure product in moderate yield (60%). The compound was utilized by another group member in his work in combinatorial chemistry.

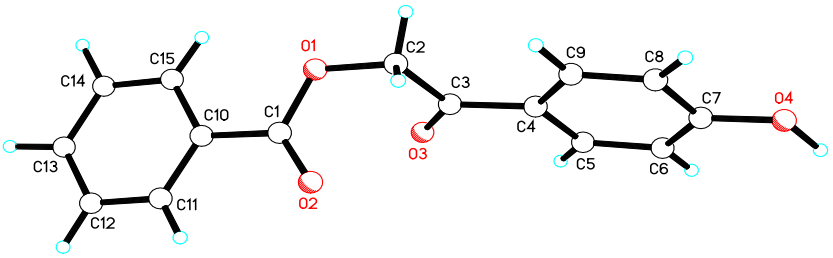

Figure 4. X-Ray Crystal Structure – pHP Benzoate **70c**. See Appendix A for details.

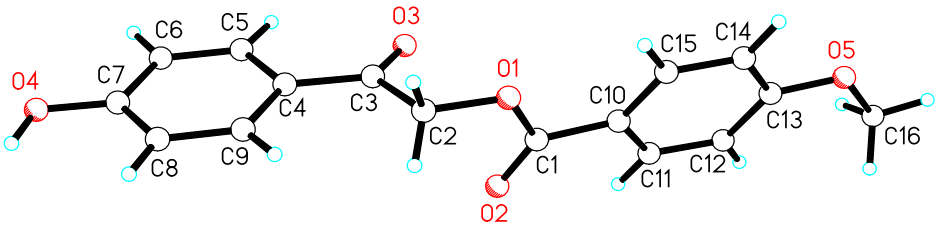

Figure 5. X-Ray Crystal Structure – pHP *p*-Methoxybenzoate **70d**. See Appendix A for details.

3. pHP Sulfonates

The synthesis of pHP mesylate **72a** and pHP tosylate **72b** (**Scheme 14**) had been previously attempted within the group[88]. The steps required to synthesize the sulfonates involve hydrolysis of pHP formate to 2,4'-dihydroxyacetophenone (**64**), protection of the alcohols with *tert*-butyldimethylsilyl (TBDMS) chloride, selective deprotection of the alcohol alpha to the carbonyl, substitution of the unprotected alcohol with a sulfonate, and finally deprotection of the phenol forming the sulfonate ester. During the photolysis of the compound by laser flash photolysis, it was discovered that the structure of the compounds synthesized in this manner were not

the desired targets with the sulfonate group thought to be attached to the oxygen alpha to the carbonyl was instead the it was attached to the oxygen of the phenol.

Scheme 14. Chimilio pHP Sulfonate Synthesis[88]

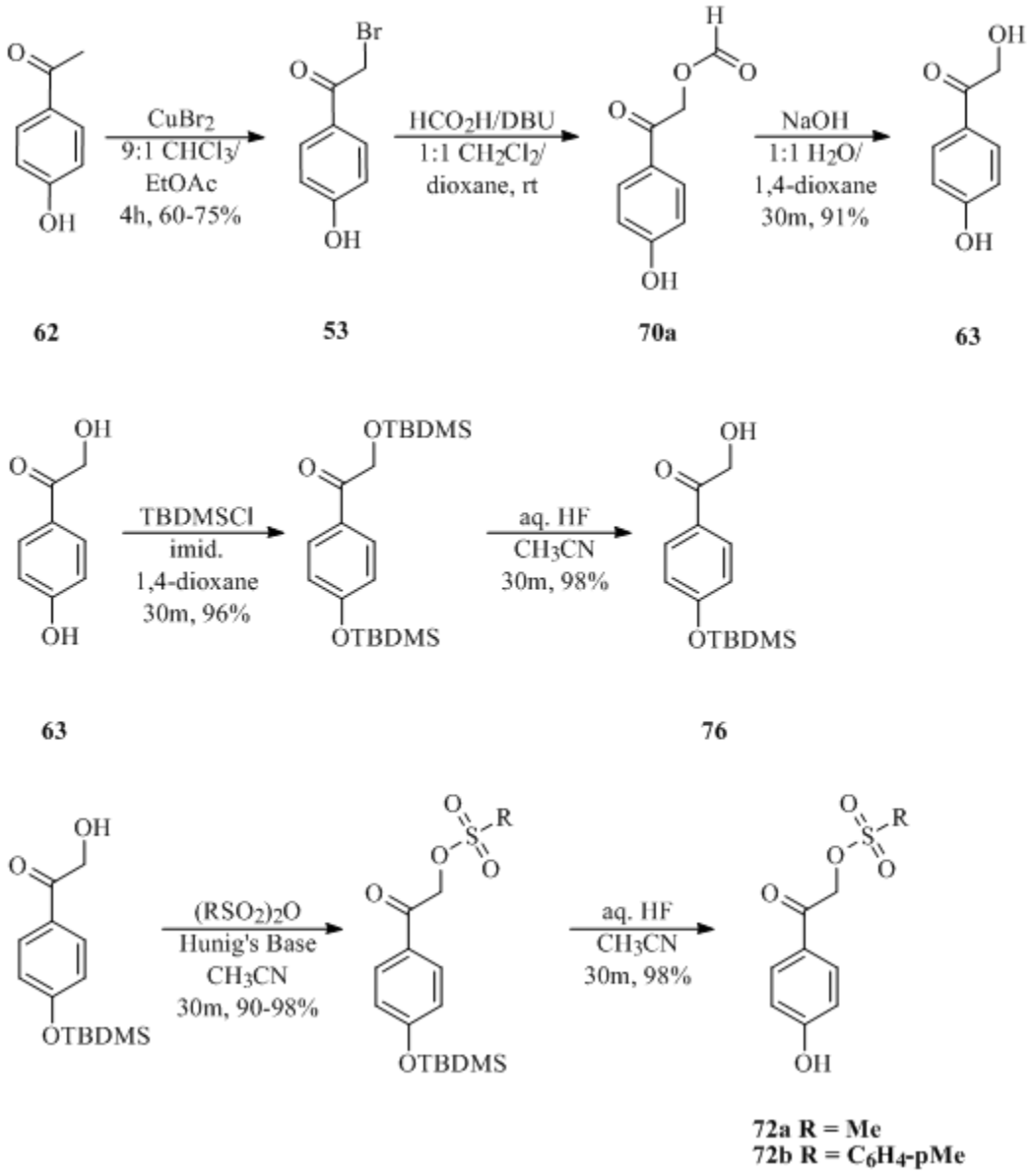

A pathway with similar steps was reported by Phillips and coworkers[67,89] in their synthesis of pHP diethyl phosphate **51a** (**Scheme 15**) and was thus employed in a revised synthetic protocol for pHP sulfonate esters. These two pathways are very similar with the main differences being the final product and when protection of the phenol should be performed. The Phillips procedure was to protect the phenol using *tert*-butyldiphenylsilyl chloride (TBDSPCl) forming silyl-protected acetophenone **73** and subsequent bromination to form protected 2-bromo acetophenone **74**. In our hands, this sequence proceeded smoothly with excellent yields (95 – 100 %) for each step. Bromination of protected acetophenone **73** was also accomplished using DDB and yielding protected 2-bromo acetophenone **74** in high yield (95%).

Scheme 15. Phillips' Synthetic Sequence[67,89]

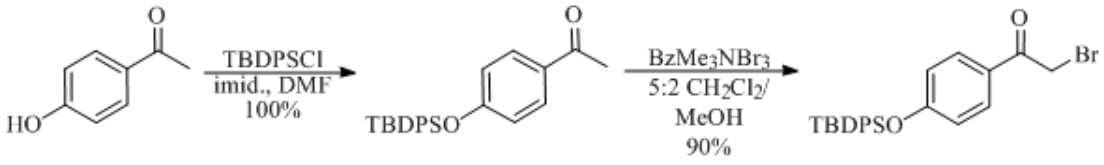

62 **73** **74**

Synthesis of α-hydroxyacetophenone **75** proved problematic. The reaction conditions outlined by Phillips and coworkers[89] yielded the desired compound and several side products. Due to the difficulty in separation of the complex product mixture, the yield of the desired product suffered (< 20%). Treatment of the reaction mixture with sodium hydroxide (NaOH) somewhat reduced the complexity of the mixture, but several compounds were still present. After several attempts to reduce

the amount of side products that formed, it was discovered that the easiest way to do this was to heat the mixture just below boiling, at a temperature around 55 – 60 °C, instead of at reflux, as recommended by Phillips and coworkers. This improved yields and with careful monitoring of the reaction, the yield was further increased (60%). Since sodium formate has low solubility in absolute ethanol, an effort to increase the formate solubility using potassium formate was employed (**Equation 25**). This modification slightly improved yields (65%) which made purifying the complicated reaction mixture a little easier.

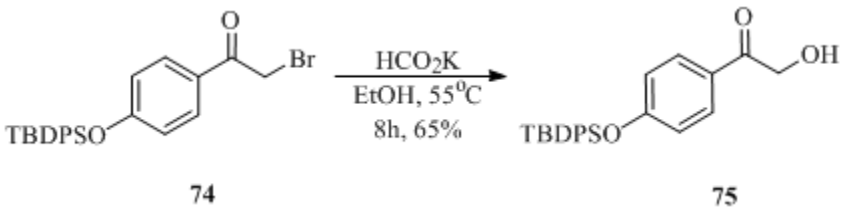

74 75

Equation 25.

An alternate synthetic pathway to pHP formate **70a** was explored. During the characterization of each of the side products of the previous reaction, a product, that was identified as the silyl-protected derivative of pHP formate, was isolated. In an effort to produce this product specifically, the solvent was changed from ethanol to acetonitrile in hopes of stopping the hydrolysis reaction that converts the formate ester to 2,4'-dihydroxyacetophenone (**75**). This method, heating silyl-protected 2-bromo-4'-hydroxyacetophenone **74** with potassium formate in acetonitrile (**Equation 26**), did indeed produce formate ester **70a** in reasonable yield (41%).

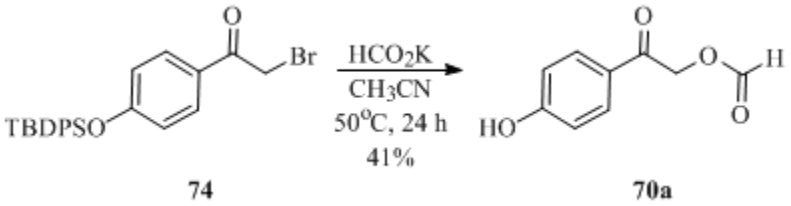

74 70a

Equation 26.

The previous work in the group (**Scheme 14**) concerning the synthesis of pHP mesylate **72a** employed a method that combined *tert*-butyldimethylsilyl protected α-hydroxyacetophenone **76** with methanesulfonyl anhydride in the presence of Hunig's base (diisopropylethylamine).[88] These reaction conditions were employed on the bulkier *tert*-butyldiphenylsilyl protected derivative of 2,4'-dihydroxyacetophenone **75.** However, several attempts of this reaction were made but the synthesis of mesylate **72a** under these conditions was unsuccessful. This reaction was also used in several attempts to synthesize pHP tosylate **72b** through the reaction of tosyl anhydride with TBDPS-protected derivative **75** with no success. The reaction conditions under which a sulfonyl anhydride was reacted with an alcohol alpha to a carbonyl have not been reported in the literature. The conditions were manipulated to mimic those found in the reactions of primary[90,91] and secondary[92] alcohols with mesyl anhydride but no products were formed.

An alternative reaction combined methanesulfonyl or *p*-toluenesulfonyl chloride with silyl-protected 2,4'-dihydroxyacetophenone **75** in pyridine. Again the reaction conditions were modeled after the conditions reported for primary alcohols.[93,94] These reaction conditions produced protected mesylate in very low yield

(< 5%) and no evidence for the formation of tosylate with tosyl chloride was observed.

Failure to produce either pHP sulfonate in useful yields prompted a study of the synthesis of model derivatives, benzyl mesylate (**77a**) and benzyl tosylate (**77b**), to discover better reaction conditions. Both derivatives have been reported to have been successfully synthesized from either benzyl alcohol (**78**)[95] (**Equation 27**) or

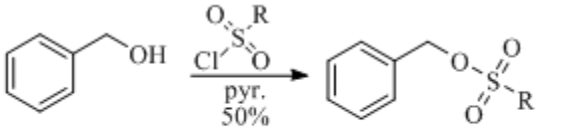

78 **77a R = Me**
77b R = C_6H_4-pMe

E**quation 27.**

from benzyl bromide (**79**)[96] (**Scheme 16**). The synthesis of benzyl mesylate **77a** was successful from both benzyl alcohol (**78**) and from benzyl bromide **(79**). The benzyl bromide (**79**) and silver salt method did, however, give higher product yields (90%).

Scheme 16. Emmons and Ferris Synthesis of Benzyl Mesylate (**77a**) and Tosylate (**77b**)[96]

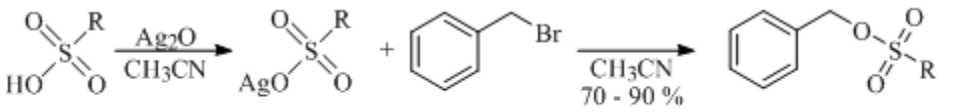

79 **77a R = Me**
77b R = C_6H_4-pMe

This method was also highly successful in the synthesis of benzyl tosylate (**77b**), producing the product in good yield (70%). Success in the synthesis of both protected pHP mesylate **80a** and protected pHP tosylate **80b** was achieved when TBDPS-protected 2-bromo-4'-hydroxyacetophenone

Scheme 17. Synthesis of pHP Mesylate **72a** and pHP Tosylate **72b**

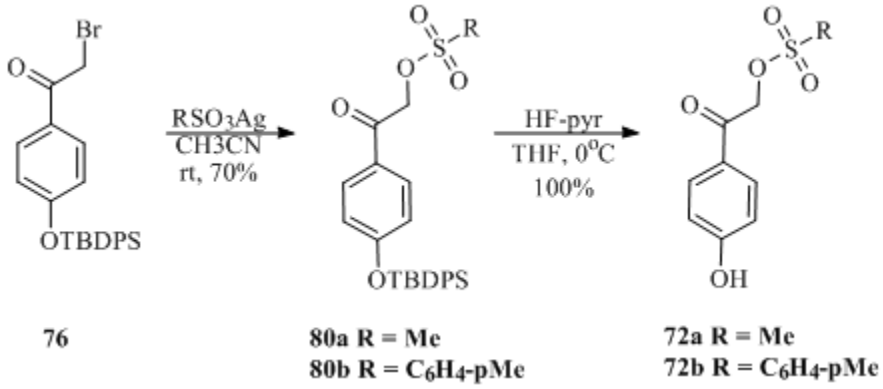

76

80a R = Me
80b R = C_6H_4-pMe

72a R = Me
72b R = C_6H_4-pMe

76 was reacted with the silver methanesulfonate or silver *p*-toluenesulfonate[96] (**Scheme 17**). Deprotection of the phenol was accomplished in excellent yield (100%) using hydrogen fluoride in pyridine.[97] pHP sulfonates **72a** and **72b** are solids and, therefore, were recrystallized and submitted for x-ray analysis for structure confirmation (**Figures 6 and 7**).

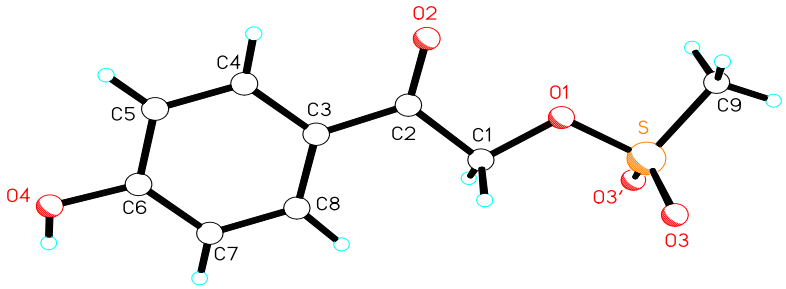

Figure 6. X-Ray Crystal Structure – pHP Mesylate **72a**. See Appendix A for details.

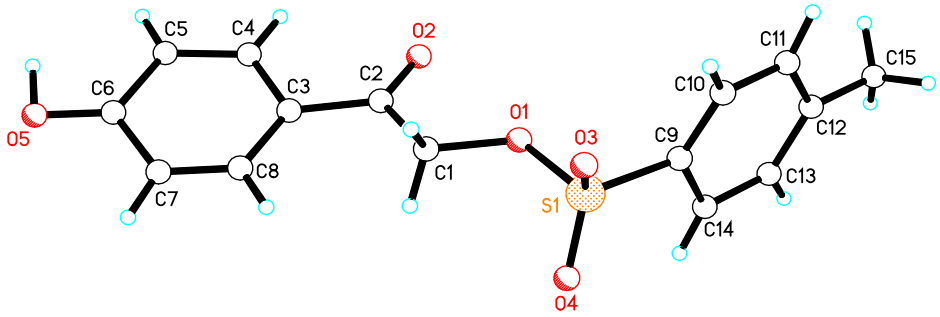

Figure 7. X-Ray Crystal Structure – pHP Tosylate **72b**. See Appendix A for details.

Stability experiments were performed under the same conditions as the photolysis conditions except the test tubes were not exposed to light. In one trial, the samples were wrapped in Aluminum foil and kept at room temperature for 3 days. Aliquots were removed, diluted, and analyzed by RP-HPLC every 24 h for 3 days. In the second trial the foil wrapped samples were placed into the photoreactor for 60 min and an aliquot was removed every 5 min and analyzed by RP-HPLC. The stability of the esters at other pHs was also evaluated. For these experiments samples were made using ammonium acetate buffered pH 3.11, 7.01, or 10.99 for the aqueous portion of the solvent. No products, either of the type formed by photolysis or by hydrolysis, were observed by HPLC for the solutions at pH 3 or 7. This suggests that both mesylate **72a** and tosylate **72b** are stable in the ground state in aqueous and buffered solutions at acidic and neutral pHs. Photosolvolysis reactions must form 2,4'-dihydroxyacetophenone (**63**). These esters were not stable at the higher pH 11 and unidentified compounds were observed in the chromatogram. Formate **70a** was not stable under any of these conditions and quickly hydrolyzes by a competing ground state reaction to 2,4'-dihydroxyacetophenone (**63**) when in contact with water. The stability of the mesylate ester was revisited, this time using a phosphate buffer adjusted to pH 3.00, 7.06, and 12.02 for the aqueous portion of the solvent. After analysis by RP-HPLC, mesylate ester **72a** was found to be stable at pH 3 and 7 for over 24 h but was not stable at pH 12 for even 1 min. The chromatogram for the solution at pH 12 showed a complex mixture of products. Of the many components in the mixture only one could be identified, 2,4'-dihydroxyacetophenone (**63**).

4. Synthesis of pHP Phenylalanine and pHP Serotonin

A synthetic pathway leading to caged biologically important molecules, specifically phenylalanine and serotonin, through either carbamate or carboxylate linkages was proposed. This route starts with Phillips' silyl-protected 2,4'-dihydroxy-acetophenone **75** and ends with caged serotonin and caged amino acids (**Scheme 18**). The first step involved reacting silyl-protected 2,4'-dihydroxyacetophenone **75** with 1,1'-carbonyldiimidazole (CDI) to form imidazole carboxylic ester **81** in low yields (25%) using the procedure reported by Mulvihill and coworkers[98]. Literature reports on the use of added bases, i.e. triethylamine (TEA)[99,100], *N*,*N*-dimethylaminopyridine (DMAP)[100,101], or sodium hexamethyldisilazide[100], promised improved product yields for this reaction. This was tried with imidazole carboxylic ester **81** synthesis using imidazole, DMAP, TEA, and Hunig's base, but no significant improvement was observed for DMAP, TEA, or Hunig's base. By adding imidazole (0.5 equivalents) to the reaction mixture, however, the yield was significantly improved (70%).

The caging of phenylalanine, glycine, and cysteine through a carbamate linkage involved displacement of imidazole from imidazole carboxylic ester **81**. Coupling ester **81** with the amino group of phenylalanine was attempted using two methods described by Elliott and coworkers[102] in their synthesis of Erythromycin. To make sure a carbamate linkage was formed, i.e. the reaction occurred at the amine group, the *tert*-butyl ester of phenylalanine **82** was used. The solvent was modified to a mixture of 1:1:1 acetonitrile/acetone/DMF and the reaction refluxed overnight. The second method involved dry DMF as the solvent with pyridine as the base. The

reaction was allowed to stir at rt overnight. The ^{1}H NMR of the crude reaction mixtures was very similar so the crude product mixtures were combined and chromatographed (1:1 hexanes/EtOAc). The isolated product was identified by NMR, ^{1}H and ^{13}C, as caged *tert*-butyl ester of phenylalanine **83** (20%). During the reaction, the silyl-protecting group was removed from the phenol thus eliminating one of the deprotection steps. Hydrolysis of *tert*-butyl ester **83** to the carboxylic acid derivative was attempted but only starting material was isolated.

The success of this synthesis with amino acids led to its application in the synthesis of pHP caged serotonin 84. The synthesis and photorelease of caged serotonin became a joint effort with an undergraduate in the lab[103]. To selectively react the phenol with imidazole carboxylic ester 81 the amine needed to be blocked. A Boc protecting group was installed (**Equation 28**). This transformation was performed using a modification of the method reported by Li and coworkers[104] and good yields (74%) of Boc-serotonin 85 were achieved. Displacement of the imidazole in an imidazole carboxylic ester by an alcohol has been reported by Rannard and Davis[105]. Their methodology was used in the displacement of imidazole by the phenol in serotonin 85 in imidazole carboxylic ester 81. Despite low yields (16%), the methodology gave the desired product 86 (**Scheme 18**).

Scheme 18. Synthesis of pHP Caged Biological Molecules

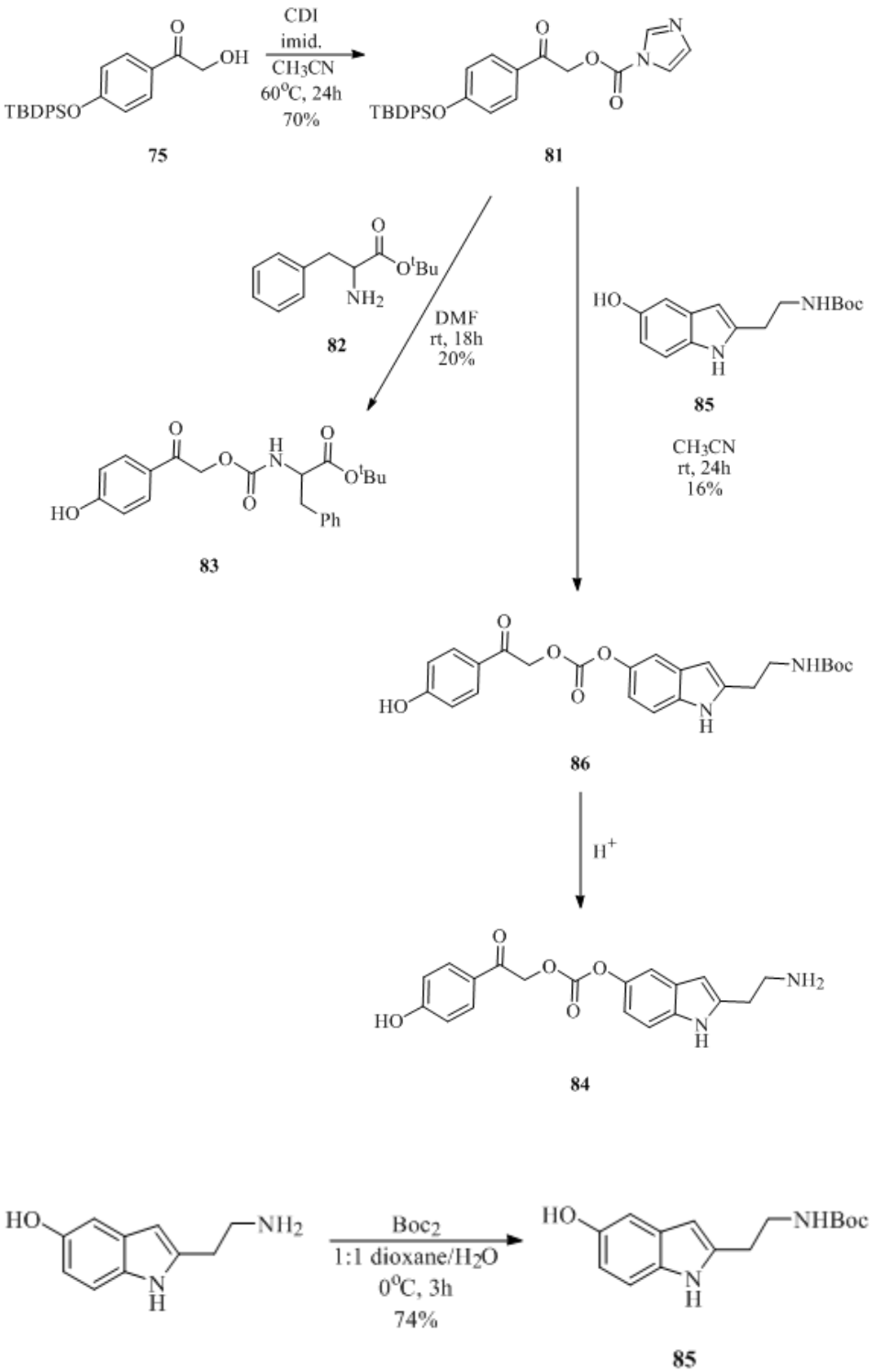

Equation 28.

B. Exploratory Photochemistry – Product Identification

1. Background

In the excited state, many competing reaction pathways lead back to the ground state of the starting material or result in product. For the purpose of this discussion, only the reaction pathways that result in the formation of product are discussed, and it is to be noted that relaxation back to the ground state does occur. However, this process was not the focus of this work.

i. Effects of Solvent

In the case of pHP esters, the solvent has an important role in the determination of which one of two pathways will be followed. The first pathway or radical pathway, which is followed in organic solvents, involves the formation and subsequent reactions of radical pairs[106] (**Scheme 19**). In this reaction pathway, the pHP ester is irradiated, promoting it to an excited state where homolytic cleavage of the chromophore-substrate bond occurs. The newly formed radical pair can combine to reform starting material or can abstract a hydrogen atom to form *p*-hydroxyacetophenone (**62**), the released substrate, and other products. This pathway was explored through the photolysis of benzoate esters **70c-e** in acetonitrile with no water present. Using liquid chromatography coupled with a mass spectromic detector (LC-MS) and ^{1}H NMR, the major products were identified as *p*-hydroxyacetophenone (**62**, ~40%) and benzoic acid (**4**, 100%), *p*-methoxybenzoic acid (**71d**, 100%), and *p*-trifluoromethylbenzoic acid (**71e**, 100%), respectively.

Scheme 19. Radical Pathway of Photorelease[106]

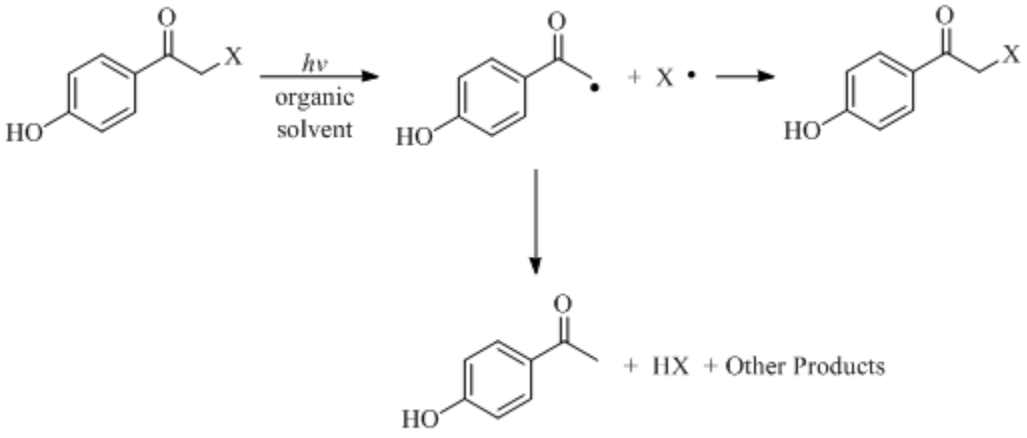

62

Several other products were present in the photolysis mixtures but their identity was not pursued. Quantitative data was obtained for these reactions using DMF as an internals standard in the ^{1}H NMR experiments. Quantum efficiencies for the disappearance of starting material (Φ_{dis}) in acetonitrile were determined (benzoate **70c**, Φ_{dis} = 0.0275; pOCH_3 benzoate **70d**, Φ_{dis} = 0.0255; and pCF_3 benzoate **70e**, Φ_{dis} = 0.0230) but they were found to be much lower than those in aqueous organic solvents (*vide infra*). The percent conversion of these reactions was kept low (~15%). When formate ester **70a** was photolyzed in 95% acetonitrile, again lower quantum efficiencies for the disappearance of starting material (Φ_{dis} = 0.0438) and a lower conversion (~10%) were observed with a complex mixture of products (*p*-hydroxybenzyl alcohol (**87**), *p*-hydroxyphenylacetic acid (**52a**), *p*-hydroxyacetophenone (**62**), and several unidentified products. These results demonstrate two of the shortcomings of this reaction pathway; low quantum

efficiencies and a complicated mixture of products. For applications as photoremovable protecting groups in biological systems, these factors in addition to the highly organic nature of the solvent system make it a less attractive choice.

The second reaction pathway, or ionic pathway, is followed in aqueous or mixed aqueous solvents, a more biologically compatible media. The advantages of aqueous solvents have been previously discussed (*vide supra*). In this reaction pathway (**Scheme 20**), the pHP ester is excited to its singlet excited state, which rapidly intersystem crosses to a triplet excited state. From here one of two events can occur, the first being decay back to the ground state and the second being the release of the substrate and formation of spirodienedione **65**. This intermediate reacts with water as part of a Favorskii-like rearrangement yielding *p*-hydroxyphenylacetic acid (**52a**, pHPAA) as the major photoproduct. This pathway had been observed in

Scheme 20. Ionic Pathway of Photorelease[84]

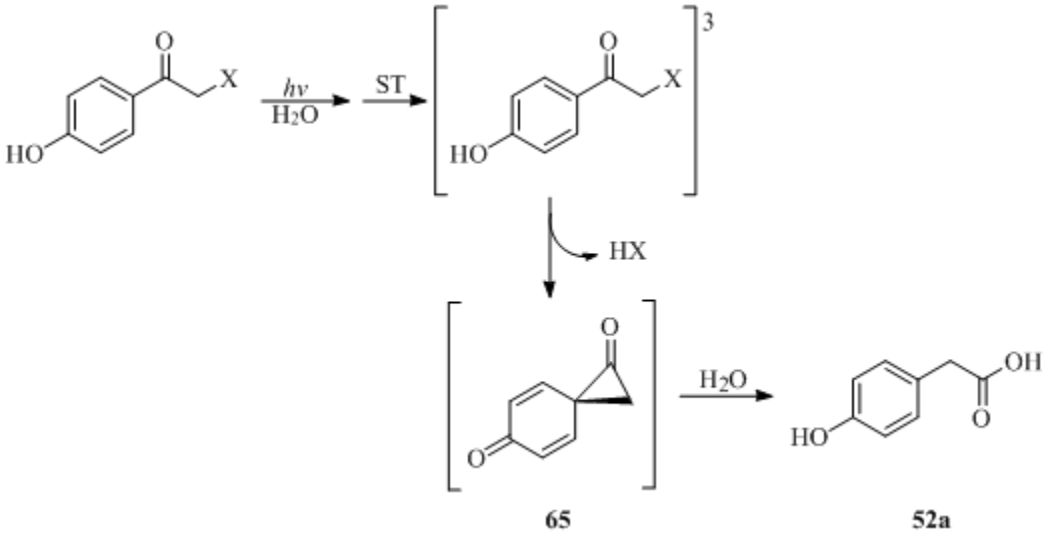

previous work where the solvent system was either water or a mixed aqueous solvent system[38,39,49,64,84]. At the high organic content of the solvent systems employed here, between 50 – 75% acetonitrile, for the photolysis of pHP formate **70a**, the pHP benzoates **70c-e**, and the pHP sulfonates **72a** and **72b**, the reaction pathway could not be anticipated. In order to obtain information on the product distribution, exploratory product experiments were performed. The photochemistry of the aforementioned pHP derivatives will be discussed in the order of formate ester followed by the benzoates and then the finally the sulfonates.

The pHP chromophore has the advantage of being more water soluble than other chromophores due to its phenolic hydroxy group. Previous literature examples[48] proved to be completely soluble in water. This is true of the derivatives that are the focus of this discussion as long as their concentrations are kept low (< 0.01mM). At higher concentrations the solubility in water decreased and acetonitrile was added to completely dissolve the solid. One of the main concerns of the photolysis experiments is the absorption of light. In order to make sure all of the light is absorbed by the sample, high concentrations (mM) are used. In the photolysis experiments, pHP formate **70a** (25 mM) and pHP mesylate **72a** (25 mM) were photolyzed in a 3:1 water/acetonitrile mixture, pHP tosylate **72b** (25 mM) was photolyzed in a 1:1 water/acetonitrile mixture, while pHP benzoates **70c-d** (10 mM) were photolyzed in 7:3 acetonitrile/water. It is interesting to note that as the substrate attached to the chromophore becomes less polar the water solubility of the pHP derivative decreases. Dominik Heger, the postdoctoral associate, analyzing these derivatives by laser flash

photolysis, also observed this trend. The percent water reported varied for each derivative; formate **70a** (100%), mesylate **72a** (100%), pOCH_3 benzoate **70d** (74%), pCF_3 benzoate **70e** (71%), tosylate **72b** (70%), and benzoate **70c** (64%).

ii. Methods of Analysis

Several spectroscopic or chromatographic tools have been used to monitor and quantify photochemical reactions. Gas chromatography coupled with mass spectromic detection (GC-MS), UV-VIS, ^{1}H NMR, and HPLC are common methods for this purpose. ^{1}H NMR and liquid chromatography were the techniques of choice for the following reasons. Attempts were made to use GC-MS in the quantitation of the photorelease reaction but the starting material and products were not detected after injection into the GC. UV-VIS has the disadvantage that the products and starting material are all chromophores with similar absorption spectra. This makes it difficult to monitor just one compound in the reaction mixture due to the overlap of the absorption bands. However, this problem can be avoided when UV-VIS is used in conjunction with HPLC. With the use of HPLC, the reaction components can be separated thus allowing for the reaction to be monitored and quantitated. UV-VIS detection can be used alone, if all of the compounds are chromophores, but can also be used in conjunction with a MS detector. The mass spectrometer comes in handy when a product is not a chromophore, or when it is necessary to verify the identity of a mixture component. One drawback of this method is the amount of time and effort that go into devising the separation method and its mode of detection. The time

commitment is very intensive during method development but after method development is complete, the samples can be run using the automatic sample injector. For LC-UV/MS analysis, a mixture of possible products was made and then analyzed making certain that base line separation was achieved with no overlapping peaks for the reaction mixture. Each compound had a distinct retention time and, when compared to pure samples, was identical to the synthetic mixture. Spiking the reaction mixture with authentic sample produced the expected changes in peak intensity. This was also used to verify product identity.

The final method used for monitoring and quantifying reactions is ^{1}H NMR. This method requires each component of the reaction mixture to have a unique functional group with its own chemical shift. The substrates that were photoreleased from the pHP chromophore fit the criteria, making the reaction easy to monitor. The disadvantage of this method is that it is very labor intensive and time consuming. In order to positively identify the components of a particular reaction mixture, the spectral or chromatographic data were compared to those of pure samples of the products. The mixture was also spiked with a small amount of a suspected product and re-analyzed noting the expected increase in the position and area of the peaks relevant to that product. In the case of ^{1}H NMR, each of the major photoproducts has a singlet with distinct absorption for either a methyl or methylene peak; the methyl group of *p*-hydroxyacetophenone (**62**) has a chemical shift of 2.23 ppm while the methylene peak of *p*-hydroxyphenylacetic acid (**52a**) is observed at 3.62 ppm. It was possible to determine the product(s) formed by location of the characteristic singlets

and to quantitate the progress of the reaction using a ratio of their areas and the areas relative to the internal standard DMF.

iii. UV-VIS Spectra and Excitation Wavelength

For each compound, UV-VIS spectra were reconstructed by factorial analysis using Specfit from LFP data (**Appendix A**) and were collected as the pHP derivatives were characterized using a spectrometer. From the LF data, when more spectra are in one frame they depict evolving absorption spectra with time in the order of shortest to longest; red, green, violet, and orange. The quality of the spectra has to be taken into account. Some subtle features can be resolved only in those spectra where low noise and numerous scans are available. In order to make comparisons of the same derivative under different conditions, the spectra should be similar in quality which was not always the case.

Comparisons of the spectra taken using the Cary 100 Bio spectrometer were made (**Table 17**). The limited solubility of the benzoates limited the amount of water that could be present in the solvent mixture. Comparisons of the spectra with 50, 70, and 100% acetonitrile show very little variation in the absorbance bands. Mesylate **72a** was also measured in varying percentages of acetonitrile and again no differences in the absorption bands were observed. From these spectra, it was decided that the best phototubes to use in the photolyses of these compounds would be those centered around 300 nm.

Table 17. UV-VIS Absorption Maxima (λ_{max}) and Extinction Coefficients (log ε) of pHP Derivatives

pHP Derivative	Solvent (% acetonitrile)			
	30	50	70	100
Formate **70a**	281 (4.04); 221 (3.06)	nd	nd	nd
Benzoate **70c**	nd	273 (4.06); 225 (3.88)	276 (4.50); 224 (4.54)	271 (5.03); 222 (5.05)
$pOCH_3$ Benzoate **70d**	nd	273 (4.16)	272 (4.64)	272 (5.09)
pCF_3 Benzoate **70e**	nd	283 (3.85); 222 (3.03)	282 (4.52); 220 (4.53)	272 (4.99); 250 (5.05)
Mesylate **72a**	281 (4.15); 221 (3.97)	281 (4.15); 221 (3.97)	nd	273 (4.21); 2.19 (4.04)
Tosylate **72b**	283 (4.20); 225 (4.30)	nd	nd	nd

nd = not determined.

2. Carboxylate Photochemistry

In the product determination experiment for pHP formate **70a**, the ^{1}H NMR spectra were recorded both before and after exposing the sample to four RPR 3000 tubes for approximately 30 min. Due to the highly organic nature of the solvent system (1:1 acetonitrile/water), it was unclear which reaction pathway would dominate. For formate irradiations for 30 minutes, subtle differences in the starting and ending spectra were noted: a decrease in the area of the large singlet at 5.56 ppm corresponding to the methylene peak in pHP formate **70a**; the appearance and increase of a singlet at 3.62 ppm; the appearance and increase of a singlet at 8.25; and differences in the aromatic region. The structure of one of the major products was determined from the chemical shift of the methylene singlet and the aromatic ring protons. It was assigned to *p*-hydroxyphenylacetic acid (**52a**) formed from the pHP chromophore. Formic acid (**71a**), identified by the singlet at 8.25, was released as the other major product by the ionic pathway (**Equation 29**). From the change in the area of the peak at 5.56 ppm, the percent conversion was calculated to be 58%.

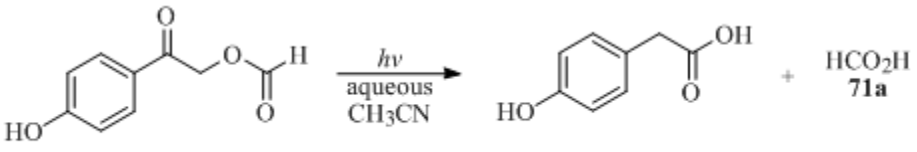

70a **52a**

Equation 29.

pHP benzoate esters **70c-e** were irradiated for 30 minutes with four RPR 3000 tubes with ^{1}H NMR spectra take before and after irradiation. Again, the anticipated reaction pathway was not certain based upon the highly organic nature of the solvent system (7:3 acetonitrile/water). Under these conditions, unsubstituted benzoate **70c** was converted to *p*-hydroxyphenylacetic acid (**52a**) and benzoic acid (**4**) was released (32% conversion), whereas the pCF_3 benzoate **70e** was converted to *p*-hydroxyphenylacetic acid (**52a**) and *p*-trifluoromethylbenzoic acid (**71e**) was released quantitatively, again following the ionic pathway (**Equation 30**). The same was found true for pOCH_3 benzoate **70d** in that the major photoproducts were *p*-hydroxyphenylacetic acid (**52a**) and released *p*-methoxybenzoic acid (**71d**, 25% conversion).

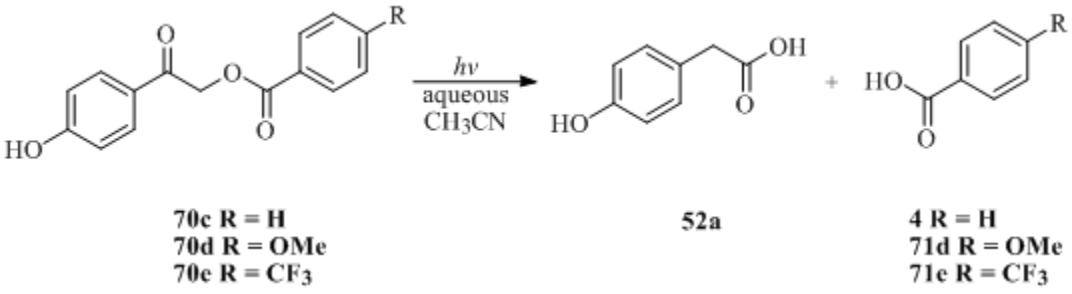

70c R = H
70d R = OMe
70e R = CF_3

52a

4 R = H
71d R = OMe
71e R = CF_3

Equation 30.

3. Sulfonate Photochemistry

Preliminary photolyses of the pHP sulfonate esters **72a** and **72b** were carried out to determine approximate yields and to determine the products. ^{1}H NMR spectra were recorded both before and after exposing the sample to four RPR 3000 tubes for 1 h containing DMF as the internal standard. The products were determined by comparisons of the spectra of authentic samples of each of the products and the spectra of the reaction mixture. The major photoproducts were determined to be the released substrate, methanesulfonic acid (**89a**) or *p*-toluenesulfonic acid (**89b**), and *p*-hydroxyphenylacetic acid (**52a**) but minor photoproducts *p*-hydroxybenzyl alcohol (**87**) and 2,4'-dihydroxyacetophenone (**63**, pHPOH) were also observed. The conversion was complete in both cases. These are very efficient and clean photoreactions that follow the ionic pathway (**Equation 31**).

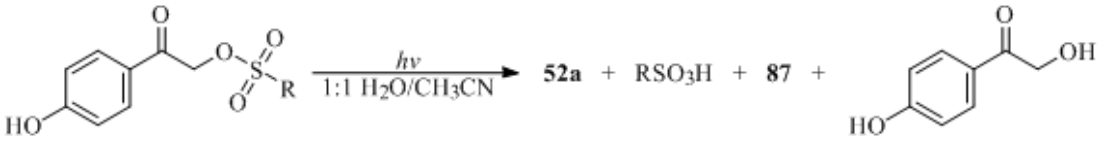

72a R = Me
72b R = C_6H_4-pMe

89a R = Me
89b R = C_6H_4-pMe

63

Equation 31.

4. New Photoproduct: Identification of *p*-Hydroxybenzyl Alcohol

After the quantum yield measurements had been completed, it was discovered that *p*-hydroxybenzyl alcohol (87, pHBA) was formed as a minor photoproduct[107]. It is the product of decarbonylation of spirodienedione intermediate 65 giving *p*-quinone methide (88) which subsequently reacts with water (Scheme 21). Because of this observation, photolysis reaction mixtures from each benzoate were analyzed for the presence *p*-hydroxybenzyl alcohol (87) by LC-MS. When the reaction mixture chromatograms were compared to those of known mixtures containing these putative photoproducts, the presence of *p*-hydroxybenzyl alcohol (87) was readily confirmed. The identification of this new photoproduct led to a re-evaluation of the ^{1}H NMR spectra of the photolysis mixtures, which revealed characteristic peaks for this minor product.

Scheme 21. Formation of *p*-Hydroxybenzyl Alcohol (87)[107]

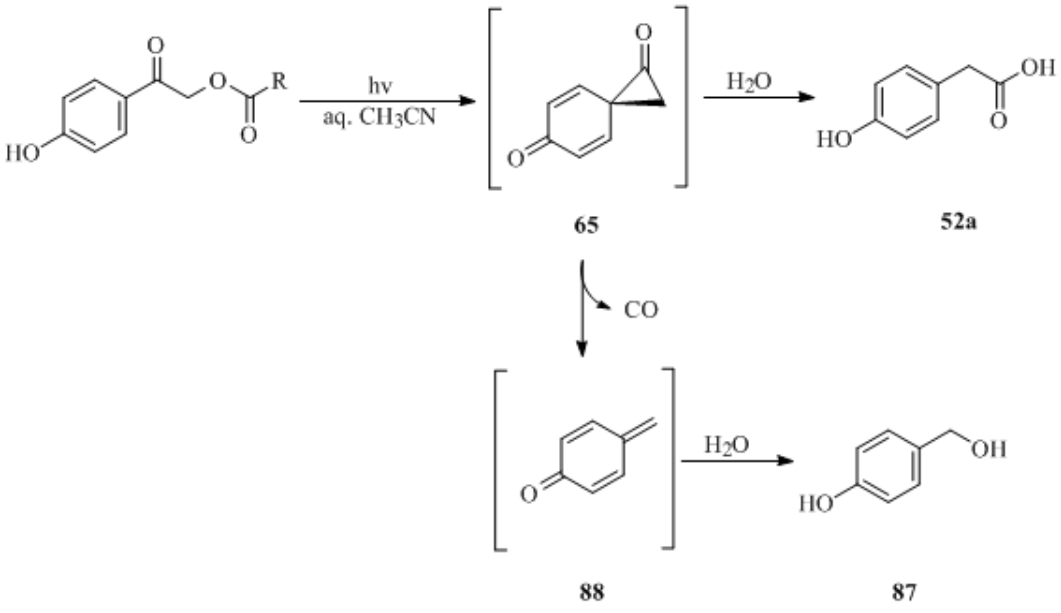

C. Quantum Efficiencies and Rates of Release: Stern-Volmer Quenching Studies

1. pHP Benzoates

Quantum efficiencies for the photolysis of benzoates **70c-e** were determined from peak area ratios for the disappearance of starting material by reverse phase high performance liquid chromatography (RP-HPLC) using biphenyl as the internal standard. Preliminary data showed quantum efficiencies for the disappearance of starting material for this series to be between 0.17 and 0.30. The quantum efficiencies determined using a more sophisticated HPLC apparatus (one equipped with an autosampler, a photo diode array detector, and a specialized C18 column designed for the separation of acid compounds (Waters XTerra)) proved to give more efficient and accurate values than the former instrumental set-up which, was used for determining the quantum efficiencies and for the quenching experiments because it was more sensitive and automated. This increased the reproducibility of the resulting quantum efficiencies for the disappearance of the starting material (Φ_{dis}) and for the appearance of products (Φ_{acid} and Φ_{pHPAA}, **Table 18**). The percent conversion for these reactions

Table 18. Disappearance and Product Appearance Quantum Efficiencies for pHP Benzoate Ester Photolyses

Ester	Benzoate **70c**	$pOCH_3$ Benzoate **70d**	pCF_3 Benzoate **70e**
Φ_{dis}	0.316 ± 0.026	0.288 ± 0.033	0.201 ± 0.044
Φ_{acid}	0.312 ± 0.044	0.263 ± 0.036	0.218 ± 0.062
Φ_{pHPAA}	0.292 ± 0.007	0.242 ± 0.033	0.160 ± 0.029

Samples were photolyzed in quartz tubes at 300 nm without degassing.

was ~ 50%. Very similar values for the quantum efficiencies for the disappearance of starting material and the appearance of each of the two products were observed. This reveals that the substrate photorelease is a primary photochemical reaction and that the photoproducts are stable once they have been formed.

2. pHP Formate and Sulfonates

i. RP-HPLC

Quantum efficiencies were determined using RP-HPLC for the formate ester and for both sulfonate esters. In each case, quantum efficiencies for the disappearance of starting material (Φ_{dis}) and the appearance of the products (Φ_{acid}, Φ_{pHPAA}, Φ_{pHBA}, and Φ_{pHPOH}) were determined using peak area ratios for the appropriate products compared with acetaminophen or biphenyl as the internal standard (**Table 19**). The conversion of these reactions was kept below 20%.

ii. ^{1}H NMR

A photolysis of formate ester **70a** was performed under the same conditions as the product identification experiment only this time the samples were analyzed every 20 minutes in order to monitor the time course of the reaction. Characteristic peak integrations for the starting material (formate **70a**, δ = 5.56 ppm) and products (*p*-hydroxyphenylacetic acid (**52a**), δ = 3.62 ppm; formic acid (**71a**), δ = 8.25) were compared to the peak integrations of the internal standard (DMF, δ = 2.77 ppm).

From this analysis and measurements of the light output, the reaction quantum efficiencies were determined (Φ_{dis} = 0.90; Φ_{acid} = 0.91; Φ_{pHPAA} = 0.88). The percent of conversion of the starting material was found to be 86%. This analysis was useful in that the results showed very similar values for the quantum efficiencies for the disappearance of starting material and the appearance of each of the two products throughout this reaction to this very high conversion. This reveals that the substrate photorelease is a primary photochemical reaction. Therefore, in the RP-HPLC experiments it assumed that the quantum efficiency for the appearance of formic acid (**71a**) would be similar to the quantum efficiency of the disappearance of the starting material.

Table 19. Quantum Efficiencies for pHP Formate and Sulfonate Esters

Ester	Formate 70a[a]	Mesylate 72a[a]	Tosylate 72b[b,c]
Φ_{dis}	0.940 ± 0.116[c]	0.932 ± 0.085[c]	1.04 ± 0.38
Φ_{acid}	0.967[d]	0.955[d]	1.00 ± 0.14
Φ_{pHPAA}	0.813 ± 0.036[c]	0.871 ± 0.011[c]	0.661 ± 0.062
Φ_{pHBA}	0.154 ± 0.012[c]	0.0798 ± 0.0006[c]	0.147 ± 0.008
Φ_{pHPOH}	nd	0.0446 ± 0.0010[c]	0.0243 ± 0.0039

[a]pHP derivatives were photolyzed in 3:1 water/acetonitrile for ^{1}H NMR and HPLC experiments. [b]pHP derivative was photolyzed in 1:1 water/acetonitrile for ^{1}H NMR and HPLC experiments. [c]Quantum efficiencies for all chromophores were determined by RP-HPLC. Samples were photolyzed in quartz test tubes ate 300 nm. [d]Quantum efficiencies were determined by ^{1}H NMR. Samples were photolyzed in Pyrex NMR tubes at 300 nm.

For the sulfonate derivative, the percent of conversion and the quantum efficiencies for the disappearance of starting material (Φ_{dis}) and the appearance of the products (Φ_{acid}, Φ_{pHPAA}, Φ_{pHBA}, and Φ_{pHPOH}) were also determined by ^{1}H NMR. This was done by comparing peak integrations for the methylene peaks of the starting esters (mesylate **72a**, δ = 5.61 ppm; tosylate **72b**, δ = 5.46 ppm) and methyl or methylene peaks of the products (methanesulfonic acid (**89a**), δ = 2.63 ppm; *p*-toluenesulfonic acid (**89b**), δ = 2.55 ppm; *p*-hydroxyphenylacetic acid (**52a**), δ = 3.62 ppm; and *p*-hydroxybenzyl alcohol (**87**), δ = 4.45 ppm) against peak integrations for a methyl group in the internal standard (DMF, δ = 2.77 ppm). Mesylate ester **72a** was examined in more detail using the method employed for formate **70a**. The quantum efficiency for the appearance of the released substrate methanesulfonic acid (**89a**, Φ_{acid}) was only quantified using ^{1}H NMR since it not an UV active chromophore. The results show that the quantum efficiency for the appearance of methanesulfonic acid (**89a**, Φ_{acid}) is similar to that of the disappearance of starting material (Φ_{dis}).

3. Quenching and Sensitation Studies

Quenching experiments using methyl sorbate were performed on benzoate **70c** and pCF_3 benzoate **70e**. At low concentrations of quencher (0 – 0.0001 M), no change in quantum efficiency for benzoate **70c** was observed. As the concentration of the quencher was increased the quantum efficiencies for the disappearance the starting materials and the appearance of products decreased. A Stern-Volmer plot was constructed plotting the quantum efficiency ratio (Φ_0/Φ_x) versus the concentration of

the quencher. The slope of the line is the Stern-Volmer constant (K_{SV}). From the K_{SV}, the triplet lifetime (τ^3) can be calculated by dividing K_{SV} by the rate of diffusion (k_{diff} = 1.33 x 10^{10} s^{-1} (weighted average based upon 7:3 acetonitrile/water solvent system). The average rates of substrate release (benzoate **70c**, k_{dis} = 7.97 x 10^7 s^{-1}; pCF_3 benzoate **70e**, k_{dis} = 2.39 x 10^8 s^{-1}) were calculated by dividing the quantum efficiency with zero quencher present by the triplet lifetime. At quencher concentrations of 0.001 M, solubility of the quencher was poor. The higher levels of quenching could not be attained and another quencher was used. Piperlyene proved to be soluble at the concentrations needed and was easily separated from the other compounds in the reaction mixture. Photolysis of benzoate esters **70c-e** were performed with increasing amounts of quencher (0.0 – 0.08 M) and the Stern-Volmer quenching data analyzed (**Figures 8, 9, and 10**). From the plots, triplet lifetimes and the rates of substrate release and were calculated as described above (**Table 20**).

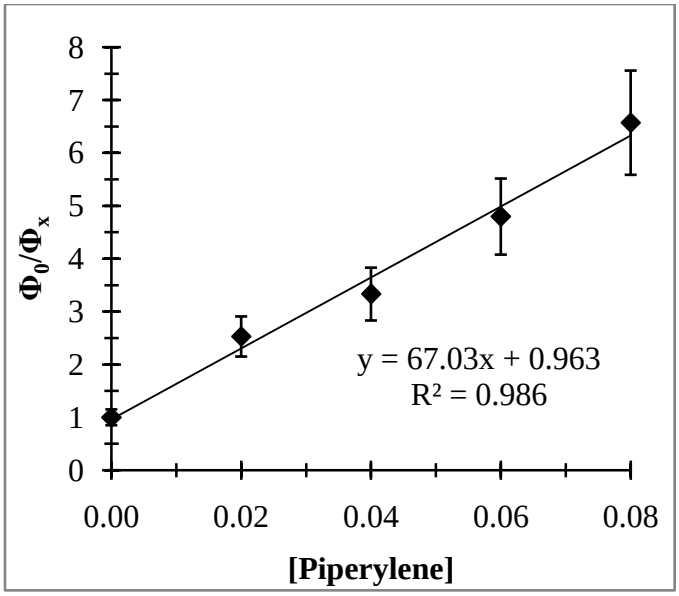

Figure 8. Stern-Volmer Quenching with Piperylene of pHP Benzoate **70c**. Samples irradiated in 7:3 acetonitrile/water at 300 nm for 1 hour.

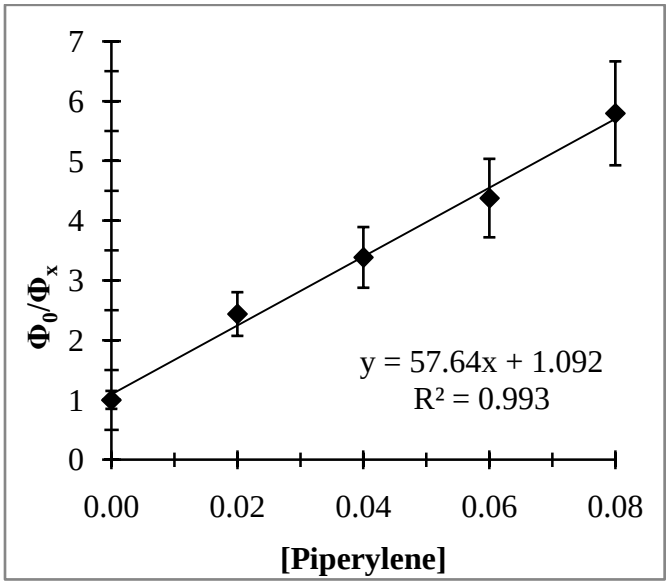

Figure 9. Stern-Volmer Quenching with Piperylene of pHP $pOCH_3$ Benzoate **70d**. Samples irradiated in 7:3 acetonitrile/water at 300 nm for 1 hour.

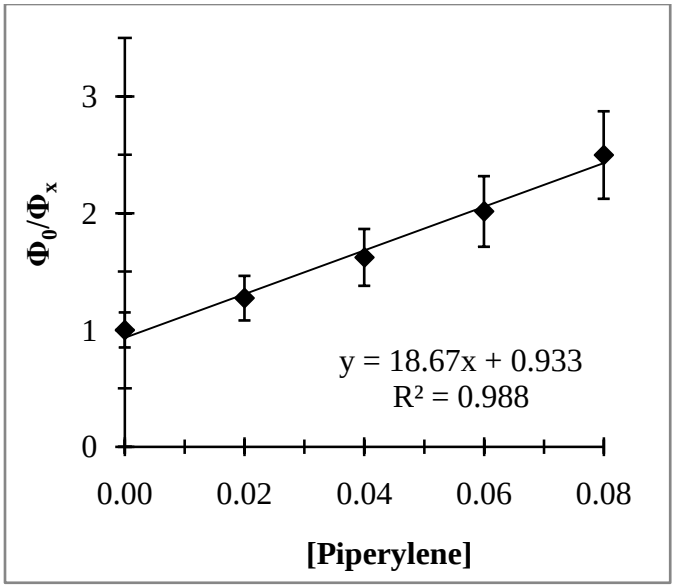

Figure 10. Stern-Volmer Quenching with Piperylene of pHP pCF_3 Benzoate **70e**. Samples irradiated in 7:3 acetonitrile/water at 300 nm for 1 hour.

Table 20. Stern-Volmer Results for Piperylene Quenching of pHP Benzoates

Ester	$\Phi_{dis, [Q] = 0}$	K_{SV}	τ^3 (ns)	k_{rel} (s^{-1})
Benzoate **70c**	0.316	67.0	5.04	6.27×10^7
$pOCH_3$ Benzoate **70d**	0.288	57.7	4.34	6.64×10^7
pCF_3 Benzoate **70e**	0.201	18.7	1.40	1.44×10^8

Samples were photolyzed in quartz test tubes at 300 nm for 1h. Piperylene concentrations ranged from 0 – 0.08 M. The solvent used was 7:3 acetonitrile/water which has a calculated $k_{diff} = 1.33 \times 10^{10}$ M^{-1} s^{-1}.

Quenching of mesylate, tosylate, and formate esters **72a**, **72b**, and **71a** was attempted using triplet quenchers such as potassium sorbate and methyl sorbate, both at very high concentrations of 2.3M and 1.0M, respectively. No quenching was observed for any of the reactions suggesting either the reaction does not proceed through a triplet pathway or that the reaction is too fast to be quenched. This would happen when rate of the triplet reaction is faster than the rate of the bimolecular quenching reaction. Based upon the concentration of the quencher ([potassium sorbate] = 2.3M; [methyl sorbate] = 1.0M) and the rate of diffusion in the mixed solvent system (3:1 water/acetonitrile, $k_{diff} = 9.08 \times 10^9\ M^{-1}s^{-1}$; 95% acetonitrile, $k_{diff} = 1.6 \times 10^{10}\ M^{-1}s^{-1}$) the average rate was calculated to be $k_{diff} = 1.9 \times 10^{10}\ M^{-1}s^{-1}$. If $k_{diff} = 1.9 \times 10^{10}\ M^{-1}s^{-1}$, then in the Stern-Volmer quenching at 1M quencher anything shorter lived than 4.5 ns could not be detected by Stern-Volmer quenching. The rates of the triplet reactions and the triplet lifetimes were later determined using picosecond pump-probe spectroscopy. All of the triplet lifetimes were less than 1 ns (*vide infra*).

Esters **70a**, **72a**, and **72b** were photolyzed to 100% conversion in acetone, a known triplet sensitizer, and analyzed by RP-HPLC. The major products observed in all three reactions were *p*-hydroxyphenylacetic acid (**52a**) and *p*-hydroxybenzyl alcohol (**87**) and in the case of tosylate **72b**, *p*-toluenesulfonic acid (**89b**) was also observed. *p*-Hydroxyacetophenone (**62**) was also observed as a product in these reactions but was only a minor product. From these experiments it was deduced that the reaction pathway is through the triplet and that 2,4'-dihydroxyacetophenone (**63**) only formed when water is present, may be a hydrolysis product from either a ground

state or an excited singlet state reaction. The quantum efficiencies were lower than those observed in aqueous organic solvents (mesylate **72a**, Φ_{dis} = 0.40; tosylate **72b**, Φ_{dis} = 0.32; formate **70a**, Φ_{dis} = 0.23). This can be explained by examining the solvent used in the analysis. As mentioned earlier, photolysis reactions in wholly organic solvents undergo a radical reaction pathway and suffer from low quantum efficiencies. When water is present, an ionic pathway with high quantum efficiencies prevails. The acetone used in these reactions was ACS grade and contained ~ 5% water, per the label. If dry acetone had been used, different products and much lower quantum efficiencies would be expected. However since the acetone contained some water, the ionic pathway dominated, based upon the observed product ratio of 5:1 for *p*-hydroxyphenylacetic acid (**52a**) to *p*-hydroxyacetophenone (**62**), but lower quantum efficiencies were observed.

D. Laser Flash Photolysis Studies

1. LFP Results: Detection of the Biradical Intermediate

Another tool available in the exploration of the photorelease reaction is laser flash photolysis (LFP) using picosecond and nanosecond pump-probe optical spectroscopy. Samples of several pHP derivatives including the benzoates, formate, and sulfonates were sent to Dr. Jakob Wirz and his colleagues at the Institut für Physikalische Chemie der Universität Basel for LFP analysis. The rates of triplet decay ($k_{\tau 3\ decay}$) were measured for each of the benzoates (benzoate **70c**, $k_{\tau 3\ decay}$ = 2.2 x 10^7 s^{-1}; $pOCH_3$ benzoate **70d**, $k_{\tau 3\ decay}$ = 1.2x 10^9 s^{-1}; pCF_3 benzoate **70e**, $k_{\tau 3\ decay}$ =

7.7 x 10^8 s^{-1}). From these measurements, the triplet lifetime (τ^3) could be calculated by taking the reciprocal of the rate of triplet decay (benzoate **70c**, τ^3 = 45.5 ns; $pOCH_3$ benzoate **70d**, τ^3 = 0.833 ns; and pCF_3 benzoate **70e**, τ^3 = 1.30 ns). It was noted that benzoate **70c** has a very long-lived triplet (τ^3 = 45.5 ns) and that it could possibly be quenched by oxygen.

Table 21. LFP Results for pHP Derivatives

pHP derivative	S^1, λ_{max} (nm)	T^1, λ_{max} (nm)	$k_{\tau 3\ rise}$	k_{ISC} (s^{-1})	$k_{\tau 3\ decay}$ (s^{-1})	τ^3 (ns)
Mesylate **72a**	320	412, 430	na	4.6 x 10^{11}	8.5 x 10^9	0.118
Tosylate **72b**	313	420	na	4.5 x 10^{11}	9.6 x 10^9	0.104
Diethyl Phosphate **51a**	313	424, 535	na	4.2 x 10^{11}	2.9 x 10^9	0.345
pCF_3 Benzoate **70e**	314	401	1.5 x 10^{10}	3.2 x 10^{11}	1.6 x 10^9	0.625
Formate **70a**	314	414	2.4 x 10^{10}	3.8 x 10^{11}	1.5 x 10^9	0.667
$pOCH_3$ Benzoate **70d**	314	408	1.4 x 10^{10}	2.8 x 10^{11}	1.2 x 10^9	0.833
Benzoate **70c**	312	405	9.0 x 10^9	3.8 x 10^{11}	8.6 x 10^8	1.16
GABA **57b**	315	400, 510	1.2 x 10^{10}	2.6 x 10^9	2.9 x 10^9	0.345
pCN Phenolate	314	422, 410	7.8 x 10^9	4.3 x 10^{11}	6.9 x 10^8	1.45
Phenolate	315	401, 422	2.8 x 10^{10}	5.3 x 10^{11}	2.6 x 10^8	3.85

Details of the analysis are given in the Experimental Section.

Wirz and Heger[109] summarize their findings for these pHP derivatives and for several other derivatives (**Table 21**). In the explanation of their analysis it was noted that the transient absorption maxima were observed for both the singlet and triplet excited states (singlet, λ_{max} = 315 nm; triplet, λ_{max} = 400 nm, 420 nm, and a broad, weak shoulder with a maximum around 510 nm); that intersystem crossing (ISC) occurred in all cases and was very fast (k_{ISC} = 2 x 10^{11} – 4 x 10^{11} s^{-1}); and that there were often delays in the rise of the triplet band ($k_{\tau 3\ rise}$ ~ 1 x 10^{10} s^{-1}) that could not be explained. It was also noted that as the triplet decays ($k_{\tau 3\ decay}$ = 7 x 10^{8} – 2 x 10^{10} s^{-1}) a new series of absorptions is revealed that are assigned biradical **89** (λ_{max} = 445, 420, and 330 nm, Equation **32**) which also rapidly decay (k_b = 1.5 x 10^{9} s^{-1}) and an unknown species (large band around 340 nm) whose decay varies with each derivative. The biradical was readily apparent for the mesylate **72a**, tosylate **72b**, and

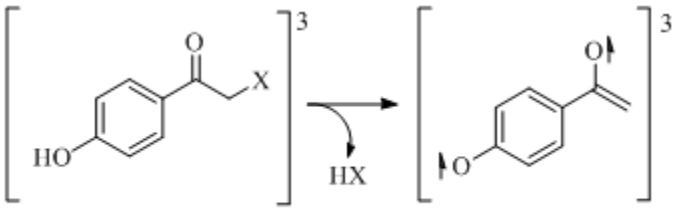

89

Equation 32.

diethyl phosphate **51a** derivatives while the unknown species was more easily detected with the benzoates and substituted phenol derivatives. Formate ester 70a,

once resolved, showed the presence of both the biradical and the unknown species. It was suggested that the rise of the unknown species with the band at 340 nm is from a competitive reaction via the triplet. This is based upon a comparison of the quantum efficiencies of the derivatives without the 340 nm band present (Φ_{dis} ~ 1) and those with the band present (Φ_{dis} ~ 0.1 – 0.4). In order for this assumption to be correct, formate 71a and the GABA 58b derivative should have quantum efficiencies less than one. The quantum efficiency for the GABA derivative (Φ_{dis} = 0.21) supports this hypothesis but the quantum efficiency for the formate ester (Φ_{dis} = 0.940) does not.

2. Oxygen Effects

In order to find out if oxygen does quench the photorelease of benzoic acid, an oxygen quenching trial was performed using benzoate **70c** in an effort to see what effect dissolved oxygen had on the photochemical reaction. Three test tubes were set up using the same conditions as the previous quantum yield experiments. One test tube was purged with oxygen for 15 min, the second was purged with argon for 15 min, and the third was left open to the atmosphere. Each tube was irradiated in a manner similar to the quantum yield determination experiments, removing an aliquot every 2 min for 18 min. The aliquots were analyzed on the Waters Aquity UPLC and their quantum efficiencies determined. The quantum efficiencies for the disappearance of starting material (Φ_{dis}) for the argon degassed, atmospheric oxygen, and oxygen saturated samples were 0.352 ± 0.042, 0.334 ± 0.040, and 0.317 ± 0.038 respectively suggesting no quenching was observed. A Stern-Volmer plot was

constructed by plotting the quantum efficiency ratio of zero quencher to that with quencher against the concentration of O_2 in solution. The concentration of the saturated oxygen solution was calculated taking the weighted average of the solubility of oxygen in acetonitrile[108] (8.21mM) and in water[108] (1.28mM) to reflect the 7:3 acetonitrile/water solvent system. This number was multiplied by 0.2 to calculate the amount of dissolved oxygen in the atmospheric oxygen sample. The Stern-Volmer plot produced the Stern-Volmer constant (K_{SV} = 16.17) from which the triplet lifetime (τ^3 = 1.2 ns) and the disappearance rate (k_{dis} = 2.9 x 10^8 s^{-1}) could be calculated. The similarities of the quantum efficiencies obtained in this experiment led to the reinvestigation of the benzoates using laser flash photolysis revealing faster rates of decay and shorter triplet lifetimes for benzoate **70c** ($k_{\tau 3\ decay}$ = 8.6 x 10^8 s^{-1}, τ^3 = 1.2 ns) and for pCF_3 benzoate **70e** ($k_{\tau 3\ decay}$ = 1.0 x 10^9 s^{-1}, τ^3 = 1.0 ns). The triplet lifetimes match and both the release rates and quantum efficiencies are similar suggesting that oxygen does not quench the reaction. The error bars in the Stern-Volmer plot are very large, which questions the validity of the correlation.

3. pH Rate Profile.

A pH rate profile of each of the esters was desired. The low water solubility of the benzoates made them undesirable for a pH study because buffer solutions require water, limiting the study to pHP formate **70a**, mesylate **72a**, and tosylate **72b**.

When pHP formate **70a** was dissolved in ammonium acetate buffers at acidic, neutral and basic pHs, an absorption band at ~ 327 nm appeared (**Table 22**). This red

shifted band was identified as belonging to the conjugate base of the formate ester in which the phenol is no longer protonated based upon the information obtained about other pHP derivatives in aqueous buffer solutions[110]. The spectra at pH 3 and 7 show bands indicative of both the protonated and non-protonated species. The conjugate base of mesylate ester **72a** is not observed under neutral conditions but is observed under basic conditions along with the protonated species. The conjugate base of tosylate ester **72b** is not observed in any of the buffered solutions. From the spectra and photolysis experiments it was determined that ammonium acetate is not a good buffer when formate **70a,** mesylate **72a**, and tosylate **72b** esters are present in mixed solvent solutions. Phosphate buffers had been studied in mixed solvent systems[111] and had a wide range of pH's where it could be used. Mesylate **72a** was dissolved in solutions made up with buffers at pH 3, 7, and 12 and the UV-VIS spectra were obtained. This buffer had the desired effect of only the protonated species being present under acidic conditions, only the conjugate base being present under basic conditions, and a mixture of the two species being present under neutral conditions. The mesylate was photolyzed under these varying conditions.

Table 22. UV-VIS Absorption Maxima (λ_{max}) and Extinction Coefficients (log ε) of pHP Derivatives in Buffered Solutions

	Ammonium Acetate Buffer		
pHP Derivative	pH 3	pH 7	pH 11
Formate **70a**	267 (4.97); 2.16 (4.70)	329 (4.09); 292 (3.95)	324 (4.38); 236 (3.02)
Mesylate **72a**	268 (3.76)	264 (4.93)	331 (3.50); 265 (4.16)
Tosylate **72b**	280 (3.24); 231 (3.06)	264 (4.15)	264 (5.08)
	Phosphate Buffer		
	pH 3	pH 7	pH 12
Mesylate **72a**	283 (4.27); 221 (4.13)	286 (4.22); 221 (4.13)	330 (4.48); 237 (4.10)

Buffered solutions (0.01 M) were made in 3:1 water/acetonitrile binary solvent systems. nd = not determined.

The pH profile of a series of pHP GABA derivatives has been obtained.[110] The data reveal a drop in the quantum efficiency of the photorelease reaction as the pH increases. Several attempts were made to photolyze sulfonate esters **72a** and **72b** and formate ester **70a** in buffered solutions. Using pH paper, the pH of the reaction solution was measured before photolysis and then again afterward. Each reaction experienced a change in pH, according to the pH paper, suggesting that the ammonium acetate buffer (0.010 M) was not able to keep the solution at a constant pH. Mesylate ester **72a** was examined in more detail and the quantum efficiencies for the disappearance of starting material were measured (pH 3, Φ_{dis} = 0.782; pH 7, Φ_{dis} = 0.646; pH 11, Φ_{dis} = 0.313). These values follow the expected trend but their validity was questioned because of the inability of the buffer to maintain the pH.

A second experiment using a phosphate buffer was performed. Buffered solutions (1.33×10^{-2} M) were made using sodium phosphate and the pH was adjusted to 3.00, 7.06, or 12.02 using phosphoric acid or saturated sodium hydroxide. These solutions were diluted with acetonitrile to make buffered solutions (0.010 M) in a 3:1 solution of water/acetonitrile. The pH of the solution was measured using a Fischer Scientific 510 pH meter equipped with an Accumet Glass Combination electrode that had been calibrated with authentic Fischer buffers giving 3.38, 7.56, and 12.45. McCalley and coworkers[112] note that many buffers are neutral or anionic acids, such as phosphate or borate, and generally show increasing pK_a with organic modifier/solvent concentrations. This shift occurs for the buffer, relative to the aqueous pH, due to a change of dissociation of the buffer with the organic modifier concentration. Mesylate **72a** was added (1.00×10^{-3} M) and the pH of the solution was again measured giving 3.32, 7.50, and 12.37. pH paper also was used to measure the pH of the beginning and ending reaction mixtures so that changes could be noted. Photolyses were performed irradiating samples made with phosphate buffer pH 3 at 254 nm and at 300 nm. The pH for these reactions held steady, according to the pH paper. The quantum efficiencies for the disappearance of starting material and the appearance of the products were measured (**Table 23**). Samples of mesylate **72a** in phosphate buffer pH 7 were irradiated at 300 nm and at 350 nm and the quantum efficiencies measured. Again, according to the pH paper, there was no change in the pH during the reaction. When the pH paper was tested after the reactions at pH 12 which had been irradiated at 300 nm and 254 nm, a color change occurred indicating

that the pH of the solution had become much more acidic. The results of the samples irradiated at 300 nm give us information about the reaction at a broader pH range than the experiments where the samples were irradiated at 254 nm and 350 nm and will be the focus.

Table 23. Quantum Efficiencies of pHP Mesylate **72a** at Different pHs

pH	Φ	λ_{excite} = 254 nm	λ_{excite} = 300 nm	λ_{excite} = 350 nm
3.4	Φ_{dis}	0.424 ± 0.141	0.786 ± 0.050	NA
	Φ_{pHPAA}	0.469± 0.256	0.784 ± 0.050	NA
	Φ_{pHBA}	0.0541± 0.0059	0.0256 ± 0.0029	NA
	Φ_{pHPOH}	0.0315± 0.0102	0.0496 ± 0.0033	NA
7.6	Φ_{dis}	NA	0.415 ± 0.092	0.275 ± 0.027
	Φ_{pHPAA}	NA	0.375 ± 0.027	0.282 ± 0.011
	Φ_{pHBA}	NA	0.0338 ± 0.0065	0.0229 ± 0.0017
	Φ_{pHPOH}	NA	0.0257 ± 0.0021	not linear
12.5	Φ_{dis}	NA	0.481 ± 0.034	0.391 ± 0.041
	Φ_{pHPAA}	NA	0.427 ± 0.029	0.215 ± 0.003
	Φ_{pHBA}	NA	0.0748 ± 0.0252	0.0409 ± 0.0017

The solvent system was 3:1 aqueous buffer/acetonitrile and all photolyses were carried out in quartz tubes. Φ_{dis} = disappearance of starting material; Φ_{pHPAA} = appearance of *p*-hydroxyphenylacetic acid (**52a**); Φ_{pHBA} = appearance of *p*-hydroxybenzyl alcohol (**87**); Φ_{pHPOH} = appearance of 2,4'-dihydroxy-acetophenone (**63**)

The results from the experiments performed at pH 3 and 7 are consistent with the results obtained for the pHP GABA derivatives in that the lower quantum efficiencies were observed at the higher pH. The quantum efficiencies measured at pH 12 do not fit with this observation and have slightly higher values than those

measured at pH 7. This is the result of an unstable pH due to buffer override and the lack of stability of mesylate **72a** at this pH. It is interesting to note the quantum efficiencies for the disappearance of starting material in the ammonium acetate solution (pH 7, $\Phi_{dis} = 0.646$) and in the phosphate buffer solution (pH 7, $\Phi_{dis} = 0.786$) are somewhat similar and that they are lower than was measured in non-buffered solutions. This difference can be attributed to the differences in the interactions between the solutes, phosphate buffer and pHP mesylate, with the binary solvent systems like water and acetonitrile or methanol.

It is common practice to measure the pH of the aqueous buffer prior to combining it with an organic solvent. Although this is a reproducible means of preparing buffers in a binary solvent system, the organic solvent can alter the pKa of the analyte/buffer and thus the pH of the solution. The use of a hydrogen electrode to measure the pH of water/acetonitrile solutions is not appropriate because of its poor response in contact with acetonitrile[113,114]. The electrode used in the measurements of pH is a glass electrode which measures the concentration of H^+ in solution thus the measurements reported above are inaccurate. In their determination of accurate pH values for reference primary standard buffer solutions in aqueous acetonitrile, Barbosa and Sanz-Nebot report evidence of preferential solvation of the buffer by the binary solvent system[111]. Preferential solvation is where a solute interacts with one of the solvents more strongly than with the other, the solute is preferentially solvated by the former. This interaction was clearly demonstrated by the lower than expected pH values of the buffer in aqueous acetonitrile when compared to solvent systems where

the "preferred" solvent was water thus changing the nature of the interactions of the buffered solution. The photorelease reaction is solvent sensitive and the ramifications of preferential solvation when binary solvent buffer systems are used are unclear. Even with inaccurate pH values, the quantum yields were measured under acidic, neutral, and basic conditions. This was verified from the shift of the λ_{max} in the UV-VIS spectra due to the relative concentrations of the pHP ester and its conjugate base.

E. Role of the Conjugate Base of pHP Chromophore

The proposed mechanism of photorelease[110] (**Scheme 22**) of the conjugate base species starts with irradiation of the pHP ester anion to a singlet excited state **90**. In this reaction mechanism, the excited state can fluoresce and return to the ground state (k_f) or intersystem cross to the triplet-excited state **91**. The triplet also has two reaction pathways it can follow. It can relax back to the ground state (k_d) or release the substrate resulting in spirodienedione intermediate **65**. From this point, the mechanism mirrors the steps taken in the formation of *p*-hydroxyphenylacetic acid (**52a**) and *p*-hydroxybenzyl alcohol (**87**, **Scheme 21**) with the subsequent reactions of spirodienedione intermediate **65**. It is suspected that lower quantum efficiencies observed for this reaction are due to the propensity of the excited states to relax back to the ground state rather than intersystem cross or undergo release the substrate.

Scheme 22. Proposed Mechanism of Photorelease from Conjugate Base of pHP Esters[110]

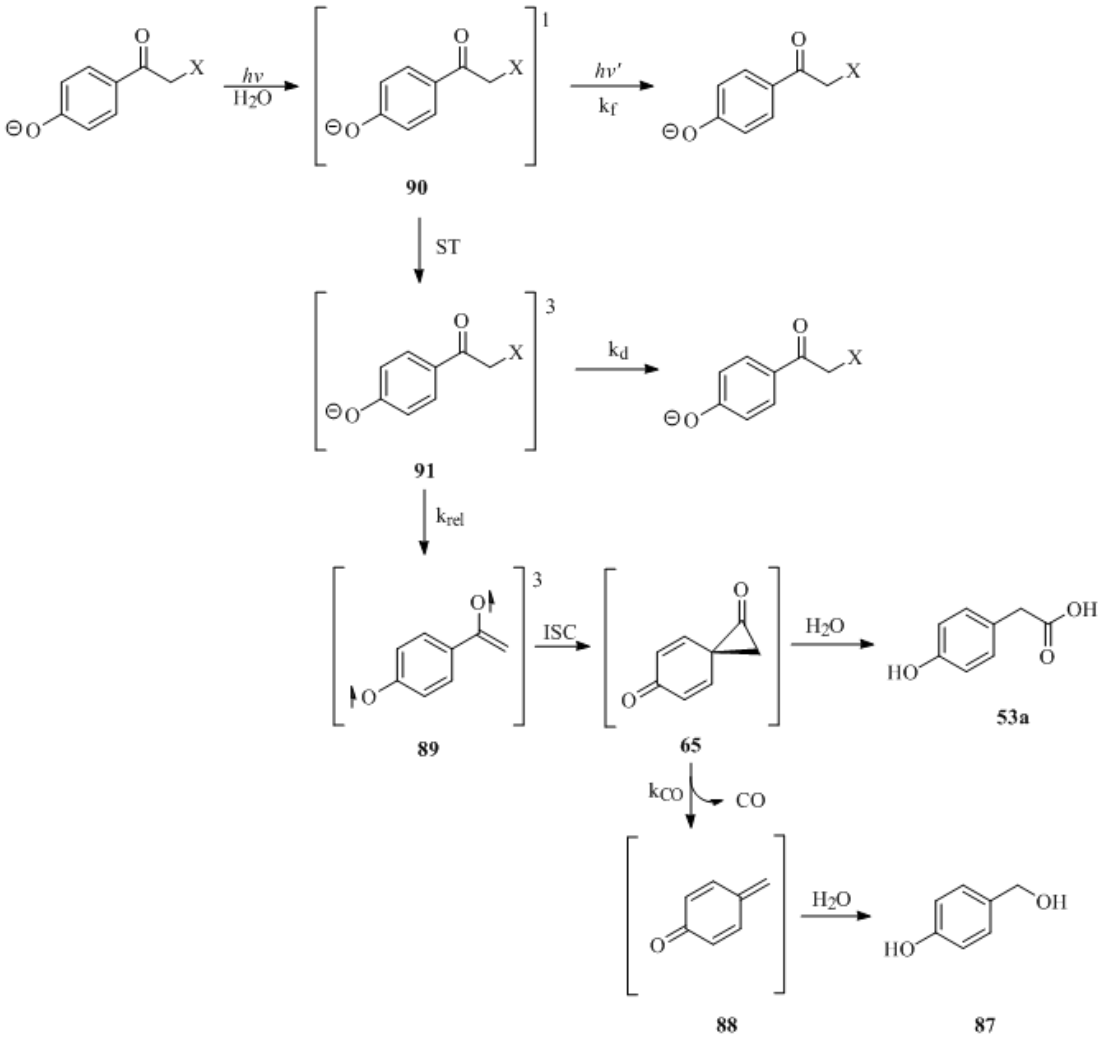

F. Time Resolved UV-VIS Spectra

1. LFP Spectra

Time resolved UV-VIS spectra for pHP benzoate **70c** (**Figure 11**) and tosylate **72b** (**Figure 12**) clearly exposed the sequence of events for the pHP photorearrangements of these esters. In each of the spectra, the rapid decay of the singlet was observed along with the rise of the triplet. The calculated triplet lifetimes for the benzoate (1.16 ns) and the tosylate (0.104 ns) are easily observed in these spectra.

Upon closer examination of the spectra of the protonated tosylate, it was realized that all of the attempts to quench the reaction failed because the reaction from the triplet ester is too fast ($k_{\tau 3\ decay} = 9.6 \times 10^9\ s^{-1}$) for bimolecular quenching (*vide supra*) and not because the reaction proceeds through a singlet state process. The decay of the triplet of the protonated triplet ester resulted in bands at 445, 420, and 330 nm, which correspond to a transient species that was observed in the tosylate **72b**, mesylate **72a**, and diethyl phosphate **51a** spectra. These absorption bands and lifetime of this intermediate are similar to those of the phenoxyl radical described by Radziszewski and coworkers[115] and thus have been assigned to triplet biradical **93**. From the information obtained from spectral data and calculations cyclization of biradical **93** to spirodienedione **65** occurs immediately following intersystem crossing[107]

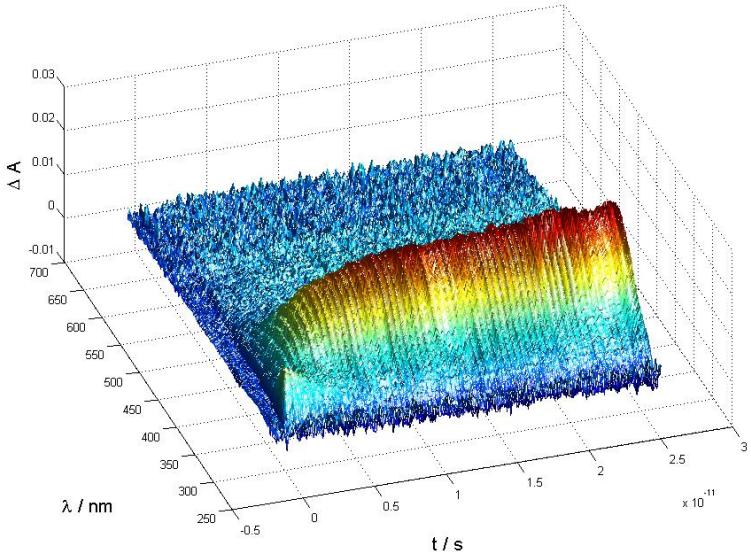

Figure 11. Time Resolved Spectra for pHP Benzoate **70c**. Picosecond transient absorption spectra were measured for pHP benzoate **70c** in aqueous acetonitrile (λ_{excite} = 266 nm).

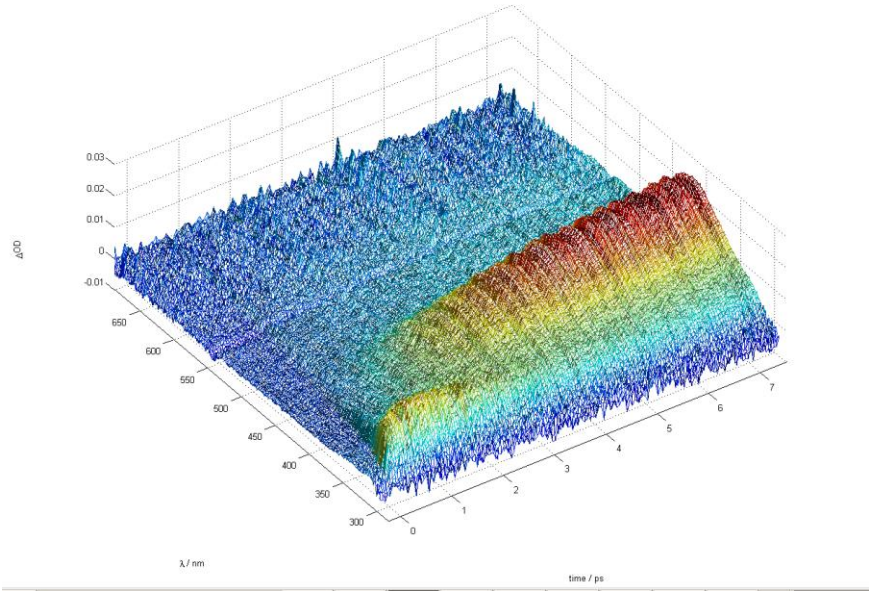

Figure 12. Time Resolved Spectra for pHP Tosylate **72b**. Picosecond transient absorption spectra were measured for pHP tosylate **72b** in aqueous acetonitrile (λ_{excite} = 266 nm).

2. Stern-Volmer Lifetime and Rate Comparison with LFP Results

A comparison between the release rates and triplet lifetimes for the Stern-Volmer quenching data and the laser flash data were made for the benzoate series and significant differences in the results were noted (**Table 24**). These differences are the result of the different photolysis conditions present in the Rayonet reactor versus picosecond pump-probe optical spectroscopy. The first major difference in the reactor is the light source. The Rayonet photoreactor uses RPR 3500, 3000, or 2540 fluorescent tubes. The latter is the mercury tube and has a fairly narrow emission range centered at 254 nm. The other two have broader emission bands (around 50 – 100 nm) and are centered at 350 nm and at 300 nm. The quantum efficiencies and Stern-Volmer studies may reflect the excitation of more than one chromophore for a

Table 24. Comparison of Stern-Volmer Quenching and Laser Flash Photolysis

	Stern-Volmer Quenching		Laser Flash Photolysis	
pHP Derivative	k_{dis} (s^{-1})	τ^3 (ns)	k_{dis} (s^{-1})	τ^3 (ns)
Benzoate **70c**	6.27×10^7	5.04	8.6×10^8	1.16
$pOCH_3$ Benzoate **70d**	6.64×10^7	4.34	1.2×10^9	0.883
pCF_3 Benzoate **70e**	1.44×10^8	1.4	1.6×10^9	0.625

given pHP derivative due to the broad emission band, which could encompass both the protonated phenolic group and its conjugate base. In comparison, the laser studies use an excitation wavelength of 266 nm which will excite a different ratio of absorptivities of the two tautomers or just be one tautomer, likely the protonated form from spectral analysis of several pHP analogs. The variation in the ratio of

acetonitrile to water in the mixed solvents may also be leading to some of the discrepancies. Several different ratios of water to acetonitrile were used (3:1. 1:1, and 3:7) depending upon the solubility limits of the more hydrophobic derivatives. The laser experiments were performed in either water or in water/acetonitrile mixed solvent systems where the solvent ratio was not recorded. These solvent mixture variations have two effects with the first being the ratio of the protonated species to the conjugate base species of the pHP ester. In solvent systems with a high organic content, the protonated species will be the dominant species present. However, as more water is added, the amount of the conjugate base species increases. The second effect of the solvent mixture variations pertains to the lifetime of the excited triplet (τ^3). Phillips ans coworkers have conclusively shown that as the amount of water increases the triplet lifetime decreases.[67] Thus modifying the solvent system affects the results of the individual experiments. Because the system is so sensitive to the solvent ratio of water to an organic component, the Stern-Volmer quenching may not be an accurate measure of the triplet lifetime even if after correcting for its effect on the diffusion rate. As more organic quencher is increasingly added (i.e., piperylene), the lifetime may increase as an effect of the added piperylene hydrocarbon giving a false measure of the bimolecular rate for energy transfer. These two factors are possible reasons for the discrepancy between the experimental results in the kinetic experiments for the benzoate series of derivatives.

G. Structural Dynamic of pHP Photochemistry

1. Ground State X-Ray Structures

In the identification of the formate, benzoate, and sulfonate esters, X-ray crystal structures were obtained in order to confirm their structure (**Figures 3 – 7**). Of the six derivatives, five resulted in crystals that were suitable for analysis but one, pCF_3 benzoate **70e**, did not. The data for each derivative were used to generate 2D and 3D structures and information about atomic coordinates, bond lengths, bond angles, hydrogen coordinates, torsion angles, and hydrogen bonds (**Appendices A and B**). The data provide the conformations of the esters in their crystalline ground states which reveal certain similarities. A qualitative comparison shows that the chromophore is planar and hydrogen bonds between neighboring molecules form planar sheets of the array. These sheets also show π-stacking between the planes. A quantitative comparison of dihedral bond angles (D1 and D2) emphasizes this and gives more detailed information about the structure of the molecule. Although there is no X-ray diffraction data published for pHP acetate **60**, the crystal structure for pHP formate **70a** has been obtained. Comparisons between the ground state conformations (crystal formate **70a** versus calculated acetate **60**) show similarities, especially in the dihedral bond angle (acetate **60**, D1 = 176°; formate **70a**, D1 = 173°).

The dihedral angle (D1) between the aryl carbon (C4), the carbonyl carbon (C3) and methylene carbon (C2) of the acyl group, and the oxygen (O1) of the leaving group (**Figure 13**) is essentially 0° in the x-ray crystal structures of pHP formate, benzoate, and sulfonate esters (**Table 25**). This places the chromophore's

aryl ring, the acyl group, and the oxygen of the leaving group all in the same plane. These values agree with those obtained by Phillips and coworkers in their calculation of the optimized structure of pHP acetate **60**[77] (**Table 24**, **Figure 14**) and pHP diethyl phosphate **51a**[67] (**Table 24**).

Figure 13. Numbering of Atoms in X-Ray Crystal Structures of pHP Carboxylates and Sulfonates.

2. Structural Changes in the Triplet Excited State

Phillips and coworkers also determined the structure of acetate ester **60** in its triplet state by both DFT calculations and by time-resolved resonance Raman spectroscopy. A comparison between the ground and triplet state structures reveal several changes in the bond lengths and bond angles within the chromophore (**Table 26**). One such change occurs in the aryl C-C bonds near the carbonyl (C1-C6 and C5-C6) which are lengthened by ~0.03 Å. Another change occurred in the acyl carbonyl C-O bond (C8-O11) which is lengthened by ~0.01 Å making it similar to the C-O single bond (C10-O10) of the acetate leaving group at ~1.35 Å. Other changes

include the shortening of the C-C bond between the aryl carbon and the carbonyl carbon of the acyl group by ~0.06 Å, the shortening of the C-C bond of the phenacyl group (C8-C9) by ~0.04 Å, and the lengthening of the C-O bond between the methylene carbon of the acyl group and the oxygen of the leaving group by ~0.05 Å. This comparison between the ground and triplet state also reveals that there are no changes in the substructure of the acetate leaving group.

Table 25. Dihedral Angles for pHP Derivatives

pHP Derivative	D1 (°)		D2 (°)		Φ_{dis}
$pOCH_3$ Benzoate **70d**[a]	C4-C3-C2-O1	179.47	C3-C2-O1-C1	71.84	0.29
Benzoate **70c**[a]	C4-C3-C2-O1	178.0(2)	C3-C2-O1-C1	74.5(3)	0.32
Acetate **60**[b]	C6-C8-C9-O10	176.0	C8-C9-O10-C12	82.3	0.4
Diethyl Phosphate **51a**[b]	O5-C10-C11-C13	164.5	P1-O5-C10-C11	91.3	0.4
Formate **70a**[a]	C4-C3-C2-O1	172.58(8)	C3-C2-O1-C1	179.89(9)	0.94
Tosylate **72b**[a]	C3-C2-C1-O1	175.1(4)	C2-C1-O1-S	178.3	1.04
Mesylate **72a**[a]	C3-C2-C1-O1	180.0	C2-C1-O1-S	180.0	0.93

[a]Obtained from x-ray diffraction data.
[b]Values obtained by theoretical calculations[65,67].

Table 26. Calculated Structural Parameters of the Ground and Triplet State of pHP Acetate **60**[77]

bond length (Å)			bond angle (°)			dihedral angle (°)		
	S^0	T^1		S^0	T^1		S^0	T^1
C1-C2	1.382	1.376	C1-C2-C3	119.7	120.2	C1-C2-C3-C4	0.0	0.7
C2-C3	1.401	1.403	C2-C3-C4	120.0	119.6	C2-C3-C4-C5	-0.1	0.5
C3-C4	1.398	1.407	C-3-C4-C5	119.8	120.8	C3-C4-C5-C6	0.1	-2.6
C4-C5	1.389	1.379	C4-C5-C6	120.9	120.5	C4-C5-C6-C1	0.0	3.5
C5-C6	1.401	1.427	C5-C6-C1	118.4	117.5	C4-C5-C6-C8	180.0	-178.8
C6-C1	1.405	1.432	C6-C1-C2	121.2	121.3	C5-C6-C8-C9	1.7	15.0
C6-C8	1.488	1.428	C6-C8-C9	117.8	126.7	C5-C6-C8-O11	-178.4	-159.6
C8-C9	1.537	1.497	C5-C6-C8	123.3	123.0	C1-C2-C3-O7	180.0	-179.3
C12-C14	1.504	1.508	C8-C9-O10	110.8	113.2	C4-C3-O7-H19	0.1	-1.1
C9-O10	1.422	1.465	C9-O10-C12	115.9	117.8	C6-C8-C9-O10	176.0	-103.2
C12-O10	1.362	1.35	O10-C12-C14	110.4	110.6	C8-C9-O10-C12	82.3	101.4
C3-O7	1.358	1.361	O10-C12-O13	123.4	124.3	C9-O10-C12-C14	-171.5	-178.8
C8-O11	1.213	1.315	C6-C8-O11	122.2	116.9	C9-O10-C12-O13	8.5	1.4
C12-O13	1.203	1.208	C3-O7-H19	109.7	109.5			
C9-H20	1.092	1.09	C2-O7-H19	117.3	117.7			
C9-H21	1.093	1.089	C8-C9-H20	110.3	109.8			
O7-H19	0.963	0.963	C8-C9-H21	109.7	110.4			
			C9-C8-O11	120.0	116.2			

In addition to the changes in the bond lengths, conformational changes within the chromophore and between the chromophore and the leaving group became prominent. In the ground state, the dihedral angle (D1) between the aryl carbon (C6), the carbonyl carbon (C8) and methylene carbon (C9) of the acyl group, and the oxygen (O10) of the leaving group (**Figure 14**) are nearly in the same plane (D1 = 176°). However, in the triplet state (**Figure 15**) the plane constituted of the acyl

group, the carbonyl and the methylene carbon (O11-C8-C9), twists out of the plane of the ring by ~20° and the leaving group oxygen deviates significantly from the ring plane ($D1^3$ = -103°). This has the effect of positioning the leaving group in an orientation that is 90° out of the plane of the acyl group. This twist aligns the aryl ring of the chromophore and the leaving group in the same plane. The leaving group is in a favorable stereoelectronic orientation for fragmentation.

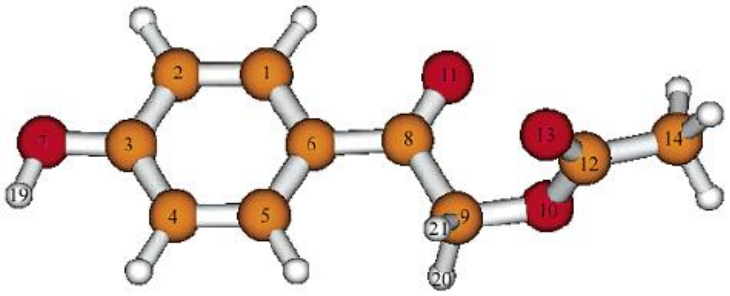

Figure 14. Optimized Structure of Ground State pHP Acetate **60**. Calculated from DFT calculation using B3LYP methods with a 6-311G** basis set. (Reprinted with permission from Reference 77. Copyright 2004 American Chemical Society.)

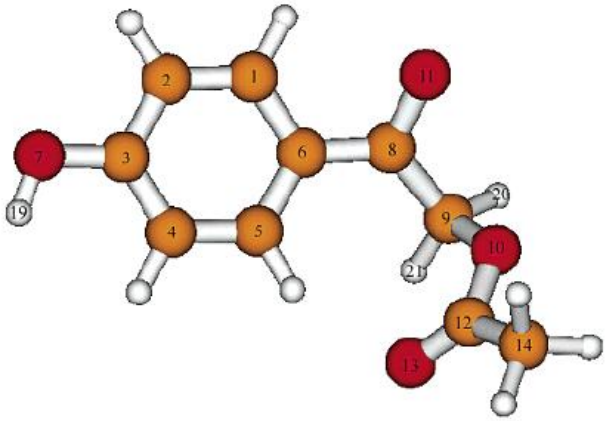

Figure 15. Optimized Structure of Triplet pHP Acetate **60**. Calculated from DFT calculation using UB3LYP methods with a 6-311G** basis set. (Reprinted with permission from Reference 77. Copyright 2004 American Chemical Society.)

This suggests that the formate ester 70a should undergo changes similar to those exhibited by the acetate 60 in going from the ground state to the triplet state. In fact, this can be suggested for the other pHP derivatives as well based upon their dihedral angles (**Table 25**).

Another angle of interest is the angle between the carbonyl and methylene carbons of the acyl group of the chromophore and the carboxylate (O-C), sulfonate (O-S), or phosphate (O-P) of the leaving group (D2, atoms in bond defined in Table 23). When the quantum efficiencies of these derivatives are compared with the D2 angle, a trend emerges; when the molecule is essentially planar (D2 ~ 180°) in the ground (crystalline) state, the quantum efficiency for the reaction is high (**Table 25**). The ground state of the mesylate is planar and the tosylate and formate are essentially planar. The conformation of the triplet ester that favors substrate release is believed to be one where the aryl ring and the carboxylate or sulfonate of the leaving group are in the same plane whereas the acyl plane of the chromophore is canted out of the plane by about 20°. Since the aryl ring and formate or sulfonate leaving groups are already planar, the rotational barrier to reach the favorable stereoelectronic state is lessened. Whereas in the benzoates, the benzoate leaving group is canted out of the plane of the aryl group and in order to reach the desired triplet conformation high rotational barriers must be overcome to rotate both the acyl and carboxylate groups. It is conceivable that the high quantum efficiencies are due to lower rotational barriers between the desired stereoelectronic conformations of the triplet state. In the

derivatives with low quantum efficiencies the molecules must subtend a larger rotation angle to achieve this desired orientation.

H. Brønsted β_{LG} Linear Free Energy Relationship.

In an effort to systematically explore the effect of the leaving group on substrate photorelease the quantum yields, Stern-Volmer quenching rates, and release rates for a series of pHP esters were examined. This information yielded valuable details about differences in the quantum efficiency and disappearance rates as the ability of the leaving group to depart changed thus showing a structure-function relationship. In physical organic chemistry, the structure-function relationship gives important information about the mechanism of the reaction. With the information available the most appropriate way to compare the efficacy of the photorelease to the pK_a of the leaving group is with a Brønsted β_{LG} (leaving group) LFER.

The earliest known free energy relationship is the correlation of acid and base strength with the effectiveness of catalysts in reactions subject to general acid-base catalysis[116]. When the rate of the reaction is dependent upon the strength of the acid or the base, a Brønsted correlation is established (**Equations 33 and 34**).

$$\log(k) = -\alpha\, pK_a + \log(C) \qquad \textbf{Equation 33.}$$

$$\log(k) = \beta\, pKa + \log(C) \qquad \textbf{Equation 34.}$$

The sensitivity of the acid-catalyzed reaction to the strength of the acid is α, whereas the sensitivity of a base-catalyzed reaction to the strength of the base is β. The α and β reaction constants indicated the extent of proton transfer in the transition state.

Another use of the Brønsted correlation is between the nucleophilicity and reactivity based upon the pK_a of the conjugate acid of the nucleophile. The equation is adapted (**Equations 35 and 36**) and the sensitivity of the reaction to the nucleophilicity of the base is indicated by the term β_{NUC}.

$$\log(k) = \beta_{NUC} \log(K_b) + \log(C) \qquad \textbf{Equation 35.}$$

$$\log(k) = \beta_{NUC} (pK_a) + \log(C') \qquad \textbf{Equation 36.}$$

The ability of a leaving group or nucleofuge to depart is often found to correlate directly with its acidity much the same way as nucleophilicity does. The same form of an equation relating the nucleofuge acidity to the rate constant can be used to correlate nucleofugality with pK_a (**Equation 37**).

$$\log(k) = \beta_{LG}(pK_a) + \log(C) \qquad \textbf{Equation 37}.$$

In this case, β_{LG} is measured which gives the sensitivity of the reaction to the acidity of the leaving group. Since the leaving group ability increases as the pKa of the acid decreases, **Equation 37** tells us that the values of β_{LG} will be negative. In a mechanistic investigation, the value of β_{LG} is used in the determination of the relative amounts of leaving group departure at the rate-determining step[117]. A Brønsted LFER was constructed comparing the rate of the disappearance of the caged ester and the pK_a of the leaving group was constructed (**Figure 16, Table 27**). From the slope of the line, the value of β_{LG} was obtained (-0.238). This value is negative which agrees with the expected value and reveals that the photorelease reaction is less sensitive to the structure and pK_a of the leaving group than is the reference deprotonation reaction of water. The rate determining step of the photorelease mechanism is thought to be

the step in which the substrate is released from the chromophore[107,118]. The modest value of β_{LG} suggests a small amount of bond cleavage to the leaving group at the transition state.

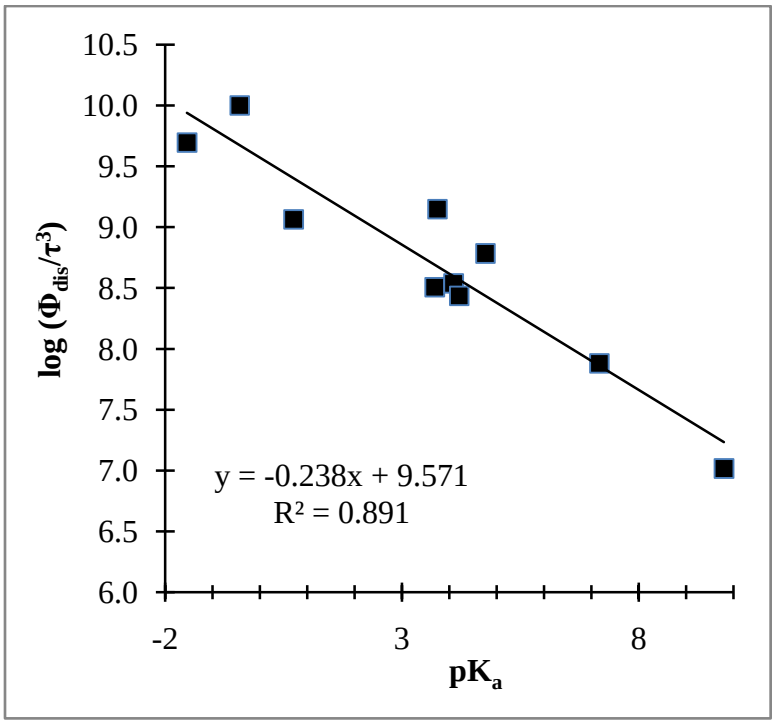

Figure 16. Brønsted Linear Free Energy Relationship. LFER between log (Φ_{dis}/τ^3) and the pK_a values of the acids released during photolysis of pHP esters aqueous acetonitrile. The straight line with slope = -0.238 and intercept = 9.571 results from a linear fit to the respective data.

Table 27. Summary of Brønsted LFER Data

pHP derivative	LG pK_a	Φ_{dis}	$k_{\tau 3\ decay}$ (s^{-1})	τ^3 (ns)	log (Φ_{dis}/τ^3)
Mesylate **72a**	-1.54	0.932	8.5×10^9	0.118	9.70
Tosylate **72b**	-0.43	1.04	9.6×10^9	0.104	10.0
Diethyl Phosphate **51a**	0.71	0.40	2.9×10^9	0.345	9.06
pCF_3 Benzoate **70e**	3.69	0.201	1.6×10^9	0.625	8.51
Formate **70a**	3.75	0.94	1.5×10^9	0.667	9.15
$pOCH_3$ Benzoate **70d**	4.09	0.288	1.2×10^9	0.833	8.54
Benzoate **70c**	4.21	0.316	8.6×10^8	1.16	8.44
GABA **57b**	4.76	0.21	2.9×10^9	0.345	8.78
pCN Phenolate	7.17	0.11	6.9×10^8	1.45	7.88
Phenolate	9.8	0.04	2.6×10^8	3.85	7.02

I. Summary: Revised Mechanism for the Photo-Favorskii Rearrangement of pHP Esters

It has been established that in aqueous or mixed aqueous solvents pHP esters follow an ionic pathway. The product identification studies of the formate, benzoate, and sulfonate esters in aqueous acetonitrile are in agreement. The proposed mechanism of the ionic pathway (**Scheme 23**) involves irradiation of the pHP ester to its singlet-excited state (S^1) which rapidly intersystem crosses to a triplet-excited state (T^1). From the triplet ester one of two things can happen, the first being decay back to the ground state and the second being the photorelease of the substrate. Substrate release is in concert with deprotonation of the phenol and is assisted by at least two water molecules[67,107] forming triplet biradical **89**. This step is the slowest step

therefore the rate-determining step of the reaction[107,118]. Cyclization of triplet biradical **89** to spirodienedione **65** follows immediately after the decay of the triplet

Scheme 23. Revised pHP Photorelease Mechanism[107]

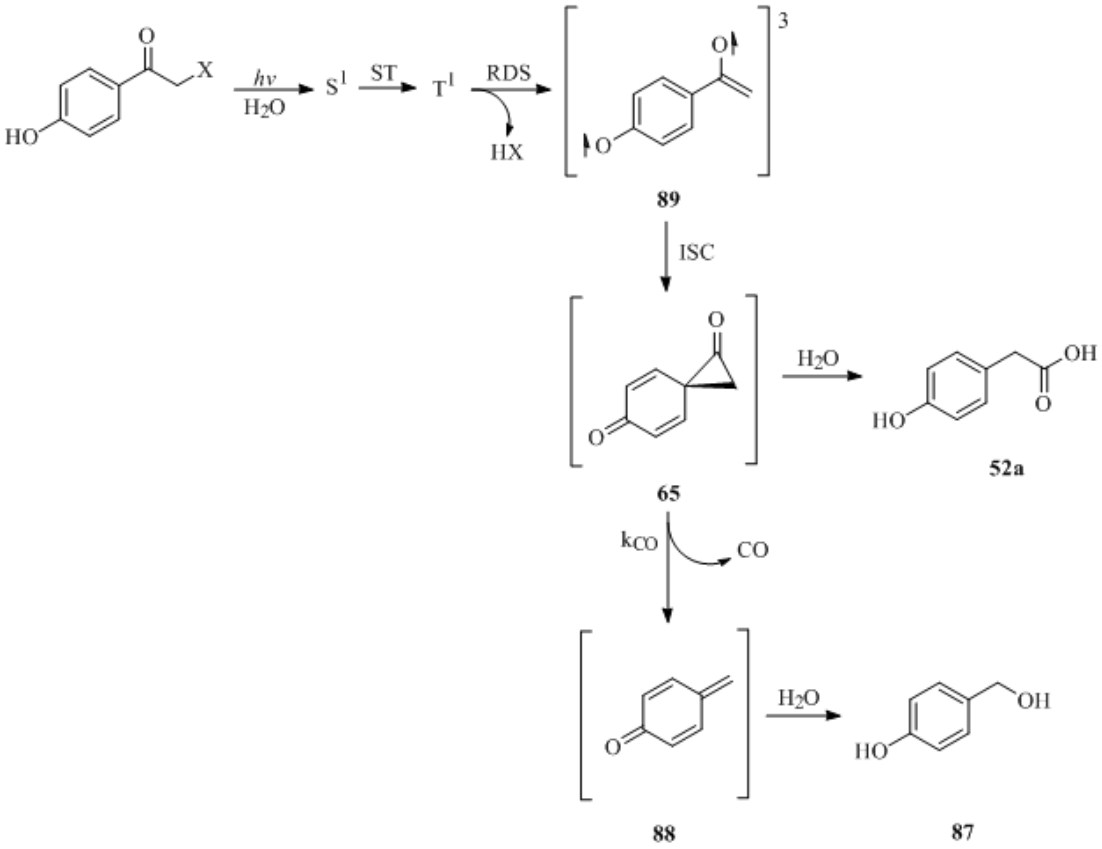

biradical to the ground state. This intermediate can either react with water as part of a Favorskii-like rearrangement yielding *p*-hydroxyphenylacetic acid (**52a**) or can undergo decarbonylation forming *p*-quinone methide (**88**) which reacts with water to form *p*-hydroxybenzyl alcohol (**87**). This mechanism is supported by the results of: the quenching of the reaction of the benzoates by a triplet quencher (piperylene); the

formation of only photoproducts *p*-hydroxyphenylacetic acid (**52a**), *p*-hydroxybenzyl alcohol (**87**), *p*-hydroxyacetophenone (**62**), and the released substrate when pHP formate, mesylate, and tosylate were photolyzed in the presence of a triplet sensitizer (acetone); the absorption bands for triplet biradical **89** and *p*-quinone methide (**88**) that were observed using laser flash photolysis[107]; the appearance and decay of singlet and triplet species in the time resolved spectra of pHP benzoate and tosylate; the calculations and time-resolved resonance Raman studies that were performed by Phillips and coworkers[65,67,77,89,118,119]; and the presence of a Brønsted correlation relating the efficacy of photorelease to the pK_a of the leaving group.

CONCLUSION

The *p*-hydroxyphenacyl group has several features that make it an attractive photoremovable protecting group. Literature examples support this statement and the benzoate, formate, and sulfonate derivatives are not exceptions. The synthesis of these targets requires few synthetic steps, which produce the desired product in good to excellent yield. The purification of these targets is simplified by the fact that these derivatives are all solids. Their solubility and stability in polar organic solvents and in water at low concentrations (pHP formate is an exception) make them ideal for use in organic synthesis and in biological applications.

The bulk of the photochemical reactions on these derivatives were performed using a low intensity commercially available Southern New England Photoreactor fitted with RPR 3000 Å lamps in order to excite the chromophore at or above 300 nm, a region of reasonable absorptivity by the pHP chromophore. Departure of the substrate or leaving group from the excited *p*-hydroxyphenacyl chromophore occurs by the heterolytic rupture of the covalent bond connecting the two. This is a primary photochemical process occurring from the triplet state. The simultaneous loss of a proton from the phenol, results in the overall extrusion of triplet oxyallyl-phenoxy biradical **89**, which is detected by its characteristic absorptions at 420 and 440 nm by LFP. The biradical relaxes to Favorskii-like intermediate dienedione **65** that goes on to two products, the rearranged *p*-hydroxyphenylacetic acid (**52a**) and the newly discovered CO extrusion product, *p*-hydroxybenzyl alcohol (**87**). The photochemical

release rate is fast (> 10^8 s^{-1}) and efficient (Φ_{dis} = 0.20 – 1.00) for the derivatives studied here.

This mechanism is supported by: 1) the results of the quenching of the reaction of the benzoates by a triplet quencher (piperylene); 2) the formation of the same photoproducts when pHP formate, mesylate, and tosylate were photolyzed in the presence of a triplet sensitizer (acetone); 3) the absorption bands for triplet biradical **93** in LFP studies and for *p*-quinone methide (**88**) by infrared and UV detection using laser flash photolysis[107]; and 4) the appearance and decay of singlet and triplet species in the time resolved UV spectra of pHP formate, benzoate, and tosylate.

A Brønsted correlation relating the log of the rate constant for photorelease to the ground state pK_a of the substrate leaving group for the pHP derivatives studied here along with those reported earlier gave a value of β_{LG} = -0.24. This indicates that there is a moderate degree of heterolytic cleavage of the carbon-leaving group bond in the transition state for the adiabatic triplet fragmentation step. These results, particularly the detection of the biradical and the Bronsted β_{LG} correlation, have added significantly to our understanding of the mechanism for the photo-Favorskii rearrangements of *p*-hydroxyphenacyl derivatives.

EXPERIMENTAL

All starting materials were purchased from Aldrich and were used without further purification unless otherwise noted. Reaction solvents were distilled prior to use. All melting points were obtained using Thomas Hoover Capillary Melting Point Apparatus and all values are uncorrected. ^{1}H and ^{13}C NMR spectra were obtained on either a Bruker 400 or 500 MHz instrument and are noted accordingly. Samples were dissolved in chloroform-d ($CDCl_3$), methanol-d_4 (CD_3OD), deuterium oxide (D_2O), acetonitrile-d_3 (CD_3CN), or dimethyl sulfoxide-d_6 (DMSO-d_6) and chemical shifts are reported in parts per million, δ. Pre-coated silica plates from Sorbent Technologies were used for thin layer chromatography (TLC) and spots were visualized under a UV lamp. Chromatographic purification was effected with flash chromatography using standard grade (32-63 μm) silica gel (Sorbent Technologies). IR spectra were obtained on a Shimatzu FTIR-8400S spectrophotometer; results reported in cm^{-1}. Samples were submitted to the Small-Molecule X-Ray Crystallography lab at the University of Kansas. HPLC analyses were conducted with an Alltech Platinum C18 analytical column (column size: 250 x 4.6 mm, particle size: 5 μm) connected to a Rainin dual pump system or with a Waters XTerra MS-C18 analytical column (column size: 2.1 x 150 mm, particle size: 5 μm) connected to a Waters Alliance HT 2795 or a Waters Aquity UPLC. UV-Vis spectra were measured on a Cary 100 Bio spectrophotometer (Varian).

Synthesis of pHP Carboxylates

2'-Bromo-4'-hydroxyacetophenone 53. Method **A**. 2-bromo-4'-hydroxyacetophenone # was prepared according to the method described by Durden and coworkers[83]. Copper (II) bromide (4.9 g, 0.22 mol) and **62** (1.5 g, 11 mmol) along with a stir bar were placed in a 100 ml round-bottom flask. A 1:1 mixture of dry EtOAc (20 ml) and dry $CHCl_3$ were added and a stopper was placed on the flask. The flask was placed in an oil bath and equipped with a condenser. The solution was refluxed for 7 hours, and then allowed to cool to room temperature, and the solution was poured through a plug of silica gel, followed by excess CH_2Cl_2. The solvent was removed in-vacuo giving a crude solid (1.8 g, 60%) which was used without further purification. Method **B**. 2-bromo-4'-hydroxyacetophenone **53** was prepared according to the method described by Rather and Reid[85]. In a 250 ml round bottom flask, p-hydroxyacetophenone **62** (1.0 g, 7.3 mmol) was dissolved in 100 ml of diethyl ether (Et_2O). The flask was equipped with a stir bar and placed in and ice bath and cooled to 0 °C. An addition funnel was used for the addition of bromine (0.37 ml, 7.3 mmol) in 100 ml Et_2O. The bromine solution was added to the flask very slowly over 20 min. making sure that the solution remained almost colorless. At the end of the addition, the ice bath was removed and the reaction mixture was allowed to warm to room temperature. The solution was transferred to a separatory funnel, washed with three 15 ml portions of DI H_2O and the organic layer was separated, dried over $MgSO_4$, and filtered. The solvent was removed by rotoevaporation leaving the crude solid (0.78 g, 50%). The crude solid was used without further purification. Method **C**.

2-bromo-4'-hydroxyacetophenone **53** was prepared according to the method described by Pasaribu and Williams[86]. In a 250 mL round-bottom flask, **62** (4.0 g, 30 mmol) was dissolved in 100 mL of 1:1 Et_2O/1,4-dioxane. The flask was placed in an ice bathe and equipped with a stir bar and an addition funnel. Dioxane dibromide (DDB, 8.0 g, 32 mmol) was placed in the funnel followed by 100 mL of 1:1 Et_2O/1,4-dioxane and added slowly to the flask over an hour, making sure that the solution remained cold. Once the addition was complete the reaction mixture was allowed to stir for 24 h then equal volumes of Et_2O and DI H_2O were added to the flask. The mixture was transferred to a separatory funnel and the organic layer was isolated, washed with 100 ml of brine, dried over $MgSO_4$, and gravity filtered. The Et_2O was removed by rotoevaporation and the dioxane was removed in vacuo. The crude solid (7.6 g, 90%) was used in most cases was used without further purification. When the solid was to be purified it was done so using flash chromatography with a 70:30 hexanes/EtOAc solvent system. The pure solid was a pink color (mp: 129 – 131°C (lit.)[84]; 120-122 °C (exp.), 90%). ^{1}H NMR (400 MHz, DMSO-d_6): δ (ppm) 10.54 (s, 1H), 7.85 (d, 2H), 6.92 (d, 2H), 4.78 (s, 2H). ^{13}C NMR (500 MHz, DMSO-d_6): δ (ppm) 198.86, 162.66, 131.46, 130.23, 115.75, 33.61. IR (KBr, cm^{-1}): 3338, 1676, 1608, 1508, 1446, 1323, 842. HRMS (m/z) calc for $C_8H_8O_2Br$ 213.96, found 214.9708 (M + H).

General Procedure for pHP Carboxylate Ester Synthesis. Carboxylate esters were synthesized according to a method based upon a method used by Buu-Hoi and Lavit[87]. Alternate synthetic approaches are noted. Brominated acetophenone **53**

was placed in a 250 mL round bottom flask and was dissolved in 100 mL of 1:1 CH_2Cl_2/1,4-dioxane and cooled to 0° C. DBU (3 equivalents) was placed in a 250 mL erlenmeyer flask along with 25 mL of the mixed solvents and placed in an ice bath. The carboxylic acid (1.3 equivalents) was mixed with 25 mL of 1:1 CH_2Cl_2/1,4-dioxane. Once the acid and base solutions were cool, the acid was slowly added to the base making sure to keep the flask cold. When the acid had dissolved, the DBU/carboxylate solution was added to the stirring solution of **53** and allowed to stir. The reaction was monitored by TLC (1:1 hexanes/EtOAc). When the reaction was judged to be complete, equal volumes of CH_2Cl_2 and H_2O were added to the reaction mixture. The organic layer was washed 3 times with 50 mL of H_2O, 50 mL saturated $NaHCO_3$ solution, and dilute HCl and then washed once with brine, dried over $MgSO_4$, and gravity filtered. The solvent was removed using rotoevaporation. Purification was performed using column chromatography.

***p*-Hydroxyphenacyl Formate 70a.** Method A. Brominated acetophenone **53** (1.2 g, 5.4 mmol), DBU (1.7 mL, 11 mmol), and formic acid **71a** (0.50 mL, 8.1 mmol) were combined in the procedure outline above. The reaction was allowed to react for 8 h. The crude solid was purified by either column chromatography (6:4 hexanes/EtOAc) or by recrystallization in EtOAc to yield a white crystalline solid (0.34 g, 1.9 mmol, 35%; mp: 146 – 147 °C). ^{1}H NMR (400 MHz, DMSO-d_6): δ (ppm) 10.58 (s, 1H), 8.46 (s, 1H), 7.91 (d, 2H), 6.94 (d, 2H), 5.54 (s, 2H). ^{13}C NMR (500 MHz, DMSO-d_6): δ (ppm) 190.1, 162.7, 161.6, 130.4, 125.2, 115.4, 65.5. IR (KBr, cm^{-1}): 3350, 2925, 1730, 1683, 1602, 1586, 1500, 822 cm^{-1}. UV-VIS (9:1

CH_3CH/H_2O) λ 220 (ε = 5,200) and 280 (ε = 10,000). HRMS (m/z) calc for $C_9H_9O_4$ 180.04, found 181.0501 (M +H). Method B. Potassium formate (2.7 g, 32 mmol) and a large stir bar were placed in a 500 mL Erlenmeyer flask. Absolute EtOH (150 mL) was added and the mixture was allowed to stir and heat at 55 – 60 °C for 15 minutes. Bromide **74** (2.0 g, 44 mmol) was added to the flask and the reaction was heated to between 55 and 60 °C 24 h. The solution was hot filtered and the ethanol was removed. The resulting solid was dissolved in EtOAc and washed twice with water and once with saturated $NaHCO_3$ and then brine. The organic layer was separated, dried, and the solvent was removed with rotoevaporation to afford a yellow solid. This solid was dissolved in acetone and purified by flash chromatography (1:1 hexane/EtOAc) to afford a white solid (0.33 g, 18 mmol, 41%; mp = 145 – 147 °C). The solid was recrystallized using 1:1 hexanes/Et_2O affording colorless crystals that were suitable for x-ray crystallography (**Figure 3**).

***p*-Hydroxyphenacyl Benzoate 70c.** Brominated acetophenone **53** (5.0 g, 23 mmol), DBU (5.2 mL, 35 mmol), and benzoic acid **4** (3.7 g, 30 mmol) were combined in the procedure outline above. The reaction was allowed to react for 24h. The crude solid after the solvent was removed was purified by either flash chromatography (1:1 hexanes/EtOAc) or by recrystallization in absolute EtOH resulting in colorless crystals (4.9 g, 19 mmol, 83%; mp: 199 – 200 (lit.)[120]; 207 – 209 °C (exp.)) that were suitable for x-ray crystallography (**Figure 4**). ^{1}H NMR (400 MHz, DMSO-d_6): δ (ppm) 10.59 (s, 1H), 8.10 (d, 2H), 8.08 (d, 2H), 7.95 (m, 1H),

7.63 (t, 2H), 6.96 (d, 2H), 5.71 (s, 2H). ^{13}C NMR (500 MHz, DMSO-d_6): δ 190.5, 165.3, 162.7, 133.6, 130.4, 129.3, 128.8, 125.4, 115.5, 66.7. IR (KBr, cm^{-1}): 3350, 1685, 1680, 1600, 1500, 840, 720, 690. UV-VIS (7:3 CH_3CN/H_2O) λ 273 (ε = 17,500) and 225 (ε = 14,500). HRMS (m/z) calc for $C_{15}H_{13}O_4$ 256.07, found 257.0814 (M + H).

***p*-Hydroxyphenacyl *p*-Methoxybenzoate 70d .** Brominated acetophenone **53** (5.0 g, 23 mmol), DBU (5.2 mL, 35 mmol), and *p*-methoxybenzoic acid **71d** (4.6 g, 30 mmol) were combined in the procedure outline above. The reaction was judged to be complete after 6 hours. The crude solid was purified by flash chromatography (7:3 hexanes/EtOAc) and then by recrystallization in 8:2 hexanes/EtOAc resulting in colorless crystals (4.9 g, 17 mmol, 75%; mp: 184 – 185 °C) that were suitable for x-ray crystallography (**Figure 5**). ^{1}H NMR (400 MHz, DMSO-d_6): δ (ppm) 10.52 (s, 1h), 7.98 (d, 2H), 7.88 (d, 2H), 7.09 (m, 4H), 6.89 (d, 2H), 5.59 (s, 2H), 3.85 (s, 3H). ^{13}C NMR (500 MHz, DMSO-d_6): δ (ppm) 191.2, 165.3, 163.7, 163.1, 131.9, 130.7, 125.9, 121.8, 115.9, 114.5, 66.8, 56.0. IR (KBr, cm^{-1}): 3357, 16805 1680, 1604, 1583, 1500. UV-VIS (7:3 CH_3CN/H_2O) λ 273 (ε = 23,300). HRMS (m/z) calc for $C_{16}H_{15}O_5$ 286.08, found 287.0919 (M + H).

***p*-Hydroxyphenacyl *p*-Trifluoromethylbenzoate 70e.** Brominated acetophenone **53** (5.0 g, 23 mmol), DBU (5.2 mL, 35 mmol), and *p*-trifluoromethylenzoic acid **71e** (5.7 g, 30 mmol) were combined in the procedure outline above. The reaction was complete after 5 days. The crude solid was purified

by flash chromatography (7:3 hexanes/EtOAc) and then by recrystallization in 9:1 hexanes/EtOAc resulting in colorless crystals (3.8 g, 12 mmol, 51%; mp: 200 – 202° C). ^{1}H NMR (400 MHz, DMSO-d_6): δ (ppm) 10.55 (s, 1H), 8.23 (d, 2H), 7.96 (d, 2H), 7.90 (d, 2H), 6.90 (d, 2H), 5.52 (s, 2H). ^{13}C NMR (500 MHz, DMSO-d_6): δ (ppm) 190.2, 164.3, 162.8, 133.0, 130.4, 125.6, 125.9, 125.3, 115.5, 67.2. IR (KBr, cm^{-1}): 3217, 1720, 1685, 1612, 1517, 1556, 1411, 821. UV-VIS (7:3 CH_3CN/H_2O)λ 222 (ε = 23,300) and 283 (ε = 12,000). HRMS (m/z) calc for $C_{16}H_{12}O_4F_3$ 324.06, found 325.0688 (M + H).

Synthesis of pHP Sulfonates and Other Caged Compounds

4-*tert*-Butyldiphenylsilylacetophenone 73. 4-*tert*-Butyldiphenylsilyl-acetophenone **73** was prepared according to the method described by Phillips and coworkers[89]. 4-Hydroxyacetophenone (**62**, 5.0 g, 37 mmol) and imidazole (6.3 g, 92 mmol) were placed in a flame dried 250 mL round bottom flask. Dry DMF (50 mL) was placed in the flask. The system was closed and placed under an argon atmosphere. With the use of a syringe *tert*-butyldiphenylsilyl chloride (TBDPSCl, 15 mL, 51 mmol) was added to the flask. The reaction mixture was allowed to stir at room temperature for 3 h. The reaction was quenched with 200 mL water and extracted three times with 150 mL of Et_2O. The organic extracts were combined and washed with brine. The organic layer was dried over $MgSO_4$ and filtered. The solvent was removed using rotoevaporation resulting in an off-white solid. The crude solid was recrystallized in absolute EtOH to produce a while solid (14 g, 37 mmol, 100%;

mp: 123-124 °C. ^{1}H NMR (500 MHz, $CDCl_3$): δ (ppm) 7.76 (d, 2H), 7.72 (m, 4H), 7.40 (m, 6H), 6.81 (d, 2H), 2.51 (s, 3H), 1.08 (s, 9H). ^{13}C NMR (500 MHz, $CDCl_3$): δ (ppm) 196.93, 160.03, 135.41, 132.14, 130.67, 130.33, 130.18, 127.94, 127.74, 119.64, 26.40, 26.34, 19.47. IR (KBr, cm^{-1}): 1685, 1112, 1685, 1508, 821. HRMS (m/z) calc for $C_{24}H_{27}O_2Si$ 175.1780, found 375.1758 (M + H).

4-*tert*-Butyldiphenylsilyloxyphenacyl bromide 74. Method A. 4-*tert*-Butyldiphenyl-silyloxyphenacyl bromide **74** was prepared according to the method described by Phillips and coworkers[89]. Benzyltrimethylammonium tribromide (4.2 g, 11 mmol) was added to a solution of **73** (4.0 g, 11 mmol) that had been dissolved in a 5:2 mixture of CH_2Cl_2 and MeOH. The mixture was allowed to stir at room temperature for 2.5 h and then was concentrated on a rotoevaporator. Water was added to the reaction flask and the mixture was extracted three times with Et_2O (30 mL). The extracts were washed with bring, dried over $MgSO_4$, and filtered. The solvent was removed with a rotoevaporator and a vacuum to yield a while solid (4.9 g, 11 mmol, 100%; mp: 51 – 54 °C. ^{1}H NMR (500 MHz, $CDCl_3$): δ (ppm) 7.70 (d, 2H), 7.65 (m, 4H), 7.37 (m, 2H), 7.35 (m, 4H), 6.73 (d, 2H), 4.25 (s, 2H), 1.00 (s, 9H). ^{13}C NMR (500 MHz, $CDCl_3$): δ (ppm) 189.96, 160.79, 135.40, 131.93, 131.08, 130.28, 128.01, 127.31, 120.01, 30.851, 26.36, 19.47. IR (KBr, cm^{-1}): 1676, 1415, 1174, 1120, 1108, 1074, 808. HRMS (m/z) calc for $C_{24}H_{25}O_2BrSi$ 453.0885, found 454.0887 (M + H). Method B. 4-*tert*-Butyldiphenylsilyloxyphenacyl bromide **75** was prepared according to the method described by Pasaribu and Williams[86]. In a 250 mL round bottom flask, acetophenone **73** (4.0 g, 11 mmol) was dissolved in 50 mL of a

1:1 mixture of Et_2O and 1,4-dioxane. The flask was placed in an ice bath and equipped with stirring and an addition funnel. Approximately 50 mL of the solvent was placed in the addition funnel. DDB (2.8 g, 11 mmol) was placed in the addition funnel and added slowly to the flask over an hour, making sure the solution remained cold. Once the addition was complete, the ice bath was removed and the solution was stirred at rt for 24 h. At the end of the time period, equal volumes of Et_2O and H_2O were added to the flask. The mixture was transferred to a separatory funnel and the organic layer was isolated. The organic layer was dried over $MgSO_4$ and filtered. The solvent was removed and by rotoevaporation and under vacuum. The crude solid (4.4 g, 9.6 mmol, 90%) was used without further purification.

4-*tert*-Butyldiphenylsilyloxy-α-hydroxyacetophenone 75. Method A. 4-*tert*-Butyldiphenylsilyloxy-α-hydroxyacetophenone **75** was prepared according to a method based on one described by Phillips and coworkers[89]. Sodium formate (0.78 g, 11 mmol) and a large stir bar were placed in a 500 mL Erlenmeyer flask. Absolute EtOH (150 mL) was added and mixture was allowed to stir and heat for 15 min. Bromide **74** (4.0 g, 8.8 mmol) was added to the flask and the reaction was heated to between 55 and 60 °C. The reaction mixture was kept at that temperature for 24 h. The solution was hot filtered and the ethanol was removed. The solid was re-dissolved in Et_2O and washed three times with water and once with brine. The organic solvent was removed with rotoevaporation to afford a yellow liquid. This liquid was diluted with acetone and purified by gravity chromatography using a gradient solvent system (hexane/Et_2O) to afford a pale yellow solid (1.3 g, 3.3 mmol,

42%; mp: 79 – 81 °C. ^{1}H NMR (500 MHz, DMSO): δ (ppm) 7.75 (d, 2H), 7.69 (m, 4H), 7.48 (m, 6H), 6.82 (d, 2H), 4.94 (s, 1H), 4.65, (d, 2H), 1.08 (s, 9H). Method B. 4-*tert*-Butyldiphenylsilyloxy-α-hydroxyacetophenone **75** was prepared according to a method based on one described by Phillips and coworkers[89]. Potassium formate (2.0 g, 24 mmol) and a large stir bar were placed in a 500 mL erlenmeyer flask. Absolute EtOH (150 mL) was added and mixture was allowed to stir and heat for 15 min. Bromide **74** (8.0 g, 18 mmol) was added to the flask and the reaction was heated to between 55 and 60 °C. The reaction mixture was kept at that temperature for 20 h. The solution was hot filtered and the ethanol was removed. The solid was re-dissolved in Et_2O and washed three times with water and once with brine. The organic solvent was removed with rotoevaporation to afford a yellow liquid. This liquid was diluted with acetone and purified by gravity chromatography using a gradient solvent system (hexane/Et_2O) to afford a pale yellow solid (4.3 g, 12 mmol, 65%; mp: 78 – 80 °C. ^{1}H NMR (500 MHz, DMSO): δ (ppm) 7.75 (d, 2H), 7.69 (m, 4H), 7.48 (m, 6H), 6.82 (d, 2H), 4.94 (s, 1H), 4.65, (d, 2H), 1.08 (s, 9H). ^{13}C NMR (500 MHz, DMSO): δ (ppm) 197.43, 159.23, 134.74, 131.24, 130.22, 129.76, 128.18, 119.59, 115.26, 64.92, 26.14, 18.89. IR (KBr, cm^{-1}): 3421, 1689, 1593, 1508, 1460, 821. HRMS (m/z) calc for $C_{24}H_{25}O_2BrSi$ 390.17, found 391.1725 (M + H).

Benzyl Mesylate (77a). Method A. Benzyl mesylate (**77a)** was prepared according to a method based on one described by Barnett and coworkers[95]. In a 100 mL round bottom flask, benzyl alcohol (**78** ,0.5 g, 4.6 mmol), methanesulfonyl chloride (0.5 mL, 6.4 mmol), and 30 mL of CH_2Cl_2 were combined. This mixture was

cooled to -78° C using a dry ice/acetone bath. Triethylamine (TEA, 1.3 mL, 9.2 mmol) was added dropwise over 20 min. The reaction mixture was allowed to stir for 1 h, the cold bath was removed and the reaction was allowed to warm to rt. The solution then was transferred to a separatory funnel and washed with water, dilute HCl, and brine. The organic layer was dried over $MgSO_4$ and the solvent was removed using a rotoevaporator. The compound was purified using column chromatography (1:1 hexanes/EtOAc) resulting in only one fraction that was submitted for NMR. ^{1}H NMR (500 MHz, DMSO): δ (ppm) 7.73 (m, 5H), 5.35 (s, 2H), 3.34 (s, 1H). ^{13}C NMR (500 MHz, DMSO): δ (ppm) 134.04, 131.82, 129.47, 128.68, 76.74, 37.05. HRMS (m/z) calc for $C_8H_{10}O_3S$ 186.23, found 209.0248 (M + Na). Method B. Benzyl mesylate (**77a**) was prepared according to the method described by Emmons and Ferris[96]. In a 100 mL round bottom flask, silver (II) oxide (0.904 g, 7.3 mmol) was dissolved in 20 mL of acetonitrile. Methanesulfonic acid (**90a**, 0.47 mL, 7.3 mmol) was dissolved in 10 mL of acetonitrile and slowly added to the reaction mixture. This mixture was allowed to stir for 30 min while benzyl bromide (**80**, 0.35 mL, 2.9 mmol) was dissolved in acetonitrile in another 100 mL round bottom flask, equipped with stirring, and was cooled to 0° C. After the 30 minutes, the silver methanesulfonate (3.22 mmol) was filtered into the round bottom containing the benzyl bromide (**79**). This reaction mixture was allowed to stir for 20 min at 0° C, then it was filtered again and the solvent was removed. The crude material was purified using column chromatography (1:1 hexanes/EtOAc) resulting in of an oil (0.49 g, 2.6 mmol, 90%). ^{1}H NMR (500 MHz, DMSO): δ (ppm) 7.34 (m,

5H), 5.21 (s, 2H), 2.83 (s, 3H). ^{13}C NMR (500 MHz, DMSO): δ (ppm) 133.43, 129.42, 128.93, 128.88, 71.51, 38.40.

Benzyl Tosylate (77b). Benzyl tosylate (**77b**) was prepared according to the method described by Emmons and Ferris[96]. In a 100 mL round bottom flask, silver (II) oxide (0.65 g, 5.3 mmol) was dissolved in 20 mL of acetonitrile. *p*-Toluenesulfonic acid (**89b**, 1.0 g, 5.3 mmol) was dissolved in 10 mL of acetonitrile and slowly added to the reaction mixture. This mixture was allowed to stir for 30 min. During this time, benzyl bromide (**79**, 0.348 mL, 2.9 mmol) was dissolved in acetonitrile in another 100 mL round bottom flask, equipped with stirring, and was cooled to 0° C. After the 30 min, the silver *p*-toluenesulfonate (3.22 mmol) was filtered into the round bottom containing the benzyl bromide (**79**). This reaction mixture was allowed to stir for 20 minutes at 0° C where it was filtered again and the solvent was removed resulting in the crude material. This material was purified using column chromatography (1:1 hexanes/EtOAc) resulting in a white solid (0.53 g, 2.0 mmol, 70%; mp: 58.5 – 58.9 °C (lit.)[121]; 52 – 54 °C (exp.)). ^{1}H NMR (500 MHz, DMSO): δ (ppm) 7.45 (m, 5H), 7.01 (d, 2H), 5.25 (s, 2H), 2.33 (s, 3H). ^{13}C NMR (500 MHz, DMSO-d_6): δ (ppm) 145.65, 130.39, 129.46, 128.80, 125.47, 76.75, 20.75. HRMS (m/z) calc for $C_{14}H_{14}SO_3Na$ 285.06, found 285.0561 (M + Na).

2-(4-(*tert*-butyldiphenylsilyloxy)phenyl)-2-oxoethyl methanesulfonate 80a. Method A. 2-(4-(*tert*-butyldiphenylsilyloxy)phenyl)-2-oxoethyl methanesulfonate **80a** was prepared according to a method based on one described by Kumar and

coworkers[94]. A 250 mL round bottom flask was flame dried and placed under and argon atmosphere. To the flask dry pyridine (10 mL) and silyl-protected-α-hydroxyacetophenone **75** (1.0 g, 2.7 mmol) were added. The reaction was then cooled to 0° C with an ice bath. Methanesulfonyl chloride (0.26 mL, 3.4 mmol) was added to the flask and the reaction was allowed to stir and slowly warm up to rt. After 24 h, the reaction was quenched with 50 mL water and washed with 75 mL EtOAc. The organic layer was washed with satd. $NaHCO_3$ and brine and was then dried over $MgSO_4$. The solvent was removed by rotoevaporation and purified by column chromatography (7: 3 hexanes/EtOAc) resulting in a white solid (0.038 g, 0.081 mmol, 3%). ^{1}H NMR (500 MHz, DMSO): δ (ppm) 7.69 (d, 2H), 7.58 (m, 4H), 7.37 (m, 6H), 6.88 (d, 2H), 5.47)s, 2H), 2.04 (s, 3H), 0.98 (s, 9H). Method B. 2-(4-(*tert*-butyldiphenylsilyloxy)phenyl)-2-oxoethyl methanesulfonate **80a** was prepared according to a method based on one described by Emmons and Ferris[96]. Silver oxide (5.0 g, 40 mmol) was placed in a 250 mL round bottom flask with a stir bar. Acetonitrile (50 mL) was added to the flask and stirred vigorously to form a suspension. Methanesulfonic acid (1.8 mL, 2.6 g, 27 mmol) was added to the silver oxide suspension. The solution was allowed to stir at room temperature for 45 minutes. In a 500 mL Erlenmeyer flask, bromide **74** (9.4 g, 21 mmol) was dissolved in 100 mL CH_3CN. After the time, the silver oxide solution was filtered and the filtrate was added to the bromide solution. This reaction mixture was stirred at 70 °C for 3 days. The mixture was filtered and the solvent removed. The yellow solid was dissolved in acetone and filtered again. Flash chromatography (7:3 hexane/Et_2O) was

used to purify the crude material resulting in a white solid (6.8 g, 14 mmol, 69 %; mp: 108 – 110 °C). ^{1}H NMR (500 MHz, DMSO): δ (ppm) 7.69 (d, 2H), 7.58 (m, 4H), 7.37 (m, 6H), 6.88 (d, 2H), 5.47 (s, 2H), 2.04 (s, 3H), 0.98 (s, 9H). ^{13}C NMR (500 MHz, DMSO): δ (ppm) 192.45, 159.88, 134.93, 131.09, 130.48, 129.16, 127.19, 119.87, 71.04, 37.42, 29.01, 18.89. IR (KBr, cm^{-1}): 1704, 1598, 1508, 1370, 1159, 821. HRMS (m/z) calc for $C_{25}H_{28}O_5SSi$ 468.14, found 469.1505 (M + H).

2-(4-(*tert*-butyldiphenylsilyloxy)phenyl)-2-oxoethyl 4-methylbenzene-sulfonate 80b. 2-(4-(*tert*-butyldiphenylsilyloxy)phenyl)-2-oxoethyl 4-methylbenzene-sulfonate **80b** was prepared according to a method based on one described by Emmons and Ferris[96]. Silver oxide (5.0 g, 40 mmol) was placed in a 250 mL round bottom flask with a stir bar. Acetonitrile (50 mL) was added to the flask and stirred vigorously to form a suspension. *p*-Toluenesulfonic acid (5.1 g, 27 mmol) was added to the silver oxide suspension. The solution was allowed to stir at rt for 45 min. In a 500 mL Erlenmeyer flask, bromide **74** (9.4 g, 21 mmol) was dissolved in 100 mL CH_3CN. After the time, the silver oxide solution was filtered and the filtrate was added to the bromide solution. This reaction mixture was stirred at 70 °C for 3 d. The mixture was filtered and the solvent removed. The orange solid was dissolved in acetone and filtered again. Flash chromatography (9:1 hexanes/Et_2O) was used to purify the crude material resulting in an off-white solid (8.0 g, 15 mmol, 70 %; mp = 120 – 122 °C). ^{1}H NMR (500 MHz, DMSO): δ (ppm) 7.90 (d, 2H), 7.80 (d, 2H), 7.70 (M, 4H), 7.54, (m, 6H), 6.82 (d, 2H), 5.41 (s, 2H), 3.42 (s, 3H), 1.08 (s, 9H). ^{13}C NMR (500 MHz, DMSO): δ (ppm) 192.45, 160.54, 145.82, 144.96, 134.92, 131.21,

130.54, 130.02, 128.39, 127.67, 126.17, 119.86, 70.98, 26.11, 21.06, 18.88. IR (KBr, cm^{-1}): 1697, 1596, 1573, 1508, 1467, 1460, 1371, 1367, 1166, 827. HRMS (m/z) calc for $C_{31}H_{32}O_5SSi$ 544.17, found 545.1818 (M + H).

***p*-Hydroxyphenacyl Mesylate 72a.** Method A. *p*-Hydroxyphenacyl mesylate **73a** was prepared according to the method described by Phillips and coworkers[89]. Protected mesylate **80a** (1.5 g, 3.2 mmol) was placed in a 100 mL round bottom flask. The flask was equipped with stirring and cooled to 0 °C. The solid dissolved in 10 mL THF and allowed to cool for 5 minutes. TBAF (1M in THF, 3.60 mL, 3.24 mmol) was added to the solution. After 15 minutes the reaction was quenched with cold DI water and extracted with EtOAc. The organic layer was washed with $NaHCO_3$, dilute HCL, and brine. The organic layer was dried over $MgSO_4$, filtered, and the solvent removed. The crude solid was purified using flash chromatography (6:4 hexanes/EtOAc) resulting in an off white solid (0.41 g, 55%, mp = 154 – 156 °C). ^{1}H NMR (500 MHz, DMSO-d_6): δ (ppm) 10.56 (s, 1H), 7.85 (d, 2H), 6.90 (d, 2H), 5.61 (s, 2H), 3.36 (s, 3H). ^{13}C NMR (500 MHz, DMSO-d_6): δ (ppm) 189.5, 162.8, 130.5, 125.1, 115.4, 70.9, 37.6. IR (KBr, cm^{-1}): 3417.63, 1683.74, 1602.74, 1579.59, 1525.59, 1442.66, 1427.23, 1367.44, 1211.21, 1168.78, 1053.06, 838.98. UV-VIS (1:1 CH_3CN/H_2O): λ 273 (ε = 16,000), 219 (ε = 11,000). HRMS (m/z) calc for $C_9H_{10}O_5S$ 230.02, found 231.0327 (M + H). Method B *p*-Hydroxyphenacyl mesylate **72a** was prepared according to a method based on one described by McDevitt and coworkers[97]. Protected mesylate **80b** (1.0 g, 2.1 mmol) was dissolved in 15 mL dry THF in a 100 mL round bottom flask. The flask was equipped with stirring and

placed in an ice bath. Hydrogen fluoride in pyridine (0.20 mL, 2.4 mmol) was slowly added to the round bottom flask. The mixture was allowed to stir for 1 h and then quenched with water. The mixture was extracted twice with 20 mL EtOAc. The organic layer was then washed with saturated $NaHCO_3$ and brine. The organic layer was dried over $MgSO_4$ and the solvent was removed using rotary evaporation. The crude solid was purified using flash chromatography (1:1 hexanes/EtOAc) resulting in a white solid (0.48 g, 2.1 mmol, 100%; mp = 155 – 157 °C). This solid was recrystallized in 9:1 hexanes/EtOAc resulting in colorless crystals suitable for x-ray crystallography (**Figure 6**).

***p*-Hydroxyphenacyl Tosylate 72b.** *p*-Hydroxyphenacyl tosylate **72b** was prepared according to a method based on one described by McDevitt and coworkers[97]. Protected tosylate **80b** (1.0 g, 1.8 mmol) was dissolved in 15 mL dry THF in a 100 mL round bottom flask. The flask was equipped with stirring and placed in an ice bath. Hydrogen fluoride in pyridine (0.18 mL, 2.0 mmol) was slowly added to the round bottom flask. The mixture was allowed to stir for 1 h and then quenched with water. The mixture was extracted twice with 20 mL EtOAc. The organic layer was then washed with saturated $NaHCO_3$ and brine. The organic layer was dried over $MgSO_4$ and the solvent was removed using rotary evaporation. The crude solid was purified using flash chromatography (1:1 hexanes/EtOAc) resulting in a white solid (0.55 g, 1.8 mmol, 100%; mp = 133 - 135° C). This solid was recrystallized in 9:1 hexanes/EtOAc resulting in colorless crystals suitable for x-ray crystallography (**Figure 7**). ^{1}H NMR (500 MHz, DMSO-d_6): δ (ppm) 10.54 (s, 1H),

7.86 (d, 2H), 7.78 (d, 2H), 7.49 (d, 2H), 6.85 (d, 2H), 5.46 (s, 2H), 2.43 (s, 3H). ^{13}C NMR (500 MHz, DMSO-d_6): δ (ppm) 188.8, 162.8, 145.0, 132.7, 130.6, 130.1, 127.7, 125.0, 115.4, 70.9, 21.1. IR (KBr, cm^{-1}): 3420, 1689, 1599, 1576, 1510, 1463, 1458, 1369, 1361, 1167, 831. UV-VIS (1:1 CH_3CN/H_2O): λ 283 (ε = 16,000) and 225 (ε = 20,000). HRMS (m/z) calc for $C_{15}H_{14}O_5S$ 306.06, found 305.0484 (M – H).

4-*tert*-Butyldiphenylsilyloxyphenacyl-1*H*-imidazole carboxylate 81. 4-*tert*-Butyldiphenylsilyloxyphenacyl-1*H*-imidazole carboxylate **81** was prepared according to a method based on one described by Chrismann and coworkers[122]. α-Hydroxyacetophenone **75** (10 g, 26 mmol), carbonyldiimidizole (CDI, 6.2 g, 39 mmol), and imidazole (0.87 g, 13 mmol) were placed in a 500 mL erlenmeyer flask. The compounds were dissolved in acetonitrile (150 mL) and allowed to stir and heat at 60 °C for 8 h. The solvent was removed with rotoevaporation to afford a yellow liquid. This liquid was diluted with acetone and purified by flash chromatography (1:1 hexane/EtOAc) to afford a pale yellow solid (8.8 g, 19 mmol, 70 %; mp = 151 – 153 °C). ^{1}H NMR (500 MHz, DMSO): δ (ppm) 8.40 (s, 1H), 7.89 (d, 2H) 7.72 (d, 5H), 7.54 (m, 6H), 7.14 (s, 1H), 6.92 (s, 2H), 5.78 (s, 2H), 1.08 (s, 9H). ^{13}C NMR (500 MHz, $CDCl_3$): δ (ppm) 190.04, 160.10, 148.11, 137.34, 134.94, 131.26, 130.58, 130.48, 130.25, 128.21, 126.96, 119.69, 117.61, 69.15, 26.16, 18.91. IR (KBr, cm^{-1}):1772, 1685, 1593, 1421, 1226, 1159. HRMS (m/z) calc for $C_{28}H_{28}N_2O_4Si$ 484.18, found 485.1896 (M + H).

***tert*-Butyl 2-(5-hydroxy-1*H*-indol-2-yl)ethylcarbamate [N-Boc-Serotonin] 85**. N-Boc-Serotonin **85** was prepared according to a method based on one described by Li and coworkers[104]. Triethylamine (2.0 mL, 14 mmol) was placed in a 250 mL round bottom flask along with a stir bar. The flask was placed in an ice bath and the TEA was cooled to 0 °C. Water (25 mL) was added to the flask along with serotonin•HCl (1.0 g, 4.7 mmol). Boc anhydride (1.5 mL, 5.2 mmol) was dissolved in 25 mL dioxane and placed in an addition funnel. The Boc solution was added to the round bottom flask over 5 min. After 15 min the ice bath was removed. The solution was allowed got stir for 3 h at which time the solution was extracted with EtOAc. The organic layer was then washed with saturated $NaHCO_3$, dilute HCl, and brine and then dried over $MgSO_4$. The drying agent was removed by filtration and the solvent was removed yielding brown oil. The crude material was purified by flash chromatography (7:3 hexanes/EtOAc) resulting in a solid (0.96 g, 3.5 mmol, 74 %; mp: 115 – 117 °C). ^{1}H NMR (500 MHz, DMSO): δ (ppm) 10.57 (s, 1H), 8.59 (s, 1H) 7.12 (d, 1H), 7.02 (s, 1H), 6.94 (s, 1H), 6.79 (s, 1H), 6.53 (s, 1H), 3.17 (m, 2H), 2.73 (m, 2H), 1.23 (s, 9H). ^{13}C NMR (500 MHz, $CDCl_3$): δ (ppm) 155.52, 150.11, 130.73, 127.87, 122.97, 155.27, 111.58, 111.19, 110.73, 102.16, 77.39, 41.86, 30.67, 28.27. IR (KBr, cm^{-1}): 3440, 3367, 3330, 1676, 1674, 1600, 1592, 1511, 1432, 1222, 842. HRMS (m/z) calc for $C_{15}H_{20}N_2O_3$ 276.15, found 277.1552 (M + H).

***p*-Hydroxyoxyphenacyl *N*-Boc-Serotonin 86**. *p*-Hydroxyphenacyl *N*-Boc-Serotonin **86** was prepared according to a method based on one described by Rannard and Davis[105]. Imidazole carboxylic ester **81** (1.5 g, 3.1 mmol), protected serotonin **85**

(0.95 g, 3.5 mmol), and potassium carbonate (1.1 g, 7.9 mmol) were dissolved in CH_3CN and allowed to stir at rt for 24 h, then the solvent was removed and the solid was dissolved in EtOAc. The organic solution was washed with water, saturated $NaHCO_3$, dilute HCl, and brine. The organic layer was then dried over $MgSO_4$, filtered, and the solvent removed. The crude material was purified by flash chromatography (1:1 hexanes/EtOAc) and a white solid was isolated (0.34 g, 0.50 mmol, 16%; mp = 169 – 171 °C). ^{1}H NMR (500 MHz, DMSO): δ (ppm) 10.87 (s, 1H), 10.37 (s, 1H), 7.77 (d, 2H) 7.24 (m, 3H), 7.04 (s, 1H), 6.76 (m, 3H), 5.34 (s, 2H), 2.99 (m, 2H), 2.56 (m, 2H), 1.98 (2, 2H), 1.23 (s, 9H). ^{13}C NMR (500 MHz, $CDCl_3$): δ (ppm) 206.50, 190.33, 162.79, 155.53, 153.86, 143.77, 134.04, 130.39, 127.25, 125.12, 124.49, 115.48, 112.30, 111.82, 109.76, 77.41, 69.15, 41.89, 30.68, 28.25. IR (KBr, cm^{-1}):3429, 3365, 3333, 1761, 1679, 1674, 1603, 1585, 1516, 1429, 1217, 839. HRMS (m/z) calc for $C_{24}H_{26}N_2O_7$ 454.2, found 455.1818 (M + H).

X-Ray Crystal Structures for pHP Derivatives (See **Appendices A and B)**

The X-ray crystallographer would like to thank the National Science Foundation (grant CHE-0079282) and the University of Kansas for funds to purchase the x-ray instrument and computers and to thank the EMSL facility at the Pacific Northwest National Laboratory in Richland, Washington for providing access to the x-ray instrument and computers used to collect the data used to solve and refine the crystal structure for pHP Tosylate **72b**.

pHP Formate 70a. Colorless crystals of $C_9H_8O_4$ are, at 100(2) K, monoclinic, space group $P2_1/c$ – C_{2h}^5 (No. 14)[123] with **a** = 8.9605(6) Å, **b** = 8.3220(6) Å, **c** = 10.6750(7) Å, β = 98.930(2)°, V = 786.38(9) Å^3 and Z = 4 molecules {d_{calcd} = 1.522 g/cm^3; μ_a(MoKα) = 0.121 mm^{-1}}. A full hemisphere of diffracted intensities (1850 10-second frames with a ω scan width of 0.30°) was measured for a single-domain specimen using graphite-monochromated MoKα radiation (λ= 0.71073 Å) on a Bruker SMART APEX CCD Single Crystal Diffraction System[124]. X-rays were provided by a fine-focus sealed x-ray tube operated at 50kV and 30mA. Lattice constants were determined with the Bruker SAINT software package using peak centers for 3517 reflections. A total of 9794 integrated reflection intensities having 2θ((MoKα)< 60.99° were produced using the Bruker program SAINT[125]; 2389 of these were unique and gave R_{int} = 0.033 with a coverage which was 99.7% complete. The data were corrected empirically for variable absorption effects using equivalent reflections; the relative transmission factors ranged from 0.949 to 1.000. The Bruker

software package SHELXTL was used to solve the structure using "direct methods" techniques. All stages of weighted full-matrix least-squares refinement were conducted using F_o^2 data with the SHELXTL Version 6.10 software package[126].

The final structural model incorporated anisotropic thermal parameters for all nonhydrogen atoms and isotropic thermal parameters for all hydrogen atoms. All hydrogen atoms were located in a difference Fourier and included in the structural model as independent isotropic atoms whose parameters were allowed to vary in least-squares refinement cycles. A total of 150 parameters were refined using no restraints, 2389 data and weights of $w = 1/ [\sigma^2(F^2) + (0.0721\ P)^2]$, where $P = [F_o^2 + 2F_c^2] / 3$. Final agreement factors at convergence are: R_1(unweighted, based on F) = 0.039 for 1979 independent absorption-corrected "observed" reflections having $2\theta(MoK\alpha) < 60.99°$ and $I > 2\sigma(I)$; R_1(unweighted, based on F) = 0.046 and wR_2(weighted, based on F^2) = 0.107 for all 2389 independent absorption-corrected reflections having $2\theta(MoK\alpha) < 60.99°$. The largest shift/s.u. was 0.000 in the final refinement cycle. The final difference map had maxima and minima of 0.47 and -0.24 $e^-/Å^3$, respectively.

pHP Benzoate 70c. Colorless crystals of $C_{15}H_{12}O_4$ are, at 100(2) K, orthorhombic, space group $P2_12_12_1 - D_2^4$ (No. 19)[123] with **a** = 8.470(1) Å, **b** = 9.844(1) Å, **c** = 14.474(2) Å, V = 1206.8(3) $Å^3$ and Z = 4 molecules {d_{calcd} = 1.410 g/cm^3; $\mu_a(MoK\alpha)$ = 0.103 mm^{-1}}. A full hemisphere of diffracted intensities (1850

10-second frames with a ω scan width of 0.30°) was measured for a single-domain specimen using graphite-monochromated MoKα radiation (λ= 0.71073 Å) on a Bruker SMART APEX CCD Single Crystal Diffraction System[124]. X-rays were provided by a fine-focus sealed x-ray tube operated at 50kV and 30mA. Lattice constants were determined with the Bruker SAINT software package using peak centers for 1901 reflections. A total of 14702 integrated reflection intensities having 2θ((MoKα)< 61.14° were produced using the Bruker program SAINT[125]; 3686 of these were unique and gave R_{int} = 0.056 with a coverage which was 99.9% complete. The data were corrected empirically for variable absorption effects using equivalent reflections; the relative transmission factors ranged from 0.877 to 1.000. The Bruker software package SHELXTL was used to solve the structure using "direct methods" techniques. All stages of weighted full-matrix least-squares refinement were conducted using F_o^2 data with the SHELXTL Version 6.10 software package[126].

The final structural model incorporated anisotropic thermal parameters for all nonhydrogen atoms and isotropic thermal parameters for all hydrogen atoms. All hydrogen atoms were located in a difference Fourier and included in the structural model as independent isotropic atoms whose parameters were allowed to vary in least-squares refinement cycles. A total of 220 parameters were refined using no restraints, 3686 data and weights of $w = 1/ [\sigma^2(F^2) + (0.0648 P)^2 + 0.2445 P]$, where $P = [F_O^2 + 2F_C^2] / 3$. Final agreement factors at convergence are: R_1(unweighted, based on F) = 0.066 for 2836 independent absorption-corrected "observed" reflections having 2θ(MoKα)< 61.14° and I>2σ(I); R_1(unweighted, based on F) = 0.089 and

wR_2(weighted, based on F^2) = 0.148 for all 3686 independent absorption-corrected reflections having 2θ(MoKα)< 61.14°. The largest shift/s.u. was 0.000 in the final refinement cycle. The final difference map had maxima and minima of 0.39 and -0.32 $e^-/Å^3$, respectively. Since the "Flack" parameter refined to a final value of 0.0(14), the absolute structure could not be reliably determined experimentally using anomalous dispersion of the x-rays.

pHP *p*-Methoxybenzoate 70d. Colorless crystals of $C_{16}H_{14}O_5$ are, at 100(2) K, monoclinic, space group $P2_1$– C_2^2 (No. 4)[123] with **a** = 8.5122(9) Å, **b** = 5.2444(6) Å, **c** = 15.108(2) Å, β = 92.049(2)°, V = 674.0(1) $Å^3$ and Z = 2 molecules {d_{calcd} = 1.411 g/cm^3; μ_a(MoKα) = 0.105 mm^{-1}}. A full hemisphere of diffracted intensities (1850 10-second frames with a ω scan width of 0.30°) was measured for a single-domain specimen using graphite-monochromated MoKα radiation (λ= 0.71073 Å) on a Bruker SMART APEX CCD Single Crystal Diffraction System[124]. X-rays were provided by a fine-focus sealed x-ray tube operated at 50kV and 30mA. Lattice constants were determined with the Bruker SAINT software package using peak centers for 2620 reflections. A total of 8175 integrated reflection intensities having 2θ((MoKα)< 61.16° were produced using the Bruker program SAINT[125]; 4008 of these were unique and gave R_{int} = 0.025 with a coverage which was 99.3% complete. The data were corrected empirically for variable absorption effects using equivalent reflections; the relative transmission factors ranged from 0.916 to 1.000. The Bruker software package SHELXTL was used to solve the structure using "direct methods"

techniques. All stages of weighted full-matrix least-squares refinement were conducted using F_o^2 data with the SHELXTL Version 6.10 software package[126].

The final structural model incorporated anisotropic thermal parameters for all nonhydrogen atoms and isotropic thermal parameters for all hydrogen atoms. All hydrogen atoms were located in a difference Fourier and included in the structural model as independent isotropic atoms whose parameters were allowed to vary in least-squares refinement cycles. A total of 246 parameters were refined using 1 restraint, 4008 data and weights of $w = 1/ [\sigma^2(F^2) + (0.0689\ P)^2]$, where $P = [F_O^2 + 2F_C^2] / 3$. Final agreement factors at convergence are: R_1(unweighted, based on F) = 0.046 for 3409 independent absorption-corrected "observed" reflections having $2\theta(MoK\alpha) < 61.16°$ and $I > 2\sigma(I)$; R_1(unweighted, based on F) = 0.055 and wR_2(weighted, based on F^2) = 0.112 for all 4008 independent absorption-corrected reflections having $2\theta(MoK\alpha) < 61.16°$. The largest shift/s.u. was 0.000 in the final refinement cycle. The final difference map had maxima and minima of 0.40 and -0.18 $e^-/Å^3$, respectively. Since the "Flack" parameter refined to a final value of 1.4(8), the absolute structure could not be reliably determined experimentally using anomalous dispersion of the x-rays.

pHP Mesylate 72a. Colorless crystals of $C_9H_{10}O_5S$ are, at 100(2) K, monoclinic, space group $P2_1/m$ - C_{2h}^2 (No. 11)[123] with **a** = 8.129(1) Å, **b** = 6.609(1) Å, **c** = 8.868(1) Å°, β = 97.535(3)°, V = 472.3(1) $Å^3$ and Z = 2 molecules {d_{calcd} =

1.619 g/cm^3; μ_a(MoKα) = 0.341 mm^{-1}}. A full hemisphere of diffracted intensities (1850 20-second frames with a ω scan width of 0.30°) was measured for a single-domain specimen using graphite-monochromated MoKα radiation (λ= 0.71073 Å) on a Bruker SMART APEX CCD Single Crystal Diffraction System[124]. X-rays were provided by a fine-focus sealed x-ray tube operated at 50kV and 35mA. Lattice constants were determined with the Bruker SAINT software package using peak centers for 2085 reflections. A total of 5835 integrated reflection intensities having 2θ((MoKα)< 60.95° were produced using the Bruker program SAINT[125]; 1551 of these were unique and gave R_{int} = 0.038 with a coverage which was 99.6% complete. The data were corrected empirically for variable absorption effects using equivalent reflections; the relative transmission factors ranged from 0.934 to 1.000. The Bruker software package SHELXTL was used to solve the structure using "direct methods" techniques. All stages of weighted full-matrix least-squares refinement were conducted using F_o^2 data with the SHELXTL Version 6.10 software package[126].

The final structural model incorporated anisotropic thermal parameters for all nonhydrogen atoms and isotropic thermal parameters for all hydrogen atoms. All hydrogen atoms were located in a difference Fourier and included in the structural model as independent isotropic atoms whose parameters were allowed to vary in least-squares refinement cycles. A total of 114 parameters were refined using no restraints, 1551 data and weights of w = 1/ [$\sigma^2(F^2)$ + (0.0573 P)^2], where P = [F_O^2 + 2F_C^2] / 3. Final agreement factors at convergence are: R_1(unweighted, based on F) =

0.042 for 1383 independent absorption-corrected "observed" reflections having $2\theta(MoK\alpha) < 60.95°$ and $I > 2\sigma(I)$; R_1(unweighted, based on F) = 0.049 and wR_2(weighted, based on F^2) = 0.106 for all 1551 independent absorption-corrected reflections having $2\theta(MoK\alpha) < 60.95°$. The largest shift/s.u. was 0.000 in the final refinement cycle. The final difference map had maxima and minima of 0.74 and -0.27 $e^-/Å^3$, respectively.

pHP Tosylate 72b. Colorless needle-shaped crystals of $C_{15}H_{14}SO_5$ are, at 296(2) K, monoclinic, space group $P2_1/c - C_{2h}^5$ (No. 14)[123] with **a** = 5.6756(4) Å, **b** = 14.2907(8) Å, **c** = 17.744(1) Å, β = 99.153(5)°, V = 1420.9(2) $Å^3$ and Z = 4 molecules {d_{calcd} = 1.432 g/cm^3; $\mu_a(CuK\alpha)$ = 2.209 mm^{-1}}. A full hemisphere of diffracted intensities (3134 5-second frames with an ω or φ scan width of 0.80°) was measured for a two-domain specimen using monochromated CuKα radiation (λ= 1.54178 Å) on a Bruker Proteum SMART 6000 Single Crystal Diffraction System[124]. X-rays were provided by a Bruker-Nonius FR591 rotating anode operating at 5kW with a 3.0 x 3.0 mm focal cup. The beam was collimated and focused with double-diffracting confocal multilayer optics (Montel mirrors). Lattice constants were determined with the Bruker SAINT software package using peak centers for 6721 reflections. A total of 11299 integrated reflection intensities having $2\theta(CuK\alpha) <$ 137.53° were produced using the Bruker program SAINT[125]; 2540 of these were unique and gave R_{int} = 0.069 with a coverage which was 94.9% complete. The data were corrected empirically[127] for variable absorption effects using equivalent

reflections; the relative transmission factors ranged from 0.830 to 1.000. The Bruker software package SHELXTL was used to solve the structure using "direct methods" techniques. All stages of weighted full-matrix least-squares refinement were conducted using F_o^2 data with the SHELXTL Version 6.10 software package[126].

The crystal initially appeared to utilize the C-centered orthorhombic space group $C222_1 - D_2^5$ (No. 20) with **a** = 5.6756(4) Å, **b** = 35.036(2) Å and **c** = 14.2907(8) Å. Merging the intensity data according to orthorhombic D_{2h}-mmm Laue symmetry gave R_{sym} = 0.088. When the structure could not be solved in this orthorhombic space group, the symmetry was reduced to monoclinic $C2_1$ [a nonstandard centered setting of $P2_1 - C_2^2$ (No. 4) with **c** as the unique axis]. The structure was solved in this space group to give an asymmetric unit that contained two crystallographically-independent molecules. When properly translated and transformed in the unit cell, these two molecules were seen to be rigorously related by the symmetry operations of space group $P2_1/c$ when the C-centered orthorhombic unit cell was transformed to the corresponding primitive monoclinic cell. The data frames were reintegrated based on the primitive monoclinic unit cell and final lattice constants were obtained. However, the structural model containing one independent $C_{15}H_{14}SO_5$ molecule in space group $P2_1/c$ would not refine below R_1 = 0.28. Incorporation of 2-domain (54/46) pseudomerohedral twinning by a twofold rotation about the orthorhombic **a** axis, reduced R_1 to 0.07.

The final structural model utilized space group $P2_1/c$ and incorporated anisotropic thermal parameters for all nonhydrogen atoms and isotropic thermal

parameters for all hydrogen atoms. All hydrogen atoms were located in a difference Fourier and included in the structural model as independent isotropic atoms whose parameters were allowed to vary in least-squares refinement cycles. A total of 248 parameters were refined using no restraints, 2540 data and weights of $w = 1/ [\sigma^2(F^2) + (0.0725\ P)^2 + 1.0148\ P]$ where $P = [F_O^2 + 2F_C^2] / 3$. Final agreement factors at convergence are: R_1(unweighted, based on F) = 0.066 for 2312 independent absorption-corrected "observed" reflections having $2\theta(CuK\alpha) < 137.53°$ and $I > 2\sigma(I)$; R_1(unweighted, based on F) = 0.071 and wR_2(weighted, based on F^2) = 0.163 for all 2540 independent absorption-corrected reflections having $2\theta(CuK\alpha) < 137.53°$. The largest shift/s.u. was 0.000 in the final refinement cycle. The final difference map had maxima and minima of 0.45 and -0.35 $e^-/Å^3$, respectively.

Photochemistry

Photolyses were performed in a Rayonet RPR-100 photochemical reactor (Southern New England Ultraviolet Company) fitted with 4 or 8 2540 Å bulbs, either 1, 2, or 4 3000 Å bulbs, or 16 3500 Å bulbs. The Rayonet reactor was turned on to warm up the lamps for 15 minutes prior to sample irradiation. Samples were irradiated in Pyrex NMR tubes or quartz test tubes at ambient temperature without degassing unless otherwise noted. The tubes were placed in a RPR merry-go-round apparatus and the counter was started at the onset of exposure to record the time of irradiation. Exposure times were controlled by manual removal of the sample from the reactor or alternatively by turning the lamps on and off. Light output experiments were performed according to the method employed by Hatchard and Parker[128] using potassium ferrioxalate as the actinometer.

General Procedure for Photolysis Product Determination (^{1}H NMR). In a 1 mL volumetric flask, 10 – 15 mg of the pHP ester was dissolved in 100 – 700 μL CD_3CN and diluted with D_2O. The solution was transferred to an NMR tube, the internal standard was added (DMF, 3.0 μL, 35 mmol), and the solution was mixed thoroughly. The NMR tube was placed into the photoreactor fitted with 254 nm, 300 nm, or 350 nm bulbs and irradiated for approximately 30 min. ^{1}H NMR spectra were taken before and after irradiation making sure to designate the integration of the internal standard. The spectrum of possible products (*p*-hydroxyphenylacetic acid **52a**, *p*-hydroxybenzyl alcohol **87**, *p*-hydroxyacetophenone **62**, formic acid **71a**,

benzoic acid **4**, *p*-methoxybenzoic acid **71d**, *p*-trifluoromethylbenzoic acid **71e**, methane sulfonic acid **89a**, and *p*-toluenesulfonic acid **89b**) with DMF was also taken so that a comparison could be made between the product and reaction mixture spectra. The disappearance of starting material and appearance of products were monitored using the integration of the signals for peaks characteristic to each compound. The percent conversion was calculated for each reaction by calculating the difference in mmol of the starting material at the beginning and at the end of the photolysis. The starting material and products in the reaction mixture were also identified by LC-MS.

Quantum Efficiency Determination (^{1}H NMR). In a 1 mL volumetric flask, 10 – 15 mg of the pHP ester was dissolved in 100 – 700 μL of CD_3CN. The solution was diluted to with D_2O and transferred to a NMR tube. Internal standard (DMF, 3 μL, 35 mmol) was added to the NMR tube and mixed thoroughly. The NMR tube was placed into the photoreactor that had been fitted with 254, 300, or 350 nm bulbs and was irradiated for 60 min. ^{1}H NMR spectra were taken at 0, 10, 20, 30, 40, 50, and 60 min making sure to designate the integration of the internal standard. The disappearance of starting material and appearance of products were monitored using the integration of the signals characteristic to each compound. The percent conversion was calculated along with the mmol of each compound in the solution. A graph was constructed plotting mmol versus time where the slope represents the change in mmol per unit time (min). The slope was then divided by the light output of the bulbs to

obtain the quantum efficiencies for the disappearance of starting material (Φ_{dis}) and the appearance of each product (Φ_{acid}, Φ_{pHPAA}, Φ_{pHBA}, and Φ_{pHPOH}).

Preliminary Quantum Efficiency Determination of pHP pCF_3 Benzoate 70e. To a 10 mL volumetric flask, 2.0 mL of a biphenyl stock solution (2.1 mM) was combined with 8.0 mL ester **70e** (5.1×10^{-3} M) dissolved in a 7:3 mixture of HPLC grade acetonitrile and water. The solution was transferred to a quartz tube and placed into a photoreactor that had been fitted with two 300 nm bulbs. The sample was irradiated for 30 min with 1.0 mL aliquots removed every 5 min. Before each aliquot was removed, the test tube was inverted 3 times to ensure proper mixing. The samples were then analyzed by HPLC so that the quantum efficiency (Φ_{dis}) could be determined.

Preliminary Quantum Efficiency Determination of pHP Benzoate 70c. To a 10 mL volumetric flask, 2.0 mL of a biphenyl stock solution (5.5 mM) was combined with 8.0 mL ester **70c** (5.3×10^{-3} M) dissolved in a 7:3 mixture of HPLC grade acetonitrile and water. The solution was transferred to a quartz tube and placed into a photoreactor that had been fitted with two 300 nm bulbs. The sample was irradiated for 30 min with 1.0 mL aliquots removed every 5 min. Before each aliquot was removed, the test tube was inverted 3 times to ensure proper mixing. The samples were then analyzed by HPLC so that the quantum efficiency (Φ_{dis}) could be determined.

Preliminary Quantum Efficiency Determination of pHP pOCH$_3$ Benzoate 70d. To a 10 mL volumetric flask, 2.0 mL of a biphenyl stock solution (6.7 mM) was combined with 8.0 mL ester **70d** (5.2×10^{-3} M) dissolved in a 7:3 mixture of HPLC grade acetonitrile and water. The solution was transferred to a quartz tube and placed into a photoreactor that had been fitted with two 300 nm bulbs. The sample was irradiated for 30 min with 1.0 mL aliquots removed every 5 min. Before each aliquot was removed, the test tube was inverted 3 times to ensure proper mixing. The samples were then analyzed by HPLC so that the quantum efficiency (Φ_{dis}) could be determined.

Quantum Efficiencies Determination of the pHP Benzoates. In a 25 mL volumetric flask, 25 mmol of benzoate **70c-e** was combined with 32 mg (0.15 mmol) biphenyl. The solids were dissolved in 17.5 mL HPLC grade acetonitrile and diluted with HPLC grade water. The solution was transferred to a quartz tube and inverted 3 times to ensure proper mixing. The quartz tube was placed in the photoreactor which had been equipped with two 300 nm bulbs and were irradiated for 40 min. At 4 min intervals, the tube was taken out of the reactor, inverted three times, and 150 μL were removed. The aliquots were placed in vials that had been acidified with 50 μL of 10% formic acid **71a** and diluted with the same solvents as above (7:3 CH_3CN/H_2O). The samples were placed in crimp top HPLC vials and submitted to be analyzed by HPLC. Using ratios of peak areas, the percent conversion and the concentrations of the starting material and products at each time could be determined. From this the quantum efficiencies were calculated (**Table 18**).

Methyl Sorbate Quenching Experiments for Benzoates 70c and 70e. In a 25 mL volumetric flask, 25 mmol of benzoate ester **70c** or **70e** and 32 mg (0.21 mmol) biphenyl were combined. The appropriate amount of HPLC grade acetonitrile was added to give a 7:3 CH_3CN/H_2O mixture after the addition of the amount of quencher which had been dissolved in acetonitrile. Varying amounts of a 0.5 M stock solution of methyl sorbate were added to the flask corresponding to the following concentrations: 0.0; 2.5×10^{-4}; 5.0×10^{-4}; 7.5×10^{-4}; 1.0×10^{-3}; 2.5×10^{-3}; 5.0×10^{-3}; 7.5×10^{-3}; and 1.0×10^{-2} M. The solution was diluted with water and mixed thoroughly. The solution was transferred to a quartz tube, inverted 3 times to mix, and placed in the photoreactor set up with two 300 nm bulbs. The solution was irradiated for 40 min removing 150 μL aliquots are 4 min intervals. The aliquots were acidified with 50 μL 10% formic acid, diluted with 1.5 mL acetonitrile, transferred to HPLC vials, and submitted for HPLC analysis. The data was analyzed and the quantum efficiencies were graphed in Stern-Volmer plots. From the K_{SV} approximate rates of starting material disappearance and triplet lifetimes were calculated.

Piperylene Quenching Experiments for pHP Benzoates. In a 25 mL volumetric flask, 25 mmol of benzoate ester **70c-e** and 32 mg (0.21 mmol) biphenyl were combined. The appropriate amount of HPLC grade acetonitrile was added to give a 7:3 CH_3CN/H_2O mixture after the addition of the amount of quencher which had been dissolved in acetonitrile. Varying amounts of a 1.0 M stock solution of methyl sorbate were added to the flask corresponding to the following concentrations: 0.0, 2.0×10^{-2}, 4.0×10^{-2}, 6.0×10^{-2}, and 8.0×10^{-2} M. The solution was diluted with

water and mixed thoroughly. The solution was transferred to a quartz tube, inverted 3 times to mix, and placed in the photoreactor set up with two 300 nm bulbs. The solution was irradiated for 60 min removing 150 μL aliquots are 5 min intervals. The aliquots were acidified with 50 μL 10% formic acid, diluted with 1.5 mL acetonitrile, transferred to HPLC vials, and submitted for HPLC analysis. The data was analyzed and he quantum yields were graphed in Stern-Volmer plots (**Figures 8 - 10**, **Table 20**).

Identification of *p*-Hydroxybenzyl Alcohol (87) in Benzoate Photolysis Mixtures. Mixtures containing **87**, **52a, 4**, **71d**, **71e**, **70c**, **70d**, and **70e** in concentrations of 5.0 mM along with biphenyl (6.0 mM) were analyzed by HPLC. For each peak the retention times and molecular ions were recorded. In a 25 mL volumetric flask, 25 mmol of benzoate **70c**, **70d**, or **70e** was combined with 32 mg (0.15 mmol) biphenyl. The solids were dissolved in 17.5 mL HPLC grade acetonitrile and diluted with HPLC grade water. The solution was transferred to a quartz tube and inverted 3 times to ensure proper mixing. The quartz tube was placed in the photoreactor which had been equipped with two 300 nm bulbs and were irradiated for 60 min. At t = 0 min and t = 60 min, the tube was taken out of the reactor, inverted three times, and 150 μL were removed. The aliquots were placed in vials that had been acidified with 50 μL of 10% formic acid **71a** and diluted with the same solvents as above (7:3 CH_3CN/H_2O). The samples were placed in crimp top HPLC vials and submitted to be analyzed by LC-MS.

Quantum Efficiency Determination of Formate and Mesylate Esters 70a and 72a. Stock solutions of esters **70a** and **72a** (100 M) were made by dissolving the solid in HPLC grade acetonitrile. A stock solution of acetaminophen (6.9×10^{-2} M) was made by dissolving the solid in HPLC grade water. In a quartz test tube, the ester (250 μL), acetaminophen (250 μL), and water (500 μL) were combined. The contents were mixed well. The tube was irradiated for 10 min. Aliquots (10 μL) were removed before the tube was irradiated and at 2 min intervals during irradiation. The aliquots were diluted with 490 μL water. The samples were then analyzed by HPLC (**Table 19**).

Quantum Efficiency Determination of Tosylate Ester 72b. A stock solution of ester **72b** (100 M) and biphenyl (5.2×10^{-2} M) were made by dissolving the solids in HPLC grade acetonitrile. In a quartz test tube, the ester (250 μL), acetaminophen (250 μL), and water (500 μL) were combined. The contents were mixed well. The tube was irradiated for 10 min. Aliquots (10 μL) were removed before the tube was irradiated and at 2 min intervals during irradiation. The aliquots were diluted with 490 μL water. The samples were then analyzed by HPLC (**Table 19**).

Quantum Yield Determination of Mesylate Ester 72b in Phosphate Buffer. Three phosphate buffer solutions (1.33×10^{-2} M) were made by dissolving sodium phosphate in HPLC grade water. The pH was adjusted to 3, 7, and 12 using phosphoric acid and concentrated sodium hydroxide. A stock solution of mesylate ester **72b** (100 M) and acetaminophen (5.3×10^{-2} M) was made by combining the

solids in a 10 mL volumetric flask and dissolving the solids in HPLC grade acetonitrile. In a quartz tube, the ester/acetaminophen mixture (250 μL) was diluted with phosphate buffer solution (750 μL of 1.33 x 10^{-2} M pH 3.03, 7.06, or 12.02) and the contents were mixed thoroughly. The tube was then irradiated for 10 min. Aliquots were removed before the tube was irradiated and at 2 min intervals during irradiation. These aliquots were diluted with 490 μL water and analyzed by HPLC (**Table 23**).

Picosecond Pump-Probe Spectroscopy[109]. Picosecond transient absorption was measured with the pump-supercontinum probe technique using a Ti/Sa laser system (Clark MXR CPA-2001; 775 nm, pulse energy = 0.9 mJ; full width at half maximum = 150 fs; operating frequency 426 Hz). Part of the beam was fed into a Clark MXR NOPA. The output at 532 nm was frequency-doubled by a β-barium borate (BBO) crystal to 266 nm and after from of a CaF_2 of 4 mm path length. The pump and probe beams were focused to a 0.04 mm^2 spot on the sample that was flowing in an optical cell of 0.3 mm thickness. The absorbance was in the range of 0.3 – 1 depending on the solubility of the compound. The probe beam and a reference signal (passing the solution besides the pump beam) were spectrally dispersed and registered with two photodiode arrays (512 pixels). Transient absorption spectra were calculated from the ratio of the two beams. Spectra were recorded with time delays ranging from 0 – 1.8 ns (to observe the triplet decay) were typically recorded with 20 ps steps, those ranging from 0 – 8 ps (to observe ISC) with 80 fs steps. The shorter measurements were corrected for chirp using a program (SPAN) kindly provided by

Prof. N. Ernsting, Berlin. To improve the signal-to-noise ratio, the data were averaged over multiple pump-probe scans (3 – 6 scans with 400 shots per temporal point). Results reported in **Table 21**.

REFERENCES

(1) Corey, E. J.; Cheng, X.-M. *The Logic of Chemical Synthesis*; John Wiley & Sons: New York, 1995.
(2) Barltrop, J. A.; Schofield, P. *Tetrahedron Letters* **1962** *16*, 697-699.
(3) Kaplan, J. H.; Forbush, B. I.; Hoffman, J. F. *Biochemistry* **1978**, *17*, 1929-1935.
(4) Givens, R. S.; Weber, J. F. W.; Jung, A. H.; Park, C.-H. *Caged Compounds*; Academic Press: New York, 1998; Vol. 29.
(5) Baldwin, J. E.; McConnaughie, A. W.; Moloney, M. G.; Pratt, A. J.; Shim, S. B. *Tetrahedron* **1990**, *46*, 6879-6884.
(6) Wang, B.; Zheng, A. *Chem. Pharm. Bull.* **1997**, *45*, 715-718.
(7) Koenings, P. M.; Faust, B. C.; Porter, N. A. *J. Am. Chem. Soc.* **1993**, *115*, 9371-9379.
(8) Sheehan, J. C.; Umezawa, K. *J. Org. Chem.* **1973**, *38*, 3771-3774.
(9) Lester, H. A.; Nerbonne, J. M. *Ann. Rev. Biophys. Bioeng.* **1982**, *11*, 151-175.
(10) Turner, A. D.; Pizzo, S. V.; Royakis, G.; Porter, N. A. *J. Am. Chem. Soc.* **1988**, *110*, 244-250.
(11) Sheehan, J. C.; Wilson, R. M. *J. Am. Chem. Soc.* **1964**, *86*, 5277-5281.
(12) Hillborn, J. W.; MacKnight, E.; Pincock, J. A.; Wedge, P. J. *J. Am. Chem. Soc.* **1994**, *116*, 3337-3346.
(13) Barltrop, J. A.; Plant, P. J.; Scholfield, P. *J. Chem. Soc. Chem. Comm.* **1966**, 822-823.
(14) Reid, V. W.; Wilk, M. *Justus Liebigs Ann. Chem.* **1954**, *590*, 91-110.
(15) Walker, J. W.; Lu, Z.; Moss, R. L. *J. Biol. Chem.* **1992**, *267*, 2459-2466.
(16) Willenbucher, R. F.; Xie, Y. N.; Eysselein, V. E.; Snape, W. J., Jr. *Am. J. Phys.* **1992**, *262*, G159-G164.
(17) Ostap, E. M.; Thomas, D. D. *Biophysical Journal* **1991**, *59*, 1235-1241.
(18) Tepe, J. J.; Williams, R. M. *J. Am. Chem. Soc.* **1999**, *121*, 2951-2995.
(19) Il'ichev, Y. V.; Schworer, M.; Wirz, J. *J. Am. Chem. Soc.* **2004**, *126*, 4581-4595.
(20) Hellrung, B.; Kamdzhilov, Y.; Schworer, M.; Wirz, J. *J. Am. Chem. Soc.* **2005**, *127*, 8934-8935.
(21) Walker, J. W.; Reid, V. W.; A., M. J.; Trentham, D. R. *J. Am. Chem. Soc.* **1988**, *110*, 7170-7177.
(22) Givens, R. S.; Kotala, M. B.; Lee, J.-I. In *Dynamic Studies in Biology*; Wiley-VCH: Weinheim, 2005, p 95-129.
(23) Zimmerman, H. E.; Sandel, V. R. *J. Am. Chem. Soc.* **1963**, *85*, 915-922.
(24) Zimmerman, H. E. *J. Phys. Chem. A* **1998**, *102*, 7725.
(25) Zimmerman, H. E. *J. Phys. Chem. A* **1998**, *102*, 5616-5621.
(26) DeCosta, D. P.; Pincock, J. A. *J. Am. Chem. Soc.* **1993**, *115*, 2180-2190.
(27) Pincock, J. A. *Accounts of Chemical Research* **1997**, *30*, 43-49.
(28) Schade, B.; Hagen, V.; Schmidt, R.; Herbrich, R.; Krause, E.; Eckardt, T.; Bendig, J. *J. Org. Chem.* **1999**, *64*, 9109-9117.

(29) Lin, W.; Lawrence, D. S. *J. Org. Chem.* **2002**, *67*, 2723-2726.
(30) Furuta, T.; Momotaka, A.; Sugimoto, M.; Hatayajma, M.; Torigai, H.; al., e. *Biochem. Biophys. Res. Commun.* **1996**, *228*, 193-198.
(31) Hagen, V.; Bendig, J.; Frings, S.; Eckardt, T.; Helm, S.; al., e. *Angewandte Chemie Int. Ed. Engl.* **2001**, *40*, 1046-1048.
(32) Schmidt, R.; Geissler, D.; Hagen, V.; Bendig, J. *J. Phys. Chem. A* **2005**, *109*, 5000-5004.
(33) Schmidt, R.; Geissler, D.; Hagen, V.; Bendig, J. *J. Phys. Chem. A* **2007**, *111*, 5768-5774.
(34) Eckardt, T.; Hagen, V.; Schade, B.; Schmidt, R.; Schweitzer, C.; Bendig, J. *J. Org. Chem.* **2002**, *67*, 703-710.
(35) Sheehan, J. C.; Wilson, R. M.; Oxford, A. W. *J. Am. Chem. Soc.* **1971**, *93*, 7222-7228.
(36) Givens, R. S.; Matuszewski, B. *J. Am. Chem. Soc.* **1984**, *106*, 6860-6861.
(37) Givens, R. S.; Athey, P. S.; Kueper, L. W.; Matuszewski, B.; Xue, J.-Y. *J. Am. Chem. Soc.* **1992**, *114*, 8708-8710.
(38) Givens, R. S.; Athey, P. S.; Matuszewski, B.; Kueper, L. W.; Xue, J.-Y.; al., e. *J. Am. Chem. Soc.* **1993**, *115*, 6001-6012.
(39) Rajesh, C. S.; Givens, R. S.; Wirz, J. *J. Am. Chem. Soc.* **2000**, *122*, 611-618.
(40) Boudebous, H.; Kosmrlj, B.; Sket, B.; Wirz, J. *J. Phys. Chem. A* **2007**, *111*, 2811-3813.
(41) Rock, R. S.; Chan, S. I. *J. Org. Chem.* **1996**, *61*, 1526-1529.
(42) Corrie, J. E. T.; Trentham, D. R. *J. Chem. Soc., Perking Trans. 1* **1992**, 2409-2417.
(43) Epstein, W. W.; Garrossian, M. *J. Chem. Soc. Chem. Comm.* **1987**, 532-533.
(44) Anderson, J. C.; Reese, C. B. *Tetrahedron Letters* **1962**, *1*, 1-4.
(45) Dhavale, D. D.; Mali, V. P.; Sudrik, S. G.; Sonawane, H. R. *Tetrahedron* **1997**, *53*, 16789-16794.
(46) Sonawane, H. R.; Bellur, N. S.; Kulkarni, D. G.; Ayyangar, N. R. *Tetrahedron* **1994**, *50*, 1243-1260.
(47) Park, C.-H.; Givens, R. S. *J. Am. Chem. Soc.* **1997**, *119*, 2453-2463.
(48) Givens, R. S.; Jung, A. H.; Park, C.-H. *J. Am. Chem. Soc.* **1997**, *119*, 8369-7370.
(49) Givens, R. S.; Weber, J. F. W.; Conrad, P. G., II; Orosz, G.; Donahue, S. L.; et. al. *J. Am. Chem. Soc.* **2000**, *122*, 2687-2697.
(50) Klinker, C.; Bowser, M. T. *Anal. Chem.* **2007**, *79*, 8747-8754.
(51) Clift, M. D.; Ji, H.; Deniau, G. P.; O'Hagan, D.; Silverman, R. B. *Biochemistry* **2007**, *46*, 13819-13828.
(52) O'Brien, K. B.; Esguerra, M.; Miller, R. F.; Bowser, M. T. *Anal. Chem.* **2004**, *76*, 5069-5074.
(53) Shikata, T.; Hashimoto, K. *J. Phys. Chem. B.* **2003**, *107*, 8701-8705.
(54) Santra, S.; Zhang, P.; Tan, W. *J. Phys. Chem. A* **2000**, *104*, 12021-12028.
(55) Niwa, O.; Kurita, R.; Horiuchi, T.; Torimitsu, K. *Anal. Chem.* **1998**, *70*, 89-93.
(56) Gee, K. R.; Kueper III, L. W.; Barnes, J.; Dudley, G.; Givens, R. S. *J. Org. Chem.* **1996**, *61*, 1228-1233.

(57) Kandler, K.; Katz, L. C.; Kauer, J. A. *Nat. Neurosci.* **1998**, *1*, 119-123.
(58) Sul, J.-Y.; Orosz, G.; Givens, R. S.; Haydon, P. G. *Neuron Glia Biology* **2004**, *1*, 3-11.
(59) Banerjee, A.; Falvey, D. E. *J. Org. Chem.* **1997**, *62*, 6245-6251.
(60) Banerjee, A.; Falvey, D. E. *J. Am. Chem. Soc.* **1998**, *120*, 2965-2966.
(61) Andrieux, C. P.; Saveant, J.-M.; Tallec, A.; Tardivel, R.; Tardy, C. *J. Am. Chem. Soc.* **1996**, *118*, 9788-9789.
(62) Andersen, M. L.; Long, W.; Wayner, D. D. M. *J. Am. Chem. Soc.* **1997**, *119*, 6590-6595.
(63) Givens, R. S.; Lee, J.-I. *Journal of Photoscience* **2003**, *10*, 37-48.
(64) Conrad, P. G., II; Givens, R. S.; Hellrung, B.; Rajesh, C. S.; Ramseier, M.; Wirz, J. *J. Am. Chem. Soc.* **2000**, *122*, 9346-9347.
(65) Ma, C.; Zuo, P.; Kwok, W. M.; Chan, W. S.; Kan, J. T. W.; Toy, P. H.; Phillips, D. L. *J. Org. Chem.* **2004**, *69*, 6641-6657.
(66) Zuo, P.; Ma, C.; Kwok, W. M.; Chan, W. S.; Phillips, D. L. *J. Org. Chem.* **2005**, *70*, 8661-8675.
(67) Ma, C.; Kwok, W. M.; Chan, W. S.; Du, Y.; Kan, J. T. W.; Toy, P. H.; Phillips, D. L. *J. Am. Chem. Soc.* **2006**, *128*, 2558-2570.
(68) Givens, R. S.; Conrad, P. G., II; Yousef, A. L.; Lee, J.-I. In *CRC Handbook of Organic Photochemistry and Photobiology*; 2nd ed.; CRC Press: New York, 2004.
(69) Zhang, K.; Corrie, J. E. T.; Munasinghe, V. R. N.; Wan, P. *J. Am. Chem. Soc.* **1999**, *121*, 5625-5632.
(70) Hagen, V.; Bendig, J.; Frings, S.; Eckardt, T.; Helm, S.; Reuter, D.; Kaupp, U. B. *J. Am. Chem. Soc.* **1997**, *119*, 4149-4159.
(71) Goeldner, M.; Givens, R. S. In *Dynamic Studies in Biology*; Wiley-VCH: Weinheim, 2005.
(72) Pelliccioli, A. P.; Wirz, J. *Photochem. Photobiol. Sci.* **2002**, *1*, 441-458.
(73) Bochet, C. G. *J. Chem. Soc., Perking Trans. 1* **2002**, 125-142.
(74) Patchornik, A.; Amit, B.; Woodward, R. B. *J. Am. Chem. Soc.* **1970**, *92*, 6333-6335.
(75) Zabadal, M.; Pelliccioli, A. P.; Klan, P.; Wirz, J. *J. Phys. Chem. A* **2001**, *105*, 10329-10333.
(76) Plistil, L.; Solomek, R.; Wirz, J.; Heger, D.; Klan, P. *J. Org. Chem.* **2006**, *71*, 8050-8058.
(77) Ma, C.; Chan, W. S.; Kwok, W. M.; Zuo, P.; Phillips, D. L. *J. Phys. Chem. B.* **2004**, *108*, 9264-9276.
(78) Wilson, R. M.; Sheehan, J. C. *J. Am. Chem. Soc.* **1969**, *91*, 7378-7380.
(79) Naitoh, K.; Yamaoka, T. *J. Chem. Soc. Perkin Trans. 2* **1992**, 663-669.
(80) Ortica, F.; Coenjarts, C.; Scaiano, J. C.; Liu, H.; Pohlers, G.; Cameron, J. F. *Chem. Mater.* **2001**, *13*, 2297-2304.
(81) Klan, P.; Pelliccioli, A. P.; Pospisil, T.; Wirz, J. *Photochem. Photobiol. Sci.* **2002**, *1*, 920-923.

(82) Usui, S.; Tanei, A. In *Book of Abstracts: 18th Conference of Physical Organic Chemistry*; Cryanski, M. K., Wozniak, K., Krygowsku, T. M., Eds.; Conference Engine: Poland, 2006, p 88.
(83) Durden, D. S.; Juorio, A. V.; Davis, B. A. *Anal. Chem.* **1980**, *52*, 1815-1820.
(84) Givens, R. S.; Weber, J. F. W.; Jung, A. H.; Park, C.-H. *Methods in Enzymology* **1998**, *291*, 1-29.
(85) Rather, J. B.; Reid, R. E. *J. Am. Chem. Soc.* **1919**, *41*, 75-83.
(86) Pasaribu, J. B.; Williams, L. R. *Aust. J. Chem.* **1973**, *26*, 1327-1331.
(87) Buu-Hoi, N. P.; Lavit, D. J. *J. Chem. Soc.* **1955**, 18-20.
(88) Chimilio, L. A., University of Kansas, 1999.
(89) Ma, C.; Kwok, W. M.; Chan, W. S.; Zuo, P.; Kan, J. T. W.; Toy, P. H.; Phillips, D. L. *J. Am. Chem. Soc.* **2005**, *127*, 1463-1472.
(90) Bratt, M. O.; Taylor, P. C. *J. Org. Chem.* **2003**, *68*, 5439-5444.
(91) Magnus, P.; Miknis, G. F.; Press, N. J.; Grandjean, D.; Taylor, G. M.; Harling, J. *J. Am. Chem. Soc.* **1997**, *119*, 6739-6748.
(92) Marino, J. P.; de Dios, A.; Anna, L. J.; de la Pradilla, R. F. *J. Org. Chem.* **1996**, *61*, 109-117.
(93) Wang, C.; Abboud, K. A.; Phanstiel, I., O. *J. Org. Chem.* **2002**, *67*, 7865-7868.
(94) Kumar, T. S.; Madsen, A. S.; Wengel, J.; Hrdlicka, P. J. *J. Org. Chem.* **2006**, *71*, 4188-4201.
(95) Barnett, D. W.; Panigot, M. J.; Curley, J., R. W. *Tetrahedron Asymmetry* **2002**, *13*, 1893-1900.
(96) Emmons, W. D.; Ferris, A. F. *J. Am. Chem. Soc.* **1953**, *75*, 2257.
(97) McDevitt, J. P.; Lansbury, J., P. T. *J. Am. Chem. Soc.* **1996**, *118*, 3818-3828.
(98) Mulvihill, M. J.; Cesario, C.; Smith, V.; Beck, P.; Nigro, A. *J. Org. Chem.* **2004**, *69*, 5124-5127.
(99) Robbins, J. D.; Boring, D. L.; Tand, W.-J.; Shank, R.; Seamon, K. B. *J. Med. Chem.* **1996**, *39*, 2745-2752.
(100) Randolph, J. T.; Waid, P.; Nichols, C.; Sauer, D.; Haviv, F.; Diaz, G.; Bammert, G.; Besecke, L. M.; Segreti, J. A.; Mohning, K. M.; Bush, E. N.; Wegner, C. D.; Greer, J. *J. Med. Chem.* **2004**, *47*, 1085-1097.
(101) Oniciu, D. C.; Dasseux, J.-L. H.; Yang, J.; Myeller, R.; Pop, E.; Denysenko, A.; Duan, C.; Huang, T.-B.; Zhang, L.; Krause, B. R.; Drake, S. L.; Lalwani, N.; Cramer, C. T.; Goetz, B.; Pape, M. E.; McKee, A.; Fici, G. H.; Lutastanksi, J. M.; Brown, S. C.; Bisfaier, C. L. *J. Med. Chem.* **2006**, *49*, 334-348.
(102) Elliott, R. L.; Pireh, D.; Griesgraber, G.; Nilius, A. M.; Ewing, P. J.; Bui, M. H.; Raney, P. M.; Flamm, R. K.; Kim, K.; Henry, R. F.; Chu, D. T. W.; Plattner, J. J.; Or, Y. S. *J. Med. Chem.* **1998**, *41*, 1651-1659.
(103) Gilkerson, M. *unpublished results* 2006.
(104) Li, T.; Fugita, Y.; Tsadu, Y.; Miyazaki, A.; Abmbo, A.; Sasaki, Y.; Jinsman, Y.; Bryant, S. D.; Lazarus, L. H.; Okada, Y. *J. Med. Chem.* **2005**, *48*, 586-592.
(105) Rannard, S. P.; Davis, N. J. *Org. Lett.* **1999**, *1*, 933-936.
(106) Wagner, P. J.; Lindstrom, M. J. *J. Am. Chem. Soc.* **1987**, *109*, 3062-3067.

(107) Givens, R. S.; Heger, D.; Hellrung, B.; Zamdzhilov, Y.; Mac, M.; Conrad, I., P. G.; Cope, E. D.; Lee, J. I.; Mata-Segreda, J. F.; Schowen, R. L.; Wirz, J. *J. Am. Chem. Soc.* **2008**, *130*, 3307-3309.
(108) Tsushima, M.; Tokuda, K.; Ohsaka, T. *Anal. Chem.* **1994**, *66*, 4551-4556.
(109) Wirz, J.; Heger, D. *unpublished results* **2007**.
(110) Stensrud, K. F.; Givens, R. S. *unpublished results* **2007**.
(111) Barbosa, J.; Sanz-Nebot, V. *Fresenius J. Anal. Chem.* **1995**, *353*, 148-155.
(112) Buckenmaier, S. M. C.; McCalley, D. V.; Euerby, M. R. *J. Chromatogr. A* **2003**, *1004*, 71-79.
(113) Rondinini, S.; Nese, A. *Electrochim. Acta* **1987**, *32*, 1499.
(114) Giammario, P.; Longhi, P.; Mussini, T. *Chim. Ind. (Milan)* **1971**, *53*, 347.
(115) Radziszewski, J. G.; Gil, M.; Gorski, A.; Spanget-Larsen, J.; Waluk, J.; Mroz, B. J. *J. Chem. Phys.* **2001**, *115*, 9733-9738.
(116) Bronsted, J. N. *Chem. Rev.* **1928**, *5*, 231-338.
(117) Anslyn, E. V.; Dougherty, D. A. *Modern Physical Organic Chemistry*; University Science Books: Sausalito, California, 2006.
(118) Chen, X.; Ma, C.; Kwok, W. M.; Guan, X.; Du, Y.; Phillips, D. L. *J. Phys. Chem. B.* **2007**, *111*, 11832-11842.
(119) Chen, X.; Ma, C.; Kwok, W. M.; Guan, X.; Du, Y.; Phillips, D. L. *J. Phys. Chem. A* **2006**, *110*, 12406-12413.
(120) Kosuge, S.; Furuta, M.; Yamaguchi, O. *Bunseki Kagaku* **1968**, *17*, 310-314.
(121) Kochi, J. K.; Hammond, G. S. *J. Am. Chem. Soc.* **1953**, *75*, 3443-3444.
(122) de Figueiredo, R. M.; Frolich, R.; Christmann, M. *J. Org. Chem.* **2006**, *71*, 4147-4154.
(123) *International Tables for Crystallography*; 4th ed. ed.; Kluwer: Boston, 1996; Vol. A.
(124) *Data Collection: SMART Software Reference Manual*; Bruker-AXS: Madison, WI, 1998.
(125) *Data Reduction: SAINT Software Reference Manual*; Bruker-AXS: Madison, WI, 1998.
(126) Sheldrick, G. M. *SHELXTL Version 6.10 Reference Manual*; Bruker-AXS: Madison, WI, 2000.
(127) Sheldrick, G. M. *Program for Emperical Absorption Correction of Area Detector Data*; University of Gottingen: Germany, 2002.
(128) Hatchard, C. G.; Parker, C. A. *Proc. R. Soc. London A* **1965**, *A220*, 518-536.

APPENDIX A

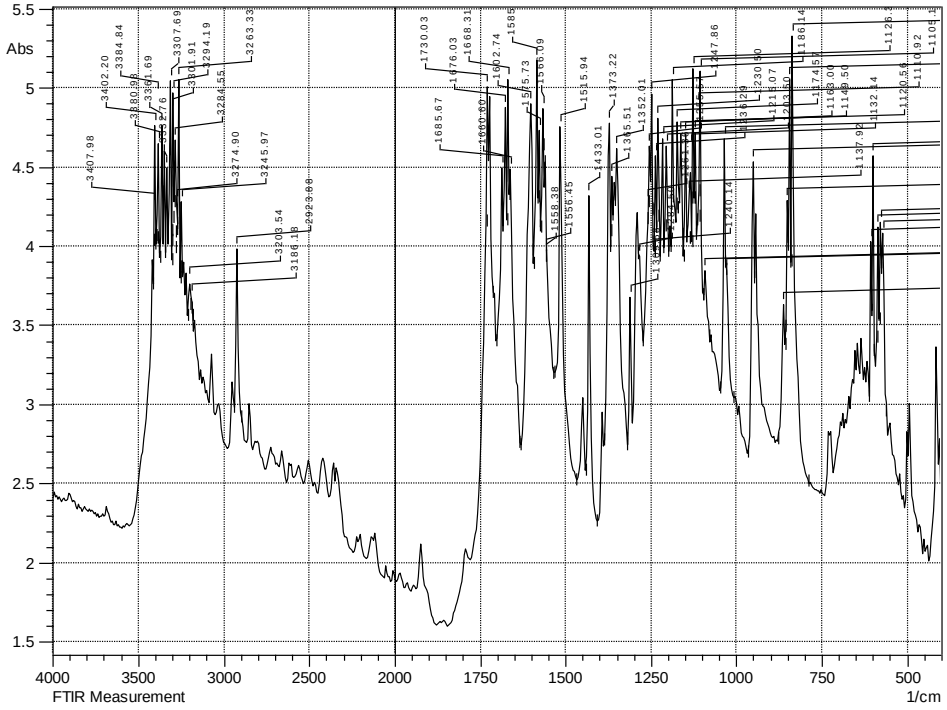

Figure 17. IR of pHP Formate **70a** (KBr).

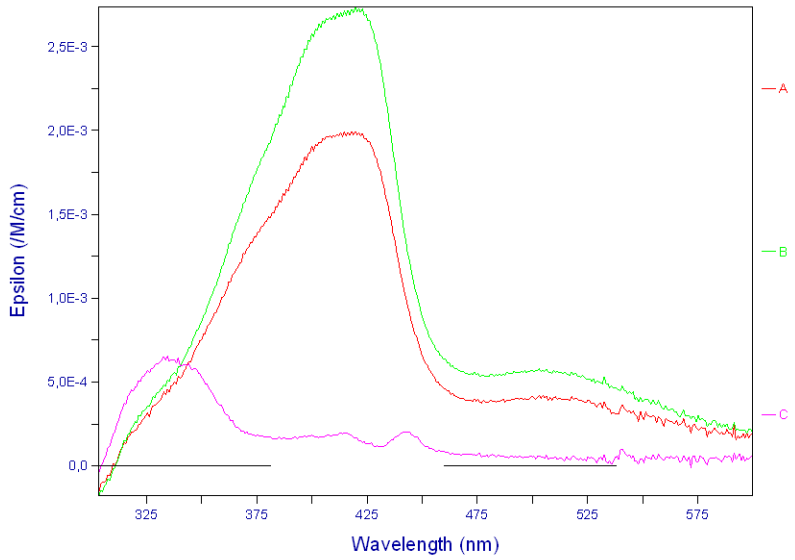

Figure 18. Laser Flash Photolysis Transient Spectra for pHP Formate **70a** in Aqueous Acetonitrile. Changes in absorption over time during photolysis represented by red, green, violet, and orange lines.

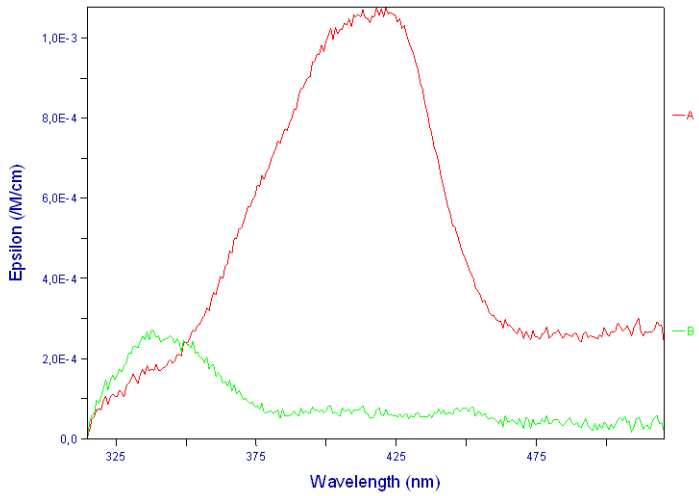

Figure 19. Laser Flash Photolysis Transient Spectra for pHP Formate **70a** in Water. Changes in absorption over time during photolysis represented by red, green, violet, and orange lines (aqueous acetonitrile).

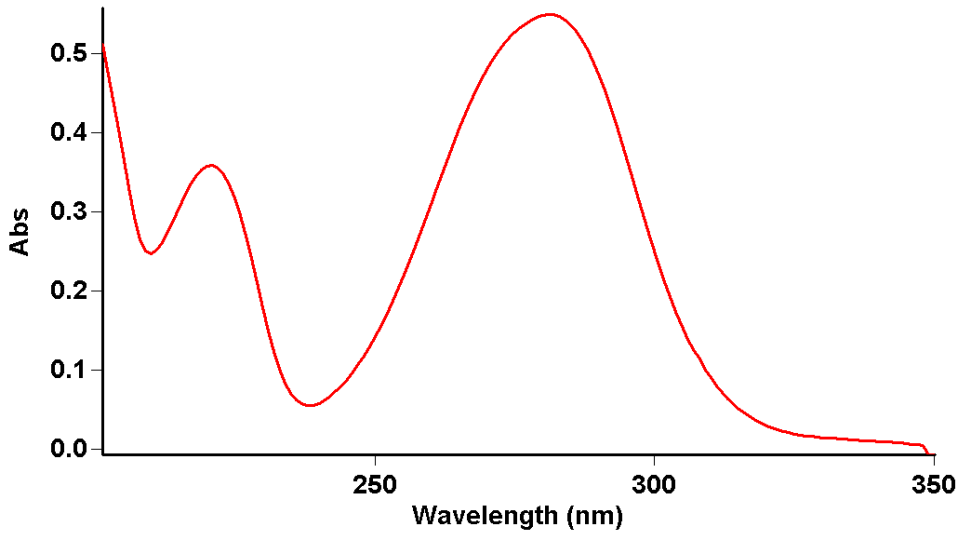

Figure 20. UV-VIS of pHP Formate **70a** (3:1 water/acetonitrile; λ_{max} = 281 nm; log ε = 4.04).

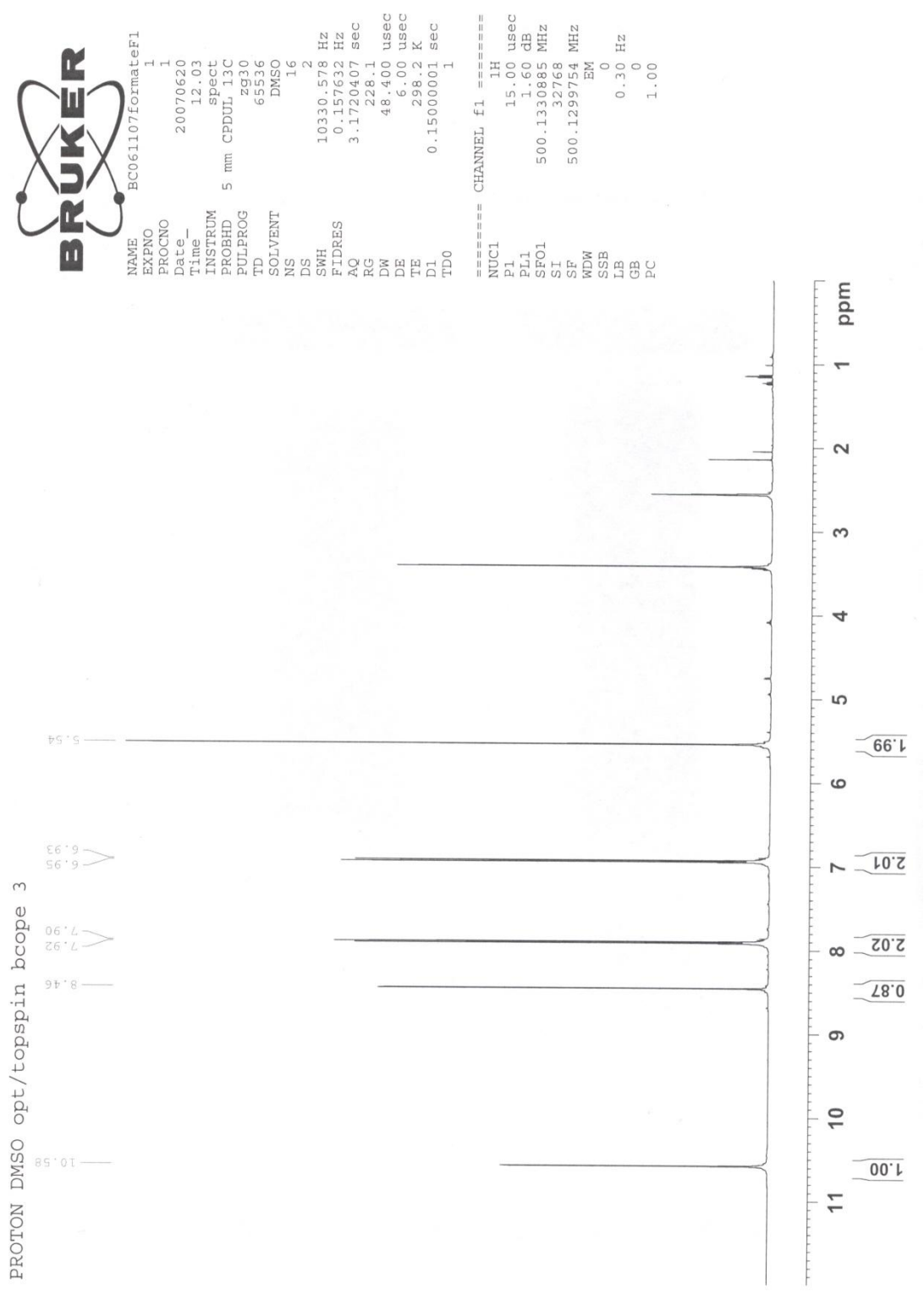

Figure 21. ^{1}H NMR of pHP Formate **70a** (DMSO-d_6).

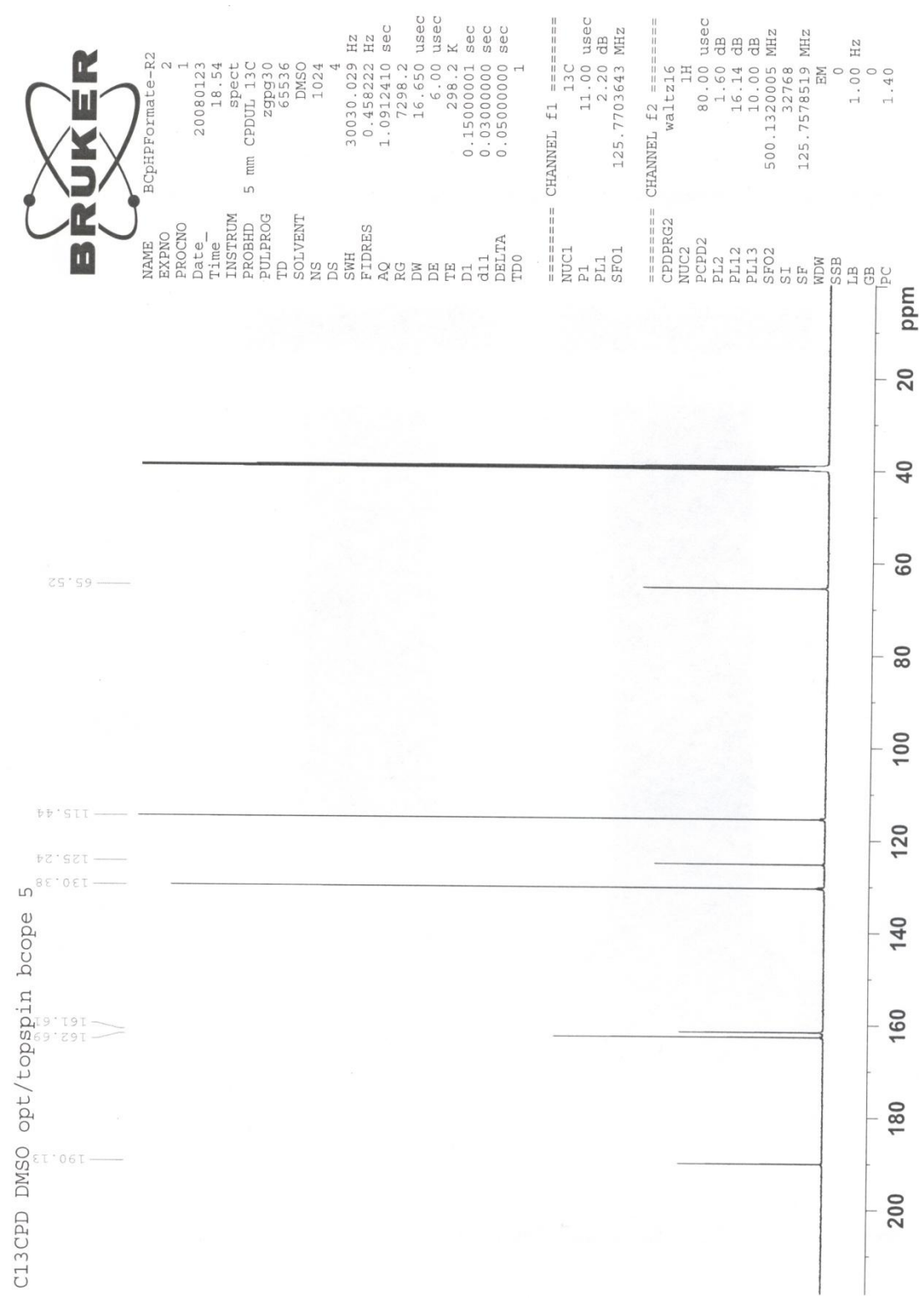

Figure 22. ^{13}C NMR of pHP Formate **70a** (DMSO-d_6).

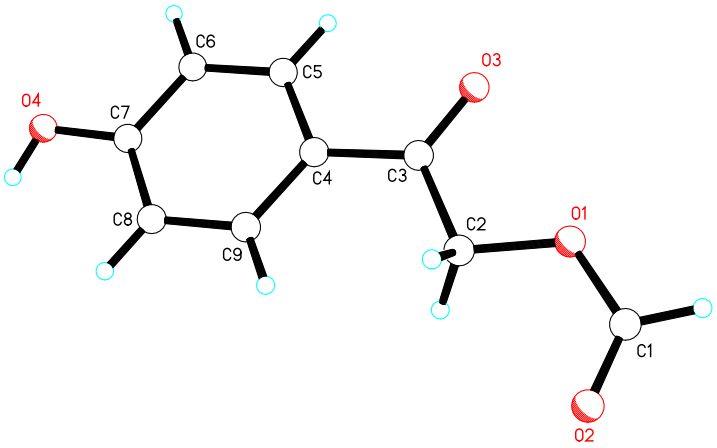

Figure 23. X-Ray Crystal Structure of pHP Formate **70a**.

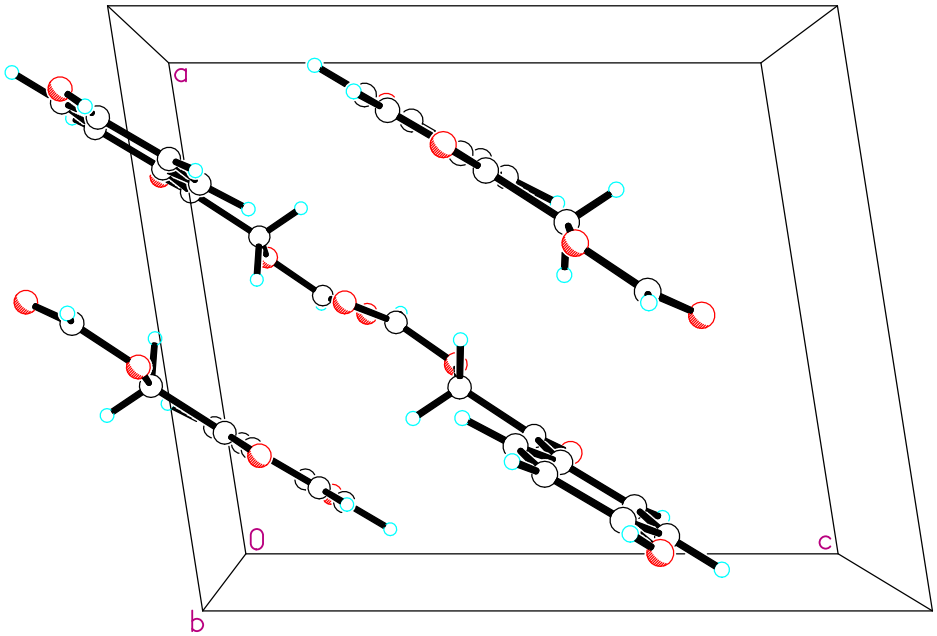

Figure 24. Orientation of pHP Formate **70a** Molecules in the Crystal Lattice.

Comments from X-Ray Crystallographer

The asymmetric unit contains one $C_9H_8O_4$ molecule. All displacement ellipsoids are drawn at the 50% probability level.

Brief Experimental Description

Colorless crystals of $C_9H_8O_4$ are, at 100(2) K, monoclinic, space group $P2_1/c$ – C_{2h}^5 (No. 14)[1] with **a** = 8.9605(6) Å, **b** = 8.3220(6) Å, **c** = 10.6750(7) Å, β = 98.930(2)°, V = 786.38(9) $Å^3$ and Z = 4 molecules {d_{calcd} = 1.522 g/cm^3; μ_a(MoKα) = 0.121 mm^{-1}}. A full hemisphere of diffracted intensities (1850 10-second frames with a ω scan width of 0.30°) was measured for a single-domain specimen using graphite-monochromated MoKα radiation (λ= 0.71073 Å) on a Bruker SMART APEX CCD Single Crystal Diffraction System[2]. X-rays were provided by a fine-focus sealed x-ray tube operated at 50kV and 30mA. Lattice constants were determined with the Bruker SAINT Software package using peak centers for 3517 reflections. A total of 9794 integrated reflection intensities having 2θ((MoKα)< 60.99° were produced using the Bruker program SAINT[3]; 2389 of these were unique and gave R_{int} = 0.033 with a coverage which was 99.7% complete. The data were corrected empirically for variable absorption effects using equivalent reflections; the relative transmission factors ranged from 0.949 to 1.000. The Bruker software package SHELXTL was used to solve the structure using "direct methods" techniques. All stages of weighted full-matrix least-squares refinement were conducted using F_o^2 data with the SHELXTL Version 6.10 software package[4].

The final structural model incorporated anisotropic thermal parameters for all nonhydrogen atoms and isotropic thermal parameters for all hydrogen atoms. All hydrogen atoms were located in a difference Fourier and included in the structural model as independent isotropic atoms whose parameters were allowed to vary in least-squares refinement cycles. A total of 150 parameters were refined using no restraints, 2389 data and weights of $w = 1/ [\sigma^2(F^2) + (0.0721\ P)^2]$, where $P = [F_O^2 + 2F_C^2] / 3$. Final agreement factors at convergence are: R_1(unweighted, based on F) = 0.039 for 1979 independent absorption-corrected "observed" reflections having $2\theta(MoK\alpha) < 60.99°$ and $I > 2\sigma(I)$; R_1(unweighted, based on F) = 0.046 and wR_2(weighted, based on F^2) = 0.107 for all 2389 independent absorption-corrected reflections having $2\theta(MoK\alpha) < 60.99°$. The largest shift/s.u. was 0.000 in the final refinement cycle. The final difference map had maxima and minima of 0.47 and -0.24 $e^-/Å^3$, respectively.

Table 28. Crystal data and structure refinement for pHP Formate **70a**.

Empirical formula	$C_9H_8O_4$
Formula weight	180.15
Temperature	100(2) K
Wavelength	0.71073 Å
Crystal system	Monoclinic
Space group	$P2_1/c$ – C_{2h}^5 (No. 14)
Unit cell dimensions	**a** = 8.9605(6) Å **α** = 90.000°
	b = 8.3220(6) Å **β** = 98.930(2)°
	c = 10.6750(7) Å **γ** = 90.000°
Volume	786.38(9) $Å^3$
Z	4
Density (calculated)	1.522 Mg/m^3
Absorption coefficient	0.121 mm^{-1}
F (000)	376
Crystal size	0.40 x 0.21 x 0.10 mm^3
Theta range for data collection	2.30° to 30.50°
Index ranges	$-12 \leq h \leq 12$, $-11 \leq k \leq 11$, $-15 \leq l \leq 14$
Reflections collected	9794
Independent reflections	2389 [R_{int} = 0.033]
Completeness to theta = 30.50°	99.7 %
Absorption correction	Multi-scan
Max. and min. transmission	1.000 and 0.949
Refinement method	Full-matrix least squares on F^2
Data / restraints / parameters	2389 / 0 / 150
Goodness-of-fit on F^2	0.988
Final R indices [I>2sigma(I)]	R_1 = 0.039, wR_2 = 0.104
R indices (all data)	R_1 = 0.046, wR_2 = 0.107
Largest diff. peak and hole	0.47 and -0.24 $e^-/Å^3$

Table 29. Atomic coordinates (x 10^4) and equivalent isotropic displacement parameters ($Å^2$ x 10^3) for pHP Formate **70a**. U(eq) is defined as one third of the trace of the orthogonalized U_{ij} tensor.

	x	y	z	U(eq)
O(1)	3891(1)	1256(1)	4042(1)	25(1)
O(2)	5118(1)	1673(1)	2383(1)	25(1)
O(3)	2168(1)	2019(1)	5676(1)	24(1)
O(4)	899(1)	9365(1)	6434(1)	24(1)
C(1)	4719(1)	812(1)	3159(1)	23(1)
C(2)	3482(1)	2925(1)	4037(1)	19(1)
C(3)	2554(1)	3173(1)	5095(1)	17(1)
C(4)	2150(1)	4822(1)	5396(1)	16(1)
C(5)	1342(1)	5058(1)	6410(1)	17(1)
C(6)	935(1)	6576(1)	6741(1)	18(1)
C(7)	1325(1)	7902(1)	6061(1)	17(1)
C(8)	2112(1)	7697(1)	5045(1)	18(1)
C(9)	2519(1)	6168(1)	4717(1)	17(1)

Table 30. Bond lengths [Å] for pHP Formate **70a**.

O(1)-C(1)	1.339(1)
O(1)-C(2)	1.437(1)
O(2)-C(1)	1.192(1)
O(3)-C(3)	1.222(1)
O(4)-C(7)	1.354(1)
O(4)-H(4O)	0.83(2)
C(1)-H(1)	0.98(1)
C(2)-C(3)	1.517(1)
C(2)-H(2A)	0.98(1)
C(2)-H(2B)	0.98(1)
C(3)-C(4)	1.468(1)
C(4)-C(9)	1.401(1)
C(4)-C(5)	1.406(1)
C(5)-C(6)	1.377(1)
C(5)-H(5)	0.97(1)
C(6)-C(7)	1.395(1)
C(6)-H(6)	1.00(2)
C(7)-C(8)	1.393(1)
C(8)-C(9)	1.384(1)
C(8)-H(8)	0.96(1)
C(9)-H(9)	0.97(1)

Table 31. Bond angles [°] for pHP Formate **70a**.

C(1)-O(1)-C(2)	115.7(1)	C(5)-C(4)-C(3)	118.2(1)
C(7)-O(4)-H(4O)	108(1)	C(6)-C(5)-C(4)	120.9(1)
O(2)-C(1)-O(1)	125.7(1)	C(6)-C(5)-H(5)	120(1)
O(2)-C(1)-H(1)	126(1)	C(4)-C(5)-H(5)	119(1)
O(1)-C(1)-H(1)	108(1)	C(5)-C(6)-C(7)	119.6(1)
O(1)-C(2)-C(3)	107.3(1)	C(5)-C(6)-H(6)	121(1)
O(1)-C(2)-H(2A)	110(1)	C(7)-C(6)-H(6)	120(1)
C(3)-C(2)-H(2A)	111(1)	O(4)-C(7)-C(8)	122.6(1)
O(1)-C(2)-H(2B)	110(1)	O(4)-C(7)-C(6)	116.9(1)
C(3)-C(2)-H(2B)	111(1)	C(8)-C(7)-C(6)	120.5(1)
H(2A)-C(2)-H(2B)	109(1)	C(9)-C(8)-C(7)	119.6(1)
O(3)-C(3)-C(4)	121.7(1)	C(9)-C(8)-H(8)	120(1)
O(3)-C(3)-C(2)	120.1(1)	C(7)-C(8)-H(8)	120(1)
C(4)-C(3)-C(2)	118.2(1)	C(8)-C(9)-C(4)	120.8(1)
C(9)-C(4)-C(5)	118.6(1)	C(8)-C(9)-H(9)	120(1)
C(9)-C(4)-C(3)	123.2(1)	C(4)-C(9)-H(9)	119(1)

Table 32. Anisotropic displacement parameters ($Å^2 \times 10^3$) for pHP Formate **70a**. The anisotropic displacement factor exponent takes the form:
$-2\pi^2[h^2 a^{*2} U_{11} + ... + 2 h k a^* b^* U_{12}]$

	U_{11}	U_{22}	U_{33}	U_{23}	U_{13}	U_{12}
O(1)	35(1)	15(1)	27(1)	1(1)	14(1)	5(1)
O(2)	26(1)	25(1)	25(1)	-2(1)	9(1)	0(1)
O(3)	30(1)	15(1)	28(1)	2(1)	10(1)	-2(1)
O(4)	35(1)	12(1)	27(1)	0(1)	15(1)	0(1)
C(1)	26(1)	20(1)	25(1)	-3(1)	6(1)	3(1)
C(2)	24(1)	13(1)	22(1)	-1(1)	7(1)	2(1)
C(3)	17(1)	15(1)	18(1)	-1(1)	2(1)	-1(1)
C(4)	17(1)	15(1)	17(1)	0(1)	3(1)	-2(1)
C(5)	18(1)	15(1)	18(1)	3(1)	4(1)	-2(1)
C(6)	20(1)	17(1)	18(1)	0(1)	6(1)	-1(1)
C(7)	20(1)	14(1)	19(1)	0(1)	4(1)	-1(1)
C(8)	21(1)	15(1)	18(1)	2(1)	5(1)	-3(1)
C(9)	19(1)	17(1)	17(1)	1(1)	5(1)	-1(1)

Table 33. Hydrogen coordinates (x 10^4) and isotropic displacement parameters ($Å^2$ x 10^3) for pHP Formate **70a**.

	x	y	z	U(eq)
H(4O)	1278(17)	10059(19)	6021(15)	40(4)
H(1)	4906(14)	-351(17)	3247(12)	24(3)
H(2A)	4402(15)	3589(15)	4164(13)	25(3)
H(2B)	2892(14)	3201(14)	3219(13)	19(3)
H(5)	1070(13)	4131(16)	6870(11)	22(3)
H(6)	354(17)	6740(17)	7461(15)	32(4)
H(8)	2385(15)	8615(17)	4587(13)	30(4)
H(9)	3018(15)	6005(17)	3988(13)	29(3)

Table 34. Torsion angles [°] for pHP Formate **70a**.

C(2)-O(1)-C(1)-O(2)	-0.78(16)
C(1)-O(1)-C(2)-C(3)	179.89(9)
O(1)-C(2)-C(3)-O(3)	-7.16(13)
O(1)-C(2)-C(3)-C(4)	172.58(8)
O(3)-C(3)-C(4)-C(9)	-177.27(9)
C(2)-C(3)-C(4)-C(9)	3.00(14)
O(3)-C(3)-C(4)-C(5)	2.21(14)
C(2)-C(3)-C(4)-C(5)	-177.52(8)
C(9)-C(4)-C(5)-C(6)	-0.73(14)
C(3)-C(4)-C(5)-C(6)	179.77(9)
C(4)-C(5)-C(6)-C(7)	0.15(15)
C(5)-C(6)-C(7)-O(4)	-179.74(9)
C(5)-C(6)-C(7)-C(8)	0.50(15)
O(4)-C(7)-C(8)-C(9)	179.69(9)
C(6)-C(7)-C(8)-C(9)	-0.56(15)
C(7)-C(8)-C(9)-C(4)	-0.03(14)
C(5)-C(4)-C(9)-C(8)	0.66(14)
C(3)-C(4)-C(9)-C(8)	-179.87(9)

Table 35. Hydrogen bonds for pHP Formate **70a** [Å and °].

D-H...A	d(D-H)	d(H...A)	d(D...A)	<(DHA)
O(4)-H(4O)...O(3)#1	0.830(17)	1.877(16)	2.6671(11)	158.5(16)

Symmetry transformations used to generate equivalent atoms: #1: x, y+1, z.

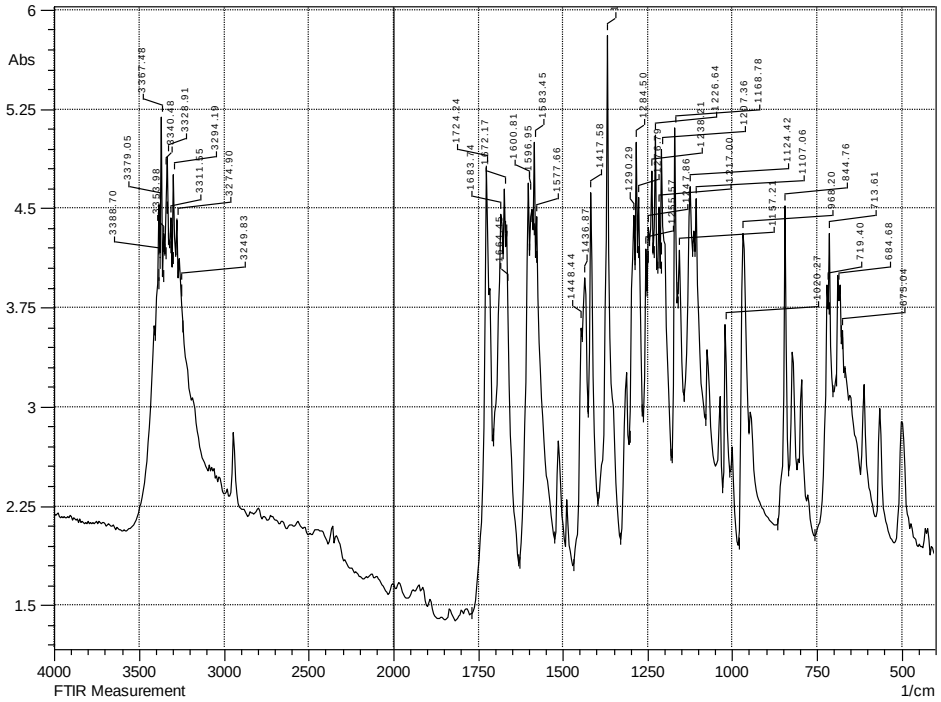

Figure 25. IR of pHP Benzoate **70c** (KBr).

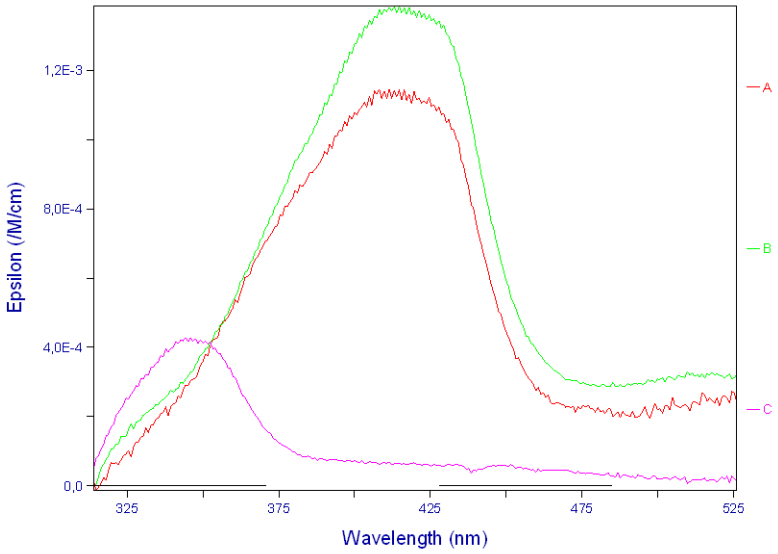

Figure 26. Laser Flash Photolysis Transient Spectra for pHP Benzoate **70c** in Aqueous Acetonitrile. Changes in absorption over time during photolysis represented by red, green, violet, and orange lines.

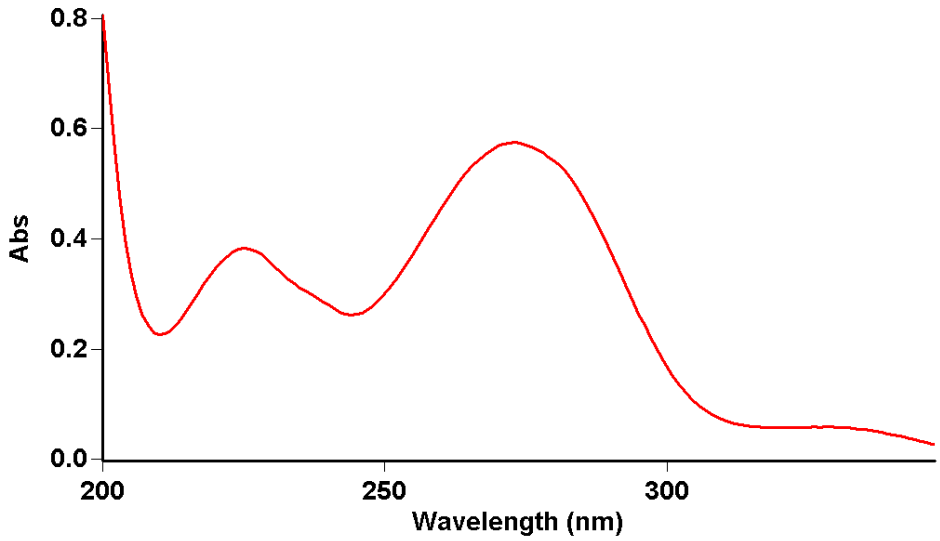

Figure 27. UV-VIS of pHP Benzoate **70c** (7:3 acetonitrile/water; λ_{max} = 276 nm; log ε = 4.50).

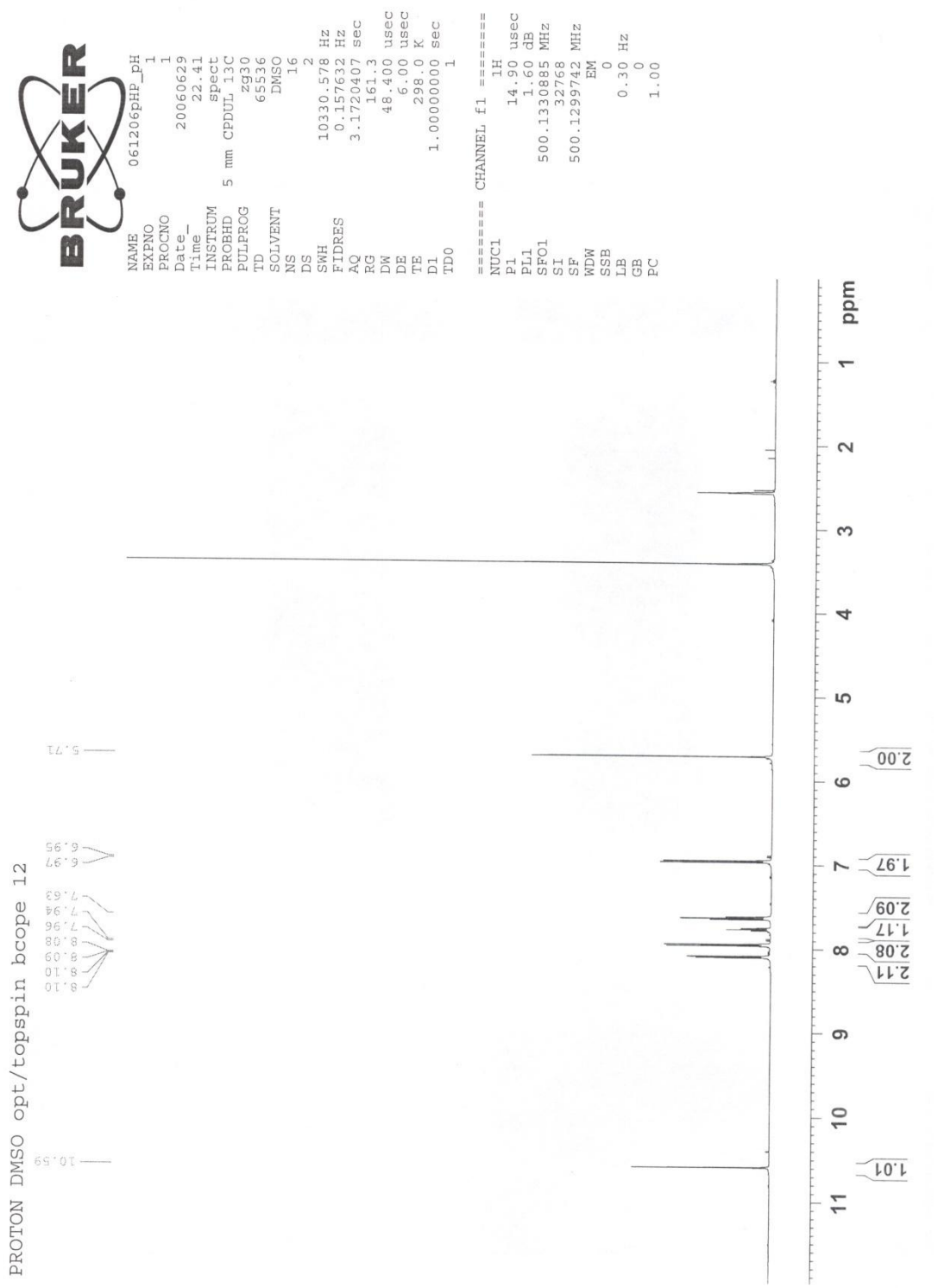

Figure 28. ^{1}H NMR of pHP Benzoate **70c** (DMSO-d_6).

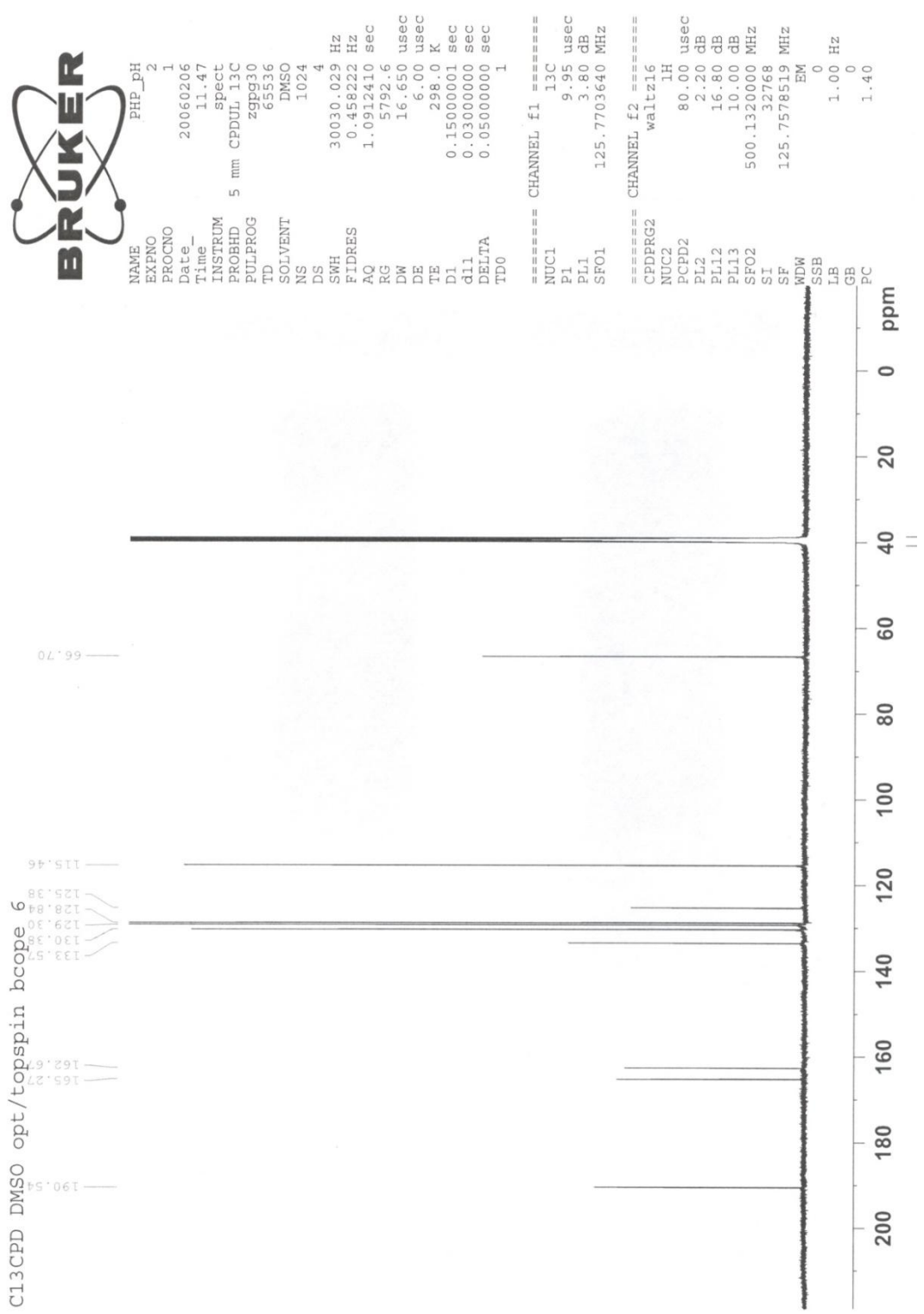

Figure 29. ^{13}C NMR of pHP Benzoate **70c** (DMSO-d_6).

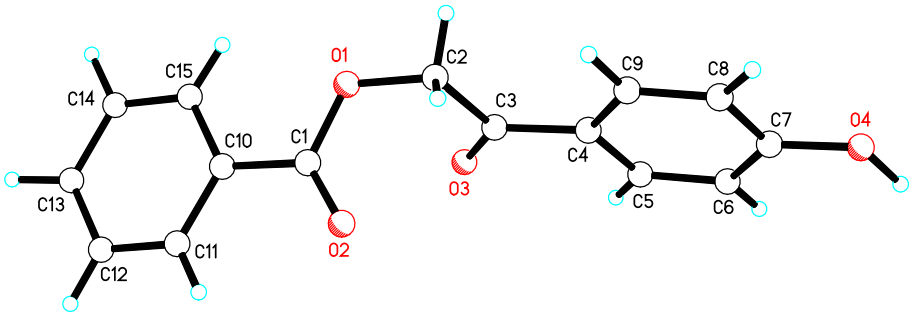

Figure 30. X-Ray Crystal Structure of pHP Benzoate **70c**.

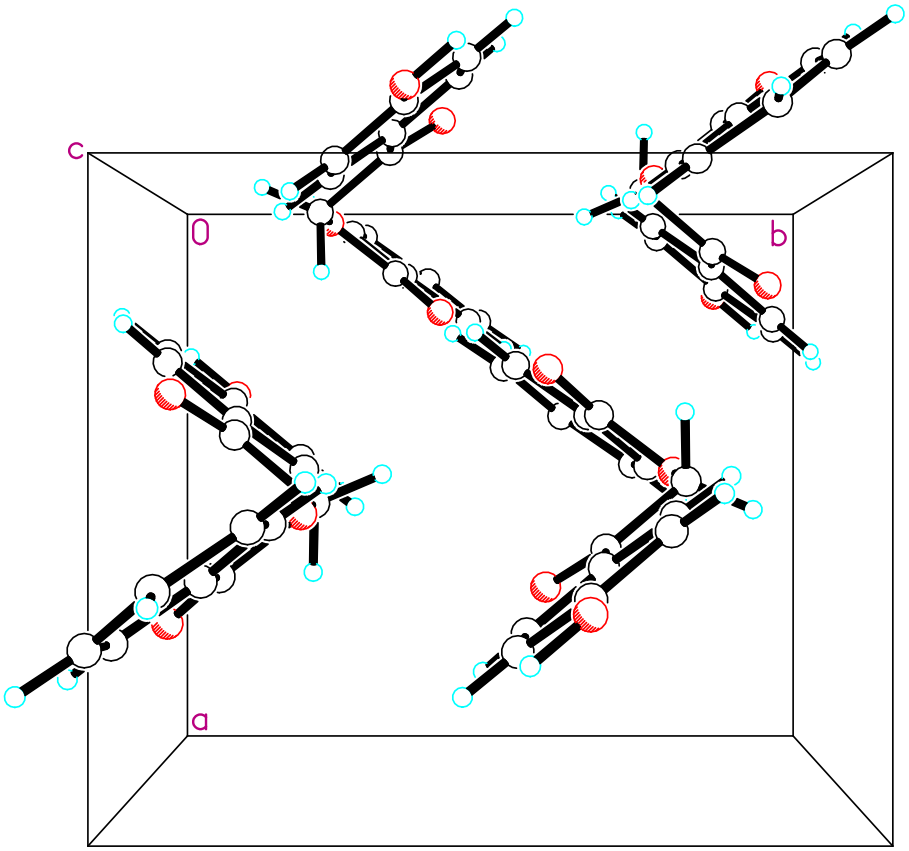

Figure 31. Orientation of pHP Benzoate **70c** in the Crystal Lattice.

Comments from X-Ray Crystallographer

The asymmetric unit contains one $C_{15}H_{12}O_4$ molecule. All displacement ellipsoids are drawn at the 50% probability level.

Brief Experimental Description

Colorless crystals of $C_{15}H_{12}O_4$ are, at 100(2) K, orthorhombic, space group $P2_12_12_1 - D_2^4$ (No. 19)[1] with **a** = 8.470(1) Å, **b** = 9.844(1) Å, **c** = 14.474(2) Å, V = 1206.8(3) $Å^3$ and Z = 4 molecules {d_{calcd} = 1.410 g/cm^3; μ_a(MoKα) = 0.103 mm^{-1}}. A full hemisphere of diffracted intensities (1850 10-second frames with a ω scan width of 0.30°) was measured for a single-domain specimen using graphite-monochromated MoKα radiation (λ= 0.71073 Å) on a Bruker SMART APEX CCD Single Crystal Diffraction System[2]. X-rays were provided by a fine-focus sealed x-ray tube operated at 50kV and 30mA. Lattice constants were determined with the Bruker SAINT software package using peak centers for 1901 reflections. A total of 14702 integrated reflection intensities having 2θ((MoKα)< 61.14° were produced using the Bruker program SAINT[3]; 3686 of these were unique and gave R_{int} = 0.056 with a coverage which was 99.9% complete. The data were corrected empirically for variable absorption effects using equivalent reflections; the relative transmission factors ranged from 0.877 to 1.000. The Bruker software package SHELXTL was used to solve the structure using "direct methods" techniques. All stages of weighted full-matrix least-squares refinement were conducted using F_o^2 data with the SHELXTL Version 6.10 software package[4].

The final structural model incorporated anisotropic thermal parameters for all nonhydrogen atoms and isotropic thermal parameters for all hydrogen atoms. All hydrogen atoms were located in a difference Fourier and included in the structural model as independent isotropic atoms whose parameters were allowed to vary in least-squares refinement cycles. A total of 220 parameters were refined using no restraints, 3686 data and weights of $w = 1/ [\sigma^2(F^2) + (0.0648\ P)^2 + 0.2445\ P]$, where $P = [F_O^2 + 2F_C^2] / 3$. Final agreement factors at convergence are: R_1(unweighted, based on F) = 0.066 for 2836 independent absorption-corrected "observed" reflections having $2\theta(MoK\alpha) < 61.14°$ and $I > 2\sigma(I)$; R_1(unweighted, based on F) = 0.089 and wR_2(weighted, based on F^2) = 0.148 for all 3686 independent absorption-corrected reflections having $2\theta(MoK\alpha) < 61.14°$. The largest shift/s.u. was 0.000 in the final refinement cycle. The final difference map had maxima and minima of 0.39 and -0.32 $e^-/Å^3$, respectively. Since the "Flack" parameter refined to a final value of 0.0(14), the absolute structure could not be reliably determined experimentally using anomalous dispersion of the x-rays.

Table 36. Crystal data and structure refinement for pHP Benzoate **70c**.

Empirical formula	$C_{15}H_{12}O_4$
Formula weight	256.25
Temperature	100(2) K
Wavelength	0.71073 Å
Crystal system	Orthorhombic
Space group	$P2_12_12_1 - D_2^4$ (No. 19)
Unit cell dimensions	**a** = 8.470(1) Å **α** = 90.000°
	b = 9.844(1) Å **β** = 90.000°
	c = 14.474(2) Å **γ** = 90.000°
Volume	1206.8(3) $Å^3$
Z	4
Density (calculated)	1.410 Mg/m^3
Absorption coefficient	0.103 mm^{-1}
F(000)	536
Crystal size	0.38 x 0.10 x 0.06 mm^3
Theta range for data collection	2.50° to 30.57°
Index ranges	$-12 \leq h \leq 12$, $-14 \leq k \leq 14$, $-20 \leq l \leq 20$
Reflections collected	14702
Independent reflections	3686 [$R_{int} = 0.056$]
Completeness to theta = 30.57°	99.9 %
Absorption correction	Empirical
Max. and min. transmission	1.000 and 0.877
Refinement method	Full-matrix least squares on F^2
Data / restraints / parameters	3686 / 0 / 220
Goodness-of-fit on F^2	1.059
Final R indices [I>2sigma(I)]	$R_1 = 0.066$, $wR_2 = 0.138$
R indices (all data)	$R_1 = 0.089$, $wR_2 = 0.148$
Absolute structure parameter	0.0(14)
Largest diff. peak and hole	0.39 and -0.32 $e^-/Å^3$

$R_1 = \Sigma \, ||F_O| - |F_C|| \, / \, \Sigma \, |F_O|$

$wR_2 = \{ \, \Sigma \, [w(F_O^2 - F_C^2)^2] \, / \, \Sigma \, [w(F_O^2)^2] \, \}^1$

Table 37. Atomic coordinates (x 10^4) and equivalent isotropic displacement parameters (Å^2 x 10^3) for pHP Benzoate **70c**. U(eq) is defined as one third of the trace of the orthogonalized U_{ij} tensor.

	x	y	z	U(eq)
O(1)	272(2)	2447(2)	1206(1)	28(1)
O(2)	1937(2)	4199(2)	1413(1)	34(1)
O(3)	-1523(2)	4245(2)	2047(1)	30(1)
O(4)	-1518(2)	3811(2)	6427(1)	30(1)
C(1)	1191(3)	3468(2)	900(2)	26(1)
C(2)	157(3)	2343(3)	2192(2)	27(1)
C(3)	-888(3)	3447(2)	2574(2)	22(1)
C(4)	-1098(3)	3522(2)	3587(2)	21(1)
C(5)	-2051(3)	4532(2)	3967(2)	23(1)
C(6)	-2211(3)	4657(2)	4914(2)	23(1)
C(7)	-1402(3)	3767(2)	5497(1)	21(1)
C(8)	-450(3)	2756(3)	5125(2)	27(1)
C(9)	-297(3)	2630(2)	4182(2)	25(1)
C(10)	1175(3)	3584(2)	-124(2)	24(1)
C(11)	2028(3)	4629(3)	-522(2)	29(1)
C(12)	2007(3)	4800(3)	-1473(2)	33(1)
C(13)	1154(3)	3917(3)	-2026(2)	29(1)
C(14)	306(3)	2855(3)	-1626(2)	29(1)
C(15)	312(3)	2686(2)	-674(2)	24(1)

Table 38. Bond lengths [Å] for pHP Benzoate **70c**.

O(1)-C(1)	1.346(3)	C(6)-H(6)	0.91(3)
O(1)-C(2)	1.433(3)	C(7)-C(8)	1.390(3)
O(2)-C(1)	1.212(3)	C(8)-C(9)	1.377(3)
O(3)-C(3)	1.221(3)	C(8)-H(8)	1.00(3)
O(4)-C(7)	1.351(3)	C(9)-H(9)	0.96(3)
O(4)-H(4O)	0.97(5)	C(10)-C(11)	1.383(3)
C(1)-C(10)	1.487(3)	C(10)-C(15)	1.397(3)
C(2)-C(3)	1.508(3)	C(11)-C(12)	1.388(3)
C(2)-H(2A)	1.00(3)	C(11)-H(11)	0.90(3)
C(2)-H(2B)	0.97(3)	C(12)-C(13)	1.384(4)
C(3)-C(4)	1.478(3)	C(12)-H(12)	0.98(3)
C(4)-C(5)	1.394(3)	C(13)-C(14)	1.394(4)
C(4)-C(9)	1.404(3)	C(13)-H(13)	0.99(2)
C(5)-C(6)	1.382(3)	C(14)-C(15)	1.387(3)
C(5)-H(5)	0.94(3)	C(14)-H(14)	1.07(4)
C(6)-C(7)	1.396(3)	C(15)-H(15)	0.90(3)

Table 39. Bond angles [°] for pHP Benzoate **70c**.

C(1)-O(1)-C(2)	114.8(2)	C(8)-C(7)-C(6)	120.0(2)
C(7)-O(4)-H(4O)	114(3)	C(9)-C(8)-C(7)	120.2(2)
O(2)-C(1)-O(1)	123.0(2)	C(9)-C(8)-H(8)	122(2)
O(2)-C(1)-C(10)	124.7(2)	C(7)-C(8)-H(8)	118(2)
O(1)-C(1)-C(10)	112.3(2)	C(8)-C(9)-C(4)	120.4(2)
O(1)-C(2)-C(3)	110.7(2)	C(8)-C(9)-H(9)	120(2)
O(1)-C(2)-H(2A)	108(1)	C(4)-C(9)-H(9)	119(2)
C(3)-C(2)-H(2A)	112(2)	C(11)-C(10)-C(15)	120.4(2)
O(1)-C(2)-H(2B)	105(2)	C(11)-C(10)-C(1)	117.9(2)
C(3)-C(2)-H(2B)	112(2)	C(15)-C(10)-C(1)	121.7(2)
H(2A)-C(2)-H(2B)	109(2)	C(10)-C(11)-C(12)	119.8(2)
O(3)-C(3)-C(4)	122.4(2)	C(10)-C(11)-H(11)	121(2)
O(3)-C(3)-C(2)	119.5(2)	C(12)-C(11)-H(11)	119(2)
C(4)-C(3)-C(2)	118.1(2)	C(13)-C(12)-C(11)	120.3(3)
C(5)-C(4)-C(9)	118.9(2)	C(13)-C(12)-H(12)	123(2)
C(5)-C(4)-C(3)	119.8(2)	C(11)-C(12)-H(12)	117(2)
C(9)-C(4)-C(3)	121.2(2)	C(12)-C(13)-C(14)	120.0(2)
C(6)-C(5)-C(4)	120.8(2)	C(12)-C(13)-H(13)	122(1)
C(6)-C(5)-H(5)	118(2)	C(14)-C(13)-H(13)	117(1)
C(4)-C(5)-H(5)	121(2)	C(15)-C(14)-C(13)	120.0(2)
C(5)-C(6)-C(7)	119.7(2)	C(15)-C(14)-H(14)	119(2)
C(5)-C(6)-H(6)	117(2)	C(13)-C(14)-H(14)	121(2)
C(7)-C(6)-H(6)	123(2)	C(14)-C(15)-C(10)	119.5(2)
O(4)-C(7)-C(8)	116.8(2)	C(14)-C(15)-H(15)	122(2)
O(4)-C(7)-C(6)	123.2(2)	C(10)-C(15)-H(15)	119(2)

Table 40. Anisotropic displacement parameters ($Å^2 \times 10^3$) for pHP Benzoate **70c**. The anisotropic displacement factor exponent takes the form: $-2\pi^2[h^2 a^{*2} U_{11} + ... + 2 h k a^* b^* U_{12}]$

	U_{11}	U_{22}	U_{33}	U_{23}	U_{13}	U_{12}
O(1)	43(1)	25(1)	16(1)	-1(1)	-1(1)	0(1)
O(2)	39(1)	42(1)	20(1)	0(1)	-5(1)	-9(1)
O(3)	38(1)	30(1)	22(1)	5(1)	-7(1)	5(1)
O(4)	35(1)	38(1)	18(1)	-4(1)	-1(1)	6(1)
C(1)	31(1)	28(1)	19(1)	1(1)	-1(1)	0(1)
C(2)	39(1)	26(1)	17(1)	1(1)	-3(1)	1(1)
C(3)	25(1)	22(1)	19(1)	2(1)	-2(1)	-3(1)
C(4)	23(1)	23(1)	17(1)	2(1)	0(1)	0(1)
C(5)	25(1)	21(1)	24(1)	3(1)	-2(1)	0(1)
C(6)	21(1)	22(1)	26(1)	0(1)	1(1)	3(1)
C(7)	21(1)	25(1)	17(1)	2(1)	0(1)	-1(1)
C(8)	31(1)	31(1)	19(1)	6(1)	1(1)	6(1)
C(9)	30(1)	24(1)	22(1)	4(1)	1(1)	6(1)
C(10)	26(1)	29(1)	18(1)	1(1)	-1(1)	3(1)
C(11)	31(1)	32(1)	24(1)	-3(1)	-4(1)	-2(1)
C(12)	34(1)	41(2)	23(1)	5(1)	4(1)	0(1)
C(13)	28(1)	43(1)	17(1)	4(1)	0(1)	5(1)
C(14)	29(1)	38(1)	21(1)	-3(1)	0(1)	1(1)
C(15)	26(1)	28(1)	20(1)	-1(1)	0(1)	2(1)

Table 41. Hydrogen coordinates (x 10^4) and isotropic displacement parameters (Å^2 x 10^3) for pHP Benzoate **70c**.

	x	y	z	U(eq)
H(4O)	-2200(70)	4530(50)	6660(30)	130(20)
H(2A)	1250(30)	2380(30)	2457(17)	28(6)
H(2B)	-290(30)	1450(30)	2299(18)	30(7)
H(5)	-2670(40)	5100(30)	3590(20)	41(8)
H(6)	-2840(40)	5350(30)	5130(20)	39(8)
H(8)	110(30)	2140(30)	5560(20)	43(8)
H(9)	300(30)	1900(30)	3923(19)	36(8)
H(11)	2580(40)	5220(30)	-170(20)	36(8)
H(12)	2610(30)	5570(30)	-1722(19)	32(7)
H(13)	1300(30)	3890(20)	-2704(16)	17(6)
H(14)	-330(40)	2150(40)	-2050(20)	58(10)
H(15)	-240(30)	2020(30)	-399(17)	16(6)

Table 42. Torsion angles [°] for pHP Benzoate **70c**.

C(2)-O(1)-C(1)-O(2)	4.0(3)
C(2)-O(1)-C(1)-C(10)	-176.01(19)
C(1)-O(1)-C(2)-C(3)	74.5(3)
O(1)-C(2)-C(3)-O(3)	1.7(3)
O(1)-C(2)-C(3)-C(4)	-178.0(2)
O(3)-C(3)-C(4)-C(5)	0.0(3)
C(2)-C(3)-C(4)-C(5)	179.8(2)
O(3)-C(3)-C(4)-C(9)	-177.0(2)
C(2)-C(3)-C(4)-C(9)	2.7(3)
C(9)-C(4)-C(5)-C(6)	-0.1(3)
C(3)-C(4)-C(5)-C(6)	-177.2(2)
C(4)-C(5)-C(6)-C(7)	0.4(3)
C(5)-C(6)-C(7)-O(4)	-178.9(2)
C(5)-C(6)-C(7)-C(8)	-0.4(3)
O(4)-C(7)-C(8)-C(9)	178.8(2)
C(6)-C(7)-C(8)-C(9)	0.2(4)
C(7)-C(8)-C(9)-C(4)	0.1(4)
C(5)-C(4)-C(9)-C(8)	-0.1(3)
C(3)-C(4)-C(9)-C(8)	177.0(2)
O(2)-C(1)-C(10)-C(11)	-2.3(4)
O(1)-C(1)-C(10)-C(11)	177.6(2)
O(2)-C(1)-C(10)-C(15)	178.6(2)
O(1)-C(1)-C(10)-C(15)	-1.4(3)
C(15)-C(10)-C(11)-C(12)	1.1(4)
C(1)-C(10)-C(11)-C(12)	-178.0(2)
C(10)-C(11)-C(12)-C(13)	-0.9(4)
C(11)-C(12)-C(13)-C(14)	0.3(4)
C(12)-C(13)-C(14)-C(15)	0.3(4)
C(13)-C(14)-C(15)-C(10)	-0.2(4)
C(11)-C(10)-C(15)-C(14)	-0.5(4)
C(1)-C(10)-C(15)-C(14)	178.6(2)

Table 43. Hydrogen bonds for pHP Benzoate **70c** [Å and °].

D-H...A	d(D-H)	d(H...A)	d(D...A)	<(DHA)
O(4)-H(4O)...O(3)#1	0.97(5)	1.71(5)	2.687(2)	177(5)

Symmetry transformations used to generate equivalent atoms: #1: -x-1/2, -y+1, z+1/2.

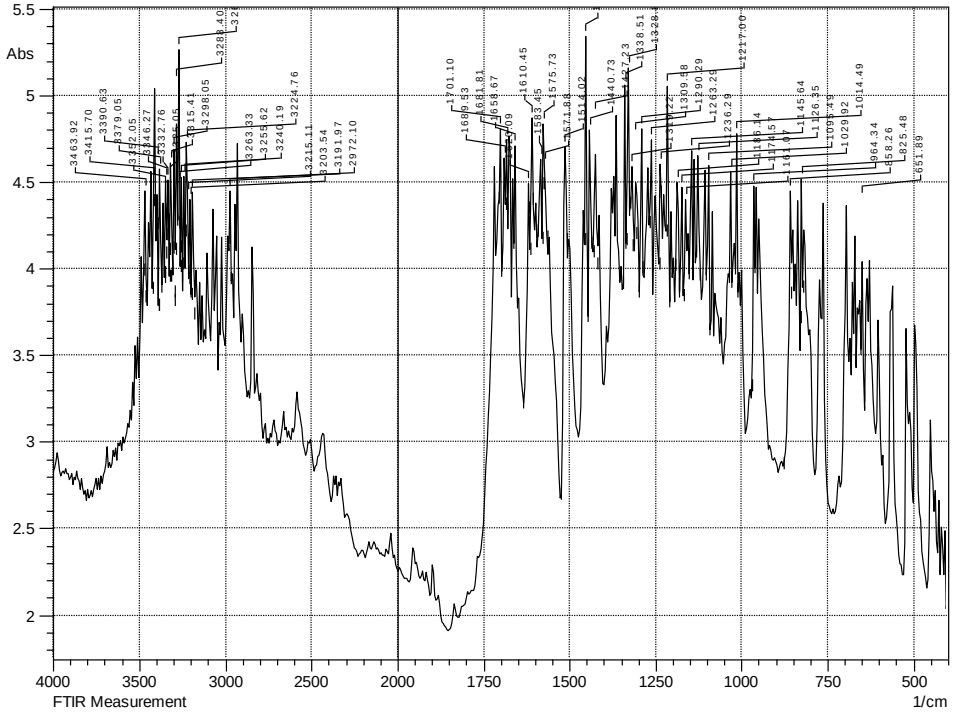

Figure 32. IR of pHP pOCH$_3$ Benzoate **70d** (KBr).

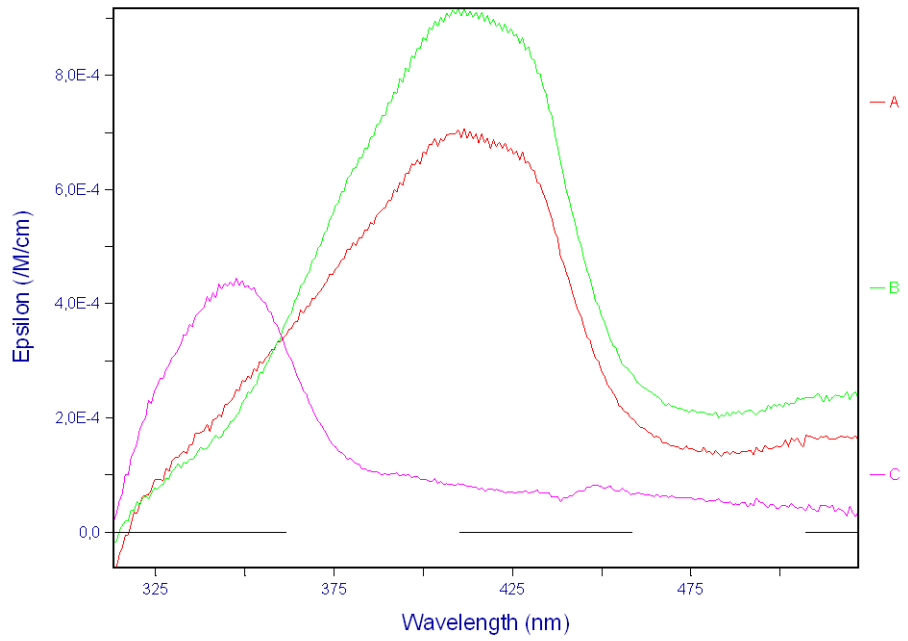

Figure 33. Laser Flash Photolysis Transient Spectra for pHP pOCH$_3$ Benzoate **70d** in Aqueous Acetonitrile. Changes in absorption over time during photolysis represented by red, green, violet, and orange lines.

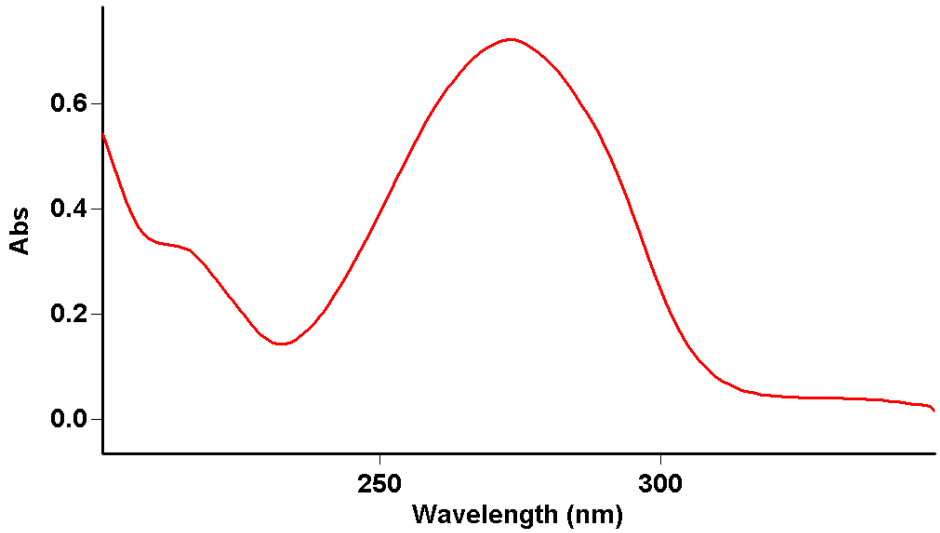

Figure 34. UV-VIS of pHP pOCH$_3$ Benzoate **70d** (7:3 acetonitrile/water; λ_{max} = 272 nm; log ε = 4.64).

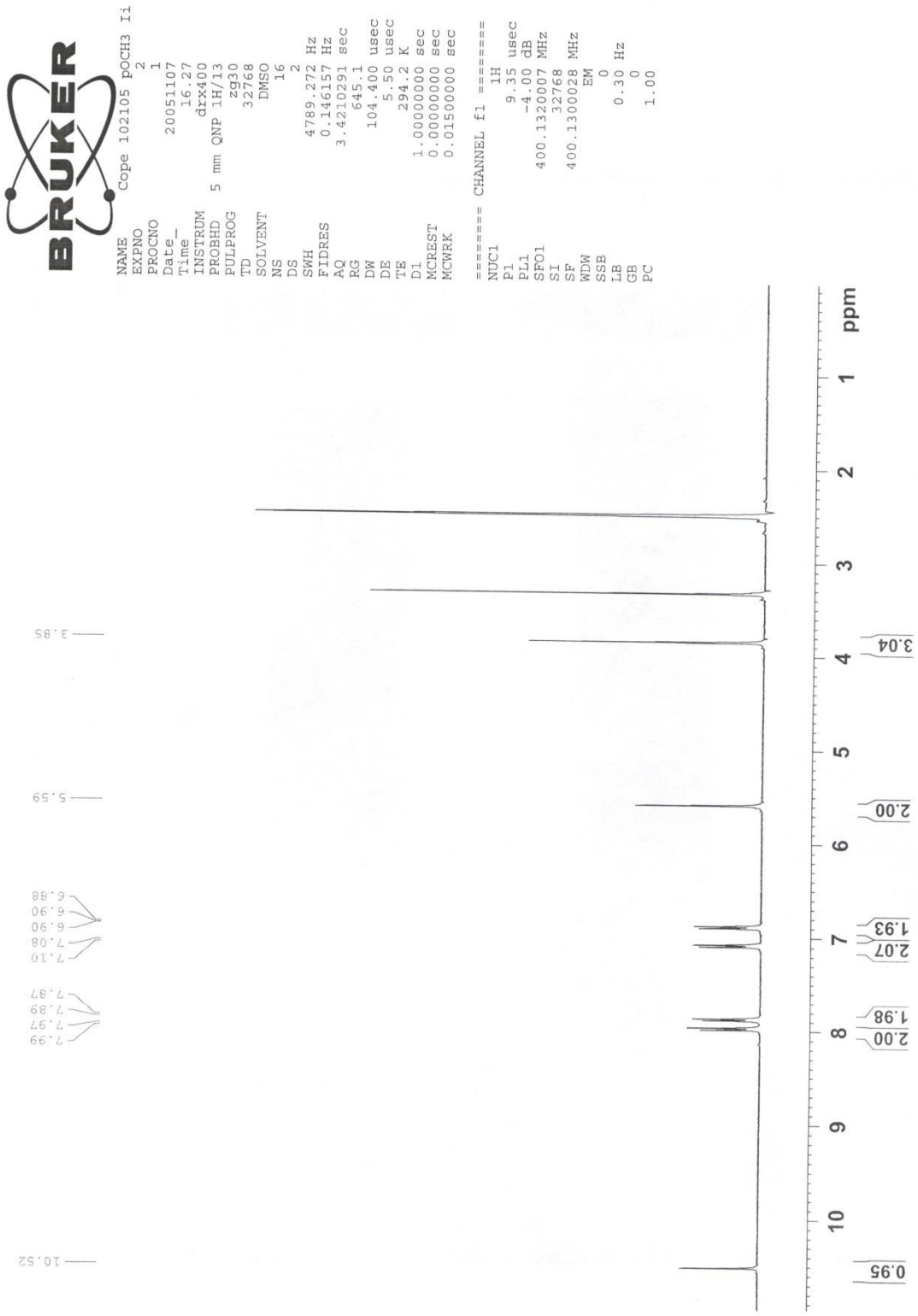

Figure 35. ^{1}H NMR of pHP pOCH$_3$ Benzoate **70d** (DMSO-d$_6$).

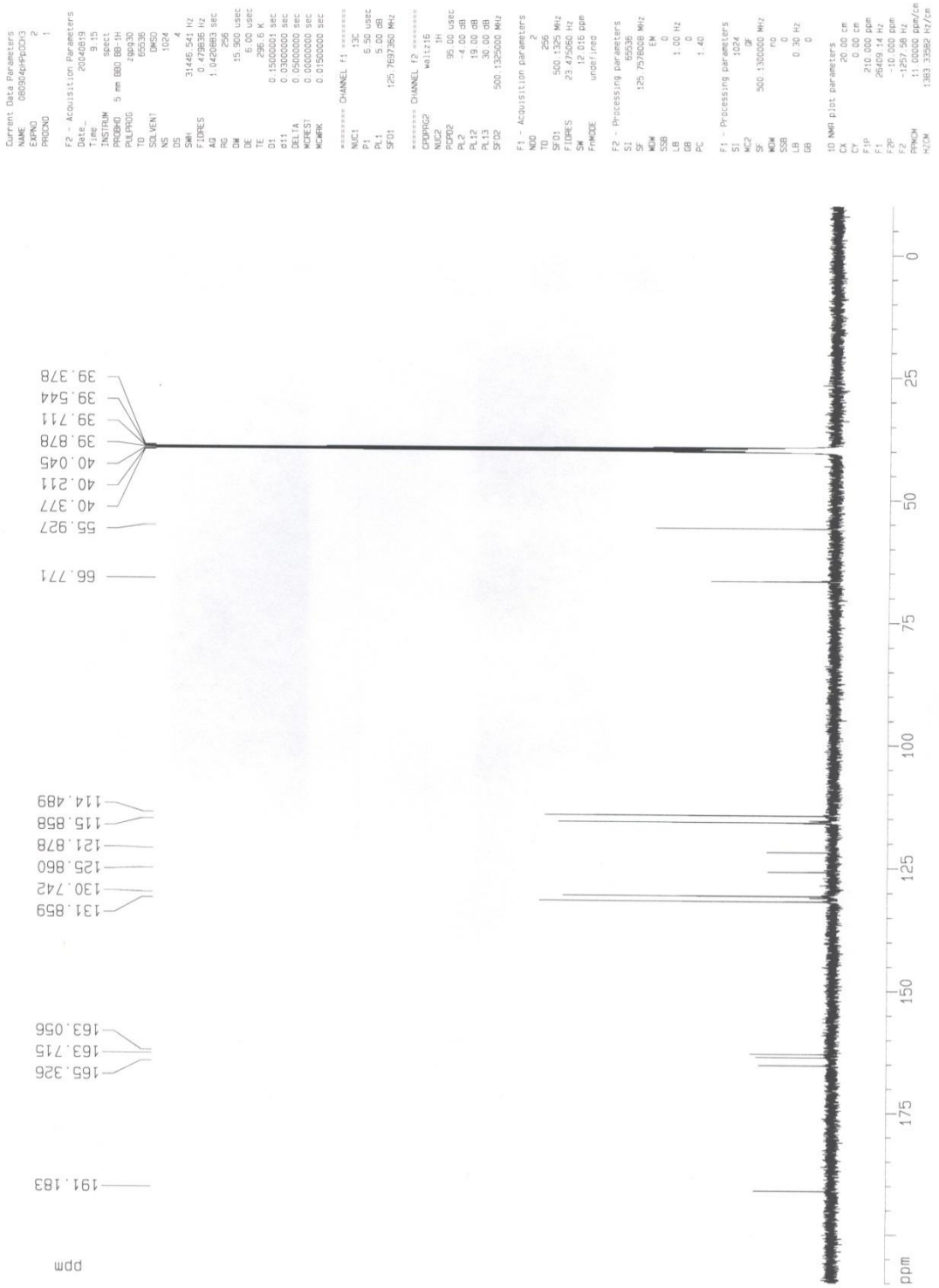

Figure 36. ^{13}C NMR of pHP $pOCH_3$ Benzoate **70d** (DMSO-d_6).

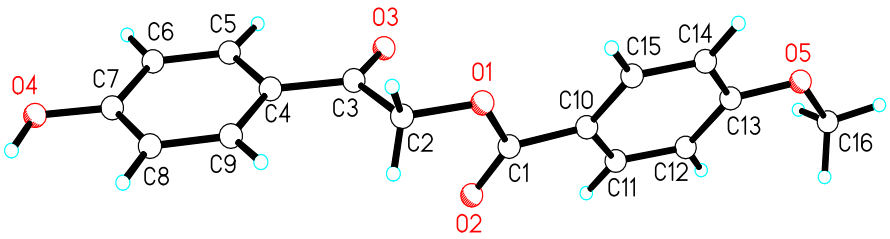

Figure 37. X-Ray Crystal Structure of pHP *p*-Methoxybenzoate **70d**.

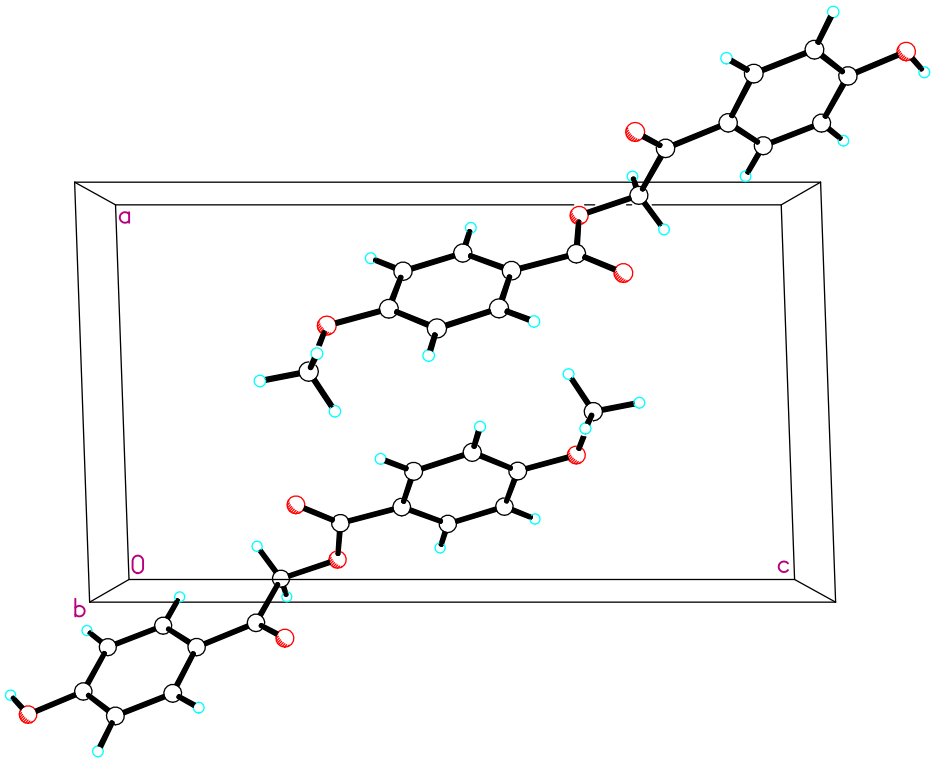

Figure 38. Orientation of $pOCH_3$ Benzoate **70d** in the Crystal Lattice.

Comments from X-Ray Crystallographer

The asymmetric unit contains one $C_{16}H_{14}O_5$ molecule. All displacement ellipsoids are drawn at the 50% probability level.

Brief Experimental Description

Colorless crystals of $C_{16}H_{14}O_5$ are, at 100(2) K, monoclinic, space group $P2_1$–C_2^2 (No. 4)[1] with **a** = 8.5122(9) Å, **b** = 5.2444(6) Å, **c** = 15.108(2) Å, β = 92.049(2)°, V = 674.0(1) $Å^3$ and Z = 2 molecules {d_{calcd} = 1.411 g/cm^3; μ_a(MoKα) = 0.105 mm^{-1}}. A full hemisphere of diffracted intensities (1850 10-second frames with a ω scan width of 0.30°) was measured for a single-domain specimen using graphite-monochromated MoKα radiation (λ= 0.71073 Å) on a Bruker SMART APEX CCD Single Crystal Diffraction System[2]. X-rays were provided by a fine-focus sealed x-ray tube operated at 50kV and 30mA. Lattice constants were determined with the Bruker SAINT software package using peak centers for 2620 reflections. A total of 8175 integrated reflection intensities having 2θ((MoKα)< 61.16° were produced using the Bruker program SAINT[3]; 4008 of these were unique and gave R_{int} = 0.025 with a coverage which was 99.3% complete. The data were corrected empirically for variable absorption effects using equivalent reflections; the relative transmission factors ranged from 0.916 to 1.000. The Bruker software package SHELXTL was used to solve the structure using "direct methods" techniques. All stages of weighted full-matrix least-squares refinement were conducted using F_o^2 data with the SHELXTL Version 6.10 software package[4].

The final structural model incorporated anisotropic thermal parameters for all nonhydrogen atoms and isotropic thermal parameters for all hydrogen atoms. All hydrogen atoms were located in a difference Fourier and included in the structural model as independent isotropic atoms whose parameters were allowed to vary in least-squares refinement cycles. A total of 246 parameters were refined using 1 restraint, 4008 data and weights of $w = 1/ [\sigma^2(F^2) + (0.0689\ P)^2]$, where $P = [F_O^2 + 2F_C^2] / 3$. Final agreement factors at convergence are: R_1(unweighted, based on F) = 0.046 for 3409 independent absorption-corrected "observed" reflections having $2\theta(MoK\alpha) < 61.16°$ and $I > 2\sigma(I)$; R_1(unweighted, based on F) = 0.055 and wR_2(weighted, based on F^2) = 0.112 for all 4008 independent absorption-corrected reflections having $2\theta(MoK\alpha) < 61.16°$. The largest shift/s.u. was 0.000 in the final refinement cycle. The final difference map had maxima and minima of 0.40 and -0.18 $e^-/Å^3$, respectively. Since the "Flack" parameter refined to a final value of 1.4(8), the absolute structure could not be reliably determined experimentally using anomalous dispersion of the x-rays.

Table 44. Crystal data and structure refinement for pHP pOCH$_3$ Benzoate **70d**.

Empirical formula	$C_{16}H_{14}O_5$	
Formula weight	286.27	
Temperature	100(2) K	
Wavelength	0.71073 Å	
Crystal system	Monoclinic	
Space group	$P2_1– C_2^2$ (No. 4)	
Unit cell dimensions	**a** = 8.5122(9) Å	**α** = 90.000°
	b = 5.2444(6) Å	**β** = 92.049(2)°.
	c = 15.1081(16) Å	**γ** = 90.000°
Volume	674.0 (1) Å^3	
Z	2	
Density (calculated)	1.411 Mg/m^3	
Absorption coefficient	0.105 mm^{-1}	
F(000)	300	
Crystal size	0.34 x 0.34 x 0.06 mm^3	
Theta range for data collection	2.70° to 30.58°	
Index ranges	$-12 \leq h \leq 12, -7 \leq k \leq 7, -21 \leq l \leq 21$	
Reflections collected	8175	
Independent reflections	4008 [R_{int} = 0.025]	
Completeness to theta = 30.58°	99.3 %	
Absorption correction	Empirical	
Max. and min. transmission	1.000 and 0.916	
Refinement method	Full-matrix least squares on F^2	
Data / restraints / parameters	4008 / 1 / 246	
Goodness-of-fit on F^2	0.991	
Final R indices [I>2sigma(I)]	R_1 = 0.046, wR_2 = 0.107	
R indices (all data)	R_1 = 0.055, wR_2 = 0.112	
Absolute structure parameter	1.4(8)	
Largest diff. peak and hole	0.40 and -0.18 e$^-$/Å^3	

$R_1 = \Sigma \, ||F_O| - |F_C|| \, / \, \Sigma \, |F_O|$

$wR_2 = \{ \, \Sigma \, [w(F_O^2 - F_C^2)^2] \, / \, \Sigma \, [w(F_O^2)^2] \, \}^{1/2}$

Table 45. Atomic coordinates (x 10^4) and equivalent isotropic displacement parameters ($Å^2$ x 10^3) for pHP pOCH_3 Benzoate **70d**. U(eq) is defined as one third of the trace of the orthogonalized Uij tensor.

	x	y	z	U(eq)
O(1)	437(1)	-1969(2)	3105(1)	28(1)
O(2)	2027(1)	1020(3)	2575(1)	31(1)
O(3)	-1458(1)	1474(2)	2353(1)	29(1)
O(4)	-3651(1)	-523(3)	-1627(1)	32(1)
O(5)	3350(1)	1566(3)	6758(1)	29(1)
C(1)	1498(2)	-98(3)	3204(1)	24(1)
C(2)	-107(2)	-2468(3)	2212(1)	26(1)
C(3)	-1176(2)	-318(3)	1874(1)	23(1)
C(4)	-1839(2)	-501(3)	957(1)	22(1)
C(5)	-2923(2)	1341(3)	659(1)	25(1)
C(6)	-3523(2)	1306(4)	-204(1)	28(1)
C(7)	-3043(2)	-598(3)	-786(1)	25(1)
C(8)	-1982(2)	-2457(3)	-496(1)	25(1)
C(9)	-1391(2)	-2407(3)	371(1)	25(1)
C(10)	1948(2)	395(3)	4140(1)	22(1)
C(11)	2944(2)	2419(3)	4350(1)	26(1)
C(12)	3445(2)	2892(3)	5218(1)	26(1)
C(13)	2926(2)	1294(3)	5888(1)	23(1)
C(14)	1920(2)	-741(3)	5686(1)	25(1)
C(15)	1439(2)	-1183(3)	4819(1)	23(1)
C(16)	4501(2)	3466(4)	6990(1)	32(1)

Table 46. Bond lengths [Å] for pHP pOCH$_3$ Benzoate **70d**.

O(1)-C(1)	1.339(2)	C(6)-H(6)	1.01(2)
O(1)-C(2)	1.435(2)	C(7)-C(8)	1.389(2)
O(2)-C(1)	1.217(2)	C(8)-C(9)	1.386(2)
O(3)-C(3)	1.216(2)	C(8)-H(8)	0.93(2)
O(4)-C(7)	1.355(2)	C(9)-H(9)	0.93(2)
O(4)-H(4O)	0.87(3)	C(10)-C(11)	1.388(2)
O(5)-C(13)	1.357(2)	C(10)-C(15)	1.399(2)
O(5)-C(16)	1.432(2)	C(11)-C(12)	1.386(2)
C(1)-C(10)	1.474(2)	C(11)-H(11)	0.95(2)
C(2)-C(3)	1.526(2)	C(12)-C(13)	1.399(2)
C(2)-H(2A)	0.93(2)	C(12)-H(12)	0.95(2)
C(2)-H(2B)	0.98(2)	C(13)-C(14)	1.395(2)
C(3)-C(4)	1.480(2)	C(14)-C(15)	1.378(2)
C(4)-C(9)	1.397(2)	C(14)-H(14)	0.97(2)
C(4)-C(5)	1.400(2)	C(15)-H(15)	0.91(2)
C(5)-C(6)	1.383(2)	C(16)-H(16A)	1.04(2)
C(5)-H(5)	0.91(2)	C(16)-H(16B)	0.98(2)
C(6)-C(7)	1.400(2)	C(16)-H(16C)	0.97(2)

Table 47. Bond angles [°] for pHP pOCH$_3$ Benzoate **70d**.

C(1)-O(1)-C(2)	115.65(12)	C(8)-C(9)-C(4)	120.96(15)
C(7)-O(4)-H(4O)	114.3(18)	C(8)-C(9)-H(9)	120.6(12)
C(13)-O(5)-C(16)	117.82(13)	C(4)-C(9)-H(9)	118.5(12)
O(2)-C(1)-O(1)	122.19(14)	C(11)-C(10)-C(15)	119.16(13)
O(2)-C(1)-C(10)	125.02(15)	C(11)-C(10)-C(1)	119.30(13)
O(1)-C(1)-C(10)	112.78(13)	C(15)-C(10)-C(1)	121.50(14)
O(1)-C(2)-C(3)	110.40(13)	C(12)-C(11)-C(10)	121.20(14)
O(1)-C(2)-H(2A)	106.4(11)	C(12)-C(11)-H(11)	120.3(12)
C(3)-C(2)-H(2A)	112.2(12)	C(10)-C(11)-H(11)	118.5(12)
O(1)-C(2)-H(2B)	103.4(12)	C(11)-C(12)-C(13)	118.89(15)
C(3)-C(2)-H(2B)	110.8(12)	C(11)-C(12)-H(12)	119.0(11)
H(2A)-C(2)-H(2B)	113.2(17)	C(13)-C(12)-H(12)	122.1(11)
O(3)-C(3)-C(4)	122.07(14)	O(5)-C(13)-C(14)	115.63(13)
O(3)-C(3)-C(2)	120.01(13)	O(5)-C(13)-C(12)	123.92(15)
C(4)-C(3)-C(2)	117.91(13)	C(14)-C(13)-C(12)	120.45(13)
C(9)-C(4)-C(5)	118.75(13)	C(15)-C(14)-C(13)	119.76(14)
C(9)-C(4)-C(3)	122.43(13)	C(15)-C(14)-H(14)	120.9(12)
C(5)-C(4)-C(3)	118.80(13)	C(13)-C(14)-H(14)	119.3(12)
C(6)-C(5)-C(4)	120.78(15)	C(14)-C(15)-C(10)	120.53(15)
C(6)-C(5)-H(5)	126.1(12)	C(14)-C(15)-H(15)	119.9(12)
C(4)-C(5)-H(5)	113.1(12)	C(10)-C(15)-H(15)	119.5(12)
C(5)-C(6)-C(7)	119.63(15)	O(5)-C(16)-H(16A)	109.1(13)
C(5)-C(6)-H(6)	119.0(12)	O(5)-C(16)-H(16B)	110.7(13)
C(7)-C(6)-H(6)	121.3(12)	H(16A)-C(16)-H(16B)	108.4(18)
O(4)-C(7)-C(8)	122.53(14)	O(5)-C(16)-H(16C)	111.9(14)
O(4)-C(7)-C(6)	117.23(14)	H(16A)-C(16)-H(16C)	109.5(16)
C(8)-C(7)-C(6)	120.24(14)	H(16B)-C(16)-H(16C)	107.2(19)
C(9)-C(8)-C(7)	119.62(14)		
C(9)-C(8)-H(8)	119.6(12)		
C(7)-C(8)-H(8)	120.7(13)		

Table 48. Anisotropic displacement parameters ($Å^2 \times 10^3$) for pHP $pOCH_3$ Benzoate **70d**. The anisotropic displacement factor exponent takes the form:
$-2\pi^2[h^2 a^{*2} U_{11} + ... + 2 h k a^* b^* U_{12}]$

	U_{11}	U_{22}	U_{33}	U_{23}	U_{13}	U_{12}
O(1)	38(1)	26(1)	18(1)	1(1)	-4(1)	-3(1)
O(2)	35(1)	39(1)	19(1)	6(1)	-1(1)	-4(1)
O(3)	37(1)	27(1)	23(1)	-8(1)	-2(1)	3(1)
O(4)	36(1)	37(1)	22(1)	-2(1)	-5(1)	7(1)
O(5)	30(1)	36(1)	21(1)	1(1)	-5(1)	-5(1)
C(1)	26(1)	26(1)	19(1)	2(1)	-2(1)	4(1)
C(2)	35(1)	24(1)	20(1)	-2(1)	-4(1)	1(1)
C(3)	27(1)	21(1)	21(1)	-1(1)	1(1)	-3(1)
C(4)	25(1)	23(1)	19(1)	0(1)	1(1)	-3(1)
C(5)	29(1)	21(1)	25(1)	-4(1)	0(1)	2(1)
C(6)	30(1)	26(1)	29(1)	2(1)	-2(1)	3(1)
C(7)	27(1)	26(1)	21(1)	0(1)	-2(1)	-2(1)
C(8)	30(1)	25(1)	19(1)	-4(1)	0(1)	0(1)
C(9)	29(1)	23(1)	22(1)	-1(1)	-3(1)	3(1)
C(10)	25(1)	23(1)	17(1)	1(1)	-1(1)	3(1)
C(11)	33(1)	24(1)	21(1)	5(1)	1(1)	-1(1)
C(12)	28(1)	25(1)	25(1)	-1(1)	-3(1)	-1(1)
C(13)	23(1)	28(1)	19(1)	0(1)	-2(1)	4(1)
C(14)	27(1)	28(1)	20(1)	5(1)	-1(1)	1(1)
C(15)	25(1)	23(1)	21(1)	1(1)	-3(1)	-1(1)
C(16)	30(1)	39(1)	27(1)	-3(1)	-5(1)	-5(1)

Table 49. Hydrogen coordinates (x 10^4) and isotropic displacement parameters ($Å^2$ x 10^3) for pHP pOCH_3 Benzoate **70d**.

	x	y	z	U(eq)
H(4O)	-3260(30)	-1650(60)	-1981(17)	65(8)
H(2A)	780(20)	-2630(40)	1881(12)	19(4)
H(2B)	-700(20)	-4060(50)	2262(13)	37(6)
H(5)	-3170(20)	2480(40)	1085(12)	21(4)
H(6)	-4330(20)	2620(40)	-394(13)	34(5)
H(8)	-1610(20)	-3660(50)	-888(13)	34(5)
H(9)	-690(20)	-3650(50)	576(12)	30(5)
H(11)	3280(20)	3490(40)	3884(12)	31(5)
H(12)	4130(20)	4300(40)	5339(12)	24(4)
H(14)	1580(20)	-1830(40)	6157(12)	27(5)
H(15)	740(20)	-2460(40)	4688(13)	28(5)
H(16A)	4730(20)	3420(50)	7672(13)	42(6)
H(16B)	4120(20)	5170(40)	6829(13)	31(5)
H(16C)	5470(20)	3200(50)	6688(14)	41(6)

Table 50. Torsion angles [°] for pHP pOCH$_3$ Benzoate **70d**.

C(2)-O(1)-C(1)-O(2)	-3.6(2)
C(2)-O(1)-C(1)-C(10)	177.27(13)
C(1)-O(1)-C(2)-C(3)	-71.84(18)
O(1)-C(2)-C(3)-O(3)	-0.4(2)
O(1)-C(2)-C(3)-C(4)	179.47(13)
O(3)-C(3)-C(4)-C(9)	172.98(16)
C(2)-C(3)-C(4)-C(9)	-6.9(2)
O(3)-C(3)-C(4)-C(5)	-5.3(2)
C(2)-C(3)-C(4)-C(5)	174.79(15)
C(9)-C(4)-C(5)-C(6)	-1.1(2)
C(3)-C(4)-C(5)-C(6)	177.29(14)
C(4)-C(5)-C(6)-C(7)	0.2(2)
C(5)-C(6)-C(7)-O(4)	-179.15(14)
C(5)-C(6)-C(7)-C(8)	0.6(2)
O(4)-C(7)-C(8)-C(9)	179.28(14)
C(6)-C(7)-C(8)-C(9)	-0.5(2)
C(7)-C(8)-C(9)-C(4)	-0.5(2)
C(5)-C(4)-C(9)-C(8)	1.2(2)
C(3)-C(4)-C(9)-C(8)	-177.08(14)
O(2)-C(1)-C(10)-C(11)	6.0(2)
O(1)-C(1)-C(10)-C(11)	-174.89(14)
O(2)-C(1)-C(10)-C(15)	-171.76(16)
O(1)-C(1)-C(10)-C(15)	7.3(2)
C(15)-C(10)-C(11)-C(12)	0.3(2)
C(1)-C(10)-C(11)-C(12)	-177.53(15)
C(10)-C(11)-C(12)-C(13)	-0.2(2)
C(16)-O(5)-C(13)-C(14)	173.96(15)
C(16)-O(5)-C(13)-C(12)	-5.5(2)
C(11)-C(12)-C(13)-O(5)	179.46(15)
C(11)-C(12)-C(13)-C(14)	0.0(2)
O(5)-C(13)-C(14)-C(15)	-179.34(14)
C(12)-C(13)-C(14)-C(15)	0.2(2)
C(13)-C(14)-C(15)-C(10)	-0.1(2)
C(11)-C(10)-C(15)-C(14)	-0.1(2)
C(1)-C(10)-C(15)-C(14)	177.65(15)

Table 51. Hydrogen bonds for pHP $pOCH_3$ Benzoate **70d** [Å and °].

D-H...A	d(D-H)	d(H...A)	d(D...A)	<(DHA)
O(4)-H(4O)...O(2)#1	0.87(3)	1.86(3)	2.7191(18)	168(3)

Symmetry transformations used to generate equivalent atoms: #1 -x, y-1/2, -z.

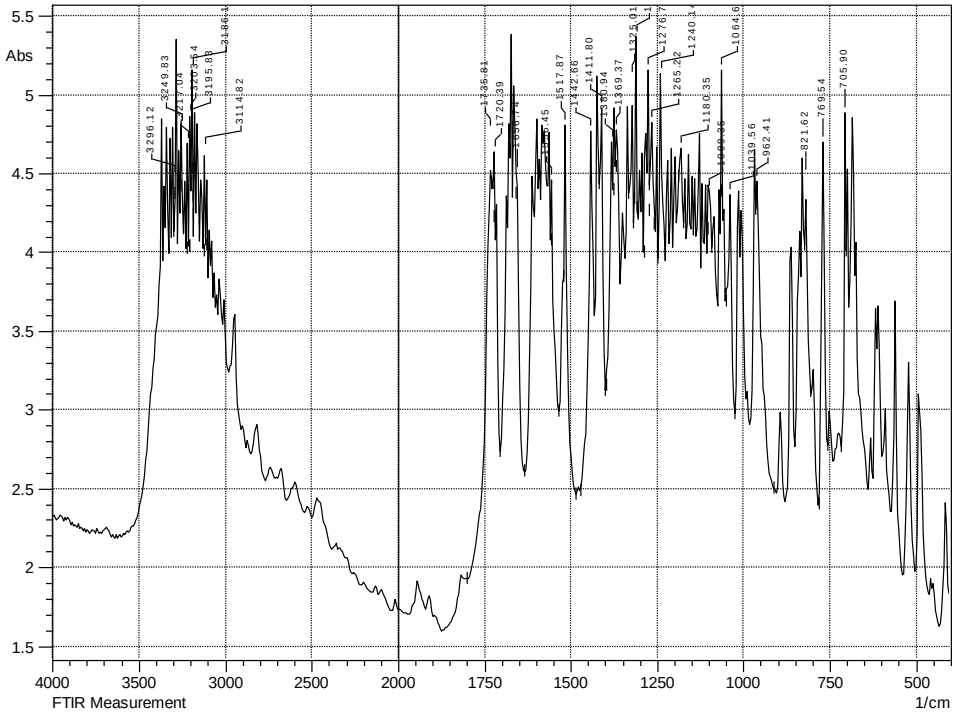

Figure 39. IR of pHP pCF_3 Benzoate **70e** (KBr).

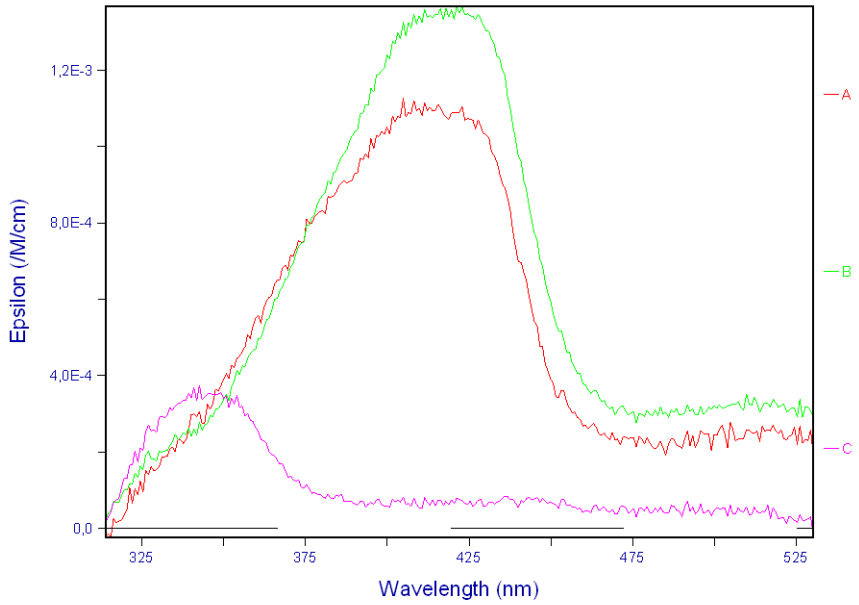

Figure 40. Laser Flash Photolysis Transient Spectra for pHP pCF_3 Benzoate **70e**. Changes in absorption over time during photolysis represented by red, green, violet, and orange lines (aqueous acetonitrile).

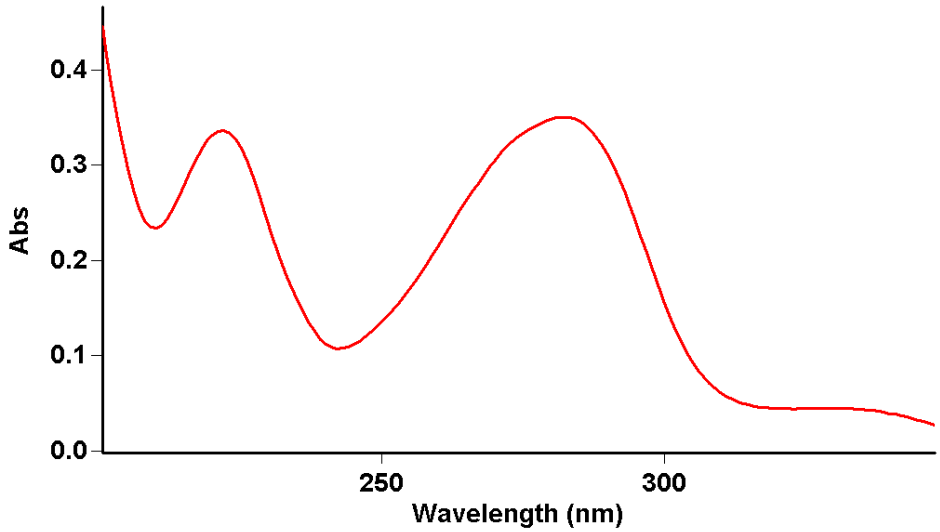

Figure 41. UV-VIS of pHP pCF_3 Benzoate **70e** (7:3 acetonitrile/water; λ_{max} = 282 nm; log ε = 4.52).

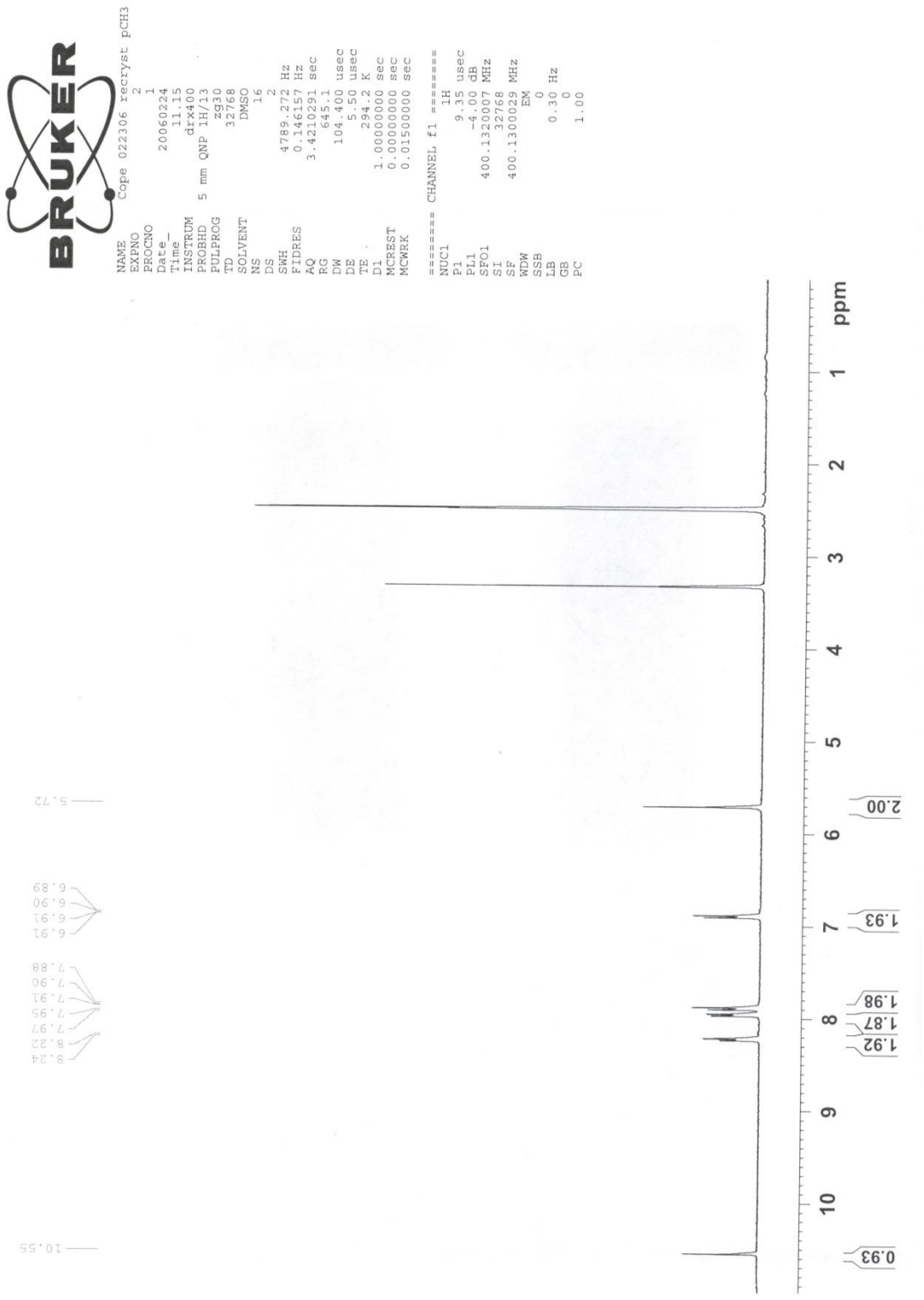

Figure 42. ^{1}H NMR of pHP pCF_3 Benzoate **70e** (DMSO-d_6).

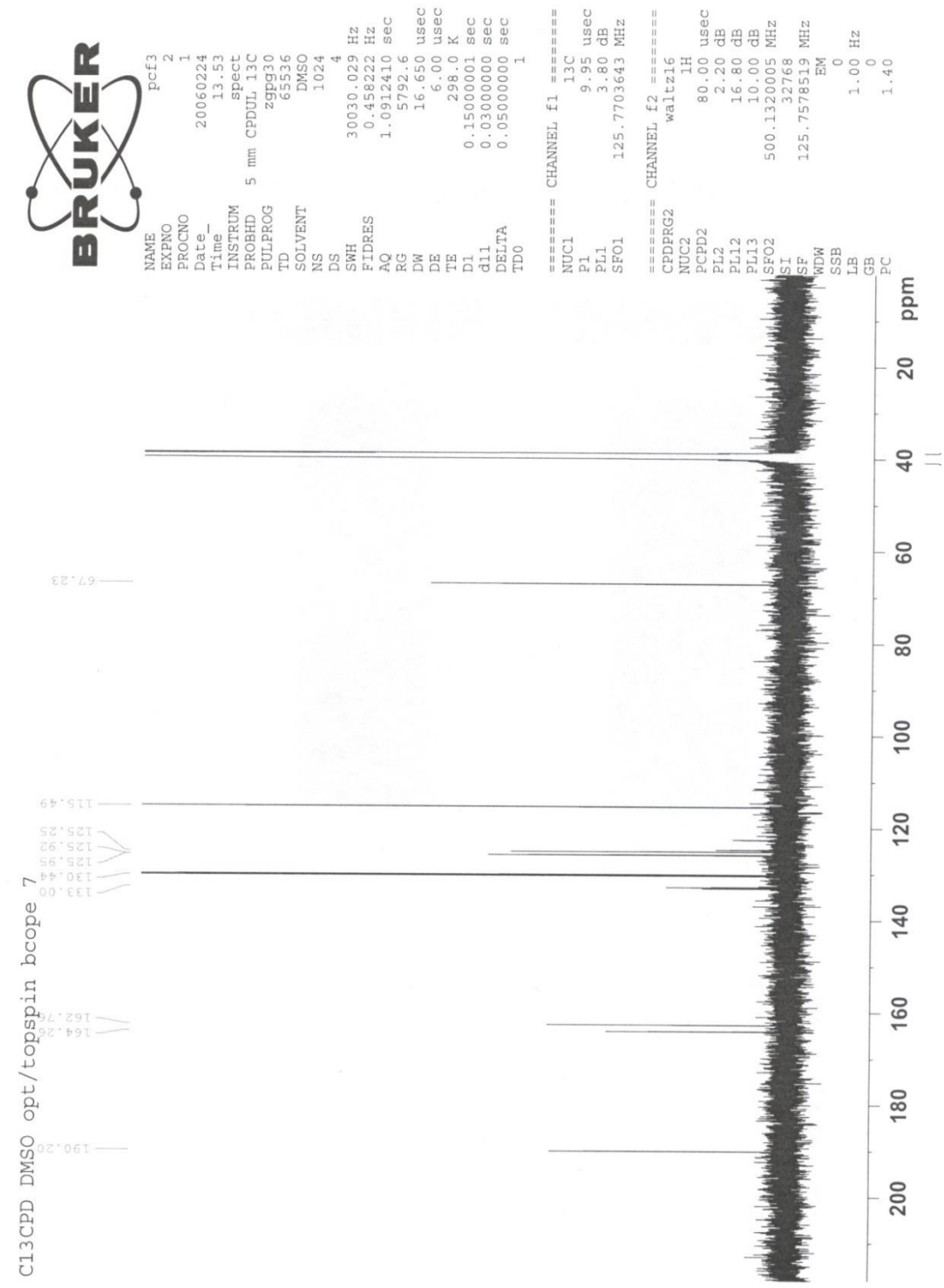

Figure 43. ^{13}C NMR of pHP pCF_3 Benzoate **70e** (DMSO-d_6).

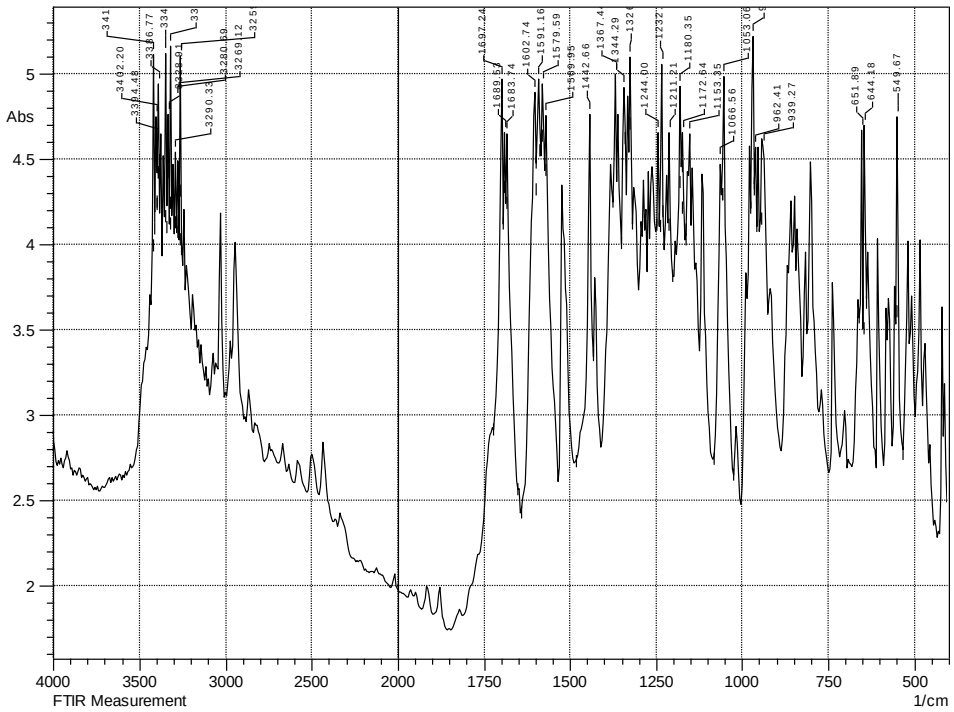

Figure 44. IR (KBr) of pHP Mesylate **72a**.

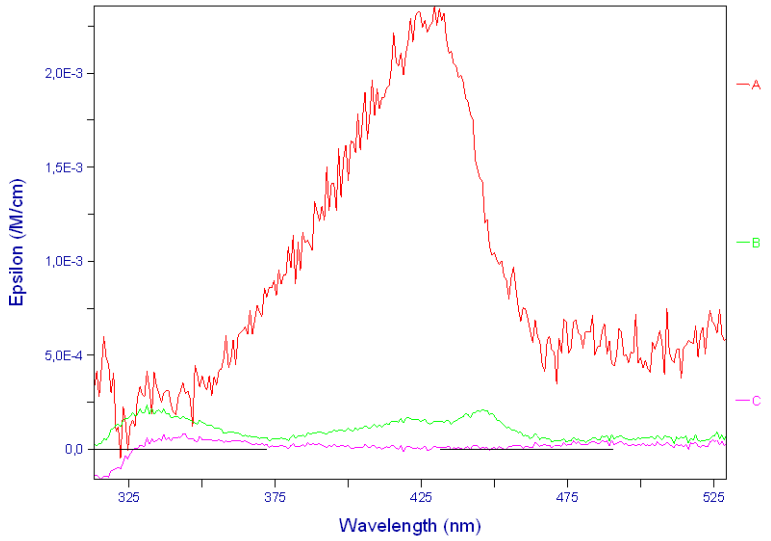

Figure 45. Laser Flash Photolysis Transient Spectra for pHP Mesylate **72a** in Aqueous Acetonitrile. Changes in absorption over time during photolysis represented by red, green, violet, and orange lines.

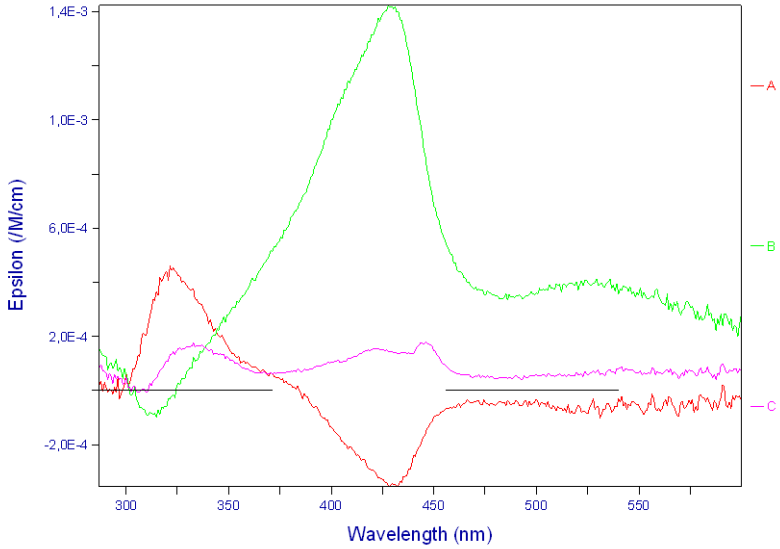

Figure 46. Laser Flash Photolysis Transient Spectra for pHP Mesylate **72a** in Water. Changes in absorption over time during photolysis represented by red, green, violet, and orange lines.

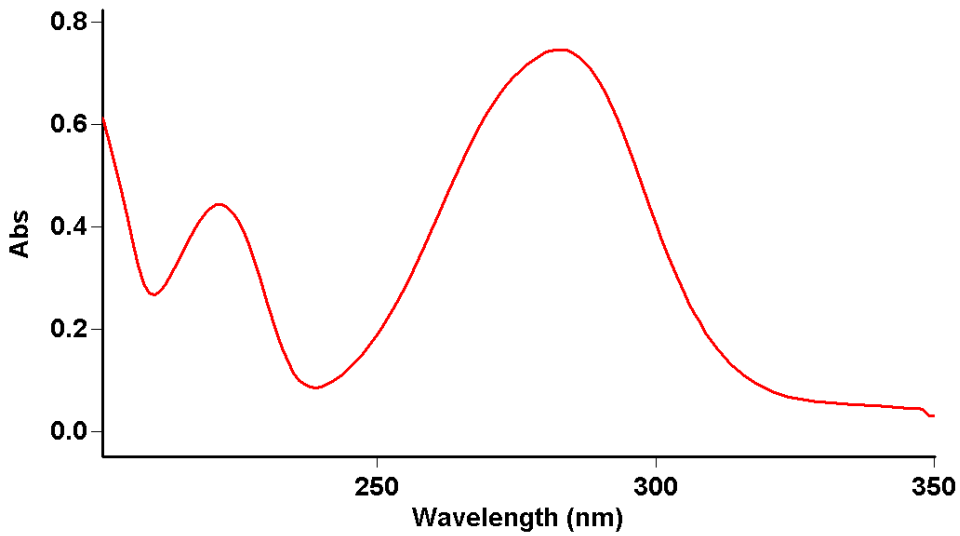

Figure 47. UV-VIS of pHP Mesylate **72a** (3:1 water/acetonitrile; λ_{max} = 281 nm; log ε = 4.15).

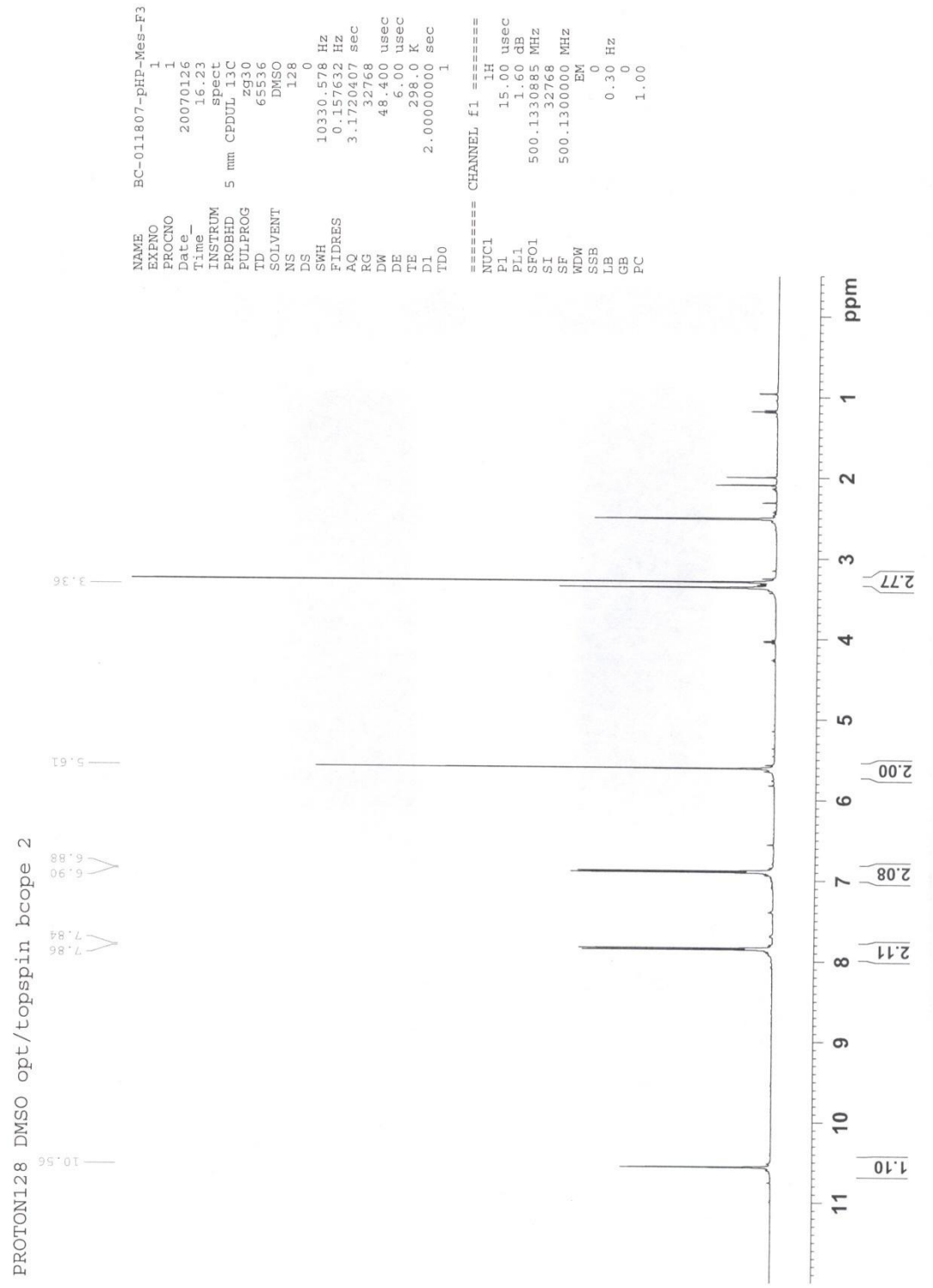

Figure 48. ^{1}H NMR of pHP Mesylate **72a** (DMSO-d_6).

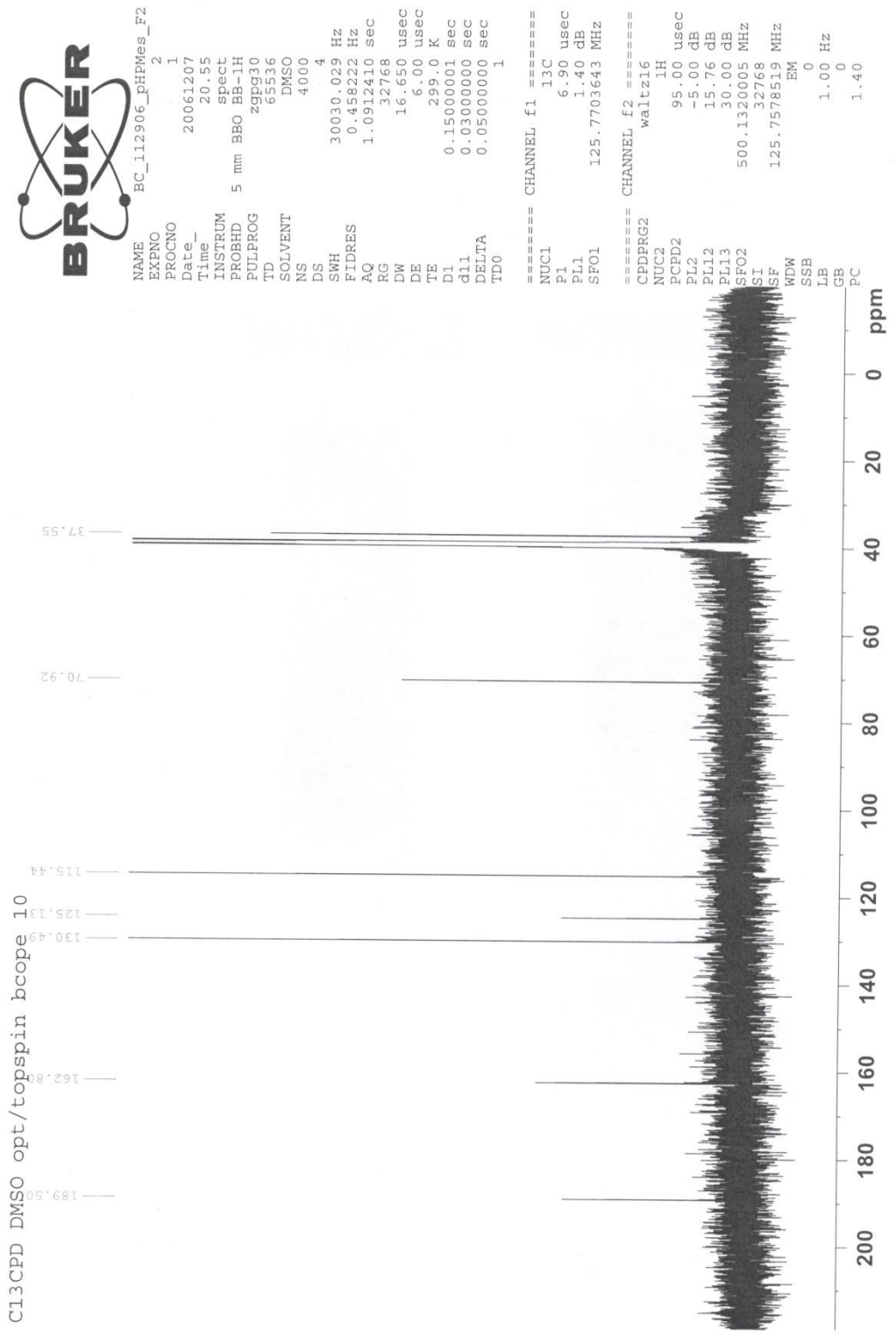

Figure 49. ^{13}C NMR of pHP Mesylate **72a** (DMSO-d_6).

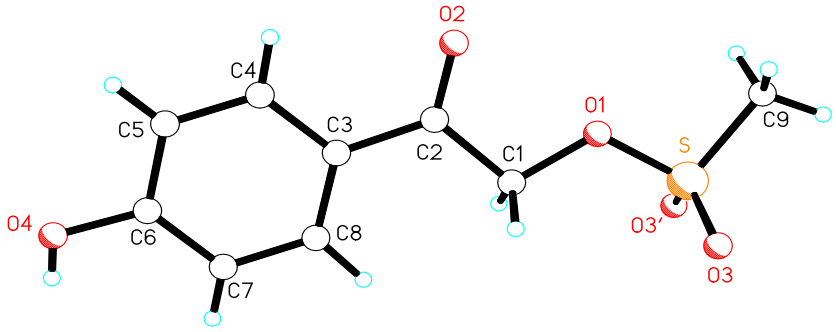

Figure 50. X-Ray Crystal Structure of pHP Mesylate **72a**.

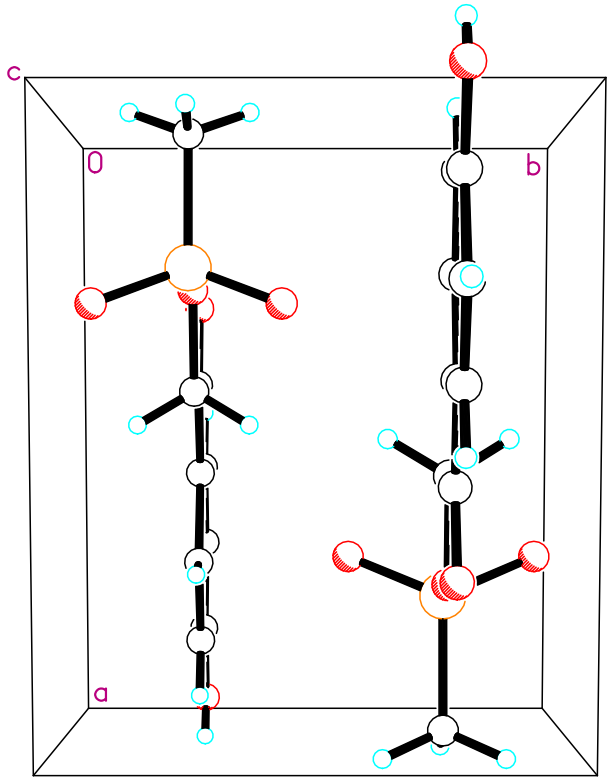

Figure 51. Orientation of pHP Mesylate **72a** in the Crystal Lattice.

Comments from X-Ray Crystallographer

The asymmetric unit contains one-half of a $C_9H_{10}O_5S$ molecule. All but one nonhydrogen atom and two hydrogen atoms of the molecule lie in the crystallographic mirror plane at y = 0.25 in the unit cell. All displacement ellipsoids are drawn at the 50% probability level.

Brief Experimental Description

Colorless crystals of $C_9H_{10}O_5S$ are, at 100(2) K, monoclinic, space group $P2_1/m$ - C_{2h}^2 (No. 11)[1] with **a** = 8.129(1) Å, **b** = 6.609(1) Å, **c** = 8.868(1) Å°, β = 97.535(3)°, V = 472.3(1) $Å^3$ and Z = 2 molecules {d_{calcd} = 1.619 g/cm^3; μ_a(MoKα) = 0.341 mm^{-1}}. A full hemisphere of diffracted intensities (1850 20-second frames with a ω scan width of 0.30°) was measured for a single-domain specimen using graphite-monochromated MoKα radiation (λ= 0.71073 Å) on a Bruker SMART APEX CCD Single Crystal Diffraction System[2]. X-rays were provided by a fine-focus sealed x-ray tube operated at 50kV and 35mA. Lattice constants were determined with the Bruker SAINT software package using peak centers for 2085 reflections. A total of 5835 integrated reflection intensities having 2θ((MoKα)< 60.95° were produced using the Bruker program SAINT[3]; 1551 of these were unique and gave R_{int} = 0.038 with a coverage which was 99.6% complete. The data were corrected empirically for variable absorption effects using equivalent reflections; the relative transmission factors ranged from 0.934 to 1.000. The Bruker software package SHELXTL was used to solve the structure using "direct methods"

techniques. All stages of weighted full-matrix least-squares refinement were conducted using F_o^2 data with the SHELXTL Version 6.10 software package[4].

The final structural model incorporated anisotropic thermal parameters for all nonhydrogen atoms and isotropic thermal parameters for all hydrogen atoms. All hydrogen atoms were located in a difference Fourier and included in the structural model as independent isotropic atoms whose parameters were allowed to vary in least-squares refinement cycles. A total of 114 parameters were refined using no restraints, 1551 data and weights of $w = 1/ [\sigma^2(F^2) + (0.0573\ P)^2]$, where $P = [F_O^2 + 2F_C^2] / 3$. Final agreement factors at convergence are: R_1(unweighted, based on F) = 0.042 for 1383 independent absorption-corrected "observed" reflections having $2\theta(MoK\alpha) < 60.95°$ and $I > 2\sigma(I)$; R_1(unweighted, based on F) = 0.049 and wR_2(weighted, based on F^2) = 0.106 for all 1551 independent absorption-corrected reflections having $2\theta(MoK\alpha) < 60.95°$. The largest shift/s.u. was 0.000 in the final refinement cycle. The final difference map had maxima and minima of 0.74 and -0.27 $e^-/Å^3$, respectively.

Table 52. Crystal data and structure refinement for pHP Mesylate **72a**.

Empirical formula	$C_9H_{10}O_5S$
Formula weight	230.23
Temperature	100(2) K
Wavelength	0.71073 Å
Crystal system	Monoclinic
Space group	$P2_1/m$ - C_{2h}^2 (No. 11)
Unit cell dimensions	**a** = 8.129(1) Å **α** = 90.000°
	b = 6.609(1) Å **β** = 97.535(3)°.
	c = 8.868(1) Å **γ** = 90.000°
Volume	472.3(1) $Å^3$
Z	2
Density (calculated)	1.619 Mg/m^3
Absorption coefficient	0.341 mm^{-1}
F(000)	240
Crystal size	0.15 x 0.13 x 0.04 mm^3
Theta range for data collection	2.32° to 30.47°
Index ranges	$-11 \leq h \leq 11$, $-9 \leq k \leq 9$, $-12 \leq l \leq 12$
Reflections collected	5835
Independent reflections	1551 [R_{int} = 0.038]
Completeness to theta = 30.47°	99.6 %
Absorption correction	Multi-scans
Max. and min. transmission	1.000 and 0.934
Refinement method	Full-matrix least squares on F^2
Data / restraints / parameters	1551 / 0 / 114
Goodness-of-fit on F^2	1.136
Final R indices [I>2sigma(I)]	R_1 = 0.042, wR_2 = 0.102
R indices (all data)	R_1 = 0.049, wR_2 = 0.106
Largest diff. peak and hole	0.74 and -0.28 $e^-/Å^3$

$R_1 = \Sigma \, ||F_O| - |F_C|| \, / \, \Sigma \, |F_O|$

$wR_2 = \{ \, \Sigma \, [w(F_O^2 - F_C^2)^2] \, / \, \Sigma \, [w(F_O^2)^2] \, \}^{1/2}$

Table 53. Atomic coordinates (x 10^4) and equivalent isotropic displacement parameters ($Å^2$ x 10^3) for pHP Mesylate **72a**. U(eq) is defined as one third of the trace of the orthogonalized U_{ij} tensor.

	x	y	z	U(eq)
S	2358(1)	2500	4680(1)	11(1)
O(1)	2633(2)	2500	2957(2)	14(1)
O(2)	2817(2)	2500	117(2)	15(1)
O(3)	2964(1)	651(2)	5385(1)	18(1)
O(4)	9979(2)	2500	-1952(2)	19(1)
C(1)	4321(2)	2500	2605(2)	12(1)
C(2)	4183(2)	2500	880(2)	11(1)
C(3)	5735(2)	2500	189(2)	11(1)
C(4)	5646(3)	2500	-1400(2)	12(1)
C(5)	7066(3)	2500	-2099(2)	13(1)
C(6)	8621(2)	2500	-1206(2)	13(1)
C(7)	8732(3)	2500	374(2)	16(1)
C(8)	7296(3)	2500	1063(2)	14(1)
C(9)	196(3)	2500	4362(2)	15(1)

Table 54. Bond lengths [Å] for pHP Mesylate **72a**.

S-O(3)#1	1.430(1)	C(3)-C(4)	1.401(3)
S-O(3)	1.430(1)	C(4)-C(5)	1.379(3)
S-O(1)	1.573(2)	C(4)-H(4)	0.92(3)
S-C(9)	1.743(2)	C(5)-C(6)	1.401(3)
O(1)-C(1)	1.446(2)	C(5)-H(5)	0.95(3)
O(2)-C(2)	1.222(2)	C(6)-C(7)	1.392(3)
O(4)-C(6)	1.359(2)	C(7)-C(8)	1.386(3)
O(4)-H(4O)	0.69(3)	C(7)-H(7)	0.85(3)
C(1)-C(2)	1.519(3)	C(8)-H(8)	1.00(3)
C(1)-H(1)	0.93(2)	C(9)-H(9A)	0.97(3)
C(2)-C(3)	1.473(3)	C(9)-H(9B)	0.97(2)
C(3)-C(8)	1.398(3)		

Table 55. Bond angles [°] for pHP Mesylate **72a**.

O(3)#1-S-O(3)	117.3(1)	C(5)-C(4)-H(4)	116(2)
O(3)#1-S-O(1)	109.9(1)	C(3)-C(4)-H(4)	122(2)
O(3)-S-O(1)	109.9(1)	C(4)-C(5)-C(6)	119.5(2)
O(3)#1-S-C(9)	110.6(1)	C(4)-C(5)-H(5)	123(2)
O(3)-S-C(9)	110.6(1)	C(6)-C(5)-H(5)	118(2)
O(1)-S-C(9)	96.4(1)	O(4)-C(6)-C(7)	122.7(2)
C(1)-O(1)-S	118.0(1)	O(4)-C(6)-C(5)	117.1(2)
C(6)-O(4)-H(4O)	106(3)	C(7)-C(6)-C(5)	120.2(2)
O(1)-C(1)-C(2)	105.7(2)	C(8)-C(7)-C(6)	119.8(2)
O(1)-C(1)-H(1)	111(1)	C(8)-C(7)-H(7)	120(2)
C(2)-C(1)-H(1)	110(1)	C(6)-C(7)-H(7)	120(2)
O(2)-C(2)-C(3)	122.3(2)	C(7)-C(8)-C(3)	120.7(2)
O(2)-C(2)-C(1)	120.0(2)	C(7)-C(8)-H(8)	116(2)
C(3)-C(2)-C(1)	117.7(2)	C(3)-C(8)-H(8)	123(2)
C(8)-C(3)-C(4)	118.7(2)	S-C(9)-H(9A)	106(2)
C(8)-C(3)-C(2)	122.3(2)	S-C(9)-H(9B)	110(1)
C(4)-C(3)-C(2)	119.0(2)	H(9A)-C(9)-H(9B)	110(1)
C(5)-C(4)-C(3)	121.1(2)		

Symmetry transformations used to generate equivalent atoms: #1: x; -y+1/2; z.

Table 56. Anisotropic displacement parameters ($Å^2 \times 10^3$) for pHP Mesylate **72a**. The anisotropic displacement factor exponent takes the form:
$-2\pi^2[h^2 a^{*2} U_{11} + ... + 2 h k a^* b^* U_{12}]$

	U_{11}	U_{22}	U_{33}	U_{23}	U_{13}	U_{12}
S	9(1)	15(1)	10(1)	0	1(1)	0
O(1)	9(1)	25(1)	10(1)	0	3(1)	0
O(2)	10(1)	20(1)	14(1)	0	0(1)	0
O(3)	16(1)	20(1)	18(1)	4(1)	-1(1)	3(1)
O(4)	9(1)	37(1)	12(1)	0	2(1)	0
C(1)	9(1)	14(1)	13(1)	0	3(1)	0
C(2)	10(1)	10(1)	14(1)	0	1(1)	0
C(3)	10(1)	12(1)	12(1)	0	1(1)	0
C(4)	9(1)	13(1)	13(1)	0	-1(1)	0
C(5)	13(1)	17(1)	8(1)	0	1(1)	0
C(6)	11(1)	16(1)	13(1)	0	3(1)	0
C(7)	10(1)	25(1)	11(1)	0	-1(1)	0
C(8)	12(1)	20(1)	10(1)	0	1(1)	0
C(9)	11(1)	20(1)	15(1)	0	2(1)	0

Table 57. Hydrogen coordinates (x 10^4) and isotropic displacement parameters (Å^2 x 10^3) for pHP Mesylate **72a**.

	x	y	z	U(eq)
H(4O)	10660(40)	2500	-1400(30)	29(9)
H(1)	4890(20)	1360(30)	3000(20)	19(5)
H(4)	4650(40)	2500	-2030(40)	41(9)
H(5)	7040(30)	2500	-3180(30)	18(7)
H(7)	9680(40)	2500	920(30)	33(8)
H(8)	7460(30)	2500	2200(30)	27(8)
H(9A)	-170(30)	2500	5360(30)	22(7)
H(9B)	-200(20)	1300(30)	3810(20)	22(5)

Table 58. Torsion angles [°] for pHP Mesylate **72a**.

O(3)#1-S-O(1)-C(1)	65.29(6)
O(3)-S-O(1)-C(1)	-65.29(6)
C(9)-S-O(1)-C(1)	180.0
S-O(1)-C(1)-C(2)	180.0
O(1)-C(1)-C(2)-O(2)	0.0
O(1)-C(1)-C(2)-C(3)	180.0
O(2)-C(2)-C(3)-C(8)	180.0
C(1)-C(2)-C(3)-C(8)	0.0
O(2)-C(2)-C(3)-C(4)	0.0
C(1)-C(2)-C(3)-C(4)	180.0
C(8)-C(3)-C(4)-C(5)	0.0
C(2)-C(3)-C(4)-C(5)	180.0
C(3)-C(4)-C(5)-C(6)	0.0
C(4)-C(5)-C(6)-O(4)	180.0
C(4)-C(5)-C(6)-C(7)	0.0
O(4)-C(6)-C(7)-C(8)	180.0
C(5)-C(6)-C(7)-C(8)	0.0
C(6)-C(7)-C(8)-C(3)	0.0
C(4)-C(3)-C(8)-C(7)	0.0
C(2)-C(3)-C(8)-C(7)	180.0

Symmetry transformations used to generate equivalent atoms: #1: x; -y+1/2; z.

Table 59. Hydrogen bonds for pHP Mesylate **72a** [Å and °].

D-H...A	d(D-H)	d(H...A)	d(D...A)	<(DHA)
O(4)-H(4O)...O(2)#2	0.69(3)	2.07(3)	2.753(2)	175(4)

Symmetry transformations used to generate equivalent atoms: #1: x; -y+1/2; z; #2: x+1; y; z.

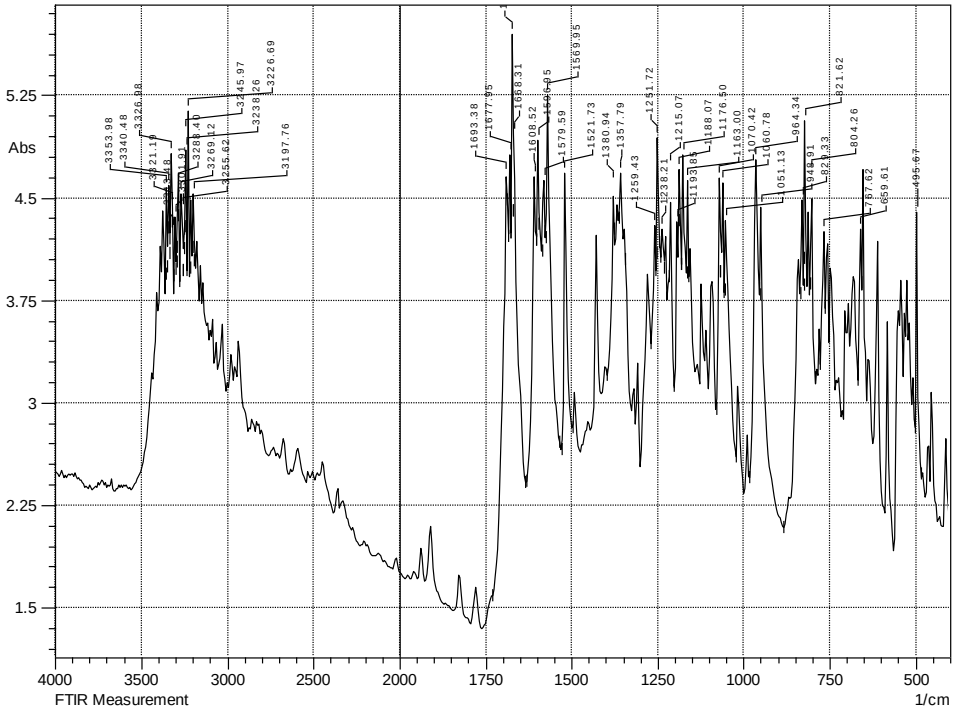

Figure 52. IR of pHP Tosylate **72b** (KBr).

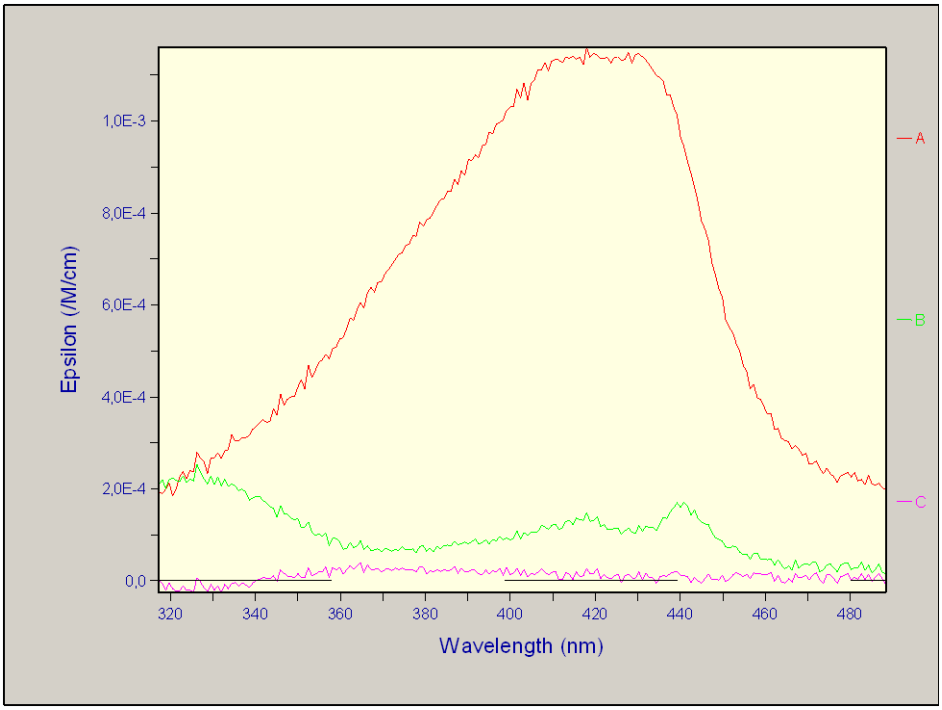

Figure 53. Laser Flash Photolysis Transient Spectra for pHP Tosylate **72b** in Aqueous Acetonitrile. Changes in absorption over time during photolysis represented by red, green, violet, and orange lines.

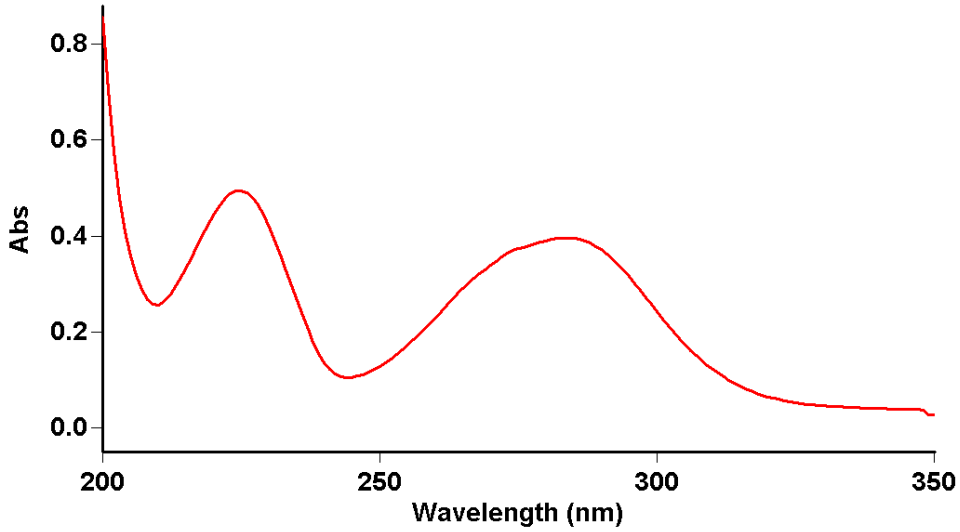

Figure 54. UV-VIS of pHP Tosylate **72b** (1:1 acetonitrile/water; λ_{max} = 283 nm; log ε = 4.20).

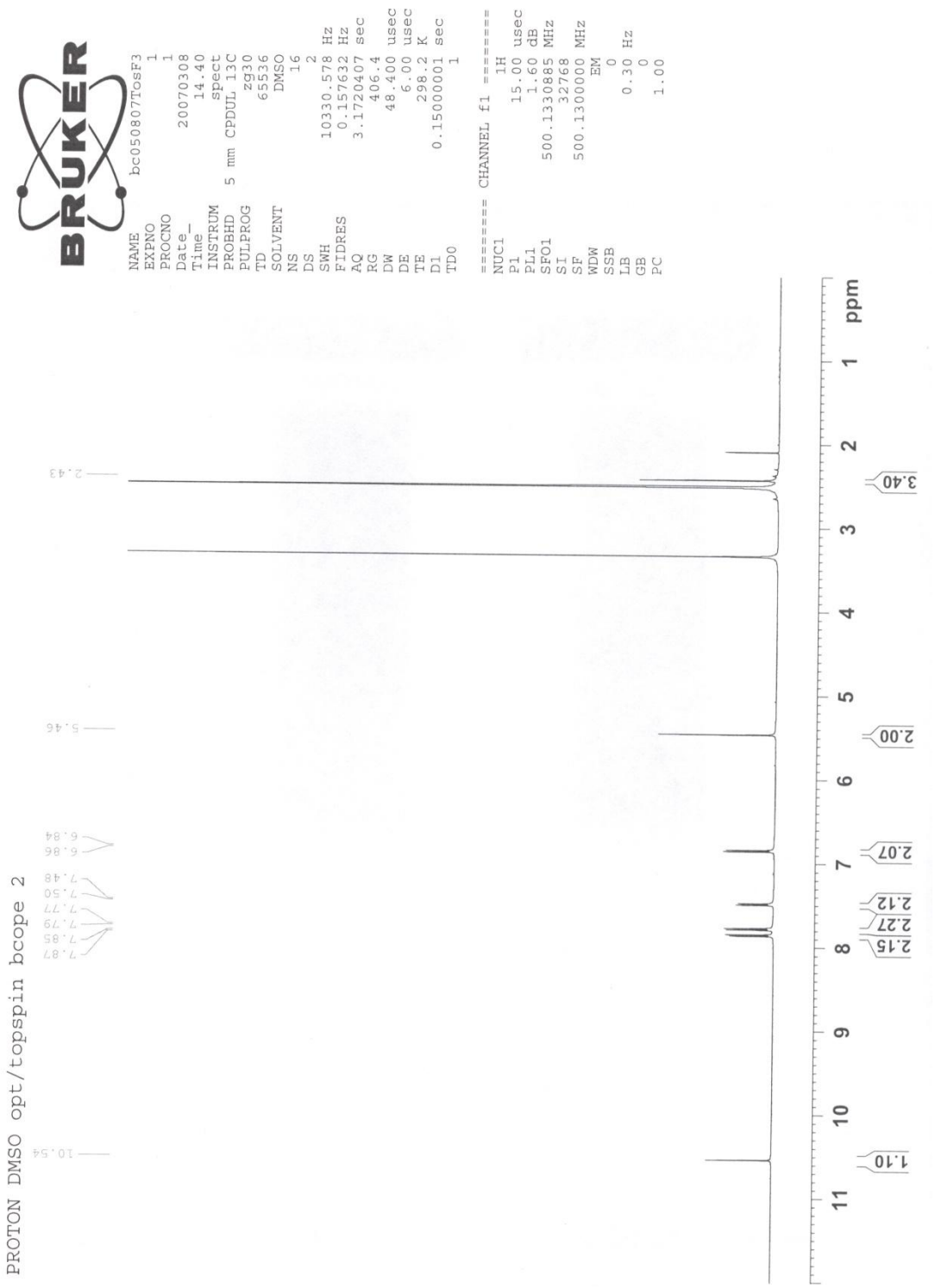

Figure 55. ^{1}H NMR of pHP Tosylate **72b** (DMSO-d_6).

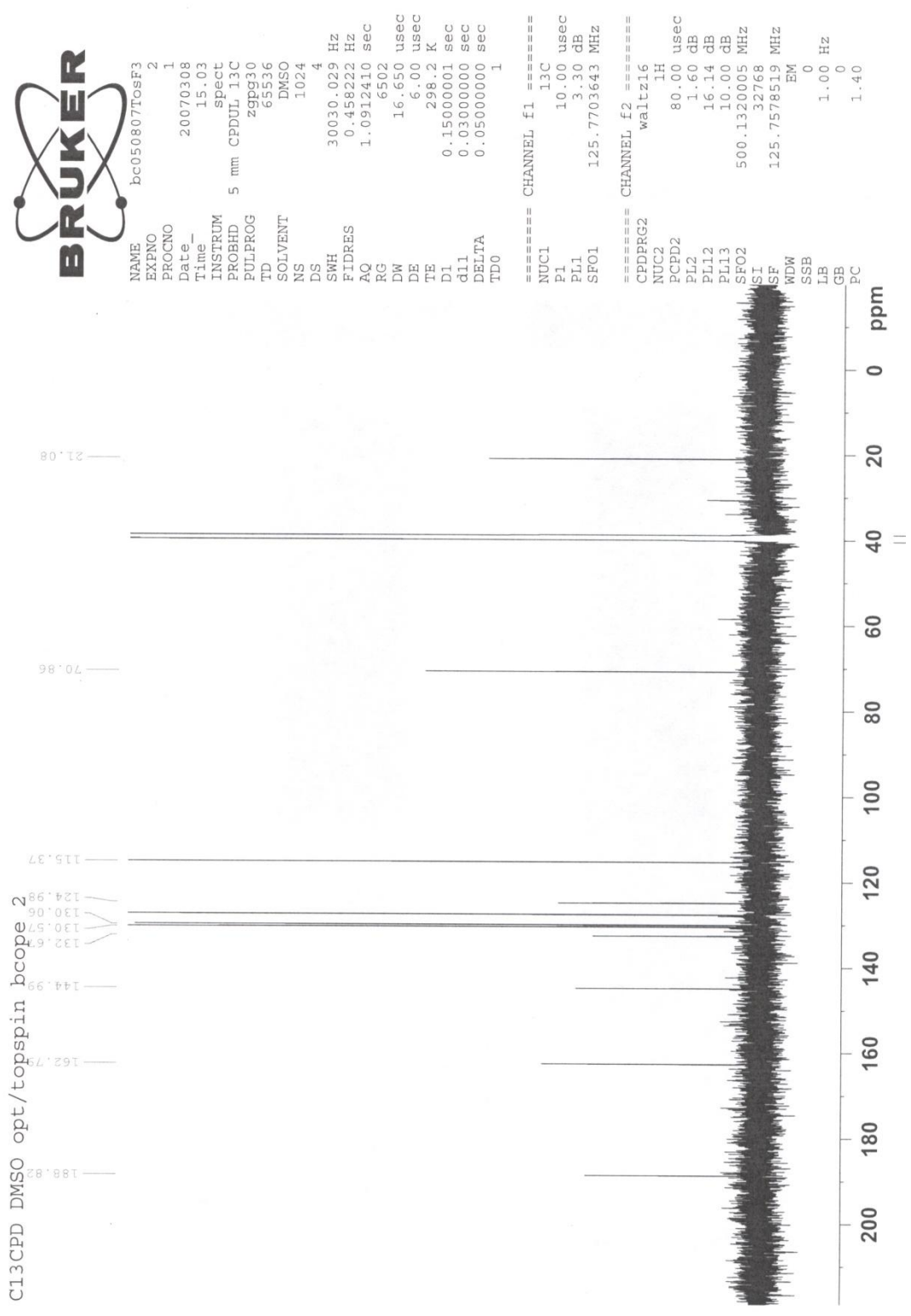

Figure 56. ^{13}C NMR of pHP Tosylate **72b** (DMSO-d_6).

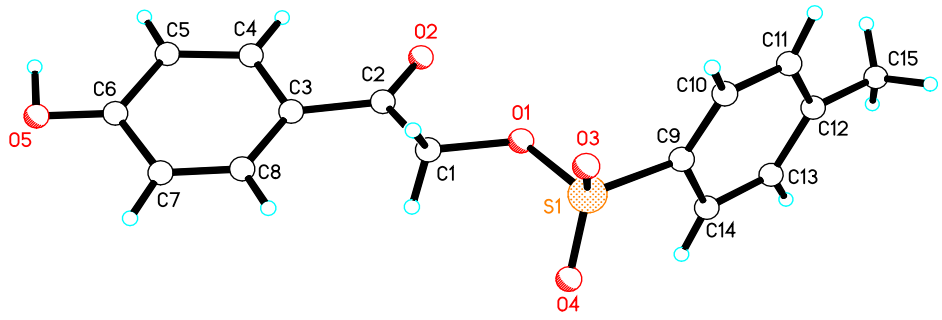

Figure 57. X-Ray Crystal Structure of pHP Tosylate **72b**.

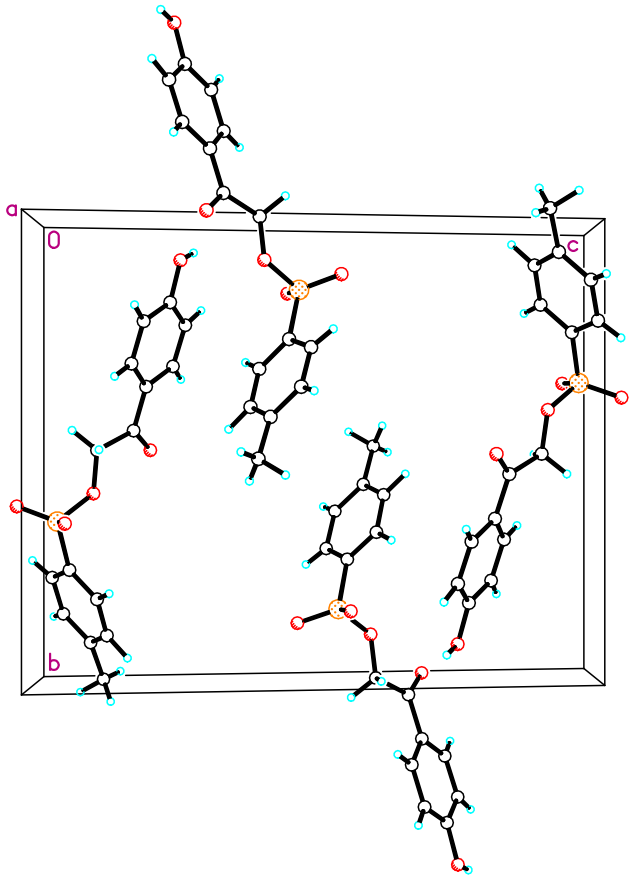

Figure 58. Orientation of pHP Tosylate **72b** in the Crystal Lattice.

Comments from Crystallographer

The asymmetric unit contains one $C_{15}H_{14}SO_5$ molecule. All displacement ellipsoids are drawn at the 50% probability level.

Brief Experimental Description

Colorless needle-shaped crystals of $C_{15}H_{14}SO_5$ are, at 296(2) K, monoclinic, space group $P2_1/c$ – C_{2h}^5 (No. 14)[1] with **a** = 5.6756(4) Å, **b** = 14.2907(8) Å, **c** = 17.744(1) Å, β = 99.153(5)°, V = 1420.9(2) Å^3 and Z = 4 molecules {d_{calcd} = 1.432 g/cm^3; μ_a(CuKα) = 2.209 mm^{-1}}. A full hemisphere of diffracted intensities (3134 5-second frames with an ω or φ scan width of 0.80°) was measured for a two-domain specimen using monochromated CuKα radiation (λ= 1.54178 Å) on a Bruker Proteum SMART 6000 Single Crystal Diffraction System[2]. X-rays were provided by a Bruker-Nonius FR591 rotating anode operating at 5kW with a 3.0 x 3.0 mm focal cup. The beam was collimated and focused with double-diffracting confocal multilayer optics (Montel mirrors). Lattice constants were determined with the Bruker SAINT software package using peak centers for 6721 reflections. A total of 11299 integrated reflection intensities having 2θ(CuKα)< 137.53° were produced using the Bruker program SAINT[3]; 2540 of these were unique and gave R_{int} = 0.069 with a coverage which was 94.9% complete. The data were corrected empirically[5] for variable absorption effects using equivalent reflections; the relative transmission factors ranged from 0.830 to 1.000. The Bruker software package SHELXTL was used to solve the structure using "direct methods" techniques. All stages of weighted

full-matrix least-squares refinement were conducted using F_o^2 data with the SHELXTL Version 6.10 software package[4].

The crystal initially appeared to utilize the C-centered orthorhombic space group $C222_1 - D_2^5$ (No. 20) with **a** = 5.6756(4) Å, **b** = 35.036(2) Å and **c** = 14.2907(8) Å . Merging the intensity data according to orthorhombic D_{2h}-mmm Laue symmetry gave R_{sym} = 0.088. When the structure could not be solved in this orthorhombic space group, the symmetry was reduced to monoclinic $C2_1$ [a nonstandard centered setting of $P2_1 - C_2^2$ (No. 4) with **c** as the unique axis]. The structure was solved in this space group to give an asymmetric unit that contained two crystallographically independent molecules. When properly translated and transformed in the unit cell, these two molecules were seen to be rigorously related by the symmetry operations of space group $P2_1/c$ when the C-centered orthorhombic unit cell was transformed to the corresponding primitive monoclinic cell. The data frames were reintegrated based on the primitive monoclinic unit cell and final lattice constants were obtained. However, the structural model containing one independent $C_{15}H_{14}SO_5$ molecule in space group $P2_1/c$ would not refine below R_1 = 0.28. Incorporation of 2-domain (54/46) pseudomerohedral twinning by a twofold rotation about the orthorhombic **an** axis, reduced R_1 to 0.07.

The final structural model utilized space group $P2_1/c$ and incorporated anisotropic thermal parameters for all nonhydrogen atoms and isotropic thermal parameters for all hydrogen atoms. All hydrogen atoms were located in a difference

Fourier and included in the structural model as independent isotropic atoms whose parameters were allowed to vary in least-squares refinement cycles. A total of 248 parameters were refined using no restraints, 2540 data and weights of $w = 1/ [\sigma^2(F^2) + (0.0725\ P)^2 + 1.0148\ P]$ where $P = [F_O^2 + 2F_C^2] / 3$. Final agreement factors at convergence are: R_1(unweighted, based on F) = 0.066 for 2312 independent absorption-corrected "observed" reflections having $2\theta(CuK\alpha) < 137.53°$ and $I > 2\sigma(I)$; R_1(unweighted, based on F) = 0.071 and wR_2(weighted, based on F^2) = 0.163 for all 2540 independent absorption-corrected reflections having $2\theta(CuK\alpha) < 137.53°$. The largest shift/s.u. was 0.000 in the final refinement cycle. The final difference map had maxima and minima of 0.45 and -0.35 $e^-/Å^3$, respectively.

Table 60. Crystal data and structure refinement for pHP Tosylate **72b**.

Empirical formula	$C_{15}H_{14}SO_5$
Formula weight	306.32
Temperature	296(2) K
Wavelength	1.54178 Å
Crystal system	Monoclinic
Space group	$P2_1/c - C_{2h}^5$ (No. 14)
Unit cell dimensions	**a** = 5.6756(4) Å α = 90.000°
	b = 14.2907(8) Å β = 99.153(5)°
	c = 17.7440(11) Å γ = 90.000°
Volume	1420.86(16) $Å^3$
Z	4
Density (calculated)	1.432 Mg/m^3
Absorption coefficient	2.209 mm^{-1}
F(000)	640
Crystal size	0.40 x 0.05 x 0.03 mm^3
Theta range for data collection	2.52° to 68.76°
Index ranges	$-6 \le h \le 6$, $-17 \le k \le 15$, $-21 \le l \le 19$
Reflections collected	11299
Independent reflections	2540 [R_{int} = 0.069]
Completeness to theta = 68.76°	94.9 %
Absorption correction	Empirical
Max. and min. transmission	1.000 and 0.830
Refinement method	Full-matrix least squares on F^2
Data / restraints / parameters	2540 / 0 / 248
Goodness-of-fit on F^2	1.209
Final R indices [I>2sigma(I)]	R_1 = 0.066, wR_2 = 0.161
R indices (all data)	R_1 = 0.071, wR_2 = 0.163
Extinction coefficient	0.002(1)
Largest diff. peak and hole	0.45 and -0.35 $e^-/Å^3$

$R_1 = \Sigma \, ||F_O| - |F_C|| \, / \, \Sigma \, |F_O|$

$wR_2 = \{ \, \Sigma \, [w(F_O^2 - F_C^2)^2] \, / \, \Sigma \, [w(F_O^2)^2] \, \}^{1/2}$

Table 61. Atomic coordinates (x 10^4) and equivalent isotropic displacement parameters ($Å^2$ x 10^3) for pHP Tosylate **72b**. U(eq) is defined as one third of the trace of the orthogonalized U_{ij} tensor.

	x	y	z	U(eq)
S	3126(2)	6514(1)	350(1)	44(1)
O(1)	2008(7)	5913(2)	947(2)	53(1)
O(2)	51(7)	4959(2)	1914(2)	56(1)
O(3)	5629(7)	6530(3)	566(3)	68(1)
O(4)	2227(9)	6189(3)	-393(2)	66(1)
O(5)	3670(8)	807(3)	2528(2)	55(1)
C(1)	2778(10)	4962(3)	1034(3)	43(1)
C(2)	1550(9)	4526(3)	1649(2)	42(1)
C(3)	2220(8)	3557(3)	1888(2)	38(1)
C(4)	802(10)	3086(4)	2338(3)	46(1)
C(5)	1269(9)	2176(4)	2570(3)	44(1)
C(6)	3165(9)	1717(3)	2336(2)	40(1)
C(7)	4622(9)	2167(3)	1902(3)	43(1)
C(8)	4144(10)	3079(4)	1677(3)	45(1)
C(9)	1851(9)	7596(3)	519(3)	42(1)
C(10)	3060(11)	8217(4)	1044(3)	46(1)
C(11)	1990(10)	9042(4)	1186(3)	49(1)
C(12)	-313(11)	9264(4)	826(3)	52(1)
C(13)	-1422(11)	8644(4)	299(4)	55(1)
C(14)	-392(11)	7806(4)	135(3)	52(1)
C(15)	-1580(18)	10138(6)	1022(5)	73(2)

Table 62. Bond lengths [Å] for pHP Tosylate **72b**.

S-O(3)	1.411(4)	C(6)-C(7)	1.376(7)
S-O(4)	1.415(4)	C(7)-C(8)	1.377(7)
S-O(1)	1.574(3)	C(7)-H(7)	0.90(5)
S-C(9)	1.753(5)	C(8)-H(8)	0.93(6)
O(1)-C(1)	1.428(6)	C(9)-C(14)	1.378(8)
O(2)-C(2)	1.207(6)	C(9)-C(10)	1.387(7)
O(5)-C(6)	1.362(6)	C(10)-C(11)	1.368(8)
O(5)-H(5O)	0.80(5)	C(10)-H(10)	0.95(6)
C(1)-C(2)	1.518(7)	C(11)-C(12)	1.398(8)
C(1)-H(1A)	0.97(5)	C(11)-H(11)	1.04(6)
C(1)-H(1B)	1.00(5)	C(12)-C(13)	1.367(8)
C(2)-C(3)	1.480(7)	C(12)-C(15)	1.509(9)
C(3)-C(8)	1.389(7)	C(13)-C(14)	1.384(8)
C(3)-C(4)	1.395(7)	C(13)-H(13)	0.79(5)
C(4)-C(5)	1.377(8)	C(14)-H(14)	0.89(7)
C(4)-H(4)	0.86(6)	C(15)-H(15A)	1.10(10)
C(5)-C(6)	1.380(7)	C(15)-H(15B)	0.84(12)
C(5)-H(5)	0.99(5)	C(15)-H(15C)	0.90(10)

Table 63. Bond angles [°] for pHP Tosylate **72b**.

O(3)-S-O(4)	117.1(3)	C(9)-C(10)-H(10)	119(4)
O(3)-S-O(1)	108.8(2)	C(10)-C(11)-C(12)	121.5(5)
O(4)-S-O(1)	108.9(2)	C(10)-C(11)-H(11)	120(3)
O(3)-S-C(9)	111.4(3)	C(12)-C(11)-H(11)	119(3)
O(4)-S-C(9)	110.6(2)	C(13)-C(12)-C(11)	117.4(5)
O(1)-S-C(9)	98.4(2)	C(13)-C(12)-C(15)	120.7(6)
C(1)-O(1)-S	116.4(3)	C(11)-C(12)-C(15)	121.9(6)
C(6)-O(5)-H(5O)	109(4)	C(12)-C(13)-C(14)	122.8(6)
O(1)-C(1)-C(2)	107.5(4)	C(12)-C(13)-H(13)	121(4)
O(1)-C(1)-H(1A)	108(3)	C(14)-C(13)-H(13)	116(4)
C(2)-C(1)-H(1A)	117(3)	C(9)-C(14)-C(13)	118.1(5)
O(1)-C(1)-H(1B)	120(3)	C(9)-C(14)-H(14)	118(4)
C(2)-C(1)-H(1B)	106(3)	C(13)-C(14)-H(14)	123(4)
H(1A)-C(1)-H(1B)	98(4)	C(12)-C(15)-H(15A)	117(5)
O(2)-C(2)-C(3)	122.2(4)	C(12)-C(15)-H(15B)	109(8)
O(2)-C(2)-C(1)	120.2(5)	H(15A)-C(15)-H(15B)	97(9)
C(3)-C(2)-C(1)	117.6(4)	C(12)-C(15)-H(15C)	112(6)
C(8)-C(3)-C(4)	117.9(5)	H(15A)-C(15)-H(15C)	103(7)
C(8)-C(3)-C(2)	124.1(4)	H(15B)-C(15)-H(15C)	118(9)
C(4)-C(3)-C(2)	118.1(4)		
C(5)-C(4)-C(3)	121.7(5)		
C(5)-C(4)-H(4)	119(3)		
C(3)-C(4)-H(4)	119(3)		
C(4)-C(5)-C(6)	118.8(5)		
C(4)-C(5)-H(5)	121(3)		
C(6)-C(5)-H(5)	119(3)		
O(5)-C(6)-C(7)	117.7(5)		
O(5)-C(6)-C(5)	121.5(5)		
C(7)-C(6)-C(5)	120.8(4)		
C(6)-C(7)-C(8)	119.8(5)		
C(6)-C(7)-H(7)	117(3)		
C(8)-C(7)-H(7)	123(3)		
C(7)-C(8)-C(3)	120.9(5)		
C(7)-C(8)-H(8)	117(4)		
C(3)-C(8)-H(8)	122(4)		
C(14)-C(9)-C(10)	120.9(5)		
C(14)-C(9)-S	118.8(4)		
C(10)-C(9)-S 1	20.3(4)		
C(11)-C(10)-C(9)	119.2(5)		
C(11)-C(10)-H(10)	121(4)		

Table 64. Anisotropic displacement parameters ($Å^2 \times 10^3$) for pHP Tosylate **72b**. The anisotropic displacement factor exponent takes the form:
$-2\pi^2[h^2 a^{*2} U_{11} + ... + 2 h k a^* b^* U_{12}]$

	U_{11}	U_{22}	U_{33}	U_{23}	U_{13}	U_{12}
S	51(1)	33(1)	51(1)	3(1)	20(1)	-4(1)
O(1)	70(3)	31(2)	65(2)	8(2)	31(2)	6(2)
O(2)	67(3)	42(2)	68(2)	1(2)	33(2)	16(2)
O(3)	45(2)	53(2)	111(3)	2(2)	24(2)	-4(2)
O(4)	92(3)	56(2)	53(2)	-6(2)	22(2)	3(2)
O(5)	58(3)	41(2)	68(2)	12(2)	14(2)	-3(2)
C(1)	50(3)	27(2)	54(3)	-2(2)	18(2)	2(2)
C(2)	52(3)	35(2)	39(2)	-3(2)	9(2)	0(2)
C(3)	45(3)	34(2)	35(2)	0(2)	6(2)	-2(2)
C(4)	48(3)	44(3)	50(3)	-3(2)	23(2)	2(2)
C(5)	44(3)	44(3)	47(2)	4(2)	14(2)	-5(2)
C(6)	43(3)	34(2)	40(2)	2(2)	2(2)	-2(2)
C(7)	38(3)	40(3)	54(3)	0(2)	10(2)	5(2)
C(8)	46(3)	39(3)	54(3)	2(2)	16(2)	-3(2)
C(9)	44(3)	39(3)	43(2)	10(2)	11(2)	-5(2)
C(10)	51(3)	40(3)	47(3)	2(2)	3(2)	-4(2)
C(11)	58(3)	40(3)	53(3)	-8(2)	14(2)	-7(2)
C(12)	62(4)	42(3)	55(3)	8(2)	23(3)	1(3)
C(13)	43(3)	53(3)	67(3)	10(3)	3(3)	8(3)
C(14)	56(3)	44(3)	54(3)	-2(2)	3(3)	-11(3)
C(15)	88(5)	53(4)	82(5)	-1(3)	31(4)	18(4)

Table 65. Hydrogen coordinates (x 10^4) and isotropic displacement parameters (Å^2 x 10^3) for pHP Tosylate **72b**.

	x	y	z	U(eq)
H(5O)	2640(100)	610(40)	2740(30)	34(14)
H(1A)	4510(90)	4950(30)	1120(20)	29(11)
H(1B)	2500(100)	4520(40)	590(30)	50(14)
H(4)	-440(100)	3370(40)	2460(30)	41(13)
H(5)	140(90)	1820(40)	2840(30)	42(13)
H(7)	5850(90)	1840(30)	1770(20)	31(11)
H(8)	5220(110)	3370(40)	1410(30)	58(16)
H(10)	4600(110)	8060(40)	1300(30)	56(16)
H(11)	2900(110)	9510(40)	1570(30)	50(14)
H(13)	-2720(100)	8740(30)	80(30)	36(14)
H(14)	-1030(130)	7430(50)	-240(40)	71(19)
H(15A)	-2830(180)	10470(60)	560(50)	120(30)
H(15B)	-2600(200)	10000(80)	1300(60)	160(50)
H(15C)	-550(180)	10600(70)	1180(50)	120(40)

Table 66. Torsion angles [°] for pHP Tosylate **72b**.

O(3)-S-O(1)-C(1)	-59.2(4)
O(4)-S-O(1)-C(1)	69.5(4)
C(9)-S-O(1)-C(1)	-175.3(4)
S-O(1)-C(1)-C(2)	178.3(3)
O(1)-C(1)-C(2)-O(2)	6.3(7)
O(1)-C(1)-C(2)-C(3)	-175.1(4)
O(2)-C(2)-C(3)-C(8)	-171.0(5)
C(1)-C(2)-C(3)-C(8)	10.5(7)
O(2)-C(2)-C(3)-C(4)	10.7(7)
C(1)-C(2)-C(3)-C(4)	-167.9(5)
C(8)-C(3)-C(4)-C(5)	-0.1(7)
C(2)-C(3)-C(4)-C(5)	178.4(5)
C(3)-C(4)-C(5)-C(6)	-1.3(8)
C(4)-C(5)-C(6)-O(5)	-178.0(4)
C(4)-C(5)-C(6)-C(7)	2.3(7)
O(5)-C(6)-C(7)-C(8)	178.2(5)
C(5)-C(6)-C(7)-C(8)	-2.0(8)
C(6)-C(7)-C(8)-C(3)	0.6(8)
C(4)-C(3)-C(8)-C(7)	0.4(7)
C(2)-C(3)-C(8)-C(7)	-178.0(5)
O(3)-S-C(9)-C(14)	159.8(4)
O(4)-S-C(9)-C(14)	27.7(5)
O(1)-S-C(9)-C(14)	-86.2(4)
O(3)-S-C(9)-C(10)	-21.8(5)
O(4)-S-C(9)-C(10)	-153.9(4)
O(1)-S-C(9)-C(10)	92.2(4)
C(14)-C(9)-C(10)-C(11)	0.8(7)
S-C(9)-C(10)-C(11)	-177.6(4)
C(9)-C(10)-C(11)-C(12)	1.3(7)
C(10)-C(11)-C(12)-C(13)	-2.8(7)
C(10)-C(11)-C(12)-C(15)	175.4(6)
C(11)-C(12)-C(13)-C(14)	2.3(8)
C(15)-C(12)-C(13)-C(14)	-175.9(6)
C(10)-C(9)-C(14)-C(13)	-1.3(7)
S-C(9)-C(14)-C(13)	177.1(4)
C(12)-C(13)-C(14)-C(9)	-0.3(8)

Table 67. Hydrogen bonds for pHP Tosylate **72b** [Å and °].

D-H...A	d(D-H)	d(H...A)	d(D...A)	<(DHA)
O(5)-H(5O)...O(2)#1	0.80(5)	1.97(6)	2.752(5)	168(5)

Symmetry transformations used to generate equivalent atoms: #1: -x, y-1/2, -z+1/2.

X-RAY CRYSTALLOGRAPHY REFERENCES

(1) *International Tables for Crystallography*; 4th ed. ed.; Kluwer: Boston, 1996; Vol. A.
(2) *Data Collection: SMART Software Reference Manual*; Bruker-AXS: Madison, WI, 1998.
(3) *Data Reduction: SAINT Software Reference Manual*; Bruker-AXS: Madison, WI, 1998.
(4) Sheldrick, G. M. *SHELXTL Version 6.10 Reference Manual*; Bruker-AXS: Madison, WI, 2000.
(5) Sheldrick, G. M. *Program for Emperical Absorption Correction of Area Detector Data*; University of Gottingen: Germany, 2002.